QUANTUM LIQUIDS AND QUANTUM CRYSTALS

Nondissipative flows in many-particle systems as a consequence of symmetry breaking

Yu. M. Poluektov*

Kharkov Physicotechnical Institute National Research Center, ul. Akademicheskaya 1, 61108, Kharkov, Ukraine

(Submitted July 6, 2002; revised August 20, 2002)
Fiz. Nizk. Temp. **29**, 3–15 (January 2003)

It is shown that undamped flows can exist in many-particle systems found in spatially nonuniform thermodynamic equilibrium states with broken symmetries. If the thermodynamic potential of the system is invariant with respect to a certain transformation which is a function of continuous parameters, then this transformation is associated with conserved flux densities and integrals of motion, the number of which is equal to the number of continuous parameters of the transformation. The stability of the superconducting and superfluid flows arising as a result of the breaking of phase symmetry is explained by the fact that the conservation laws associated with these states, which do not correspond to an absolute minimum of the thermodynamic potential, do not allow them to be destroyed. © *2003 American Institute of Physics.* [DOI: 10.1063/1.1542371]

1. INTRODUCTION

Systems of many interacting particles can be found in states that admit the existence of flows which are unaccompanied by energy dissipation. Nondissipative electron flows (superconductivity) were discovered in metals by Kamerlingh Onnes in 1911,[1] and nondissipative mass flows (superfluidity) were discovered in liquid ^{4}He a quarter of a century later by Kapitsa.[2] The superfluid properties of liquid ^{3}He at millidegree temperatures were detected in the early 1970s.[3] In ^{3}He there can be nondissipative transport not only of mass but of other characteristics, spin in particular. In 1986 Bednorz and Müller discorved[4] that nondissipative flows of charges exist in materials having an extremely complex internal structure (high-T_c superconductors). There are other systems in which flows unaccompanied by energy dissipation are possible, e.g., materials with a magnetic structure and liquid crystals. The problem of nondissipative flows and superfluidity in ^{4}He and ^{3}He, magnets, and excitonic insulators has been discussed from various points of view by Sonin.[5]

One notices that flows without dissipation can exist in systems with very different internal structures and particle statistics. This apparently indicates that the appearance of nondissipative (superfluid) flows in many-particle systems with different internal structures has a unified cause. The connection between the superconducting properties and the existence of a complex-valued parameter that breaks the symmetry of the state with respect to a phase transformation was first demonstrated in the famous paper by Ginzburg and Landau.[6] The ideas of Ref. 6 were extended to superfluid ^{4}He by Ginzburg and Pitaevskiĭ in Ref. 7 (a modified version of the theory is set forth in Ref. 8). We note that the breaking of symmetry with respect to phase transformations is also taken into account, although in implicit form, in the the famous Landau theory of superfluidity,[9] through the introduction of a superfluid velocity and a density of the superfluid component, which are related to the modulus and phase of the complex order parameter.[7] In spite of the fact that the fundamental role of broken phase symmetry in the existence of nondissipative flows is perfectly clear from Refs. 6 and 7, in many papers at the present time the phenomena of superfluidity and superconductivity are being attributed to circumstances that, although they may be accompanied by transitions to states with nondissipative flows, are not essential and necessary for the appearance of such flows (macroscopically occupied state, the presence of pairing, characteristic features of the quasiparticle energy spectrum, etc.).

In the present paper we show in general form that current states arise in systems of many interacting particles found in spatially nonuniform thermodynamic equilibrium states with broken symmetries with respect to certain kinds of transformations. These currents may involve the transport not only of charge or mass but also of other characteristics, e.g., magnetization, angular momentum, etc. If the thermodynamic potential is invariant with respect to the transformations in question, then an integral of motion is associated to each such flow. The result of this study is essentially an analog of Nöther's theorem,[10] well known in field theory, for the case of a many-particle nonrelativistic system. According to Nöther's theorem, to each transformation of functions of the field and coordinates which does not affect the action there are associated s currents and the same number of dynamical invariants, where s is the number of continuous parameters on which the transformation depends. Spatial transformations and transformations of internal symmetries are considered. A special study is made of symmetry with respect to phase transformations, the breaking of which is associated with the appearance of superfluid and superconducting properties. The stability of states having superfluid flows and not corresponding to an absolute minimum of the thermodynamic potential is explained by the fact that the destruction of these flows is prevented by a conservation law due to the phase symmetry. For the example of flows of

magnetization near a domain wall in a ferromagnet we consider nonconserved localized nondissipative flows.

2. STATEMENT OF THE PROBLEM

According to the Landau theory of second-order phase transitions,[11,12] a phase transition to a state with lower symmetry can be described as the appearance of certain additional characteristics of the system—order parameters—which, generally speaking, can be functions of the spatial coordinates. The assumption that spatially nonuniform thermodynamic equilibrium states with order parameters depending on the coordinates can exist even under spatially uniform external conditions is of fundamental importance for the treatment that follows. The spatial nonuniformity is associated with a certain energy, and the thermodynamic potential density therefore depends not only on the order parameter but also on its gradients.

Suppose that a system of many particles enclosed in a volume V is characterized by (in addition to the thermodynamic variables, which we choose as the temperature T and chemical potential μ) a multicomponent order parameter

$$\varphi=(\varphi_1,\varphi_2,\ldots\varphi_L), \tag{1}$$

the components of which are the coordinate-dependent functions $\varphi_a(\mathbf{r})$ $(a=1,2,\ldots L)$, where L is the number of components of the order parameter. The multicomponent character of the order parameter may be of various natures, e.g., the components of a vector or tensor. In the case of a multiband superconductor the components of the order parameter describe the electrons of different conduction bands.[13] Different components can correspond to different types of anomalous averages (single-particle, pair). Without specifying the particular microscopic nature of the order parameter, we shall assume that the functions $\varphi_a(\mathbf{r})$ are complex. The formulas for the case of real-valued order parameters can be obtained in an obvious way from the formulas given below. We assume that the thermodynamic potential density depends on both the thermodynamic variables and on the order parameter and its gradients:

$$\omega=\omega(\mu,T:\varphi,\varphi^*,\nabla\varphi,\nabla\varphi^*). \tag{2}$$

The components of the order parameter are functions of the thermodynamic variables μ and T. We shall assume that there are no external fields, and therefore ω does not depend explicitly on the spatial coordinates. A generalization to the case when such a dependence does exist presents no fundamental difficulties. The total thermodynamic potential of the system,

$$\Omega(\mu,T)=\int_V d^3r\,\omega(\mu,T;\varphi,\varphi^*,\nabla\varphi,\nabla\varphi^*), \tag{3}$$

is a function of the thermodynamic variables and a functional of the order-parameter components $\varphi_a(\mathbf{r})$. In the theory of second-order phase transition it is assumed that the thermodynamic potential near a line of transitions can be expanded in a series in powers of the order parameter and its gradients. However, we shall not specify the dependence of ω on φ and $\nabla\varphi$, so that the treatment that follows does not rely on the possibility of such an expansion.

The order parameter is found from the requirement that the thermodynamic potential be minimum. By varying Ω with respect to the functions $\varphi_a(\mathbf{r})$ under the condition that the variation $\delta\varphi_a(\mathbf{r})$ vanish at the boundary, we obtain the Lagrange–Euler equations[14] determining the components of the order parameter in the thermodynamic equilibrium state:

$$\frac{\partial\omega}{\partial\varphi_a}-\nabla\frac{\partial\omega}{\partial\nabla\varphi_a}=0. \tag{4}$$

Equations (4) have the solution $\varphi=0$. The region of the (μ,T) plane in which such a solution corresponds to the absolute minimum of the thermodynamic potential is called the normal or symmetric phase. Regions in which $\varphi\neq0$ correspond to phases with broken symmetries.

Using Eqs. (4), we find the total number of particles in the system:

$$N=-\frac{\partial\Omega}{\partial\mu}=-\int_V d^3r\frac{\partial'\omega}{\partial\mu}-\sum_a\int_S d\mathbf{s}\left(\frac{\partial\omega}{\partial\nabla\varphi_a}\frac{\partial\varphi_a}{\partial\mu}+\text{c.c.}\right), \tag{5}$$

where the prime on the differentiation sign means that only the explicit dependence of ω on μ is taken into account, and the abbreviation c.c. denotes the complex conjugate. The analogous formula with the substitution $\mu\to T$ determines the total entropy S. The total energy is expressed by the formula

$$E=\int_V d^3r\left(\omega-\mu\frac{\partial'\omega}{\partial\mu}-T\frac{\partial'\omega}{\partial T}\right)-\sum_a\int_S d\mathbf{s}\left[\frac{\partial\omega}{\partial\nabla\varphi_a}\left(\frac{\partial\varphi_a}{\partial\mu}\mu+\frac{\partial\varphi_a}{\partial T}T\right)+\text{c.c.}\right]. \tag{6}$$

Generally speaking, the surface terms in Eqs. (5) and (6) are nonzero.

We define a set of new functions $\varphi'_a(\mathbf{r};\lambda)$ related to the old functions $\varphi_a(\mathbf{r})$ by the expression

$$\varphi'_a(\mathbf{r},\lambda)=\sum_b\int d^3r'T_{ab}(\mathbf{r},\mathbf{r}';\lambda)\varphi_b(\mathbf{r}'), \tag{7}$$

where $T_{ab}(\mathbf{r},\mathbf{r}';\lambda)$ is an $L\times L$ matrix in the space of indices enumerating the components of the order parameter and depends on a set of s continuous real parameters $\lambda=(\lambda_1,\lambda_2,\ldots,\lambda_s)$. It is convenient to choose these matrices as unitary, so that

$$\sum_c\int d^3r''T^*_{ca}(\mathbf{r}'',\mathbf{r})T_{cb}(\mathbf{r}'',\mathbf{r})=\sum_c\int d^3r''T^*_{ac}(\mathbf{r},\mathbf{r}'')T_{bc}(\mathbf{r}',\mathbf{r}'')=\delta_{ab}\delta(\mathbf{r}-\mathbf{r}'). \tag{8}$$

Here the normalization of the order-parameter components is preserved:

$$\sum_a\int d^3r|\varphi_a(\mathbf{r})|^2=\sum_a\int d^3r|\varphi'_a(\mathbf{r})|^2.$$

We assume that the thermodynamic potential density is invariant with respect to the linear transformations (7), and therefore

$$\Omega = \int_V d^3r\,\omega(\varphi(\mathbf{r}),\varphi^*(\mathbf{r}),\nabla\varphi(\mathbf{r}),\nabla\varphi^*(\mathbf{r}))$$

$$= \int_V d^3r\,\omega(\varphi'(\mathbf{r}),\varphi'^*(\mathbf{r}),\nabla\varphi'(\mathbf{r}),\nabla\varphi'^*(\mathbf{r})). \qquad (9)$$

The functions $\varphi'_a(\mathbf{r};\lambda)$ also satisfy the Lagrange–Euler equations (4). Thus, in addition to the state determined by the set of functions $\varphi_a(\mathbf{r})$, there can be states determined by the set of functions $\varphi'_a(\mathbf{r},\lambda)$, which depend on s continuous parameters, i.e., there exist infinitely many states which differ in the values of λ but for which the value of the thermodynamic potential is the same. This means that there is degeneracy of the states in the many-particle system.

3. DENSITIES OF NONDISSIPATIVE FLOWS

In what follows it is sufficient to consider infinitesimal transformations. One can always choose the set of continuous parameters λ in such a way that if all these parameters equal zero, the functions $\varphi_a(\mathbf{r})$ and $\varphi'_a(\mathbf{r})$ coincide. In this case at small values of λ we have

$$T_{ab}(\mathbf{r},\mathbf{r}';\lambda) = \delta_{ab}\delta(\mathbf{r}-\mathbf{r}') + \sum_{\nu=1}^{s} \Theta^{\nu}_{ab}(\mathbf{r},\mathbf{r}')\lambda_\nu, \qquad (10)$$

where the generator of the transformation is

$$\Theta^{\nu}_{ab}(\mathbf{r},\mathbf{r}') = \left.\frac{\partial T_{ab}(\mathbf{r},\mathbf{r}';\lambda)}{\partial\lambda_\nu}\right|_{\lambda=0}.$$

We note that, by virtue of the unitarity conditions (8), the following condition holds:

$$\Theta^{\nu}_{ab}(\mathbf{r},\mathbf{r}') = -\Theta^{\nu*}_{ba}(\mathbf{r},\mathbf{r}'). \qquad (11)$$

Substituting (10) into (7), we obtain

$$\varphi'_a(\mathbf{r}) = \varphi_a(\mathbf{r}) = \delta\varphi_a(\mathbf{r}), \qquad (12)$$

where

$$\delta\varphi_a(\mathbf{r}) = \sum_{b=1}^{L}\sum_{\nu=1}^{s}\int d^3r'\,\Theta^{\nu}_{ab}(\mathbf{r},\mathbf{r}')\varphi_b(\mathbf{r}')\lambda_\nu.$$

Using the invariance of the thermodynamic potential (9) with respect to infinitesimal transformations (12) and taking the Lagrange–Euler equations (4) into account, we obtain the relation

$$\sum_{a=1}^{L}\sum_{\nu=1}^{s}\int d^3r\nabla\left[\frac{\partial\omega}{\partial\nabla\varphi_a}\Psi_{a\nu}(\mathbf{r}) + \text{c.c.}\right]\lambda_\nu = 0, \qquad (13)$$

where

$$\Psi_{a\nu}(\mathbf{r}) = \sum_{b=1}^{L}\int d^3r'\,\Theta^{\nu}_{ab}(\mathbf{r},\mathbf{r}')\varphi_b(\mathbf{r}').$$

By virtue of the arbitrariness of the values of the small parameters λ_ν, it follows from (13) that

$$\sum_a \int d^3r\nabla\left[\frac{\partial\omega}{\partial\nabla\varphi_a}\Psi_{a\nu}(\mathbf{r}) + \text{c.c.}\right] = 0. \qquad (14)$$

Equations (14) are a set of s continuity equations ($\nu = 1,2,\ldots,s$)

$$\operatorname{div}\mathbf{j}_\nu = 0, \qquad (15)$$

where the flux densities have the form

$$\mathbf{j}_\nu = \sum_a\left[\frac{\partial\omega}{\partial\nabla\varphi_a}\Psi_{a\nu}(\mathbf{r}) + \text{c.c.}\right]. \qquad (16)$$

We see that there are s flux densities corresponding to the s continuous parameters in the transformation (7). As we know, the flux densities are defined nonuniquely, up to a vector with zero divergence. Flows of physical quantities in systems with broken symmetries are considered in the method of quasiaverages in Ref. 15 (see also Ref. 16).

4. INTEGRALS OF MOTION

In the previous Section we obtained expressions for s flux densities and the corresponding continuity equations. The existence of continuity equations implies the existence of conserved quantities—integrals of motion. For finding the integrals of motion it is insufficient to consider a stationary state, and one must use the dynamical equations describing the evolution of the order parameter in time. Here the differential form of the conservation equations is

$$\frac{\partial\pi_\nu}{\partial t} + \operatorname{div}\mathbf{j}_\nu = 0, \qquad (17)$$

where π_ν are the densities of the quantities whose fluxes densities are $\mathbf{j}_\nu$. Integrating (17) over the volume and assuming that the total flux through the boundary of the volume is zero,

$$\int_S d\mathbf{s}\cdot\mathbf{j}_\nu = 0, \qquad (18)$$

were find that the quantities

$$\Pi_\nu = \int_V d^3r\,\pi_\nu(\mathbf{r}) \qquad (19)$$

are integrals of motion. Let us find the densities π_ν and, hence, the integrals of motion (19). In a phenomenological approach this can be done using the Lagrangian formalism. We shall treat the thermodynamic potential density as a potential energy density and introduce a kinetic energy density related to the change of the order parameter in time:

$$\kappa = \kappa(\mu,T;\varphi,\varphi^*,\dot\varphi,\dot\varphi^*). \qquad (20)$$

Then we write the Lagrangian density in the form

$$\Lambda(\varphi,\varphi^*,\nabla\varphi,\nabla\varphi^*,\dot\varphi,\dot\varphi^*)$$

$$= \kappa(\varphi,\varphi^*,\dot\varphi,\dot\varphi^*) - \omega(\varphi,\varphi^*,\nabla\varphi,\nabla\varphi^*). \qquad (21)$$

We assume that there are no time-dependent external fields, so that the Lagrangian is explicitly dependent on neither the coordinates nor time. Then, in analogy with how this was done for the steady-state case, we arrive at the conservation laws (17), where the densities of the conserved quantities have the form

$$\pi_\nu(\mathbf{r}) = \sum_a\left[\frac{\partial\kappa}{\partial\dot\varphi_a}\Psi_{a\nu}(\mathbf{r}) + \text{c.c.}\right]. \qquad (22)$$

Thus, if the thermodynamic potential of the system is invariant with respect to the transformations (7), containing s continuous parameters, then there are s conserved quantities Π_ν—integrals of motion.

In addition to the s continuity equations (17), which are valid because of the invariance of the thermodynamic potential with respect to the symmetry transformations (7), we also have the energy conservation law due to the invariance of the thermodynamic potential with respect to a translation in time:

$$\frac{\partial \vartheta}{\partial t} + \operatorname{div} \mathbf{j}^{(\varepsilon)} = 0, \tag{23}$$

where the energy density is

$$\vartheta = \sum_a \left(\frac{\partial \Lambda}{\partial \dot{\varphi}_a} \dot{\varphi}_a + \frac{\partial \Lambda}{\partial \dot{\varphi}_a^*} \dot{\varphi}_a^* \right) - \Lambda, \tag{24}$$

and the energy flux density is

$$\mathbf{j}^{(\varepsilon)} = \sum_a \left(\frac{\partial \Lambda}{\partial \nabla \varphi_a} \dot{\varphi}_a + \text{c.c.} \right). \tag{25}$$

If the total energy flux through the boundary is zero, $\int_S d\mathbf{s} \cdot \mathbf{j}^{(\varepsilon)} = 0$, then the total energy

$$\Xi = \int_V d^3 r \, \vartheta(\mathbf{r}) \tag{26}$$

is a dynamical invariant. We note that in a state of equilibrium the energy Ξ is equal to the total thermodynamic potential and not to the total energy E, which is given by formula (6). This is because the dynamics of the order parameter is considered at fixed thermodynamic variables μ, T. In a stationary state the energy flux density vanishes, so that the flows in a thermodynamic equilibrium state do not transport energy.

Nonstationary phenomena in a many-particle system are accompanied by energy dissipation, a fact which was not taken into account in the derivation of the continuity equations (17). Dissipation can be taken into account in our phenomenological approach by specifying a dissipative function in addition to the Lagrangian.[17] Then the right-hand sides of equations (17) would be nonzero, and the quantities Π_ν would vary in time, relaxing to their equilibrium values. Thus Π_ν are integrals of motion only when dissipative processes are neglected, as is the situation in classical mechanics also. In this paper we shall not consider dissipative phenomena in many-particle systems.

5. KINETIC ENERGY

In the phenomenological approach the kinetic energy density must be specified in additon to the thermodynamic potential density. Taking into account certain general requirements, let us refine the form of the kinetic energy. The kinetic energy must be real-valued and, since we are describing nondissipative processes, invariant with respect to time inversion. In addition, it should be invariant with respect to phase transformations. In quantum mechanics, as we know, the operation of time inversion involves changing the sign of the time derivative and replacing the wave function by its complex conjugate. Accordingly, in order for the kinetic energy to remain invariant under the transformations

$$t \to -t, \quad \varphi \to \varphi^*, \tag{27}$$

the following condition must hold:

$$\kappa(\varphi, \varphi^*, \dot{\varphi}, \dot{\varphi}^*) = \kappa(\varphi, \varphi^*, -\dot{\varphi}, -\dot{\varphi}^*). \tag{28}$$

We note that if the order parameter is a spinor, then the time inversion operation is somewhat different from (27).[16] In this paper we restrict discussion to the case when operation (27) is valid. As in classical mechanics,[14] we shall take into account terms up to quadratic in the velocities or, here, in the derivatives $\dot{\varphi}, \dot{\varphi}^*$. In classical mechanics the kinetic energy does not contain terms linear in the velocities and depends only on the squares of the velocities. In the case of complex variables, condition (28) can also hold for terms linear in the quantities $\dot{\varphi}, \dot{\varphi}^*$. In addition, the kinetic energy, like any observable quantity, must be invariant with respect to the phase transformations

$$\varphi \to \varphi e^{i\chi}, \tag{29}$$

where χ is a real number. Taking into account everything we have said, we write the kinetic energy in the form

$$\begin{aligned} \kappa(\varphi, \varphi^*, \dot{\varphi}, \dot{\varphi}^*) = & \sum_a \left[A_a(\varphi^*, \varphi) \dot{\varphi}_a - A_a(\varphi, \varphi^*) \dot{\varphi}_a^* \right] \\ & + \sum_{ab} \left[B_{ab}(\varphi^*, \varphi) \dot{\varphi}_a \dot{\varphi}_b \right. \\ & + B_{ab}(\varphi, \varphi^*) \dot{\varphi}_a^* \dot{\varphi}_b^* \\ & \left. + D_{ab}(\varphi, \varphi^*) \dot{\varphi}_a^* \dot{\varphi}_b \right]. \end{aligned} \tag{30}$$

By virtue of the requirements that the kinetic energy be real and invariant with respect to time inversion (28), the following conditions must hold for the coefficients (30):

$$\begin{aligned} & A_a(\varphi, \varphi^*) = -A_a^*(\varphi^*, \varphi), \\ & B_{ab}(\varphi, \varphi^*) = B_{ba}(\varphi, \varphi^*) = B_{ab}^*(\varphi^*, \varphi), \\ & D_{ab}(\varphi, \varphi^*) = D_{ba}^*(\varphi, \varphi^*) = D_{ba}(\varphi^*, \varphi). \end{aligned} \tag{31}$$

The requirement of phase invariance leads to the conditions

$$\begin{aligned} & A_a(\varphi^* e^{-i\chi}, \varphi e^{i\chi}) e^{i\chi} = A_a(\varphi^*, \varphi), \\ & B_{ab}(\varphi^* e^{-i\chi}, \varphi e^{i\chi}) e^{2i\chi} = B_{ab}(\varphi^*, \varphi), \\ & D_{ab}(\varphi^* e^{-i\chi}, \varphi e^{i\chi}) = D_{ab}(\varphi^*, \varphi). \end{aligned} \tag{32}$$

Taking into account only the leading terms of the expansion of the coefficients in (30) in powers of the order parameter, we obtain the simplest possible form of the kinetic energy:

$$\begin{aligned} \kappa(\varphi, \varphi^*, \dot{\varphi}, \dot{\varphi}^*) = & -i \sum_a \beta_a (\varphi_a^* \dot{\varphi}_a - \varphi_a \dot{\varphi}_a^*) \\ & + \frac{1}{2} \sum_{ab} \gamma_{ab} \dot{\varphi}_a^* \dot{\varphi}_b, \end{aligned} \tag{33}$$

where $\beta_a = \beta_a^*$ and $\gamma_{ab} = \gamma_{ba}^*$ are phenomenological constants. The requirements on the symmetry of the thermodynamic potential with respect to other transformations can impose additional conditions on the coefficients in the expression for the kinetic energy. We note that the form of the energy (33) is analogous to the choice of a kinetic energy containing terms linear in the time derivative of the wave function when the Schrödinger equation is obtained by the Lagrangian method.[14] If we use this simplified form for the kinetic energy, we obtain the following expression for the densities of conserved quantities:[22]

$$\pi_\nu = -i\sum_a \beta_a(\varphi_a^*\Psi_{a\nu} - \varphi_a\Psi_{a\nu}^*) + \frac{1}{2}\sum_{ab}(\gamma_{ab}^*\dot{\varphi}_b^*\Psi_{a\nu} + \gamma_{ab}\dot{\varphi}_b\Psi_{a\nu}^*). \quad (34)$$

We note that the given quantities are nonzero under stationary conditions $\dot{\varphi}=0$ in the case when the kinetic energy contains terms linear in $\dot{\varphi}$. This occurs if the order parameter is complex. In the case of many-particle systems with complex order parameters the integrals of motion which are nonzero in stationary equilibrium states substantially determine the stability of the current states in such systems.

For a kinetic energy density (33) the density of the energy integral (24) has the form

$$\vartheta = \frac{1}{2}\sum_{ab}\gamma_{ab}\dot{\varphi}_a^*\dot{\varphi}_b + \omega(\varphi,\varphi^*,\nabla\varphi,\nabla\varphi^*) \quad (35)$$

and does not contain terms linear in the time derivatives of the order parameter. Defining the canonical momenta

$$p_a = \frac{\partial\Lambda}{\partial\dot{\varphi}_a^*} = -i\beta_a\varphi_a + \frac{1}{2}\sum_b \gamma_{ab}\dot{\varphi}_b \quad (36)$$

and changing from velocities to momenta in Eq. (35), we obtain the Hamiltonian

$$\mathcal{H} = -2i\sum_{ab}\beta_b\gamma_{ab}^{-1}(p_a^*\varphi_b - p_a\varphi_b^*) + 2\sum_{ab}\gamma_{ab}^{-1}(p_a p_b^* + \beta_a\beta_b\varphi_a\varphi_b^*) + \omega(\varphi,\varphi^*,\nabla\varphi,\nabla\varphi^*), \quad (37)$$

where γ^{-1} is the inverse matrix of γ. We note that the Hamiltonian contains terms linear in the momenta. By substituting (37) into the canonical equations

$$\dot{\varphi}_a = \frac{\partial\mathcal{H}}{\partial p_a^*},\quad \dot{p}_a = -\frac{\partial\mathcal{H}}{\partial\varphi_a^*} + \nabla\frac{\partial\mathcal{H}}{\partial\nabla\varphi_a^*}, \quad (38)$$

we obtain the dynamical equations for the order parameter in Hamiltonian form.

6. SPATIAL SYMMETRIES

Let us consider the consequences that flow from the symmetry of the system with respect to spatial translations and rotations. We assume that the thermodynamic potential of the system is not affected by a translation of the system by a vector $\mathbf{r}_0$: $\varphi'(\mathbf{r}) = \varphi(\mathbf{r}+\mathbf{r}_0)$. Then the matrix of the transformation (7) and the quantities (10) and (13) have the form

$$T_{ab}(\mathbf{r},\mathbf{r}',\mathbf{r}_0) = \delta_{ab}\delta(\mathbf{r}'-\mathbf{r}-\mathbf{r}_0),\quad \Theta_{ab}^\nu(\mathbf{r},\mathbf{r}') = \delta_{ab}\nabla_\nu\delta(\mathbf{r}'-\mathbf{r}),\ \Psi_{a\nu}(\mathbf{r}) = \nabla_\nu\varphi_a(\mathbf{r}). \quad (39)$$

The momentum flux density due to the existence of the order-parameter field is described by the tensor

$$j_{\nu i}^{(I)} = \sum_a\left[\frac{\partial\omega}{\partial\nabla_i\varphi_a}\nabla_\nu\varphi_a + \text{c.c.}\right], \quad (40)$$

and the momentum density has the form

$$\pi_\nu^{(I)} = \sum_a\left[\frac{\partial\kappa}{\partial\dot{\varphi}_a}\nabla_\nu\varphi_a + \text{c.c.}\right]. \quad (41)$$

If the kinetic energy is chosen in the form (33), then

$$\pi_\nu^{(I)} = -i\sum_a\beta_a(\varphi_a^*\nabla_\nu\varphi_a - \varphi_a\nabla_\nu\varphi_a^*) + \frac{1}{2}\sum_{ab}(\gamma_{ab}^*\dot{\varphi}_b^*\nabla_\nu\varphi_a + \gamma_{ab}\dot{\varphi}_b\nabla_\nu\varphi_a^*). \quad (42)$$

We note that for complex fields the momentum density is nonzero even in stationary states $\dot{\varphi}=0$—in particular, under conditions of thermodynamic equilibrium.

If the system is invariant with respect to rotations in coordinate space $\varphi'(\mathbf{r}) = \varphi(g^{-1}\mathbf{r})$, with $(g^{-1}\mathbf{r})_i = \Sigma_j R_{ji}(g)x_j$, where $R_{ji}(g)$, the matrix of three-dimensional rotations g, is specified by a set of three parameters, e.g., the Euler angles, then the angular momentum associated with the order-parameter field is conserved. However, in the case when the rotations do not affect the components of the order parameter, i.e., they do not get mixed, the momentum conservation law is not independent but is a consequence of momentum conservation. The angular momentum flux density and angular momentum density are expressed in terms of the momentum flux density (40) and momentum density (41):

$$j_{\nu i}^{(L)} = \sum_{m,\mu}\varepsilon_{\nu m\mu}x_m j_{\mu i}^{(I)},\ \pi_\nu^{(L)} = \sum_{m,\mu}\varepsilon_{\nu m\mu}x_m\pi_\mu^{(I)}, \quad (43)$$

where $\varepsilon_{\nu m\mu}$ is an antisymmetric tensor. If the thermodynamic potential of the system is invariant with respect to simultaneous rotations in coordinate space and in the space of order-parameter components, then a nontrivial conservation law arises in relation to rotation. This case is considered in the next Section.

7. INTERNAL SYMMETRIES

In the previous Section we considered transformations affecting only the spatial coordinates of the order parameter components. We now consider transformations with the matrix form

$$T_{ab}(\mathbf{r},\mathbf{r}';\lambda) = T_{ab}(\lambda)\,\delta(\mathbf{r}-\mathbf{r}'), \quad (44)$$

which do not affect the spatial coordinates. Following the terminology adopted in field theory,[10] we call the symmetries associated with such transformations "internal." For infinitesimal transformations we can write

$$T_{ab}(\lambda) = \delta_{ab} + \sum_{\nu=1}^{s}\Theta_{ab}^\nu\lambda_\nu,\quad \Theta_{ab}^\nu = \left.\frac{\partial T_{ab}(\lambda)}{\partial\lambda_\nu}\right|_{\lambda=0}, \quad (45)$$

and, according to condition (11),

$$\Theta_{ab}^\nu + \Theta_{ba}^{\nu*} = 0. \quad (46)$$

The flux density due to the symmetry transformation (44) has the form

$$j_{\nu i}^{(M)} = \sum_{ab}\left[\frac{\partial\omega}{\partial\nabla_i\varphi_a}\varphi_b - \frac{\partial\omega}{\partial\nabla_i\varphi_b^*}\varphi_a^*\right]\Theta_{ab}^\nu, \quad (47)$$

and the density of the corresponding conserved quantity is

$$\pi_\nu^{(M)}=\sum_{ab}\left(\frac{\partial\kappa}{\partial\dot\varphi_a}\varphi_b-\frac{\partial\kappa}{\partial\dot\varphi_b^*}\varphi_a^*\right)\Theta_{ab}^\nu. \tag{48}$$

If the kinetic energy is chosen in the form (33), then

$$\pi_\nu^{(M)}=-\sum_{ab}(\beta_a+\beta_b)\varphi_a^*\varphi_b\Theta_{ab}^\nu + \frac{1}{2}\sum_{abc}(\gamma_{ac}^*\dot\varphi_c\varphi_b-\gamma_{bc}\dot\varphi_c\varphi_a^*)\Theta_{ab}^\nu. \tag{49}$$

An example of a system which is invariant with respect to internal symmetry transformations is a ferromagnet, the thermodynamic potential of which contains an exchange energy ω_e. In the case of cubic symmetry, the exchange energy density has the form[18]

$$\omega_e=\frac{1}{2}\alpha\sum_{i=1}^{3}\frac{\partial\mathbf{M}}{\partial x_i}\frac{\partial\mathbf{M}}{\partial x_i}, \tag{50}$$

where α is a phenomenological constant, and $\mathbf{M}$ is the magnetic moment density. In this case the components of the order parameter are the projections of the vector $\mathbf{M}$. Expression (50) is obviously invariant with respect to rotations of the magnetic moment density through an arbitrary angle $\theta=\theta\mathbf{n}$:

$$M_a'(\mathbf{r})=\sum_{b=1}^{3}R_{ab}(\theta)M_b(\mathbf{r}), \tag{51}$$

where $R_{ab}(\theta)$ is an orthogonal rotation matrix, and $\mathbf{n}$ is a unit vector specifying the direction of the axis of rotation. In this case $\Theta_{ab}^\nu=-\varepsilon_{\nu ab}$, and the flux density has the well-known form[19]

$$j_{\nu i}^{(M)}=\alpha[\mathbf{M}\times\nabla_i\mathbf{M}]_\nu. \tag{52}$$

In a thermodynamic equilibrium state the flux density (52) is nonzero, e.g., in regions near domain walls. The dynamical equations for the magnetization in a ferromagnet[18,19] can be obtained in a Lagrangian approach if the angle variables specifying the orientation of the magnetization vector are chosen as the generalized coordinates.

It can happen that the thermodynamic potential is altered by some spatial and internal transformations separately but remains invariant under the combined transformations. Suppose that the spatial coordinates transform according to the rule

$$x_i'=\sum_k a_{ik}(\lambda)x_k,\quad\text{where}\quad\sum_i a_{ik}(\lambda)a_{il}(\lambda)=\delta_{kl}, \tag{53}$$

and that there is a simultaneous rotation, specified by the same set of parameters λ, in the space of order-parameter components, so that

$$T_{ab}(\mathbf{r},\mathbf{r}';\lambda)=T_{ab}(\lambda)\,\delta\left(x_i'-\sum_k a_{ik}(\lambda)x_k\right). \tag{54}$$

In this case

$$\Psi_{a\nu}(\mathbf{r})=\sum_{i,k}\theta_{ik}^\nu x_k\nabla_i\varphi_a(\mathbf{r})+\sum_b\Theta_{ab}^\nu\varphi_b(\mathbf{r}), \tag{55}$$

where

$$\theta_{ik}^\nu=\left.\frac{\partial a_{ik}(\lambda)}{\partial\lambda_\nu}\right|_{\lambda=0},\quad \Theta_{ab}^\nu=\left.\frac{\partial T_{ab}(\lambda)}{\partial\lambda_\nu}\right|_{\lambda=0}.$$

The continuity equation (17) is then valid for the total densities

$$j_{\nu i}=j_{\nu i}^{(L)}+j_{\nu i}^{(M)},\quad \pi_\nu=\pi_\nu^{(L)}+\pi_\nu^{(M)},$$

where $j_{\nu i}^{(M)}$ and $\pi_\nu^{(M)}$ are given by formulas (47)–(49) and describe the contribution to the total angular momentum in consequence of the multicomponent nature of the order parameter; this contribution is an analog of the spin moment in quantum field theory.[10] The orbital angular momentum density and flux density are given by the expressions

$$j_{\nu i}^{(L)}=\frac{1}{2}\sum_a\sum_{ik}\left[\frac{\partial\omega}{\partial\nabla_i\varphi_a}(\nabla_l\varphi_a x_k-\nabla_k\varphi_a x_l)+\text{c.c.}\right]\theta_{kl}^\nu, \tag{56}$$

$$\pi_\nu^{(L)}=\frac{1}{2}\sum_a\sum_{ik}\left[\frac{\partial\kappa}{\partial\dot\varphi_a}(x_k\nabla_i\varphi_a-x_i\nabla_k\varphi_a)+\text{c.c.}\right]\theta_{ik}^\nu. \tag{57}$$

With the kinetic energy chosen in the form (33), we have

$$\pi_\nu^{(L)}=-\frac{i}{2}\sum_a\sum_{ik}[\beta_a\varphi_a^*(x_k\nabla_i\varphi_a-x_i\nabla_k\varphi_a)-\text{c.c.}]\theta_{ik}^\nu + \frac{1}{4}\sum_{ab}\sum_{ik}[\gamma_{ab}^*\dot\varphi_b^*(x_k\nabla_i\varphi_a-x_i\nabla_k\varphi_a)+\text{c.c.}]\theta_{ik}^\nu. \tag{58}$$

The conservation of total angular momentum in the case discussed is a new independent conservation law.

8. PHASE SYMMETRY

An important type of internal symmetry is symmetry with respect to phase transformations with a constant value of the phase (phase transformations of the first kind). This symmetry does not have such a clear interpretation as does symmetry with respect to translations and rotations, for example. The existence of phase symmetry is due to the quantum nature of the structure of the substance. In quantum field theory, phase symmetry is associated with charge conservation.[10] In the nonrelativistic quantum theory of many particles one considers electrically neutral systems consisting of neutral particles or of particles with charges of different sign, so that it is assumed *a priori* that charge conservation holds. Here the breaking of the phase symmetry of a state entails the possibility of existence of superfluid flows, i.e., flows of charge in superconductors and superfluid mass flows in liquid helium.

In the case of phase transformations $\varphi\to\varphi'=\varphi e^{i\chi}$ we obtain

$$T_{ab}(\mathbf{r},\mathbf{r}';\chi)=\delta_{ab}e^{i\chi}\delta(\mathbf{r}-\mathbf{r}'),\quad \Theta_{ab}=i\,\delta_{ab}. \tag{59}$$

We note that for spatially nonuniform states the complex nature of the field is essential, and the field cannot be made real by means of a phase transformation of the first kind. The general formulas (47) and (48) taken together with (59) imply the following expressions for the flux density and the density of the conserved quantity associated with phase symmetry:

$$\mathbf{j}^{(\chi)}=i\sum_a\left(\frac{\partial\omega}{\partial\nabla\varphi_a}\varphi_a-\frac{\partial\omega}{\partial\nabla\varphi_a^*}\varphi_a^*\right), \tag{60}$$

$$\pi^{(\chi)}=i\sum_a\left(\frac{\partial\kappa}{\partial\dot\varphi_a}\varphi_a-\frac{\partial\kappa}{\partial\dot\varphi_a^*}\varphi_a^*\right). \tag{61}$$

If the kinetic energy is chosen in the form (33), then the phase symmetry is associated with the integral of motion

$$\pi^{(\chi)}=2\sum_a\beta_a|\varphi_a|^2+\frac{i}{2}\sum_{ab}(\gamma_{ab}^*\dot\varphi_b^*\varphi_a-\gamma_{ab}\dot\varphi_b\varphi_a^*). \tag{62}$$

We note that for the Schrödinger equation in quantum mechanics the density of the conserved quantity associated with the phase symmetry of the Lagrangian and Hamiltonian has the meaning of a probability density, and the integral of motion is the total probability.

When the components of the complex order parameter are written in term of the modulus and phase,

$$\varphi_a=\eta_a e^{i\xi_a},$$

formula (62) takes the form

$$\pi^{(\chi)}=2\sum_a\beta_a\eta_a^2+\frac{1}{2}\sum_{ab}\{(\gamma_{ab}^*+\gamma_{ab})\eta_a\times[\eta_b\dot\xi_b\cos(\xi_a-\xi_b)-\dot\eta_b\sin(\xi_a-\xi_b)]+i(\gamma_{ab}^*-\gamma_{ab})\times\eta_a[\dot\eta_b\cos(\xi_a-\xi_b)+\eta_b\dot\xi_b\sin(\xi_a-\xi_b)]\}. \tag{63}$$

We see that the density of the conserved quantity (63), like any other observable quantity, depends only on the phase difference or the derivatives of the phases, since observable quantities are invariant with respect to the phase transformations (29).

For systems with broken phase symmetry Eqs. (4) have the spatially nonuniform solutions

$$\varphi_a(\mathbf{r})=\eta_a e^{i\mathbf{q}\cdot\mathbf{r}}, \tag{64}$$

where the modulus η_a is independent of the coordinates, and $\mathbf{q}$ is a constant vector. Substitution of the function (64) into Eq. (4) will lead to a system of L nonlinear algebraic equations, which determine the moduli of the order-parameter components as functions of the quantity q. This system has solutions of the form (64) at sufficiently small values of q. At values of q exceeding a certain critical value q_c, solutions of the form (64) do not exist. It is easy to see that the total momentum is conserved in states described by solutions (64). The possibility of conserving momentum in spatially nonuniform states is an important feature of systems with a complex order parameter. Indeed, if the system as a whole is translated by an arbitrary vector $\mathbf{r}_0$, then the function (64) is multiplied by an exponential factor with a constant phase,

$$\varphi_a(\mathbf{r}+\mathbf{r}_0)+\varphi_a(\mathbf{r})e^{i\mathbf{q}\cdot\mathbf{r}_0},$$

and, by virtue of the phase invariance of the thermodynamic potential, this does not lead to any change in it. According to the results of Sec. 6, solution (64) describes a state of the system with conserved total momentum, with a density determined by the formula

$$\pi^{(I)}=2\mathbf{q}\sum_a\beta_a\eta_a^2. \tag{65}$$

We note that the state (64) is equivalent to that determined in the microscopic approach,[20]—a spatially uniform, translationally noninvariant state of a superfluid system with nonzero total momentum.

Up till now we have not specified the form of the dependence of the thermodynamic potential on the order parameter and its derivatives. To write an explicit expression for the fluxes, we must specify the dependence of the thermodynamic potential on the gradients. We restrict consideration of the thermodynamic potential to terms quadratic in the gradients, choosing it in the form

$$\omega_g=\frac{1}{2}\sum_{ab}\sum_{ik}c_{ab}^{ik}\nabla_i\varphi_a^*\nabla_k\varphi_b, \tag{66}$$

where $c_{ab}^{ik}=c_{ba}^{ki*}$. Then the momentum flux density becomes

$$j_{ki}^{(I)}=\frac{1}{2}\sum_{ab;l}(c_{ab}^{il*}\nabla_l\varphi_b^*\nabla_k\varphi_a+c_{ab}^{il}\nabla_l\varphi_b\nabla_k\varphi_a^*)=\frac{1}{2}q_k\sum_{ab;l}(c_{ab}^{il*}+c_{ab}^{il})\eta_a\eta_b q_l. \tag{67}$$

For the state under consideration, the density of the conserved quantity and its flux density (60), (61), which follow from the condition of phase invariance, are

$$\pi^{(\chi)}=2\sum_a\beta_a\eta_a^2,\quad j_i^{(\chi)}=\frac{1}{2}\sum_{ab;l}(c_{ab}^{il*}+c_{ab}^{il})\eta_a\eta_b q_l. \tag{68}$$

We see that the quantity in (68) is related to the density and the momentum flux density by the relations

$$\pi_i^{(I)}=q_i\pi^{(\chi)},\quad j_{ki}^{(I)}=q_k j_i^{(\chi)}, \tag{69}$$

so that in the given state with a constant flux density the conservation laws that follow from the translational and phase invariance of the thermodynamic potential actually have identical consequences. This is true only in the case (64). One could, as is customary, define the superfluid velocity $\mathbf{v}_s$ and density ρ_s:

$$\mathbf{v}\propto\mathbf{q},\quad \rho_s\propto\sum_a\beta_a\eta_a^2,$$

after having substituted the momentum density in the form $\boldsymbol{\pi}^{(I)}=\rho_s\mathbf{v}_s$. The conservation law for $\boldsymbol{\pi}^{(\chi)}$ thus acquires the meaning of conservation of the superfluid mass (at constant T and μ). We note that in this approach for describing the dynamics of a system with a single complex order parameter one can obtain an equation, analogous to the Gross–Pitaevskiĭ equation,[19] describing the dynamics of a slightly nonideal Bose gas.

9. NONCONSERVED FLOWS

Up till now we have been considering flows in systems whose thermodynamic potential is invariant with respect to the continuous transformations (7). For such flows, which are naturally called conserved, the divergence is equal to zero in the stationary state and obeys the continuity equation (17) in the nonstationary state. In the case when the thermo-

dynamic potential is not invariant, it is natural to retain the definitions of the flux densities. However, in this latter case the divergence of these flux densities is nonzero, and in place of (15) we obtain

$$\operatorname{div}\mathbf{j}_\nu=\sigma_\nu, \tag{70}$$

where the function σ_ν has the meaning of a source density. Integrating (70) over the volume, we find that the total production of the physical quantities transported by the flux density $\mathbf{j}_\nu$ is equal to the total flux through the boundary of the volume under consideration. If the total flux through the boundary is equal to zero, then the total amount of the physical quantity produced is also zero, although the source of this quantity may be locally nonzero.

Under nonstationary conditions with a noninvariant thermodynamic potential the conservation equation has the form

$$\frac{\partial\pi_\nu}{\partial t}+\operatorname{div}\mathbf{j}_\nu=\sigma_\nu, \tag{71}$$

where $\mathbf{j}_\nu$ and π_ν are given by formulas (16) and (22). In this case the quantities Π_ν (19) are no longer integrals of motion, even in the case when the total flux through the boundary is zero.

An example of a system in which nonconserved nondissipative flows exist is a ferromagnet with domain walls. The thermodynamic potential ω_f of a ferromagnet includes, in addition to the exchange energy (50), which is invariant with respect to rotation of the magnetic moment (51), an anisotropy energy that breaks this invariance:

$$\omega_a=\frac{\beta}{2}[M^2-(\mathbf{M}\cdot\mathbf{n})^2], \tag{72}$$

where $\mathbf{n}$ is the axis of anisotropy and β is the anisotropy constant. In this case the flux density of the magnetization is, as before, given by formula (52), and the source density is given by the formula

$$\sigma_\nu^{(M)}=\beta(\mathbf{n}\cdot\mathbf{M})[\mathbf{n}\times\mathbf{M}]_\nu. \tag{73}$$

Associated with the magnetization field are the momentum flux density and source density

$$j_{\nu i}^{(I)}=\alpha\nabla_i\mathbf{M}\cdot\nabla_\nu\mathbf{M}, \quad \boldsymbol{\sigma}^{(I)}=\nabla\omega_f \tag{74}$$

and the orbital angular momentum flux density and source density

$$j_{\nu i}^{(L)}=\alpha\sum_a[\mathbf{r}\times\nabla M_a]_\nu\nabla_i M_a, \quad \boldsymbol{\sigma}^{(L)}=[\mathbf{r}\times\boldsymbol{\sigma}^{(I)}]. \tag{75}$$

Near a Bloch domain wall[21] lying in the yz plane one has

$$M_x=0, \quad M_y=M\sin\vartheta, \quad M_z=M\cos\vartheta,$$

and the angle ϑ specifying the orientation of the magnetization, which is assumed to have a constant magnitude, satisfies the equation

$$\nabla_x^2\vartheta-\frac{\beta}{\alpha}\sin\vartheta\cos\vartheta=0. \tag{76}$$

The localized solution of this equation has the form

$$\cos\vartheta=-\tanh\sqrt{\frac{\beta}{\alpha}}x. \tag{77}$$

In this case the magnetization flux density and source density have the following nonzero components:

$$j_{xx}^{(M)}=-\alpha M^2\nabla_x\vartheta, \quad \sigma_x^{(M)}=-\beta M^2\sin\vartheta\cos\vartheta. \tag{78}$$

We see that Eq. (76) follows from the continuity equation (70) for the magnetization. The nonzero momentum flux density and source density have the form

$$j_{xx}^{(I)}=\alpha M^2(\nabla_x\vartheta)^2, \quad \sigma_x^{(I)}=\beta M^2\nabla_x(\sin^2\vartheta). \tag{79}$$

The continuity equation for the momentum gives a first integral of equation (76). Let us also give the nonzero orbital angular momentum flux density and source density:

$$j_{yx}^{(L)}=\alpha zM^2(\nabla_x\vartheta)^2, \quad j_{zx}^{(L)}=-\alpha yM^2(\nabla_x\vartheta)^2,$$
$$\sigma_y^{(L)}=\beta zM^2\nabla_x(\sin^2\vartheta), \quad \sigma_z^{(L)}=-\beta_y M^2\nabla_x(\sin^2\vartheta). \tag{80}$$

Thus, near a domain wall there are localized flows which, by virtue of the equilibrium character of the state, are not accompanied by energy dissipation. However, unlike the flows generated by a phase transformation, these flows are not associated with integrals of motion. Such states can be stable only in the case when they correspond to an absolute minimum of the thermodynamic potential.

10. CONCLUSION

It follows from the above discussion that the appearance of nondissipative flows in many-particle systems is due to extremely general causes which are largely independent of the details of their internal structure. One can identify several conditions that must hold for the existence of flows without energy dissipation. First, the system must be found in a state whose symmetry is broken, so that, besides the usual thermodynamic variables, the state will be characterized by some additional variables—order parameters. Second, this state must be spatially nonuniform, i.e., the components of the order parameters must be functions of the spatial coordinates. In that case the system is described by a set of real or complex fields. Third, the complete absence of dissipation is realized only in the case when the system is found in a stationary thermodynamic equilibrium state, corresponding to a local or absolute minimum of the thermodynamic potential. It was shown that then, as in field theory,[10] corresponding to each continuous transformation of the order parameter that preserves the value of the thermodynamic potential there are a conserved flux density and an integral of motion. Flows without dissipation can also exist in the case when the state of the system is spatially nonuniform but its thermodynamic potential is noninvariant with respect to symmetry transformations. In that case the flow generated by the given symmetry will not be an integral of motion.

An additional energy is associated with the spatial nonuniformity of the order parameter, and therefore such a state can be stable only under certain conditions. As we have said, it is stable if an absolute minimum of the thermodynamic potential is realized, i.e., if the increase in energy due to the nonuniformity is compensated by a lowering of the other contributions to the total energy of the system. An example of such a system is a ferromagnet with a domain structure. If the deformed state corresponds to a local and not an absolute minimum of the thermodynamic potential, then the state is

metastable, and its lifetime is determined by the size of the potential barrier separating it from another state with a lower value of the thermodynamic potential. Finally, the deformed state of the system may not correspond to an absolute minimum of the thermodynamic potential but be associated with some conservation law that prevents the system from spontaneously passing to a state with a lower value of the thermodynamic potential. In the latter case the state corresponding to a local minimum of the thermodynamic potential will be just as stable as a state corresponding to the absolute minimum of the thermodynamic potential. This is apparently the situation in systems ordinarily called superconducting and superfluid. An important feature of these systems is that their order-parameter field is complex, and consequently the phase invariance of the state is broken in this case. Since the phase of a complex order parameter is not an observable quantity (only a phase difference or phase gradient can be observed), all of the observable quantities and, in particular, the thermodynamic potential are independent of the phase and are invariant with respect to phase transformations. Thus the phase symmetry of the thermodynamic potential is exact, unlike the symmetries associated with translations and rotations, and it cannot be broken by any interactions. Since the phase symmetry is exact, a conserved flux and an integral of motion are always associated with it. Yet another feature of complex fields, the importance of which, in our view, has not received the attention it deserves, is that the kinetic energy of such fields contains a contribution linear in the time derivatives of the order parameters. For this reason a system with broken phase symmetry has a nonzero integral of motion in the stationary state. The presence of such an integral of motion prevents the system from spontaneously passing to a state with a lower value of the thermodynamic potential. Because of this property, in systems with broken phase symmetry the current states, although they do not correspond to the absolute minimum of the thermodynamic potential, are extremely stable. For example, a superconducting ring carrying an induced current was held for over two and a half years at a temperature below T_c with no detectable decrease in current.[1] Under strictly fixed external conditions the current states (except, perhaps, for low-dimensional systems) would have an infinite lifetime. Unavoidable fluctuations of the external parameters, primarily the temperature, will bring the system out of the equilibrium state, and any deviations from thermodynamic equilibrium and nonstationary processes present in the system will lead to energy dissipation and damping of the flow.

In this paper we have not dealt with the problem of critical currents. In this connection we note that the equations for the order parameters have stationary solutions at sufficiently low fluxes. For fluxes exceeding a certain critical value there are no stationary solutions, and the system can be found only in a nonstationary state, which is accompanied by energy dissipation. The stationarity can be broken at even lower values of the fluxes in the case when the stationary flow loses stability. Despite the analogy in the theoretical description of superfluid ^{4}He and superconductors,[6,7] it should be emphasized that there is a substantial difference in the behavior of these objects under unsteady conditions. For a slight nonstationarity the dissipative effects in superfluid ^{4}He are small, and its superfluid properties are well manifested even under slightly nonequilibrium conditions. For superconductors the dynamical equation has a diffusional form,[22] and nonstationary processes can lead to strong energy dissipation and rapid destruction of the superconducting properties.

Nonconserved nondissipative flows, since no conservation laws are associated with them, can exist stably only in states corresponding to the absolute minimum of the thermodynamic potential. Therein lies the essential difference between nondissipative flows in ferromagnets[5] or liquid crystals, for example, where the symmetry, as a rule, is approximate, and in superconductors and superfluids, where an exact phase symmetry is broken.

The existence of a complex order-parameter field, dependent on the coordinates, is sufficient for explaining why nondissipative flows appear. However, within a phenomenological approach it is impossible to determine the structure of the order parameter or the nature of the onset of a complex field. The answers to these questions must be given by a microscopic theory of systems with broken symmetries. On the microscopic level the nature of the appearance of a complex field in superconductors was explained by Gor'kov,[23] who associated the order parameter of Ginzburg–Landau theory with a pair-type anomalous average (pair correlation). The appearance of pair correlations also leads to a change in the spectrum of quasiparticle excitations in superconductors. As a rule, an energy gap appears in the spectrum, and this is often perceived to be a hallmak of supercondtivity. Meanwhile, it is well known that in superconductors containing paramagnetic impurities, the energy gap vanishes at a certain impurity concentration.[22] However, this does not lead to vanishing of the superconducting properties, since the phase symmetry of the system remains broken on account of the complex order parameter, which remains nonzero. In certain directions in momentum space the energy gap also vanishes in the A phase of superfluid ^{3}He.[24] These examples and also the foregoing treatment show that the presence of a gap in the spectrum of excitations, although it affects many properties of the superconductor, has no relation to the existence of flows unaccompanied by dissipation, i.e., to the phenomenon of superfluidity itself.

Landau also linked the property of superfluidity in liquid ^{4}He to the form of the quasiparticle energy gap. According to Landau, the phenomenon of superfluidity can occur if the famous criterion which he introduced is met.[9,19] Sixty years after publication of Landau's paper,[9] which played a key role in the development of the theory of superfluidity, many new experimental data on the structure of liquid ^{4}He have been obtained, and new theoretical ideas have been developed. Studies of the spectrum of excitations in ^{4}He by the method of inelastic neutron scattering show that its form is not fundamentally altered at the transition from the superfluid to the normal phase,[25] and, consequently, the Landau criterion is met even in the normal phase. The Landau criterion is also met for the spectra of excitations in other nonsuperfluid liquids. It seems natural to conclude that, as in the case of superconductors, the superfluid properties of a system of bosons are not related to the form of the spectrum of elementary excitations or, for that matter, excitations of other types.

As to the Landau theory of superfluidity,[9] its success in describing superfluid properties is due, as we have said, to the introduction of a superfluid velocity and density for taking into account the breaking of the phase symmetry. The role of the Landau criterion was investigated by Volovik[22] in an analysis of the superfluid properties of the A phase of ^{3}He, and it was concluded that exceeding the Landau velocity is not crucial for the existence of a nondissipative flow of the superfluid component. An explanation of superfluidity in ^{4}He as being a consequence of the breaking of phase symmetry was given in the paper by Ginzburg and Pitaevskiĭ.[7] The restricted domain of applicability of that theory, even in its modified form,[8] is due to the use of an expansion of the thermodynamic potential near T_λ in powers of the modulus of the order parameter. However, the main idea of that paper—to describe the superfluid properties through the introduction of a complex order parameter—is undoubtedly correct not only near the temperature of the λ transition but also in the entire existence region of the superfluid phase.

Let us make a few remarks about the microscopic nature of the complex field in a superfluid boson system. The phase symmetry at the microscopic level can be broken as a result of the appearance of single-particle anomalous quasiaverages $\langle a_{\mathbf{k}}\rangle$ and $\langle a_{\mathbf{k}}^+\rangle$, where $a_{\mathbf{k}}$ and $a_{\mathbf{k}}^+$ are the annihilation and creation operators for Bose particles with momentum $\mathbf{k}$. In a spatially uniform case such quasiaverages exist only for $\mathbf{k}=0$, but under spatially nonuniform conditions they are nonzero even for $\mathbf{k}\neq 0$. It follows from a microscopic treatment[26] that in a system of bosons there always exist pair anomalous quasiaverages $\langle a_{\mathbf{k}}a_{\mathbf{k}'}\rangle$, $\langle a_{\mathbf{k}}^+ a_{\mathbf{k}'}^+\rangle$ in addition to the single-particle anomalous quasiaverages. In the self-consistent-field approximation,[26] anomalous averages of a large number of particles are expressed in terms of single-particle and pair anomalous averages. In a more exact approximation this is not so, and there are independent correlations of more than two particles. Thus, in a Bose system with predominant repulsion between particles, as is probably the case in ^{4}He, there should exist at least two complex fields associated with the single-particle and pair anomalous averages, i.e., the order parameter should be two-component. The model of superfluid Bose systems with two condensates was investigated in Ref. 27. In the case when the interaction between particles in the Bose system has a predominantly attractive character, single-particle anomalous averages cannot exist, and the single-component order parameter is formed only by pair anomalous averages.[28]

As we have seen, breaking of symmetry and spatial nonuniformity of the order parameter in a state of thermodynamic equilibrium are sufficient conditions for the existence of nondissipative flows. It is of interest to answer the question: are these conditions necessary, or are there other possible mechanisms of creation of nondissipative flows? There is no proof of their necessity. Alternative versions can be expected in low-dimensional systems, for example. The author is inclined to assume that symmetry breaking should take place in all cases in which nondissipative flows arise and thus is also a necessary condition for the existence of nondissipative flows.

The author thanks S. V. Peletminskiĭ for a discussion of this study.

*E-mail: antarasov@kipt.kharkov.ua

[1] E. A. Lynton, *Superconductivity*, 4th ed., Chapman and Hall, London (1971), Mir, Moscow (1974).
[2] P. L. Kapitsa, Nature (London) **141**, 74 (1938).
[3] D. D. Osheroff, R. C. Richardson, and D. M. Lee, Phys. Rev. Lett. **28**, 885 (1972).
[4] J. G. Bednorz and K. A. Müller, Z. Phys. B: Condens. Matter **64**, 189 (1986).
[5] É. B. Sonin, Usp. Fiz. Nauk **137**, 267 (1982) [Sov. Phys. Usp. **25**, 409 (1982)].
[6] V. L. Ginzburg and L. D. Landau, Zh. Éksp. Teor. Fiz. **20**, 1064 (1950).
[7] V. L. Ginzburg and L. P. Pitaevskiĭ, Zh. Éksp. Teor. Fiz. **34**, 1240 (1958) [Sov. Phys. JETP **7**, 858 (1958)].
[8] V. L. Ginzburg and A. A. Sobyanin, Usp. Fiz. Nauk **120**, 153 (1976) [Sov. Phys. Usp. **19**, 773 (1976)].
[9] L. D. Landau, Zh. Éksp. Teor. Fiz. **11**, 592 (1941).
[10] N. N. Bogoliubov and D. V. Shirkov, *Introduction to the Theory of Quantized Fields*, 3rd ed., Wiley, New York (1980), Nauka, Moscow (1973).
[11] L. D. Landau, Zh. Éksp. Teor. Fiz. **7**, 19 (1937).
[12] L. D. Landau and E. M. Lifshitz, *Statistical Physics*, 2nd ed., Pergamon Press, Oxford (1969), Nauka, Moscow (1964).
[13] Yu. M. Poluéktov and V. V. Krasil'nikov, Fiz. Nizk. Temp. **15**, 1251 (1989) [Sov. J. Low Temp. Phys. **15**, 691 (1989)].
[14] H. Goldstein, *Classical Mechanics*, Addison-Wesley, Cambridge, Mass. (1950), Nauka, Moscow (1975).
[15] S. V. Peletminskiĭ and A. I. Sokolovskiĭ, Teor. Mat. Fiz. **18**, 121 (1974).
[16] A. I. Akhiezer and S. V. Peletminskiĭ, *Methods of Statistical Physics*, Pergamon Press, Oxford (1981), Nauka, Moscow (1977).
[17] Yu. M. Poluéktov and V. V. Slezov, "Forces and energy dissipation in disordered nonequilibrium superconductors" [in Russian], KhFTI Preprint 87-44, Kharkov Physicotechnical Institute, Kharkov (1987).
[18] A. I. Akhiezer, V. G. Bar'yakhtar, and S. V. Peletminskii, *Spin Waves*, North-Holland, Amsterdam (1968), Nauka, Moscow (1967).
[19] L. D. Landau and E. M. Lifshitz, *Statistical Physics*, 3rd ed. (with L. P. Pitaevskiĭ), Vol. 2, Pergamon Press, Oxford (1980), Nauka, Moscow (1978).
[20] N. N. Bogolyubov Jr., M. Yu. Kovalevskiĭ, S. V. Peletminskiĭ, A. N. Tarasov, and A. M. Kurbatov, Fiz. Élem. Chastits At. Yadra **16**, 875 (1985) [Sov. J. Part. Nucl. **16**, 389 (1985)].
[21] L. D. Landau and E. M. Lifshitz, in *L. D. Landau. Collected Works* [in Russian], Vol. 1, Nauka, Moscow (1969), p. 128.
[22] A. M. Gulyan and G. F. Zharkov, *Superconductivity in External Fields* [in Russian], Nauka, Moscow (1990).
[23] L. P. Gor'kov, Zh. Éksp. Teor. Fiz. **36**, 1918 (1959) [Sov. Phys. JETP **9**, 1364 (1959)].
[24] G. E. Volovik, Usp. Fiz. Nauk **143**, 73 (1984) [Sov. Phys. Usp. **27**, 363 (1984)].
[25] I. V. Bogoyavlenskii, L. V. Karnatsevich, Zh. A. Kozlov, V. G. Kolobrodov, V. B. Priezzhev, A. V. Puchkov, and A. N. Skomorokhov, Fiz. Nizk. Temp. **20**, 626 (1994) [Low Temp. Phys. **20**, 489 (1994)].
[26] Yu. M. Poluektov, Fiz. Nizk. Temp. **28**, 604 (2002) [Low Temp. Phys. **28**, 429 (2002)].
[27] S. I. Shevchenko, Fiz. Nizk. Temp. **11**, 339 (1985) [Sov. J. Low Temp. Phys. **11**, 282 (1985)].
[28] P. S. Kondratenko, Teor. Mat. Fiz. **22**, 278 (1975).

Translated by Steve Torstveit

On the suprathermal distribution in an anisotropic phonon system in He II

I. N. Adamenko* and K. E. Nemchenko

V. N. Karazin Kharkov National University, 4 Svobody Sq., Kharkov 61077, Ukraine

A. F. G. Wyatt

School of Physics, University of Exeter, Exeter EX4 4QL, United Kingdom
(Submitted July 25, 2002; revised September 24, 2002)
Fiz. Nizk. Temp. **29**, 16–21 (January 2003)

The equation that describes the suprathermal distribution of high-energy phonons (*h* phonons) created in anisotropic phonon systems in superfluid helium is obtained. The solution of this equation enables the derivation of the value of suprathermal ratio *S* as the ratio of the actual distribution to the Bose–Einstein one, its dependences on the momentum of the *h* phonons, the anisotropy parameters, and the temperature of the low-energy phonons from which the *h* phonons are created. We analyze this equation to obtain an estimate of the value of the ratio between the *h*-phonon number density in anisotropic and isotropic phonon systems and draw conclusions about the dependence of *S* on the relevant parameters. © *2003 American Institute of Physics.* [DOI: 10.1063/1.1542372]

1. INTRODUCTION

For a phonon system in superfluid ^{4}He (He II) the rates of kinetic processes are determined by the unusual form of the phonon energy-momentum dependence. At zero pressure the phonon dispersion curve in He II bends upwards,[1–3] and this causes spontaneous decay of phonons with energies $\varepsilon < \varepsilon_c = 10$ K.[4,5] For these phonons, the energy and momentum conservation laws allow processes in which the phonon numbers in the initial and final states do not equal one another. The fastest process among these is the three-phonon process $(3pp)$, in which one phonon decays to two phonons or two phonons interact to create one phonon. The rate of these three-phonon processes was obtained in Refs. 6 and 7, in the two extreme limits; and the general case was calculated in Ref. 8.

At higher energies the phonon dispersion curve bends downwards, and at $\varepsilon > \varepsilon_c$ the phonon spectrum becomes nondecaying. Here the most rapid process is the four-phonon process $(4pp)$, in which there are two phonons in the initial and final states.

The rate of three-phonon processes ν_{3pp} is obtained using Landau's Hamiltonian in first-order perturbation theory, and the rate of four-phonon ν_{4pp} processes is determined by second-order perturbation theory.[9–11] This is quantitatively evaluated and confirmed by experiment.[12] The difference between the orders of perturbation theory results in the strong inequality $\nu_{3pp} \gg \nu_{4pp}$. Thus the phonons of superfluid ^{4}He form two subsystems: one of low energy (*l* phonons) with $\varepsilon < \varepsilon_c$, which very quickly attains equilibrium; and the other of high-energy phonons (*h* phonons), which goes to equilibrium relatively slowly.

The angles between the phonons which take part in $3pp$ is small due to the smallness of the deviation of the energy-momentum dispersion from linearity, $\varepsilon = cp$. Thus in isotropic phonon systems, when all directions in momentum space are uniformly occupied, equilibrium is not attained isotropically in the short term because interactions involve only phonons within a limited solid angle. Thus, all thermodynamic parameters of the *l* subsystem become functions of angle.[11] In the long term, four-phonon processes and diffusion in angular space bring about complete equilibrium. This quasidiffusion is determined by fast three-phonon interactions involving small angles.[13–15]

The situation is quite different in highly anisotropic phonon systems. Here the momenta of all phonons are in a narrow cone with solid angle Ω_p, which has a value close to the typical angle for three-phonon processes. Such strongly anisotropic phonon systems have been created in liquid ^{4}He (Refs. 16–20). This pure and isotropic superfluid can have such a low temperature that one can neglect the existence of thermal excitations. Low-energy phonons are injected by a heater and then propagate along the direction normal to the surface of the heater. In momentum space all the phonons lie in a narrow cone of solid angle $\Omega_p = 0.125$ sr.

In such experiments[16–20] the unusual phenomenon of the creation of high-energy phonons was observed. These *h* phonons are created by a pulse of *l* phonons, which has a temperature an order of magnitude less than the energy of the high-energy phonons that it creates. The theory of this unique phenomenon was proposed in Refs. 21 and 22. A further development of the theory[23–28] shows that in strongly anisotropic phonon systems there exists an asymmetry between processes of creation and decay for the *h* phonons. Such an asymmetry causes the distribution function of *h* phonons in the anisotropic phonon system to be *S* times greater than that in the Bose–Einstein distribution. Moreover, it is possible to have $S \gg 1$. Using the notation of Ref. 23, we will call such an unusual distribution of *h* phonons a suprathermal distribution, and the parameter *S*, the suprathermal ratio.

In this paper we derive an exact equation that allows us to calculate the suprathermal ratio and to determine its dependences on momentum, anisotropy parameter, and temperature. We analyze the contribution of all possible pro-

cesses that lead to the formation of suprathermal distributions in anisotropic phonon systems. From this equation we derive an estimate of the average value of the suprathermal ratio S: the ratio of the number density of h phonons in the anisotropic and isotropic phonon systems.

2. THE INEQUALITIES FOR DETERMINING OF THE STATIONARY DISTRIBUTION FUNCTION OF PHONONS IN AN ANISOTROPIC PHONON SYSTEM

The attainment of equilibrium in the subsystem of h phonons can be described by the kinetic equation for the distribution functions, which can be written as

$$\frac{dn_1}{dt}=N_b(\mathbf{p}_1)-N_d(\mathbf{p}_1), \tag{1}$$

where

$$N_b(\mathbf{p}_1)=\int_{\Omega_b} W(\mathbf{p}_1,\mathbf{p}_2|\mathbf{p}_3,\mathbf{p}_4)n_3n_4(1+n_1)(1+n_2) \times\delta(\varepsilon_1+\varepsilon_2-\varepsilon_3-\varepsilon_4)\,\delta(\mathbf{p}_1+\mathbf{p}_2-\mathbf{p}_3-\mathbf{p}_4) \times d^3p_2d^3p_3d^3p_4 \tag{2}$$

is the number of phonons with momentum $\mathbf{p}_1$ created per unit time as the result of four-phonon $(4pp)$ interactions;

$$N_d(\mathbf{p}_1)=\int_{\Omega_d} W(\mathbf{p}_1,\mathbf{p}_2|\mathbf{p}_3,\mathbf{p}_4)n_1n_2(1+n_3)(1+n_4) \times\delta(\varepsilon_1+\varepsilon_2-\varepsilon_3-\varepsilon_4)\,\delta(\mathbf{p}_1+\mathbf{p}_2-\mathbf{p}_3-\mathbf{p}_4) \times d^3p_2d^3p_3d^3p_4 \tag{3}$$

is the number of phonons that decay per unit time; $W(\mathbf{p}_1,\mathbf{p}_2|\mathbf{p}_3,\mathbf{p}_4)=W(\mathbf{p}_3,\mathbf{p}_4|\mathbf{p}_1,\mathbf{p}_2)$ defines the transition probability density for $4pp$ processes, which have been calculated;[25] Ω_b and Ω_d each represent a set of three solid angles, one for each momentum over which the function is integrated, i.e., Ω_{bi} and Ω_{di} $(i=2,3,4)$. These maximum angles are determined by the anisotropy of the phonon system and the angles in the $4pp$ interactions. In the isotropic case $\Omega_{bi}=\Omega_{di}$. In relations (1)–(3) and below we consider $p_1\geqslant p_c=k_B\varepsilon_c/c$ (i.e., phonon "1" is the h_1 phonon), while the other three phonons can be l phonons or h phonons. The stationary distribution function is determined by the equality

$$N_b=N_d. \tag{4}$$

For isotropic phonon systems $\Omega_{bi}=\Omega_{di}$, and equality (4) gives:

$$n_1n_2(1+n_3)(1+n_4)=n_3n_4(1+n_1)(1+n_2). \tag{5}$$

The solution of this equation is the Bose–Einstein distribution

$$n_i^{(0)}=\{\exp(\varepsilon_i/T)-1\}^{-1}. \tag{6}$$

In an anisotropic phonon system, when the initial phonons are inside a narrow cone with solid angle $\Omega_p\leqslant 4\pi$, the result differs from (5) and (6). In this case the limits of integration in (2) and (3) with respect to angular variables are defined by the inequalities

$$\Omega_i\leqslant\Omega_p. \tag{7}$$

Here $i=3,4$ for creation processes, and $i=2$ for decay processes. The angular variables for the final phonons have no such restrictions.

Such asymmetry for the initial and final states results in the inequality $\Omega_b\neq\Omega_d$. In this case in anisotropic phonon systems the equality (4) cannot be satisfied by solution (5), and the Bose-Einstein distribution is not a solution of equation (4).

In highly anisotropic phonon systems, when Ω_p is less than the typical solid angle for four-phonon processes, the stationary distribution of h phonons will be substantially different from the Bose–Einstein distribution (6) in magnitude and in momentum dependence.

The integrals (2) and (3) can be written as a sum of five terms with definite ranges of integration. These terms correspond to the different processes that are possible for the interactions of h phonons between themselves and with l phonons:

$$\begin{aligned}&1)\ h_1+l_2\leftrightarrow l_3+l_4;\quad 2)\ h_1+l_2\leftrightarrow h_3-l_4;\\ &3)\ h_1+l_2\leftrightarrow h_3+h_4;\quad 4)\ h_1+h_2\leftrightarrow h_3+l_4;\\ &5)\ h_1-h_2\leftrightarrow h_3+h_4.\end{aligned} \tag{8}$$

The arrow to the right indicates the decay of an h_1 phonon, and to the left, creation. We define the rates $\nu_{b,d}^{(n)}$ of creation (b) and decay (d) processes with distribution function n for h phonons by the equalities:

$$N_{b\alpha}=n_1^{(0)}\nu_{b\alpha}^{(n)};\ \ N_{d\alpha}=n_1\nu_{d\alpha}^{(n)};\quad (\alpha=1,2,3,4,5). \tag{9}$$

As N_b is the sum over all $N_{b\alpha}$, we rewrite relation (4) as follows:

$$n_1^{(0)}\sum_{\alpha=1}^{5}\nu_{b\alpha}^{(n)}=n_1\sum_{\alpha=1}^{5}\nu_{d\alpha}^{(n)}. \tag{10}$$

We take into account that $3pp$ processes instantaneously establish equilibrium (on the time scale of h-phonon creation and propagation) in the subsystem of l phonons, which occupy the solid angle Ω_{3pp} that is typical for $3pp$. The phonon pulses in experiments[16–20] have Ω_p close to Ω_{3pp}.[13–15] Therefore in this case we can consider that the l phonons in the pulse have a Bose–Einstein distribution:

$$n(\mathbf{p}_1)=n_l^{(0)},\ \text{ at }\ p_l<p_c. \tag{11}$$

For the stationary distribution of h phonons, the distribution function can be written in the form:

$$n(\mathbf{p}_h)=S(\mathbf{p}_h)n_h^{(0)},\ \text{ at }\ p_h>p_c. \tag{12}$$

Starting from equalities (10)–(12), we have

$$\sum_{\alpha=1}^{5}\nu_{b\alpha}^{(n)}=S(\mathbf{p}_1)\sum_{\alpha=1}^{5}\nu_{d\alpha}^{(n)}. \tag{13}$$

This equation is an integral equation with respect to the unknown function $S(\mathbf{p}_1)$. For decay processes when h_1 combines with an l or h phonon, the rate is independent of or a linear functional of S, respectively. For creation processes if initially there are zero, one, or two h phonons then the rate is independent, a linear functional, or a quadratic functional, respectively. Therefore the desired function $S(\mathbf{p}_1)$ is absent in the rates $\nu_{b1}^{(n)}$, $\nu_{d1}^{(n)}$, $\nu_{d2}^{(n)}$, $\nu_{d3}^{(n)}$ if one takes into account

that $1-n_h \approx 1$. The rates $\nu_{b2}^{(n)}$, $\nu_{b4}^{(n)}$, $\nu_{d4}^{(n)}$, $\nu_{d5}^{(n)}$ include linear functionals, and $\nu_{b3}^{(n)}$, $\nu_{b5}^{(n)}$ include quadratic functionals. Using these facts, we present the rates from (9) as

$$\begin{aligned}
&\nu_{b1}^{(n)} = \nu_{b1}^{(0)}; \quad \nu_{d1}^{(n)} = \nu_{d1}^{(0)};\\
&\nu_{d2}^{(n)} = \nu_{d2}^{(0)}; \quad \nu_{d3}^{(n)} = \nu_{d3}^{(0)};\\
&\nu_{b2}^{(n)} = S_{b2}(\mathbf{p}_1)\,\nu_{b2}^{(0)}; \quad \nu_{b4}^{(n)} = S_{b4}(\mathbf{p}_1)\,\nu_{b4}^{(0)};\\
&\nu_{d4}^{(n)} = S_{d4}(\mathbf{p}_1)\,\nu_{d4}^{(0)}; \quad \nu_{d5}^{(n)} = S_{d5}(\mathbf{p}_1)\,\nu_{d5}^{(0)};
\end{aligned} \tag{14}$$

and

$$\nu_{b3}^{(n)} = S_{b3}^2(\mathbf{p}_1)\,\nu_{b3}^{(0)}; \quad \nu_{b5}^{(n)} = S_{b5}^2(\mathbf{p}_1)\,\nu_{b5}^{(0)}; \tag{15}$$

where

$$\nu_{b,d\alpha}^{(0)} = \nu_{b,d\alpha}^{(n_0)}(S=1) \tag{16}$$

are the rates calculated with distribution function (6). The above equations define $S_{b,d\alpha}$, which are functionals of the function $S(\mathbf{p}_h)$.

Using (14)–(16), we can write relation (13) as

$$\begin{aligned}
&\{SS_{d5}\nu_{d5}^{(0)} - S_{d5}^2\nu_{b5}^{(0)}\} + \{SS_{d4}\nu_{d4}^{(0)} - S_{b3}^2\nu_{b3}^{(0)}\}\\
&\quad + \{S\nu_{d3}^{(0)} - S_{b4}\nu_{b4}^{(0)}\} + \{S\nu_{d2}^{(0)} - S_{b2}^2\nu_{b2}^{(0)}\} = \nu_{b1}^{(0)} - S\nu_{d1}^{(0)}.
\end{aligned} \tag{17}$$

For isotropic phonon systems, when $\Omega_{bi} = \Omega_{di}$, relations (2), (3) give $\nu_{b\alpha}^{(0)} = \nu_{d\alpha}^{(0)} = \nu_{\alpha}^{(\mathrm{isotr})}$. In this case Eq. (17) has the solution $S(\mathbf{p}_h) \equiv \mathbf{1}$, and, according to (12), we get the Bose–Einstein distribution (6) for all phonons in an isotropic system.

3. ASYMMETRY OF PROCESSES OF *h*-PHONON CREATION AND DECAY, RESULTING IN A SUPRATHERMAL DISTRIBUTION IN AN ANISOTROPIC PHONON SYSTEM

In anisotropic phonon systems, when $\Omega_{bi} \neq \Omega_{di}$ the creation rate $\nu_{b\alpha}^{(0)}$ can be significantly different from the decay rate $\nu_{d\alpha}^{(0)}$. In Refs. 25 and 26 the rates of all five processes of creation and decay are calculated for phonons with momentum $\mathbf{p}_1$ directed along the axis of symmetry of the pulse, chosen as the Z axis, so $\theta_1 = 0$. These rates we denote $\nu_{b,d}$, where the superscript (0) is understood.

The main role in (17) is played by a type-1 process that describes the exchange of phonons between the l and h systems. For a pulse typically used in the experiments[16–20] the values are: anisotropy parameter $\Omega_p = 0.125$ sr and temperature $T = 1$ K. Then the minimum value of the ratio $\nu_{b1}/\nu_{d1} = 30$ at $p_1 = p_c$; it grows quickly with increasing p_1 and becomes equal to infinity at $p_1 \geqslant p_0$ (see Fig. 1). The limiting momentum p_0 is determined by the solid angle Ω_p and the conservation laws of energy and momentum, which govern the interaction of l phonons with such h_1 phonons. The corresponding analytical expressions and detailed discussion of the rates and their dependences on momentum shown in Fig. 1, are given in Refs. 25 and 26.

An infinite lifetime coupled with a finite creation rate of h phonons with $p_1 \geqslant p_0$ means that in anisotropic phonon systems, type-1 processes cannot effect a dynamic equilibrium between the h and l subsystems. However such an equilibrium can be provided by type-4 processes, because $\nu_{d4} > \nu_{b4}$ in the momentum region where $\nu_{d1} = 0$ (see Fig. 1). Using the numerical values for rates calculated for the anisotropic phonon system (see Fig. 1), equation (17) can be satisfied for $S \gg 1$. As a result, in anisotropic phonon systems, the stationary distribution function of such h phonons is many times greater than the Bose–Einstein one (6) and has a different energy dependence, which is determined by the momentum-dependent rates shown in Fig. 1.

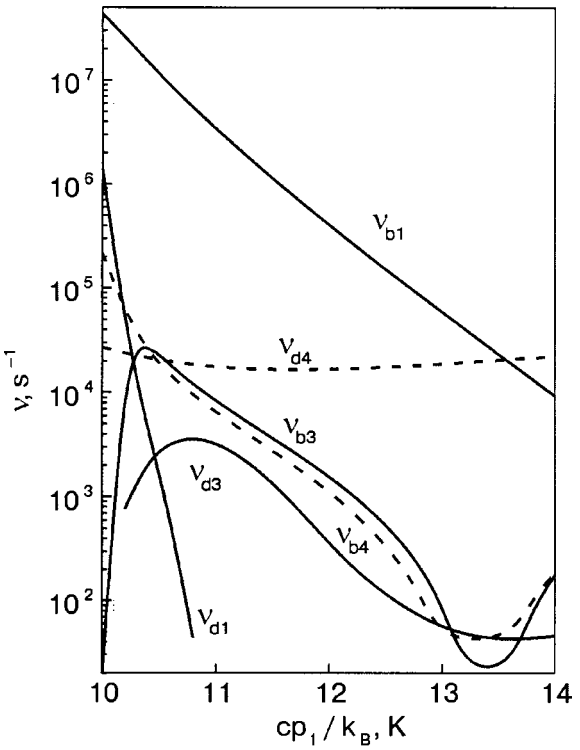

FIG. 1. The momentum dependences of the creation rates ν_b and decay ν_d rates, at $T = 1$ K and $\Omega_p = 0.125$ sr, for all the processes which exchange phonons between the l- and h-phonon systems.

In the left-hand side of (17) the rates that have the same power of S and describe mutually compensating processes are separated in curved braces. These compensating processes in (17) are of two fundamentally different types. The second and the third braces describe processes which exchange phonons between the l and h systems. At the same time, type-4 decay processes are partly compensated by type-3 creation processes (but not by type-4 creation processes), and type-3 decay processes partly compensate type-4 creation process (but not type-3 creation process). The first and fourth curved braces describe processes that conserve the number of h phonons. Here decay is compensated by creation in processes of the same type.

The presence in (17) of processes that conserve and do not conserve the number of h phonons makes it useful to consider the expression obtained from (17) by averaging the anisotropic phonon system over $\mathbf{p}_1$. We define the average as

$$\langle A \rangle = \frac{\int_{\Omega_p} A n_1^{(0)} d^3 p_1}{\int_{\Omega_p} n_1^{(0)} d^3 p_1}. \tag{18}$$

Then one should take into account the following equalities, which are obtained by reindexing the variables of integration:

$$\int_{\Omega_p} N_{d2}(\mathbf{p}_1)d^3p_1 = \int_{\Omega^{(3)}_{d2}} N_{b2}(\mathbf{p}_1)d^3p_1, \tag{19}$$

$$\int_{\Omega_p} N_{d5}(\mathbf{p}_1)d^3p_1 = \int_{\Omega^{(3)}_{d5}} N_{b5}(\mathbf{p}_1)d^3p_1, \tag{20}$$

$$\int_{\Omega_p} N_{d3}(\mathbf{p}_1)d^3p_1 = \int_{\Omega^{(3)}_{d3}} N_{b4}(\mathbf{p}_1)d^3p_1, \tag{21}$$

$$\int_{\Omega_p} N_{d4}(\mathbf{p}_1)d^3p_1 = \int_{\Omega^{(3)}_{d4}} N_{b3}(\mathbf{p}_1)d^3p_1, \tag{22}$$

where $\Omega^{(3)}_{d\alpha}$ is the solid angle of the created $\mathbf{p}_3$ phonon in decay processes of the type α.

From the conservation laws of energy and momentum it follows that at the typical momenta of the phonons taking part in the decay processes, the created $\mathbf{p}_3$ phonon remains inside the initial phonon pulse. This fact allows us to consider approximately that $\Omega^{(3)}_{d\alpha} = \Omega_p$. In this case the averaging of (17) with (19)–(22) taken into account gives:

$$\langle S S_{d4} \nu^{(0)}_{d4} \rangle - \langle S_{b4} \nu^{(0)}_{b4} \rangle = 2\langle \nu^{(0)}_{b1} \rangle - 2\langle S \nu^{(0)}_{d1} \rangle. \tag{23}$$

This result can be rewritten in the form

$$\langle S^2 \rangle \tilde{\nu}^{(0)}_{d4} - \langle S \rangle \tilde{\nu}^{(0)}_{b4} = 2\overline{\nu^{(0)}_{b1}} - 2\langle S \rangle \overline{\nu^{(0)}_{d1}}, \tag{24}$$

where $\overline{\nu^{(0)}_{b1}} = \langle \nu^{(0)}_{b1} \rangle$, and the other average values of the rates $\tilde{\nu}^{(0)}_{b1,d4}$ are determined by the obvious equalities of the respective terms in Eqs. (23) and (24). The solution of Eq. (24) is

$$\langle S \rangle = \frac{4\overline{\nu^{(0)}_{b1}}}{\sqrt{(2\tilde{\nu}^{(0)}_{d1} - \tilde{\nu}^{(0)}_{b4})^2 + 8\tilde{\nu}^{(0)}_{d4}\overline{\nu^{(0)}_{b1}}} + 2\tilde{\nu}^{(0)}_{d1} - \tilde{\nu}^{(0)}_{b4}}. \tag{25}$$

Using this solution we can estimate the value of $\langle S \rangle$ if we replace the rates in (25) (shown in Fig. 1) by their average values calculated over the range $10\ \mathrm{K} < cp_1/k_B < 20\ \mathrm{K}$, at $\theta_1 = 0$. These rates we denote $\overline{\nu_{b,d}}$. In this case

$$2\overline{\nu_{d1}} - \overline{\nu_{b4}} \ll \sqrt{8\overline{\nu_{b1}\nu_{d4}}} \tag{26}$$

and from (25) we have

$$\langle S \rangle \approx \sqrt{2\frac{\overline{\nu^{(0)}_{b1}}}{\overline{\nu^{(0)}_{d4}}}} = 30. \tag{27}$$

This relation has a simple physical meaning. The value of $\langle S \rangle$ is defined as the square root of the ratio of the rate of growth of the number of h phonons by type-1 processes to the rate of decrease of the number of h phonons by type-4 processes, which are partly compensated by type-3 processes.

According to (17) and results obtained for $\nu_{b2,d2}$ and $\nu_{b5,d5}$ (Refs. 25 and 26), it follows that S depends strongly on the angle θ_1 between the direction of the phonon $\mathbf{p}_1(p_1, \theta_1, \varphi_1)$ and the Z axis of symmetry of the anisotropic phonon system. Therefore, according to Refs. 25 and 26, over a relatively wide region of momentum $\mathbf{p}_1$ the creation rate of h phonons with $\theta_1 = 0$, for the second and the fifth processes, is greater than the decay rate. Since the total number of h phonons is separately conserved in processes 2 and 5, the h phonons will concentrate in momentum space near the Z axis. With increasing θ_1, the number of h phonons decreases, so that there will be relatively few h_1 phonons at large $\theta_1 < \theta_p$ in the pulse. This result agrees with the results of experiments,[17,19] where the h-phonon cone is found to be narrower than the l-phonon cone.

The suprathermal ratio S is also a function of the temperature of the l phonons, because according to Refs. 25 and 26 the rates of creation and decay of all five processes become smaller, at different rates, with decreasing temperature. Thus, at $\Omega_p = 0.125$ sr and $p_1 \approx p_c$, according to Ref. 26, with decreasing temperature from 1 K to 0.7 K the rates ν_{b1} and ν_{d1} becomes smaller by ≈ 5 and ≈ 6 times, respectively, the rates ν_{b2} and ν_{d2} by ≈ 9 and ≈ 6 times, the rates ν_{b3} and ν_{d3} by ≈ 70 and ≈ 65 times, the rates ν_{b4} and ν_{d4} by ≈ 80 and ≈ 95 times, and the rates ν_{b5} and ν_{d5} by ≈ 85 and ≈ 100 times, respectively. In general, the suprathermal ratio increases as the temperature decreases.

Although in this paper we are concerned with the value of S averaged over momentum, we do expect that S is strongly peaked just above p_c, where $\nu_{d4} - \nu_{d3}$ is small and ν_{b3} has a maximum.[26] However, the situation is complicated, as S is also expected to vary with angle within the beam.

4. CONCLUSION

In this paper we have shown that the asymmetry between the processes of decay and creation of high-energy phonons in long enough phonon pulses created in experiments[16–20] in superfluid helium results in a suprathermal distribution. Then the quasi-equilibrium distribution function of the h phonons differs from the Bose–Einstein distribution by a factor $S(p)$.

We have obtained an equation (17) whose solution determines the value of the suprathermal ratio S and its dependence on momentum $\mathbf{p}_1$, anisotropy parameter Ω_p, and temperature T. Expressions that describe mutually compensating processes are separated in (17) by curved braces. These compensated processes have two different principal types: the first type describes processes that exchange phonons between the l and h systems, and the second type conserves the number of h phonons. That is why we consider the expressions (23), obtained from (17) by averaging with respect to all $\mathbf{p}_1$ of the anisotropic phonon system.

Starting from relation (23) and the available results for the rates of creation and decay of phonons with momentum $\mathbf{p}_1(p_1, \theta_1 = 0, \varphi_1)$ directed along the symmetry axis Z (see Fig. 1), an estimate is made of the average value $\langle S \rangle$ of the suprathermal ratio. The full evaluation of the suprathermal ratio S and its dependence on the parameters $\mathbf{p}_1$, Ω_p, and T will only be possible after calculation of all the rates in (17) at arbitrary angles θ_1. We plan to carry out this calculation. At present we have only the values of all the rates $\nu_{b,d}$ for the case $\theta_1 = 0$. This estimation of and the analysis of Eqs. (17) and (23) indicates that the distribution function of h phonons can exceed the Bose–Einstein energy distribution by two orders of magnitude in anisotropic phonon systems. We find that $\langle S \rangle$ depends strongly on the parameters $\mathbf{p}_1$, Ω_p, and T. Besides the creation $\langle S \rangle$ of a more complete theory of the suprathermal distribution, we plan to carry out experiments to observe this very unusual phenomenon occurring in phonon pulses in He II.

We express our gratitude to EPSRC of the UK (grant GR/N18796 and GR/N20225), and to GFFI of Ukraine (grant N02.07/000372) for support for this work.

*E-mail: adamenko@pem.kharkov.ua

[1] H. J. Marris and W. E. Massey, Phys. Rev. Lett. **25**, 220 (1970).
[2] J. Jackle and K. W. Kerr, Phys. Rev. Lett. **27**, 654 (1971).
[3] W. G. Stirling, *75th Jubilee Conference on ^4He*, J. G. M. Armitage (Ed.), World Scientific, Singapure (1983), p. 109.
[4] R. C. Dynes and V. Narayanamurti, Phys. Rev. Lett. **33**, 1195 (1974).
[5] A. F. G. Wyatt, N. A. Lockerbie, and R. A. Sherlock, Phys. Rev. Lett. **33**, 1425 (1974).
[6] S. Havlin and M. Luban, Phys. Lett. A **42**, 133 (1972).
[7] H. J. Maris, Phys. Rev. A **8**, 1980 (1972).
[8] M. A. H. Tucker, A. F. G. Wyatt, I. N. Adamenko, K. E. Nemchenko, and A. V. Zhukov, Fiz. Nizk. Temp. **25**, 657 (1999) [Low Temp. Phys. **25**, 488 (1999)].
[9] L. D. Landau, Zh. Éksp. Teor. Fiz. **11**, 592 (1941).
[10] S. G. Eckstein, Y. Eckstein, J. B. Ketterson, and J. H. Vignos, *Phys. Acoustics* **2**, Academic Press, New York (1970), p. 244.
[11] I. M. Khalatnikov, *Theory of Superfluidity*, Nauka, Moscow (1971) (in Russian).
[12] M. A. H. Tucker and A. F. G. Wyatt, J. Phys.: Condens. Matter **4**, 7745 (1992).
[13] I. N. Adamenko and M. I. Kaganov, Zh. Éksp. Teor. Fiz. **53**, 886 (1967). [Sov. Phys. JETP **26**, 537 (1968)].
[14] V. L. Gurevich and B. D. Laĭkhtman, Zh. Éksp. Teor. Fiz. **69**, 1230 (1975). [Sov. Phys. JETP **42**, 628 (1975)].
[15] V. L. Gurevich and B. D. Laĭkhtman, Zh. Éksp. Teor. Fiz. **70**, 1907 (1976). [Sov. Phys. JETP **43**, 993 (1976)].
[16] M. A. H. Tucker and A. F. G. Wyatt, Physica B **194**, 549 (1994).
[17] M. A. H. Tucker and A. F. G. Wyatt, Physica B **194**, 551 (1994).
[18] M. A. H. Tucker and A. F. G. Wyatt, J. Phys.: Condens. Matter **6**, 2813 (1994).
[19] M. A. H. Tucker and A. F. G. Wyatt, J. Phys.: Condens. Matter **6**, 2825 (1994).
[20] M. A. H. Tucker and A. F. G. Wyatt, J. Low Temp. Phys. **113**, 621 (1998).
[21] I. N. Adamenko, K. E. Nemchenko, A. V. Zhukov, M. A. H. Tucker, and A. F. G. Wyatt, Phys. Rev. Lett. **82**, 1482 (1999).
[22] A. F. G. Wyatt, M. A. H. Tucker, I. N. Adamenko, K. E. Nemchenko, and A. V. Zhukov, Phys. Rev. B **6**, 9402 (2000).
[23] A. F. G. Wyatt, M. A. H. Tucker, I. N. Adamenko, K. E. Nemchenko, and A. V. Zhukov, Phys. Rev. B **62**, 3029 (2000).
[24] A. F. G. Wyatt, M. A. H. Tucker, I. N. Adamenko, K. E. Nemchenko, and A. V. Zhukov, Physica B **280**, 36 (2000).
[25] I. N. Adamenko, K. E. Nemchenko, and A. F. G. Wyatt, J. Low Temp. Phys. **125**, 1 (2001).
[26] I. N. Adamenko, K. E. Nemchenko, and A. F. G. Wyatt, J. Low Temp. Phys. **126**, 1471 (2002).
[27] I. N. Adamenko, K. E. Nemchenko, and A. F. G. Wyatt, J. Low Temp. Phys. **126**, 609 (2002).
[28] I. N. Adamenko, K. E. Nemchenko, and A. F. G. Wyatt, Fiz. Nizk. Temp. **28**, 123 (2002) [Low Temp. Phys. **28**, 85 (2002)].

This article was published in English in the original Russian journal. Reproduced here with stylistic changes by AIP.

SUPERCONDUCTIVITY, INCLUDING HIGH-TEMPERATURE SUPERCONDUCTIVITY

Odd resistive response in superconductors with bianisotropic pinning

V. A. Shklovskij[a)]

Institute of Theoretical Physics, National Research Center "Kharkov Physicotechnical Institute," 1 ul. Akademicheskaya 1, 61108 Kharkov, Ukraine; V. N. Karazin Kharkov National University, pl. Svobody 4, 61077 Kharkov, Ukraine

A. A. Soroka

Institute of Theoretical Physics, National Research Center "Kharkov Physicotechnical Institute," 1 ul. Akademicheskaya 1, 61108 Kharkov, Ukraine

(Submitted June 13, 2002)
Fiz. Nizk. Temp. **29**, 22–38 (January 2003)

A theoretical study is made of the odd resistive response (i.e., having odd parity with respect to inversion of the magnetic field) of a superconductor in the mixed state in the presence of bianisotropic pinning and a small isotropic Hall effect. The components of the odd magnetoresistivity in the directions longitudinal and transverse to the current are obtained in a two-dimensional stochastic model of bianisotropic pinning based on the Fokker–Planck equations in the approximation of noninteracting vortices and to a first approximation in the small Hall constant. Both naturally occurring and artificially produced realizations of this model are possible. It is shown that the nonlinear anisotropic properties of the magnetoresistivities are naturally related to the principal critical currents and saturation currents of the system under study. Scaling relations for the Hall conductivity in terms of the longitudinal and transverse magnetoresistivities obtained are discussed, and scaling and its stability in the basal X and Y geometries of the problem are examined. © *2003 American Institute of Physics.*
[DOI: 10.1063/1.1542373]

1. INTRODUCTION

One of the topical problems in the physics of superconductors in the mixed state when vortex pinning is present in them is the influence of pinning on the Hall effect and observed resistive response.[1–16] The first problem studied theoretically was the Hall effect in superconductors with a random distribution of point pinning centers. For a weak isotropic pinning it was found on the basis of a phenomenological approach[1] and collective pinning theory[2] that a universal (independent of the form of the vortex phase and the dynamical regime of the vortices) scaling $\rho_{xy} \propto \rho_{xx}^2$ obtains, which had been observed in a number of experimental studies.[3,4] It was shown in Refs. 1 and 2 that the Hall conductivity is not affected by a weak random disorder, and its anomalous behavior[5] as a function of magnetic field and temperature is due not to pinning but to the magnetic field and temperature dependence of the Hall constants. In the phenomenological model of Wang, Dong, and Ting (WDT)[6] the surface force acting on the vortex in the flow of current around its core and the force due to the counterflow of current inside the core are explicitly taken into account, and that leads to explicit dependence of the Hall constant on the pinning force and the velocity of the vortex; this is the fundamental difference from the theory set forth in Refs. 1 and 2. In the scaling law $\rho_{xy} \propto \rho_{xx}^{\beta}$ that follows from the WDT model the exponent β can take different values depending on the dynamical regime of the vortex.

Another limiting case in the study of the Hall resistive response in the mixed state arises in the presence of uniaxial anisotropy of the pinning, which in high-temperature superconductors is due to a system of unidirectional planar pinning centers—mainly twins.[7–9,11–15,17] A phenomenological theory of superconductors with uniaxial anisotropy was developed in Refs. 11–13. In Refs. 14 and 17 a two-dimensional stochastic model of anisotropic pinning was proposed. In Ref. 15 this model was supplemented by anisotropy of the Hall conductivity and the form of the pinning potential was specified, making it possible to calculate the observable effects analytically in the nonlinear case (the linear case is considered in Ref. 14). In Ref. 15, in contrast to Ref. 17, the dependence of the resistive response on the magnetic field direction was taken into account, and the even and odd components of the resistance were investigated theoretically. (Note: Everywhere in this paper the terms even and odd will refer to parity under inversion of the magnetic field, and the terms longitudinal and transverse will mean with respect to the direction of the current). It was shown that the expressions for the odd longitudinal $\rho_{\parallel}^{-}$ and transverse $\rho_{\perp}^{-}$ magnetoresistivities consist of both nonlinear Hall contributions due to the directed motion of the vortices along the planes of the pinning centers (the so-called "guiding," or "G" effect)[21–23] and contributions due to the dependence of the anisotropic vortex dynamics on the magnetic field direction. The mutual influence of the G effect and Hall effect was investigated and the scaling relations were examined.

In Ref. 7 an odd longitudinal magnetoresistivity $\rho_{\parallel}^{-}$ was first observed experimentally in a $YBa_2Cu_3O_{\delta-7}$ single crys-

tal containing unidirectional twins. In that paper the phenomenological model of Ref. 12 was used to obtain the dependence of the Hall magnetoresistivities $\rho_{Hl}(H)$ and $\rho_{Ht}(H)$ in the L and T geometries $\mathbf{j}\|\mathbf{m}$ and $\mathbf{j}\perp\mathbf{m}$, where $\mathbf{m}$ is a unit vector perpendicular to the planes of the twins, from the functions $\rho_{\|}^{-}(H)$ and $\rho_{\perp}^{-}(H)$ measured at an angle $\alpha=45°$ between the current density vector $\mathbf{j}$ lying in the ab plane and the planes of the twins (where the value of $\rho_{\|}^{-}(H)$ was expected to be maximal). It turned out that the behavior of the functions $\rho_{Hl}(H)$ and $\rho_{Ht}(H)$ differ substantially, and on that basis it was concluded that the influence of twins on the Hall constant is anisotropic, and that fact in turn causes an odd longitudinal component $\rho_{\|}^{-}$ to appear. Anisotropy of the Hall conductivity was investigated experimentally in Ref. 8, where below the characteristic temperature for the onset of vortex pinning at twins a decreasing ratio $\sigma_H^{\perp}/\sigma_H^{\|}$ was observed ($\sigma_H^{\perp}$ and $\sigma_H^{\|}$ are the Hall conductivities when the $\mathbf{j}$ vector is directed perpendicular to and parallel to the planes of the twins). In Ref. 8 the anisotropy of the Hall conductivity due to the influence of twins was explained on the basis of the WDT theory,[6] generalized to take into account the pinning anisotropy caused by the twins. The influence of the form of the vortex phase and of vortex pinning at twins on the behavior of the Hall conductivity and scaling was investigated in Ref. 9 (for $\alpha=45°$). Two types of phase transitions were observed, depending on the magnetic field direction with respect to the twin planes (specified by the angle θ): in the region $\theta>\theta^*$ a transition from the Bragg glass to the liquid phase is observed (at $T=T_m$), and in the region $\theta<\theta^*$, a transition from a Bose glass to the liquid phase (at $T=T_{Bg}$). In both cases a scaling law $\rho_{xy}\propto\rho_{xx}^{\beta}$ is found, with an exponent $\beta=1.4$ for $\theta>\theta^*$ and $\beta=2$ for $\theta<\theta^*$; this relation is independent of the values of the temperature, magnetic field, current density, and angle θ (within the respective regions) and insensitive to the phase transition. A monotonic decline of $\sigma_{xy}(T)$ to the temperatures T_m and T_{Bg} was observed, and also a sharp divergence at $T<T_m$ in the Bragg phase and saturation at $T<T_{Bg}$ in the Bose phase; in the Bragg phase a dependence of $\sigma_{xy}(T)$ on the pinning was observed. It was thus concluded that the behavior of the Hall conductivity and the form of the scaling are substantially different in the Bose and Bragg phases, and the latter depends on the type of disorder (the value $\beta=1.4$ corresponds to point disorder, and $\beta=2$ to correlated disorder).

We note that the experimental results[7,8] indicate a violation of the Onsager relation for the kinetic coefficients ($\sigma_{xy}=-\sigma_{yx}$); this is due to the influence of twins on the Hall conductivity of an isotropic sample. It should be noted that scaling relations of a general form, expressing the components of the conductivity tensor $\hat{\sigma}$ (including the Hall conductivity σ_{xy}, σ_{yz}) in terms of the observable current–voltage characteristics in the L and T geometries have been obtained in the framework of a phenomenological model of anisotropic pinning;[13] in Ref. 15 a scaling relation for the Hall conductivity in the presence of anisotropic pinning was obtained in terms of the observable magnetoresistivities at an arbitrary angle between the current direction and the twin planes; this scaling relation differs substantially from the power-law scaling obtained in the isotropic case.[1]

A feature of the theoretical model of anisotropic pinning considered in Refs. 11–15 and 17 is the existence of a critical current j_c only for the direction strictly perpendicular to the planes of the twins ($\alpha=0$); for any other direction $j_c(\alpha)=0$ ($0<\alpha\leqslant\pi/2$). Nevertheless, measurements of the resistive response for a solid vortex phase always show[9,23] that $j_c(\alpha)>0$ for any angles α (although $j_c(\alpha)$ may be anisotropic). Thus the model of uniaxial anisotropy of the pinning cannot take into account the j_c anisotropy of the solid vortex phase.[9,23] The simplest model in which j_c anisotropy is realized for any angles α in the presence of a planar pinning potential is the model of bianisotropic pinning with a composite potential formed by a superposition of two periodic planar pinning potentials acting in mutually perpendicular directions. The experimental realization of bianisotropic pinning, both in naturally occurring[24] and in artificially created[25] pinning structures, is based on the presence of two mutually orthogonal systems of planar, unidirectional, equidistant pinning centers. It should be noted that at the present time there have been few experimental studies of the resistive properties of superconductors, and then only ones with uniaxial anisotropy of the pinning.[7–9,11] For the case of bianisotropic pinning there are no such studies as yet (the first theoretical paper on this subject appeared only in 2002).[16] We understand that a study of superconductors with a bianisotropic pinning potential created by mutually orthogonal systems of twins and nanocracks[25] and also a system of mutually orthogonal narrow strips of magnetic materials (Co,Ni) deposited on superconducting films is planned for the near future.[26,27]

In this paper we investigate theoretically the odd (with respect to inversion of the magnetic field) resistive response of a superconductor in the mixed state in the presence of bianisotropic pinning and a small Hall effect, and the case of an isotropic Hall constant[14] is considered. Formulas for the observed resistive characteristics of the system—the odd and even longitudinal and transverse magnetoresistivities $\rho_{\|,\perp}^{\pm}(j,T,\alpha)$ as functions of the current density j, temperature T, and angle α specifying the direction of the current density vector with respect to the axes of anisotropy (see Fig. 1) have been obtained in the framework of a two-dimensional stochastic model of bianisotropic pinning on the basis of the Fokker–Planck equation in the approximation of noninteracting vortices and in a first approximation in the small Hall constant.[16] The small Hall effect does not affect the expressions for the even components of the magnetoresistivity $\rho_{\|,\perp}^{+}(j,T,\alpha)$, but it does give rise to magnetoresistivity components which are odd in the magnetic field, $\rho_{\|,\perp}^{-}(j,T,\alpha)$. In the absence of the Hall effect the properties of the observed (even with respect to magnetic field) magnetoresistivities and the resulting anisotropy of the critical current and guided motion of the vortices have been studied in detail theoretically in Refs. 18 and 19. The nonlinear behavior of the observed magnetoresistivities $\rho_{\|,\perp}^{\pm}(j,T,\alpha)$ in a stochastic model of bianisotropic pinning, both in the presence and absence of the Hall effect, are determined by the properties of the functions $\nu_{x,y}(j,T,\alpha)$, the probabilities of a vortex overcoming the xy components of the pinning potential, which describe the vortex dynamics in relation to the corresponding systems of planar pinning centers. The behavior of the functions $\rho_{\|,\perp}^{-}(j,T,\alpha)$ results from the evolution of the

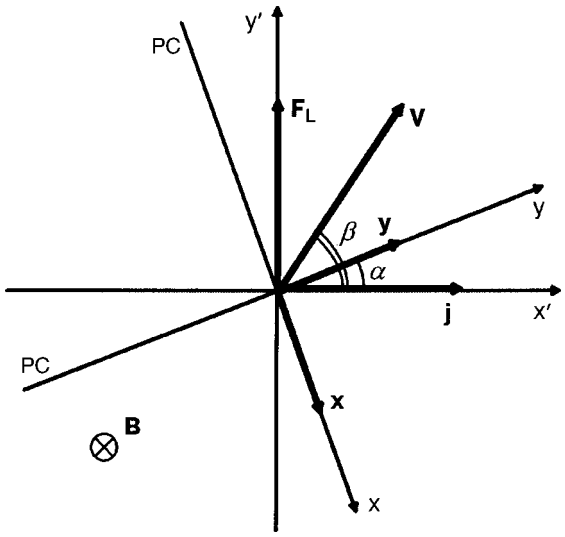

FIG. 1. Coordinate system xy associated with two mutually orthogonal systems of pinning centers (their arrangement is specified by the anisotropy vectors **x**, **y**, which are perpendicular to their planes, and the coordinate system $x'y'$, tied to the direction of the current (the current density vector **j** is directed along the $0x'$ axis); α is the angle between vectors **y** and **j**, β is the angle between the velocity vector **v** of the vortices and the vector **j**; **B** is the magnetic field vector, and F_L is the Lorentz force.

vortex dynamics with changing current and temperature and is due to the realization of certain combinations of regimes of the vortex dynamics with respect to the two systems of pinning centers. The quantitative and qualitative analysis of these functions is done in terms of the functions $\nu_{x,y}(j,T,\alpha)$ and is clearly demonstrated with the aid of a diagram of the dynamical states of the vortex system on the j_xj_y plane.[19] The interrelationship between the nonlinear anisotropic properties of $\rho^{-}_{\parallel,\perp}$ and the principal (in the directions of the axes of anisotropy) critical currents $j_c^{x,y}(T)$ and saturation currents $j_s^{x,y}(T)$ of the given system are analyzed. New scaling relations[16] for the Hall conductivity in the bianisotropic pinning model are discussed in terms of the observed magnetoresistivities $\rho^{\pm}_{\parallel,\perp}(j,T,\alpha)$ are discussed, and the scaling and its stability in the basal X and Y geometries are analyzed.

The material of this article is divided into Sections as follows. In Sec. 2 the two-dimensional stochastic model of bianisotropic pinning based on the Fokker–Planck equations is set forth, and expressions are obtained for the average velocity of the vortex system in a first approximation in the small Hall constant. In Sec. 3 formulas for the nonlinear conductivity and resistivity tensors and all components of the observable magnetoresistivities $\rho^{\pm}_{\parallel,\perp}$ are obtained in general form. In Sec. 4 the general form of the bianisotropic pinning potential is made specific to its possible experimental realizations, and exact expressions for the probability functions ν_x and ν_y in particular cases are discussed. In Sec. 5 the observable magnetoresistivities $\rho^{-}_{\parallel,\perp}$ are analyzed comprehensively. In Sec. 6 the scaling relations are considered in the framework of the specified model. In the Conclusion we state the main findings of this study.

2. STOCHASTIC MODEL OF BIANISOTROPIC PINNING

Let us consider the problem of the vortex dynamics in a superconducting sample in the presence of bianisotropic pinning created by two orthogonal systems of planar unidirectional equidistant pinning centers, these systems in general having different concentrations of pinning centers and depths of the pinning potentials. The preferred directions along which the pinning forces are exerted by the corresponding systems of pinning centers are characterized by pinning anisotropy vectors **x** and **y** (see Fig. 1).

The two-dimensional pinning potential of such a system of planar defects is assumed to be additive and periodic in the anisotropy directions, i.e.,

$$U_p(x,y)=U_{pa}(x)+U_{pb}(y), \tag{1}$$

where

$$U_{pa}(x)=U_{pa}(x+a),\ U_{pb}(y)=U_{pb}(y+b),$$

and a and b are constant periods.

To solve the problem of the vortex dynamics in the presence of bianisotropic pinning we use the Fokker–Planck method. The Langevin equation for a vortex moving with velocity **v** in a magnetic field $\mathbf{B}=\mathbf{n}B$ (where $B\equiv|\mathbf{B}|$, $\mathbf{n}=n\mathbf{z}$, **z** is a unit vector along the z axis, and $n=\pm1$) has the following form:

$$\eta\mathbf{v}+n\alpha_H\mathbf{v}\times\mathbf{z}=\mathbf{F}_L+\mathbf{F}_p+\mathbf{F}_{\rm th}, \tag{2}$$

where $\mathbf{F}_L=n(\Phi_0/c)\mathbf{j}\times\mathbf{Z}$ is the Lorentz force (Φ_0 is the magnetic flux quantum, c is the speed of light, and **j** is the current density); $\mathbf{F}_p=-\nabla U_p$ is the pinning force (U_p is the pinning potential), $\mathbf{F}_{\rm th}$ is the force of thermal fluctuations, η is the electronic viscosity constant, and α_H is the Hall constant. The fluctuational force $\mathbf{F}_{\rm th}(t)$ is Gaussian white noise, the stochastic properties of which are specified by the relations

$$\langle F_{{\rm th},i}(t)\rangle=0,\ \langle F_{{\rm th},i}(t)F_{{\rm th},j}(t')\rangle=2\tilde{T}\delta_{ij}\eta\delta(t-t'), \tag{3}$$

where $\tilde{T}$ is the temperature in energy units. Using relations (3), we can reduce Eq. (2) to a system of Fokker–Planck equations:

$$\eta\mathbf{S}+n\alpha_H\mathbf{S}\times\mathbf{z}=(\mathbf{F}_L-\mathbf{F}_p)p-\tilde{T}\nabla P, \tag{4}$$

$$\frac{\partial P}{\partial t}=-\nabla\cdot\mathbf{S}, \tag{5}$$

where $P(\mathbf{r},t)$ is the probability density for finding a vortex at time t at the point $\mathbf{r}=(x,y)$, and $\mathbf{S}(\mathbf{r},t)\equiv P(\mathbf{r},t)\mathbf{v}(\mathbf{r},t)$ is the probability flux density for the vortex velocity. The average vortex velocity $\langle\mathbf{v}\rangle$ is by definition equal to $\int\int\mathbf{S}d^2\mathbf{r}/\int\int Pd^2\mathbf{r}$.

In the steady-state case Eq. (4) for the functions $P=P(x,y)$ and $\mathbf{S}=(S_x(x,y),S_y(x,y))$ reduces to the equations

$$\begin{cases}\eta S_x+n\alpha_H S_y=F_xP-\tilde{T}(\partial P/\partial x),\\ -n\alpha_H S_x+\eta S_y=F_yP-\tilde{T}(\partial P/\partial y),\end{cases} \tag{6}$$

where

$$F_x=F_{Lx}-dU_{pa}/dx,\ F_y=F_{Ly}-dU_{pb}/dy.$$

The stationarity condition for Eq. (5) leads to the relation

$$\partial S_x/\partial x+\partial S_y/\partial y=0. \tag{7}$$

Because the pinning potential is additive, the probability density for finding vortices can be written in factorized form: $P(x,y)=P_a(x)P_b(y)$.

In this paper the Hall constant α_H is assumed small compared to the electronic viscosity η. We introduce a dimensionless small parameter $\epsilon \equiv \alpha_H/\eta$ ($\epsilon \ll 1$) and a parameter $\delta \equiv n\epsilon$.

To zeroth order in the parameter δ (the case of a negligible Hall effect) the expressions for the components of the average velocity of a vortex have the form[18]

$$\langle v_x\rangle = \tilde{\nu}_x(F_{Lx})/\eta; \quad \langle v_y\rangle = \tilde{\nu}_y(F_{Ly})/\eta, \tag{8}$$

where $\tilde{\nu}_i(F) \equiv F\nu_i(F)$, $i=x,y$ (expressions for $\nu_i(F)$ are given in formula (11) of Ref. 18), the function $\nu_i(F)$ has the physical meaning of the probability that the vortices will overcome the potential barriers of the pinning centers in the x and y directions under the influence of an external effective force F (see Ref. 15 for more details).

We now obtain expressions for the components of the average velocity of a vortex with allowance for the Hall effect in a first approximation with respect to the small parameter δ ($|\delta| \ll 1$). The functions P_a, P_b and a_x, b_y (defined in formula (9) of Ref. 18) in this case can be written as

$$\begin{cases} P_a = P_{a0} + \delta P_{a1}, \\ P_b = P_{b0} + \delta P_{b1}, \end{cases} \quad \begin{cases} a_x = a_0 + \delta a_{x1}, \\ b_y = b_0 + \delta b_{y1}, \end{cases} \tag{9}$$

where P_{a1}, P_{b1} and a_{x1}, b_{y1} are the corrections to the functions P_{a0}, P_{b0} and a_0, b_0 (the zeroth approximation in δ) due to taking the small Hall effect into account (the functions P_{a1}, a_{x1} and P_{b1}, a_{y1} are obviously periodic with periods a and b, respectively). Working by analogy with the $\delta = 0$ case,[18] we use formulas (6) and (7) and obtain expressions for a_{x1} and b_{y1}:

$$\begin{cases} a_{x1} = \tilde{\nu}_y(F_{Ly})(P_{a0}(x) - P_{a0}(0)), \\ b_{y1} = -\tilde{\nu}_x(F_{Lx})(P_{b0}(y) - P_{b0}(0)). \end{cases} \tag{10}$$

Differential equations for P_{a1} and P_{b1} are obtained from the system of equations for a_x and b_y:

$$\begin{cases} F_x P_{a1} - \tilde{T} dP_{a1}/dx = a_{x1}, \\ F_y P_{b1} - \tilde{T} dP_{b1}/dy = b_{y1}. \end{cases} \tag{11}$$

Equations (11) are analogous to the equations for the zeroth approximation, but now on the right-hand side are the x- and y-dependent functions a_{x1} and b_{y1}. The solution of equations (11) consists of the function

$$P_{a1}(x) = (1/\tilde{T}^2)\tilde{v}_y(F_{Ly}) a_0 0_a^2 f(x) \int_x^{x+a} d\xi \int_\xi^{\xi+a} d\zeta / f(\zeta),$$
$$f(x) = \exp[-(F_{Lx}x - U_p(x))/\tilde{T}] \tag{12}$$

and the function $P_{b1}(y)$ obtained formally from $P_{a1}(x)$ by the change of variable $x \to y$, the indices $x \leftrightarrow y$, and $a \to b$, $a_0 \to b_0$, $\theta_a \to \theta_b$.

From the definition of the average velocity $\langle \mathbf{v} \rangle$ of a vortex its components to a first approximation in the small parameter δ are

$$\langle v_x\rangle = \tilde{\nu}_x[1 - \delta(\tilde{\nu}_x A_1/aa_0)]/\eta,$$
$$\langle v_y\rangle = \tilde{\nu}_y[1 - \delta(\tilde{\nu}_y B_1/bb_0)]/\eta, \tag{13}$$

where $A_1 \equiv \int_0^a P_{a1} dx$, $B_1 \equiv \int_0^b P_{b1} dy$. For A_1 and B_1 by identity transformations we obtain the following representation:

$$A_1 = -aa_0 \tilde{\nu}_y d/dF_{Lx}(1/\tilde{\nu}_x),$$
$$B_1 = bb_0 \tilde{\nu}_x d/dF_{Ly}(1/\tilde{\nu}_y). \tag{14}$$

By substituting formulas (14) into (13), we finally obtain the following expressions for the components of the average velocity of a vortex in the presence of a small Hall effect in a first approximation in the parameter gd:

$$\langle v_x\rangle = \tilde{\nu}_x[F_{Lx} - \delta\tilde{\nu}_y(F_{Ly})]/\eta,$$
$$\langle v_y\rangle = \tilde{\nu}_y[F_{Ly} + \delta\tilde{\nu}_x(F_{Lx})]/\eta. \tag{15}$$

The derivation of formulas (15) with the use of an expansion in the small parameter δ presupposes satisfaction of the conditions $|F_{Lx}| \gg |\delta\tilde{\nu}_y(F_{Ly})|$, $|F_{Ly}| \gg |\delta\tilde{\nu}_x(F_{Lx})|$. Consequently, expressions (15) for the components of the average velocity of a vortex are valid in the region of angles α satisfying the condition $\epsilon \ll \tan\alpha \ll \epsilon^{-1}$. In Secs. 3 and 5 the resistive properties are considered for this region of angles. The case of angles α close to the X and Y geometries is considered separated in Sec. 6.

3. NONLINEAR CONDUCTIVITY AND MAGNETORESISTIVITY TENSORS AND THE EXPERIMENTALLY OBSERVABLE MAGNETORESISTIVITIES

The electric field induced by a moving vortex system is

$$\mathbf{E} = (1/c)\mathbf{B} \times \langle \mathbf{v} \rangle = n(B/c)(-\langle v_y\rangle \mathbf{x} + \langle v_x\rangle \mathbf{y}). \tag{16}$$

From formulas (15) and (16) we obtain the magnetoresistivity tensor $\hat{\rho}$ for the nonlinear Ohm's law $\mathbf{E} = \hat{\rho}(\mathbf{j})\mathbf{j}$:

$$\hat{\rho} = \begin{pmatrix} \rho_{xx} & \rho_{xy} \\ \rho_{yx} & \rho_{yy} \end{pmatrix} = \begin{pmatrix} \nu_y(F_y) & -\delta\nu_x(F_{Lx})\nu_y(F_{Ly}) \\ \delta\nu_x(F_{Lx})\nu_y(F_{Ly}) & \nu_x(F_x) \end{pmatrix}. \tag{17}$$

The components of the tensor $\hat{\rho}$ are measured in units of $\rho_f \equiv (\Phi_0 B/\eta c^2)$—the magnetoresistivity to the flux flow; $F_x = F_{Lx} - \delta F_{ly}\nu_y(F_{Ly})$, $F_y = F_{Ly} + \delta F_{Lx}\nu_x(F_{Lx})$ are the components of the external force acting along the vectors $\mathbf{x}$ and $\mathbf{y}$, respectively.

As is seen from Eq. (17), in the general nonlinear case the off-diagonal components of the tensor $\hat{\rho}$ satisfy the Onsager relation ($\rho_{xy} = -\rho_{yx}$). We also note that the components ρ_{xy} and ρ_{yx} depend on the parameter δ explicitly, while the diagonal components ρ_{xx} and ρ_{yy} depend on it implicitly, in terms of the arguments F_y and F_x. All the components of the tensor $\hat{\rho}$ (unlike the components of the tensor $\hat{\sigma}$) are functions of the current density, temperature, and angle α.

The conductivity tensor $\hat{\sigma}$ (the components of which are measured in units of $1/\rho_f$), wich is the inverse of the tensor $\hat{\rho}$, has the form

$$\hat{\sigma} = \begin{pmatrix} \sigma_{xx} & \sigma_{xy} \\ \sigma_{yx} & \sigma_{yy} \end{pmatrix} = \begin{pmatrix} \nu_y(F_y)^{-1} & \delta \\ -\delta & \nu_x(F_x)^{-1} \end{pmatrix}. \tag{18}$$

The off-diagonal components of the tensor $\hat{\sigma}$ are, up to a factor of the sign, equal to the dimensionless Hall constant ϵ, which also satisfies the Onsager relation ($\sigma_{xy} = -\sigma_{yx}$). In the diagonal components the dependence on the parameter δ, by analogy with the tensor $\hat{\rho}$, is implicit.

The experimentally measurable quantities are referred to a coordinate system tied to the current (see Fig. 1). The longitudinal $E_\parallel$ and transverse $E_\perp$ components of the electric field (relative to the direction of the current) are related to E_x and E_y by the simple relations

$$\begin{cases} E_{\parallel} = E_x \sin\alpha + E_y \cos\alpha, \\ E_{-} = -E_x \cos\alpha - E_y \sin\alpha. \end{cases} \tag{19}$$

In the presence of the Hall effect the longitudinal $\rho_{\parallel} = E_{\parallel}/j$ and transverse $\rho_{\perp} = E_{\perp}/j$ magnetoresistivities must be separated into components which are even, $\rho^{+} = [\rho(n) + \rho(-n)]/2$, and odd, $\rho^{-} = [\rho(n) - \rho(-n)]/2$, with respect to the magnetic field. To do this we find the even $\nu^{+} = [\nu(n) + \nu(-n)]/2$ and odd $\nu^{+} = [\nu(n) - \nu(-n)]/2$ components of the functions $\nu_x(F_x)$ and $\nu_y(F_y)$ appearing in Eq. (17) (the functions $\nu_x(F_{Lx})$ and $\nu_y(F_{Ly})$ are even with respect to the magnetic field in view of the assumed evenness of $\nu(F)$). In the region of angles bounded by the condition $\epsilon \ll \tan\alpha \ll \epsilon^{-1}$, in which the functions $\nu_x(F_x)$ and $\nu_y(F_y)$ can be expanded in the small parameter δ, we have for these components, with an accuracy up to terms $\sim \delta^3$,

$$\begin{cases} \nu_x^{+}(F_x) = \nu_x(F_{Lx}), \\ \nu_x^{-}(F_x) = -\delta \nu_x'(F_{Lx}) \tilde{\nu}_y(F_{Ly}), \end{cases} \quad \begin{cases} \nu_y^{+}(F_y) = \nu_y(F_{Ly}), \\ \nu_y^{-}(F_y) = -\delta \nu_y'(F_{Ly}) \tilde{\nu}_x(F_{Lx}), \end{cases} \tag{20}$$

where the prime denotes the derivative, $\nu'(F) \equiv d\nu(F)/dF$.

Using formulas (19) and (20), we obtain expressions for the even and odd components of the longitudinal $\rho_{\parallel}$ and transverse $\rho_{\perp}$ magnetoresistivities:[16]

$$\begin{cases} \rho_{\parallel}^{+} = \nu_y(F_{Ly}) \sin^2\alpha + \nu_x(F_{Lx}) \cos^2\alpha, \\ \rho_{-}^{+} = [\nu_x(F_{Lx}) - \nu_y(F_{Ly})] \sin\alpha \cos\alpha, \end{cases} \tag{21}$$

$$\begin{cases} \rho_{\parallel}^{-} = \nu_y^{-}(F_y) \sin^2\alpha + \nu_x^{-}(F_x) \cos^2\alpha, \\ \rho_{\perp}^{-} = \delta \nu_x(F_{Lx}) \nu_y(F_{Ly}) + [\nu_x^{-}(F_x) - \nu_y^{-}(F_y)] \sin\alpha \cos\alpha. \end{cases} \tag{22}$$

The even components of the magnetoresistivity $\rho_{\parallel,\perp}^{+}$, being a combination of the functions ν_x and ν_y, reflect the nonlinear dynamics of vortices in a superconductor with bianisotropic pinning. Formulas (21) for $\rho_{\parallel,\perp}^{+}$ do not depend on the parameter δ to a first approximation in that parameter, i.e., they correspond to the case $\delta = 0$ which was investigated in detail theoretically in Refs. 18 and 19. The odd components of the magnetoresistivity, $\rho_{\parallel,\perp}^{-}$ are of a Hall origin. They are proportional to the parameter δ and are a combination of the functions ν_x, ν_y and their derivatives ν_x', ν_y'. Below we shall study the properties of the magnetoresistivity $\rho_{\parallel,\perp}^{-}$ on the basis of the model bianisotropic pinning potential used in Refs. 15, 18, and 19.

The dimensionless functions $\nu_x(F, \tilde{T})$ and $\nu_y(F, \tilde{T})$ (F denotes the arguments F_{Lx}, F_x of the function ν_x and F_{Ly}, F_y of the function ν_y), which have the physical meaning of the probabilities of a vortex overcoming the potential barriers of the corresponding systems of pinning centers—the main nonlinear components of the problem. In the nonlinear case the functions $\nu_{x,y}$ correspond to a smoothed steplike resistive transition, and the functions ν_x' and ν_y' have the form of spikes located in the region of nonlinearity of the transition (see below). In the regions of nonlinearity of the functions ν_x and ν_y with respect to current and temperature (or, in other words, in regions of nonlinearity of the pinning viscosity) the corresponding dependences of the experimentally observable magnetoresistivities manifest pronounced nonlinearity. It can be noticed from formulas (21) and (22) that in the nonlinear case $\rho_{\parallel}^{+}$ and $\rho_{\perp}^{+}$ are combinations of smoothed steplike transitions (steps): $\rho_{\parallel}^{-}$ is a combination of spikes, and $\rho_{\perp}^{-}$ is a combination of steps and spikes.

We note the connection of the four components of the magnetoresistivity to the properties of the functions $\nu_{x,y}$. We introduce the X and Y geometries, in which $\mathbf{j} \| \mathbf{x}$ ($\alpha = \pi/2$) and $\mathbf{j} \| \mathbf{y}$ ($\alpha = 0$). Here there exist only the longitudinal even magnetoresistivities $\rho_{\parallel}^{x}(j, \tilde{T}) = \nu_y(j, \tilde{T})$ and $\rho_{\parallel}^{y}(j, \tilde{T}) = \nu_x(j, \tilde{T})$, while $\rho_{\perp}^{x} = \rho_{\perp}^{y} \equiv 0$ (here we have temporarily dropped the superscript "+" from the quantities $\rho_{\parallel,\perp}^{-}$). Thus, measurement of the longitudinal even magnetoresistivities in the X and Y geometries allows one to obtain the current and temperature dependences of the functions $\nu_{x,y}$, which are sufficient for obtaining all forms of the magnetoresistivities $\rho_{\parallel,\perp}^{\pm}(j, \tilde{T})$ to a first approximation in the parameter δ at arbitrary angles α, since the functions $\nu_{x,y}$ appearing in formulas (21) and (22) can be written as $\nu_x(F_{Lx}, \tilde{T}) = \nu_x(j_y, \tilde{T}) = \rho_{\parallel}^{y}(j_y, \tilde{T})$; $\nu_y(F_{Ly}, \tilde{T}) = \nu_y(j_x \tilde{T}) = p_{\parallel}^{x}(j_x, \tilde{T})$ and, consequently, to recover $\nu_x'(F_{Lx}, \tilde{T})$ and $\nu_y'(F_{Ly}, \tilde{T})$.

4. PROPERTIES OF THE PROBABILITY FUNCTIONS $\nu_{x,y}(j, \tau, \alpha, p, \varepsilon, k)$ FOR OVERCOMING OF THE PERIODIC PINNING POTENTIALS

The nonlinear properties of the odd observable magnetoresistivities $\rho_{\parallel}^{-}$, as can be seen from formulas (20) and (22), are completely determined by the behavior of the functions $\nu_x(F_{Lx}, \tilde{T})$, $\nu_y(F_{Ly}, \tilde{T})$, $\nu_x'(F_{Lx}, \tilde{T})$, and $\nu_y'(F_{Ly}, \tilde{T})$, which depend on the form of the pinning potential (see the definition in formula (11) of Ref. 18). In analogy with Refs. 15 and 18, let us make this potential specific to HTSCs of the YBCuO type, where the experimental realization of anisotropic pinning centers can be twins, nanotracks, or gaps between planes of the layered superconductor.[20,25,26] For each of these cases the order parameter is depressed in the region of the pinning center, and, consequently, it is energetically favorable for the vortices to be localized in that region.

Analysis of the Hall resistive properties will be done on the basis of the same pinning potentials U_{pa} and U_{pb} as in Ref. 18 (formulas (19) and Fig. 2 of that paper), which lead to formulas (20) for the function $\nu(f, \tau, \varepsilon)$. Quantitative and qualitative analyses of its behavior as a function of all the parameters and the corresponding asymptotic expressions are discussed in detail in Ref. 15. The characteristic curves of $\nu(f, \tau, \varepsilon)$ as a function of the parameters f and τ (see Figs. 4 and 5 of Ref. 15) describe the nonlinear dynamics of the vortex system as a function of the temperature and of the external force exerted on the vortex perpendicular to the pinning center. It can be seen from those figures that the shape of the $\nu(f)$ and $\nu(\tau)$ curves is determined by the values of the respective fixed parameters τ and f. The monotonically increasing function $\nu(f)$ reflects the nonlinear transition from the regime of thermally activated flux flow (the TAFF regime) to the regime of free flux flow (the FF regime) as the external force is increased at low temperatures ($\tilde{T} \ll U_0$), whereas at high temperatures ($\tilde{T} \geqslant U_0$) the FF regime is realized in the entire range of variation of the external force (at low forces because of the effect of thermal fluctuations on the vortices). Analogously, the monotonically increasing function $\nu(\tau)$ reflects the nonlinear transition from a dy-

namical state corresponding to the value of the external force at zero temperature to the saturation FF regime.

A characteristic feature of the odd magnetoresistivities (22) is the presence in them of not only the functions ν themselves but also their derivatives with respect to the external force. Mathematically the origin of these derivatives is due to the odd components of the functions ν [see Eqs. (20)]. The latter, in turn, have a simple physical meaning. The dynamics of the vortex system in the presence of the Hall effect depends substantially on the magnetic field direction. The effective external forces $F_x = F_{Lx} - n\epsilon F_{Ly}\nu_y(F_{Ly})$ and $F_y = F_{Ly} + n\epsilon F_{Lx}\nu_x(F_{Lx})$ appearing in the expressions for $\rho_\parallel$ and $\rho_\perp$ (for one of the magnetic field directions) and acting on the vortices along the pinning anisotropy vectors **x** and **y** (perpendicular to the pinning center) contain contributions both from the components of the Lorentz force and the components of the Magnus force. Depending on the magnetic field direction, which is specified by the factor $n = \pm 1$, the pairs of components of the Lorentz and Magnus forces can be codirectional or oppositely directed, and the resultant force will be different in these cases; accordingly, the resistive response will be different. The behavior of the functions ν in relation to the parameters f and τ follows directly from the properties of the probability function ν.

The $\nu'(f)$ curve has the form of a spike located in the region of the nonlinear transition, and it goes to zero in the linear regimes (for $f \to 0, \infty$). For $f \leqslant 1$ one has $\nu'(\tau = 0) \equiv 0$ (this is because $\nu(f) \equiv 0$ for $\tau = 0$ in the region $f \leqslant 1$), and the function $\nu'(t)$ also has the form of a spike with a zero limit for $\tau \to \infty$; for $f > 1$ the function $\nu'(t)$ decreases monotonically from the value $\nu'(f,0)$ to zero for $\tau \to \infty$.

The transition to dimensionless parameters, which allow one to take different potentials U_{pa}, U_{pb} into account in the general case, is done in the same way as in Ref. 18. The temperature will be characterized by the parameter $\tau = \tilde{T}/U_0$, the current density will be measured in units of $j_c = cU_0/(\Phi_0 d)$, $U_0 = (U_{x0}, U_{y0})^{1/2}$ is the average depth of the potential wells, $\varepsilon = (\varepsilon_x \varepsilon_y)^{1/2}$ is the average concentration of pinning centers, and $k = (\varepsilon_y/\varepsilon_x)^{1/2} = (a/b)^{1/2}$ and $p = (U_{x0}/U_{y0})^{1/2}$ are measures of the corresponding anisotropies. We recall that the dimensionless parameters f_{Lx} and f_{Ly}, which specify the ratio of the Lorentz force components F_{Lx} and F_{Ly} to the corresponding pinning forces $F_{px} = U_{0x}/d$, $F_{py} = U_{0y}/d$, are equal to $f_{Lx} = njp^{-1}\cos\alpha$ and $f_{Ly} = -njp\sin\alpha$. The dimensionless parameters f_x and f_y, which specify the ratio of the external forces perpendicular to the pinning centers, F_x and F_y, to the pinning forces have the form $f_x = F_x/F_{px} = njp^{-1}[\cos(\alpha) + n\epsilon v_y(f_{Ly}, \tau)\sin\alpha]$ and $f_y = F_y/F_{py} = njp[-\sin\alpha - n\epsilon\nu_x(f_{Lx}, \tau)\cos\alpha]$. The values of the external force $F = F_x$, $F = F_y$ at which the heights of the potential barriers of the potentials U_{pa} and U_{pb} vanish at $\tilde{T} = 0$ correspond to the dimensionless critical currents $j_c^x(\alpha) \approx 1/(p\sin\alpha)$, $j_c^y(\alpha) \approx p/\cos\alpha$ (with accuracy to quantities $\nu_x\epsilon\cot\alpha \ll 1$, $\nu_y\epsilon\tan\alpha \ll 1$, respectively). For $\tilde{T} = 0$ the principal critical currents along the pinning anisotropy vectors **x** and **y** are equal to $j_c^x \equiv j_c^x(\pi/2) \approx p^{-1}$, $j_c^y \equiv j_c^y(0) \approx p$. In the general case of nonzero temperature the critical currents $j_c^x(\tau, \alpha)$ and $j_c^y(\tau, \alpha)$ depend on temperature and correspond for a given angle α to a change in the vortex dynamics from the TAFF regime to a nonlinear regime in relation to the systems of pinning centers with pinning anisotropy vectors **x** and **y**. The condition that determines the temperature region in which the concept of critical currents has physical meaning is $0 < \tilde{T} \ll U_0$ (for $\tilde{T} \geqslant U_0$ the transition from the TAFF to the nonlinear regime is smeared, and the concept of critical current loses physical meaning). In analogy with the critical currents $j_c^x(\tau, \alpha)$ and $j_c^y(\tau, \alpha)$ one can define the saturation currents $j_s^x(\tau, \alpha)$ and $j_s^y(\tau, \alpha)$ at which the nonlinear regime of vortex dynamics gives way to the FF regime at the corresponding systems of pinning centers $j_s^x = j_s^x(\pi/2)$, $j_s^y = j_s^y(0)$ are the principal saturation currents along the pinning anisotropy vectors **x** and **y**, and $j_s^x(\alpha) = j_s^x/\sin\alpha$, $j_s^y(\alpha) = j_s^y/\cos\alpha$).

5. ODD MAGNETORESISTIVITIES

Let us discuss the odd longitudinal and transverse magnetoresistivities caused by the Hall effect on the basis of the bianisotropic pinning potential introduced previously (formula (19) in Ref. 18). We obtain analytic formulas for them by substituting the corresponding expressions for the $\nu_{x,y}$ functions (calculated according to formula (20) of Ref. 18) into formula (22):

$$\begin{cases} \rho_\parallel^- = n\epsilon j \sin\alpha\cos\alpha[p^{-1}\cos\alpha\,\nu_y(pj\sin\alpha, \tau, \varepsilon_y) \\ \qquad \times \nu_x'(p^{-1}j\cos\alpha, \tau, \varepsilon_x) \\ \qquad - p\sin\alpha\,\nu_x(p^{-1}j\cos\alpha, \tau, \varepsilon_x) \\ \qquad \times \nu_y'(pj\sin\alpha, \tau, \varepsilon_y), \\ \rho_\perp^- = n\epsilon\nu_x(p^{-1}j\cos\alpha, \tau, \varepsilon_x)\,\nu_y(pj\sin\alpha, \tau, \varepsilon_y) \\ \qquad + n\epsilon j\sin\alpha\cos\alpha[p^{-1}\sin\alpha\,\nu_y(pj\sin\alpha, \tau, \varepsilon_y), \\ \qquad \times \nu_x'(p^{-1}j\cos\alpha, \tau, \varepsilon_x) \\ \qquad + p\cos\alpha\,\nu_x(p^{-1}j\cos\alpha, \tau, \varepsilon_x) \\ \qquad \times \nu_y'(pj\sin\alpha, \tau, \varepsilon_y). \end{cases} \tag{23}$$

The behavior of the resistivity curves $\rho_{\parallel,\perp}^-(j)$ and $\rho_{\parallel,\perp}^-(\tau)$ is a consequence of the character of the action of the Hall effect on the vortices in the case of nonlinear dynamics of the vortex system and, according to formulas (22), is completely determined by the properties of the even and odd components of the functions $\nu_x(F_x)$ and $\nu_y(F_y)$. The magnetoresistivity $\rho_\parallel^-$ is a combination of odd components of the functions $\nu_{x,y}$. The influence of the Hall effect on the magnetoresistivity $\rho_\parallel^-$ is due to the fact that the resultant forces F_x and F_y contain Magnus force components, which depend on the direction of the magnetic field. This gives rise to odd components of the functions $\nu_x(F_x)$ and $\nu_y(F_y)$ in regions oftheir nonlinearity, these components being proportional to the corresponding Magnus force components in those regions [see formula (20)]. The magnetoresistivity $\rho_\perp^-$ contains contributions from both even and odd components of the functions $\nu_{x,y}$. The Hall contribution to the magnetoresistivity $\rho_\perp^-$ from the even components (the first term in formula (23) for $\rho_\perp^-$) reflects the nonlinear (in current and temperature) Hall effect due to vortex pinning on both systems of pinning centers and is directly related to the action of the Magnus force on the vortices. This effect is more efficient in the case when the vortices are found in the FF regime of motion with respect to both systems of pinning centers, i.e.,

when the influence of the latter can be neglected. If the vortex pinning on one of the systems of pinning centers is appreciable, so that with respect to that system of pinning centers the guided motion of vortices (the G effect) is realized, then the Magnus force acting perpendicular to the velocity and, hence, the pinning centers of that system, is suppressed by the pinning force (if the vortices move along the $0x$ axis, then the action of the Magnus force along the $0y$ axis is suppressed by pinning, and vice versa), and the Hall contribution to the magnetoresistivity $\rho_{\perp}^{-}$ from the even components of the functions $\nu_{x,y}$ is negligible.

Thus the physical origin of the Hall contributions to the magnetoresistivity $\rho_{\parallel,\perp}^{-}$ lies in the realization of certain combinations of dynamical regimes of the vortices with respect to both systems of pinning centers, and the behavior of the functions $\rho_{\parallel,\perp}^{-}(j,\tau)$ is determined by the evolution of the vortex dynamics upon a change of current and temperature. In Refs. 16 and 19 a description and analysis of the vortex dynamics in a stochastic model of bianisotropic pinning in the presence of the Hall effect is done with the aid of the dynamical state diagram of the vortex system on the $j_x j_y$ plane. Since the changes of the critical currents and saturation currents due the Hall effect are negligible, one can neglect the difference in the form of the diagram for opposite directions of the magnetic field, and use that diagram (see Fig. 2) to elucidate the behavior of the functions ν and ν^{-} in different regions of the diagram and to analyze the resistivity curves $\rho_{\parallel,\perp}^{-}(j,\tau)$ accordingly.

The plane of Fig. 2 is divided by lines $j_x = j_c^x(\tau)$, $j_y = j_c^y(\tau)$ and $j_x = j_s^x(\tau)$, $j_y = j_s^y(\tau)$ into several regions corresponding to all possible different dynamical states of the vortex system in the given model. The end of the vector **j**, which has the coordinates $(j\sin\alpha, j\cos\alpha)$, belongs to some one of these regions, depending on the values of j and α. We introduce the critical angles $\alpha^* = \tan^{-1}(j_c^x/j_c^y)$, $\alpha_1^* = \tan^{-1}(j_c^x/j_s^y)$, and $\alpha_2^* = \tan^{-1}(j_s^x/j_c^y)$ (the angles α^*, α_1^*, and α_2^* are formed by rays passing through the origin of coordinates and the respective crossing points of the pairs of lines $j_x = j_c^x$ and $j_y = j_c^y$, $j_x = j_c^x$ and $j_y = j_s^y$, and $j_x = j_s^x$ and $j_y = j_c^y$). In Fig. 2 the unshaded region FP corresponds to the full pinning regime ($j_x < j_c^x$, $j_y < j_c^y$); here TAFF dynamics of the vortices is realized in respect to both systems of pinning centers, and $\nu_x \simeq 0$, $\nu_y \simeq 0$. The region NT_x corresponds to the nonlinear transition regime in the linear TAFF and FF regimes of vortex motion in the direction of the vector **x** (due to pinning on the system of pinning centers parallel to the $0y$ axis); in this region $j_c^y < j_y < j_s^y$ ($j_c^y(\alpha) < j < j_s^y(\alpha)$) and $0 < \nu_x < 1$, $\nu_x^{-} \neq 0$, $\nu_y \simeq 0$, $\nu_y^{-} \simeq 0$. Similarly, the region NT_y corresponds to a nonlinear transition regime between the direction of the vector **y** (due to pinning on the system of pinning centers parallel to the $0x$ axis); here $j_c^x < j_x < j_s^x$ ($j_c^x(\alpha) < j < j_s^x(\alpha)$) and $\nu_x \simeq 0$, $\nu_x^{-} \simeq 0$, $0 < \nu_y < 1$, $\nu_y^{-} \neq 0$. The region FG_x, shaded with horizontal lines, corresponds to a regime of guided motion of the vortices along the pinning centers parallel to the $0x$ axis (the FG_x regime), in which $j_x < j_c^x$, $j_y > j_s^y$ ($j_s^y(\alpha) < j < j_c^x(\alpha)$), and $\nu_x \simeq 1$, $\nu_y \simeq 0$, $\nu_x^{-} \simeq 0$, $\nu_y^{-} \simeq 0$. Region FG_y, shaded with vertical lines, corresponds to the regime of guided motion of the vortices along the pinning centers parallel to the $0y$ axis (the FG_y regime); here $j_x > j_s^x$, $j_y < j_c^y$ ($j_s^x(\alpha) < j < j_c^y(\alpha)$), and $\nu_x \simeq 0$, $\nu_y \simeq 1$, $\nu_x^{-} \simeq 0$, $\nu_y^{-} \simeq 0$. Finally, the FF region, shaded by both horizontal and vertical lines, corresponds to the regime of free flow of magnetic flux with respect to both systems of pinning centers and, consequently, an isotropic resistive response (FF regime); here $j_x > j_s^x$, $j_y > j_s^y$ ($j > j_s^x(\alpha), j > j_s^y(\alpha)$), and $\nu_x \simeq 1$, $\nu_y \simeq 1$, $\nu_x^{-} \simeq 0$, $\nu_y^{-} \simeq 0$. Thus it is only in the region of the nonlinear regimes NT_x and NT_y that the values of ν_x^{-} and ν_y^{-} and, hence, the corresponding (proportional to them) contributions to $\rho_{\parallel,\perp}^{-}$, are nonzero.

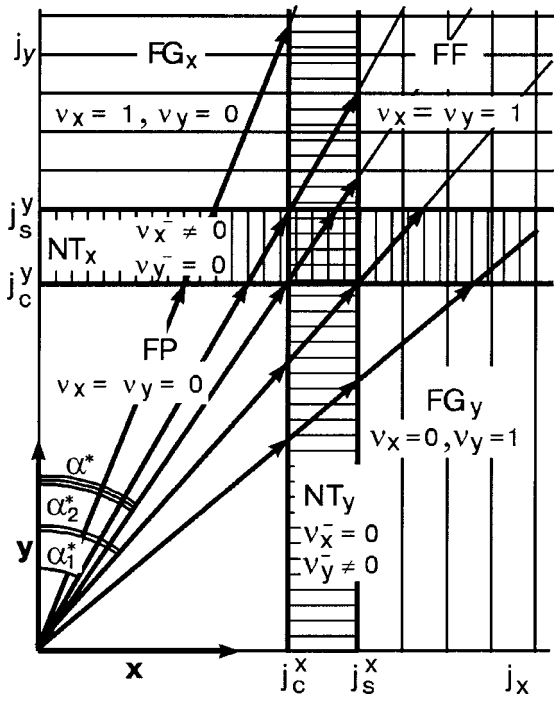

FIG. 2. Dynamical state diagram of a vortex system on the $j_x j_y$ plane and the characteristic values $\nu_x^{\pm}$, $\nu_y^{\pm}$ in each of its regions. j_c^x, j_s^x and j_c^y, j_s^y are the principal critical currents and saturation currents along the pinning anisotropy vectors **x** and **y**, respectively; FP is the full pinning region, NT_x and NT_y are regions of nonlinear transitions between the linear TAFF and FF regimes of vortex motion in the directions of the $0x$ and $0y$ axes, respectively. FG_x and FG_y are the regions of directed (guided) motion of the vortices along the $0x$ and $0y$ axes, respectively, and FF is the region of free flux flow; α^*, α_1^*, and α_2^* are characteristic critical angles (see text).

In accordance with these results it is easy to track the sequence of dynamical regimes in which the vortex system will be found as the current is increased at a fixed temperature and a given angle α and, hence, to explain the qualitative form of the resistivity curves $\rho_{\parallel,\perp}^{-}(j)$. Let us discuss three cases in which their form is different. For $\alpha < \alpha_1^*$ we obtain the following sequence of regimes as the current increases: $\mathrm{FP} \rightarrow \mathrm{NT}_x \rightarrow \mathrm{FG}_x \rightarrow \mathrm{NT}_y \rightarrow \mathrm{FF}$, which corresponds to the following sequence of transition currents between regimes: $j_c^y(\alpha) < j_s^y(\alpha) < j_c^x(\alpha) < j_s^x(\alpha)$. In this case, in accordance with formula (20), only the component $\nu_y^{-}(F_y)$ contributes to $\rho_{\parallel}^{-}(j)$ in the region of currents $j_c^x(\alpha) < j < j_s^x(\alpha)$ (it arises on account of the y component of the Magnus force $F_{My} \approx \epsilon F_{Lx}$, corresponding to the FF regime of vortex motion along the $0x$ axis in the region of nonlinearity of ν_y). The contribution of the components $\nu_x^{-}(F_x)$ to $\rho_{\parallel}^{-}(j)$, on the other hand, are negligible, so that in the region of nonlinearity of ν_x the x component of the Magnus force, $F_{Mx} = -\epsilon F_{Ly}\nu_y(F_{Ly})$, is approximately zero owing to the TAFF regime of motion of vortices along the $0y$ axis. The function

$\rho_{\perp}^{-}(j)$ has, in addition to the contribution from the component $\nu_y^-(F_y)$ in the current region $j_c^x(\alpha)<j<j_s^x(\alpha)$, there also exists a contribution $n\epsilon\nu_x(F_{Lx})\nu_y(\varphi_{Lx})$ from the even components $\nu_x^+(F_x)$, $\nu_y^+(F_y)$ in the current region $j>j_c^x(\alpha)$, where $\nu_x\approx 1$ and ν_y is outside the TAFF region. The case $\alpha>\alpha_2^*$ can be considered in an analogous way. In that case one obtains the following sequence of regimes with increasing current: $\mathrm{FP}\rightarrow\mathrm{NT}_y\rightarrow\mathrm{FG}_y\rightarrow\mathrm{NT}_x\rightarrow\mathrm{FF}$, which corresponds to the following sequence of transition currents between regimes: $j_c^x(\alpha)<j_s^x(\alpha)<j_c^y(\alpha)<j_s^y(\alpha)$. In this case the function $\rho_{\parallel}^{-}(j)$ is nonzero in the region $j_c^y(\alpha)<j<j_s^y(\alpha)$ on account of the contribution from the component $\nu_x^-(F_x)$. The function $\rho_{\perp}^{-}(j)$ contains, in addition to this last, a contribution $n\epsilon\nu_x(F_{Lx})\nu_y(F_{Lx})$ in the current region $j>j_c^y(\alpha)$, where $\nu_y\approx 1$, and ν_x lies outside the TAFF region. Finally, we consider the case $\alpha_1^*<\alpha<\alpha_2^*$. In this region of angles the nonlinear regimes NT_x and NT_y overlap in a certain interval of currents, and, as a result, the function $\rho_{\parallel,\perp}^{-}(j)$ contains components $\nu_x^-(F_x)$ and $\nu_y^-(F_y)$. For example, in the region of angles $\alpha_1^*<\alpha<\alpha^*$, when the current reaches the value $j_c^x(\alpha)$ the nonlinear NT_y regime (in the direction of the $0y$ axis) begins to exist along with the NT_x regime (in the direction of the $0x$ axis). Therefore, at this current, together with the component $\nu_y^-(F_y)$ (due to the y component of the Magnus force, $F_{My}\approx\epsilon\tilde{\nu}_x(F_{Lx})$) a component $\nu_x^-(F_x)$ appears (due to the x component of the Magnus force $F_{Mx}\approx-\epsilon\tilde{\nu}_y(F_{Ly})$). In the region of angles $\alpha^*<\alpha<\alpha_2^*$, when the current reaches the value $j_c^y(\alpha)$, the nonlinear NT_x regime begins to exist along with the nonlinear NT_y regime. Therefore, at this current a component $\nu_y^-(F_y)$ appears along with the component $\nu_x^-(F_x)$. The contribution $n\epsilon\nu_x(F_{Lx})\nu_y(F_{Lx})$ to the function $\rho_{\perp}^{-}(j)$ continues to exist in the current region $j>j_c^x(\alpha)$ for $\alpha_1^*<\alpha<\alpha^*$ and in the current region $j>j_c^y(\alpha)$ for $\alpha^*<\alpha<\alpha_2^*$, when neither of the functions ν_x nor ν_y is found in the TAFF regime of vortex dynamics.

With the aid of the state diagram one can also analyze the qualitative form of the resistivity curves $\rho_{\parallel,\perp}^{-}(\tau)$ in the temperature region where the concepts of critical currents and saturation curves have physical meaning. If one considers the breakaway of the vortices from the pinning centers under the influence of thermal fluctuations and defines the vortex depinning temperature $\tilde{T}_{dp}(j,\alpha,p,\varepsilon,k)$ as the value at which the vortex system goes over into the FF regime of dynamics at given parameters j, α, p, ε, and k, then the condition of applicability of the state diagram for analysis of the functions $\rho_{\parallel,\perp}^{-}(\tau)$ has the form $\tilde{T}\ll\tilde{T}_{dp}$ (Ref. 19). The influence of temperature on the state diagram consists in a monotonic decrease of the value of the critical currents and an increase in the values of the saturation currents with increasing temperature in their domain of definition; this allows one to track the dynamics of the vortices and to explain qualitatively the dependences $\rho_{\parallel,\perp}^{-}(\tau)$. We note that their characteristic form is due to the vortex dynamics, which depends on j and α at $\tau=0$.

By analogy with Ref. 19, where in the bianisotropic pinning model in the absence of the Hall effect the observed dependences $\rho_{\parallel,\perp}^{+}(j,\tau)$ were investigated, one can show that in the model under consideration, with a small Hall effect, the diversity and qualitative form of the $\rho_{\parallel,\perp}^{-}(j,\tau)$ curves at fixed parameters p, ε, k, and t, j, respectively, are due to the influence of the set of values of these parameters (except j) on the values of the principal currents j_c^x, j_s^x, j_c^y, and j_s^y that form the dynamical state diagram, and also the geometric factor—the value of the angle α, which determines the sequence of states of the vortex system on the diagram as the current or temperature is increased. Indeed, it follows from an analysis of the diagram that at a given value $\epsilon\ll 1$ the currents $j_{c,s}^x(\tau,p,\varepsilon k)$ and $j_{c,s}^y(\tau,p,\varepsilon/k)$ determine the existence region and the value of the observed resistive responses $\rho_{\parallel,\perp}^{-}(j,\tau)$. As was shown in Ref. 19, the influence of the "internal" parameters p, ε, and k and the temperature (the parameter τ) on the values of the currents j_c^x, j_s^x, j_c^y, and j_s^y can be characterized as follows. With increasing τ there occurs a decrease in the principal critical currents j_c^x, j_c^y and an increase in the principal saturation currents j_s^x, j_s^y, so that the FP region on the diagram is narrowed and the NT region widened. With increasing ε there occurs an increase of both pairs of principal currents j_c^x, j_c^y and j_s^x, j_s^y, so that the functions $\nu_{x,y}$ decrease monotonically with increasing ε; however, the increase of the second pair of currents occurs significantly faster than the first, and, as a result, a widening of the NT region and a less significant widening of the FP region occur on the diagram. The parameters p and k describe anisotropy of the bianisotropic pinning potential and determine the anisotropy of the critical currents and saturation currents. Growth of the parameter p and/or decline of the parameter k lead to a decrease in the values of the pair of critical and saturation currents j_c^x, j_s^x and an increase in the values of the pair j_c^y, j_s^y. Here the NT_x region is shifted upward, the NT_y region is shifted to the left, and, accordingly, the FP region becomes longer and narrower.

Let us now analyze the behavior of the magnetoresistivities $\rho_{\parallel}^{-}$ and $\rho_{\perp}^{-}$ as functions of current and temperature with the aid of formulas (23); such an analysis corresponds qualitatively to the analysis given above for the state diagram. The expressions for $\rho_{\parallel}^{-}$ and $\rho_{\perp}^{-}$ contain combinations of factors of the form

$$\nu_x'(f_{Lx},\tau,\varepsilon_x)\nu_y(f_{Ly},\tau,\varepsilon_y),$$

$$\nu_x(f_{Lx},\tau,\varepsilon_x)\nu_y'(f_{Ly},\tau,\varepsilon_y),$$

$$\nu_x(f_{Lx},\tau,\varepsilon_x)\nu_y(f_{Ly},\tau,\varepsilon_y),$$

and the properties of their current and temperature dependences follow directly from the properties of the corresponding dependences of the functions $\nu_{x,y}$ at the given values of the fixed parameters p, ε_x, ε_y, and τ (for the current dependences) or j (for the temperature dependences) and the angle α. The functions $\nu_x'(j)\nu_y(j)$ and $\nu_x(j)\nu_y'(j)$ have a bell-shaped form, and the functions $\nu_x'(\tau)\nu_y(\tau)$ and $\nu_x(\tau)\nu_y'(t)$ have a bell-shaped or monotonically decreasing form, depending on the absolute values (moduli) of the arguments f_{Lx} and f_{Ly} of the functions $\nu_{x,y}$ in relation to unity. The functions $\nu_x(j)\nu_y(j)$ and $\nu_x(\tau)\nu_y(\tau)$ have the form of a smoothed steplike transition.

Let us illustrate the behavior of $\rho_{\parallel,\perp}^{-}(j,\tau)$ for a number of values of the angle α and a certain set of parameter values $\epsilon=0.01$, $p=1.4$, $\varepsilon=0.1$, $k=10$, $\tau=0.1$, and $j=1.7$, which makes for a clearer picture by providing wide regions of the nonlinear regimes with pronounced resistive responses in

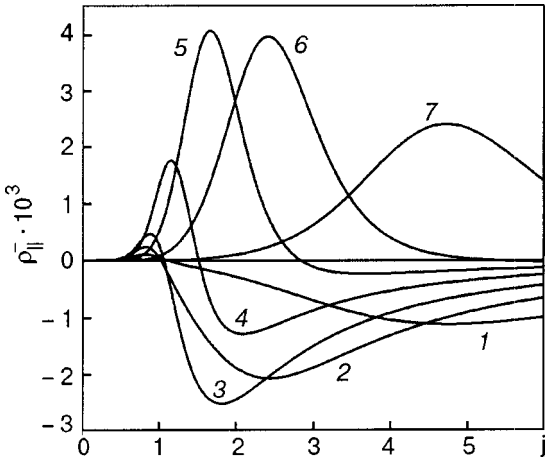

FIG. 3. The function $\rho_{\parallel}^{-}(j)$ for several values of the angle α [deg]: 10 (*1*), 20 (*2*), 30 (*3*), 45 (*4*), 60 (*5*), 70 (*6*), and 80 (*7*) for $\epsilon=0.01$, $p=1.4$, $\tau=0.1$, $\varepsilon=0.1$, $k=10$.

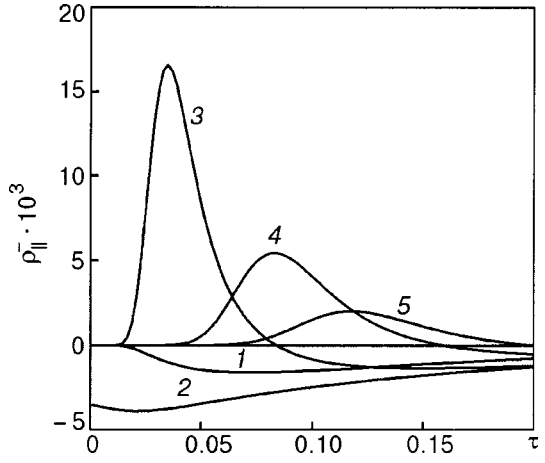

FIG. 4. The function $\rho_{\parallel}^{-}(\tau)$ for several values of the angle α [deg]: 20 (*1*), 30 (*2*), 45 (*3*), 60 (*4*), 70 (*5*) for $\epsilon=0.01$, $p=1.4$, $j=1.7$, $\varepsilon=0.1$, and $k=10$.

them. This set of parameters corresponds to the following pairs of critical and saturation currents: $j_c^x\simeq 0.5$, $j_s^x\simeq 2$, and $j_c^y\cong 0.5$, $j_s^y\simeq 1$ and critical angles $\alpha^*\simeq 45°$, $\alpha_1^*\simeq 27°$, $\alpha_2^*\simeq 76°$ (as a criterion for determining the values of the critical and saturation currents we use the condition that the tangents to the $\nu_{x,y}$ curves at the corresponding points make an angle of 45° to the abscissa).

In the nonlinear case the current dependence of the magnetoresistivity $\rho_{\parallel}^{-}$ (see Fig. 3) is a superposition of bell-shaped functions of different signs, and their resultant form is determined by the relative contribution of these functions, this contribution, in turn, depending on the values of the parameters and the angle α. We note that in the magnetoresistivities $\rho_{\parallel,\perp}^{-}$ there is an external dependence on the angle α, on account of the factors $\sin\alpha$ and $\cos\alpha$, and an internal dependence via the arguments $f_{Lx}=p^{-1}j\cos\alpha$ and $f_{Ly}=pj\sin\alpha$ of the functions $\nu_{x,y}$. It is seen in Fig. 3 that with increasing angle α the contribution to $\rho_{\parallel}^{-}(j)$ from the odd component $\nu_x^{-}(f_x)$ increases, and that from the odd component $\nu_y^{-}(f_y)$ decreases (according to the state diagram, both components exist in the region of angles $\alpha_1^*<\alpha<\alpha_2^*$). Indeed, in accordance with formula (23), with increasing angle α the external angular dependences $\sin\alpha\cos^2\alpha$ and $\sin^2\alpha\cos\alpha$ have qualitatively similar behavior; the component $\nu_x^{-}(f_x)$ increases and the component $\nu_y^{-}(f_y)$ decreases on account of the increase and decrease of the corresponding components of the Magnus forces, $|f_{Mx}|=\epsilon\tilde{\nu}_y(f_{Ly})$ and $f_{My}=-\epsilon\tilde{\nu}_x(f_{Lx})$. The qualitative form of the temperature dependence of the resistivity $\rho_{\parallel}^{-}$ (see Fig. 4) can be either the same as the current dependences (in which case the same kind of relationship, with a superposition of bell-shaped functions, is manifested upon variation of the angle α), or else it can be a function with a finite (non-TAFF) limit as $\tau\to 0$ (see curve *2* in Fig. 4); as was shown above, this is determined by the values of the dimensionless forces f_{Lx} and f_{Ly} with respect to unity, i.e., the set of values of the parameter p, k, ε, j and angle α (which specify the corresponding regime on the state diagram). The magnetoresistivity $\rho_{\parallel}^{-}$ exists only in the nonlinear regimes (in regions of nonlinearity of the functions $\nu_x^{-}(f_x)$ and $\nu_y^{-}(f_y)$); it is proportional to the dimensionless Hall constant ϵ and of the same order of magnitude with it. Because of the external dependence on α, one has $\rho_{\parallel}^{-}\equiv 0$ at $\alpha=(0,\pi/2$. The function $\rho_{\parallel}^{-}(j)$ has a limit of zero for $j\to 0$ and for $j\to\infty$. The function $\rho_{\parallel}^{-}(j)$ has the TAFF limit for $\tau\to 0$ if $p^{-1}j\cos\alpha\leqslant 1$ and/or $pj\sin\alpha\leqslant 1$, and a finite (non-TAFF) limit if $p^{-1}j\cos\alpha>1$ and $pj\sin\alpha>1$; for $\tau\to\infty$ the limit of $\rho_{\parallel}^{-}(\tau)$ is equal to zero. The current and temperature dependences of $\rho_{\parallel}^{-}$ can have a change of sign (see Figs. 3 and 4), since the magnetoresistivity $\rho_{\parallel}^{-}$ contains positive terms entering with different signs.

The current dependence of the magnetoresistivity $\rho_{\perp}^{-}$ at low temperatures (see Fig. 5) is a superposition of a smoothed steplike transition and bell-shaped functions. The qualitative form of the temperature dependence of the magnetoresistivity $\rho_{\perp}^{-}$ (see Fig. 6) is either analogous to the current dependences or differs from them for the same reason as for the resistivity $\rho_{\parallel}^{-}$. Like the dependences of the longitudinal magnetoresistivity, the change in form of the $\rho_{\perp}^{-}(j)$ and $\rho_{\perp}^{-}(\tau)$ curves with increasing angle α occurs on account of an increase in the odd component $\nu_x^{-}(f_x)$ and a decrease of the odd component $\nu_y^{-}(f_y)$. The magnetoresistivity $\rho_{\perp}^{-}$ is

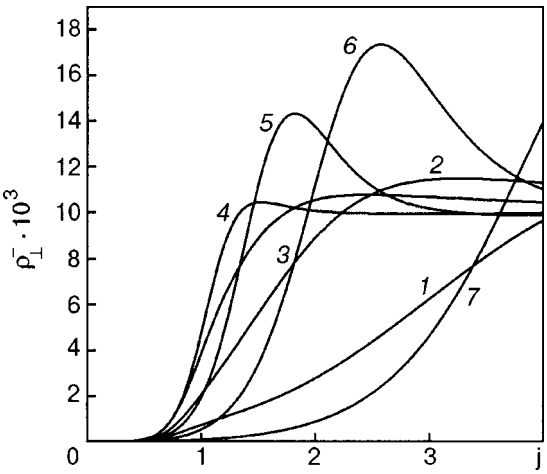

FIG. 5. The function $\rho_{\perp}^{-}(j)$ for several values of the angle α [deg]: 10 (*1*), 20 (*2*), 30 (*3*), 45 (*4*), 60 (*5*), 70 (*6*), and 80 (*7*) for $\epsilon=0.01$, $p=1.4$, $\tau=0.1$, $\varepsilon=0.1$, and $k=10$.

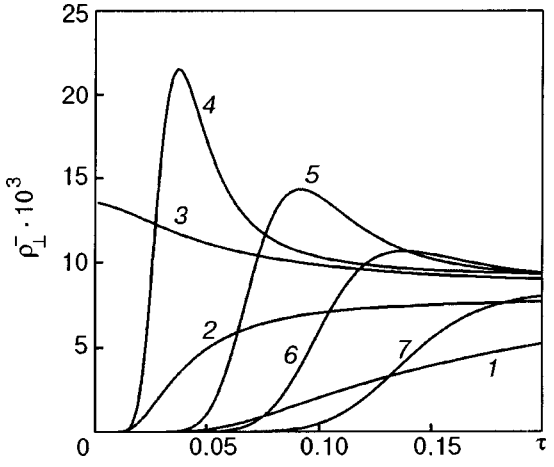

FIG. 6. The function $\rho_\perp^-(\tau)$ for several values of the angle α [deg]: 10 (*1*), 20 (*2*), 30 (*3*), 45 (*4*), 60 (*5*), 70 (*6*), and 80 (*7*) for $\epsilon=0.01$, $p=1.4$, $j=1.7$, $\varepsilon=0.1$, and $k=10$.

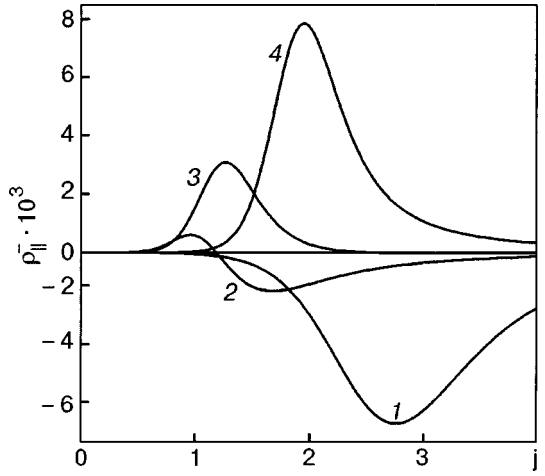

FIG. 7. The function $\rho_\parallel^-$ for several values of the parameter p: 0.7 (*1*), 1.2 (*2*), 1.4 (*3*), and 2 (*4*) for $\epsilon=0.01$, $\alpha=25^0$, $\tau=0.1$, $\varepsilon=0.1$, $k=1$.

proportional to the dimensionless Hall constant ϵ and has the same order of magnitude. Unlike $\rho_\parallel^-$, the magnetoresistivity $\rho_\perp^-$ exists even in the linear regime at high currents and temperatures on account of the contribution $n\epsilon\nu_x\nu_y$; because the external dependence on α makes $\rho_\perp^- \equiv 0$ for $\alpha=0,\pi/2$. At low temperatures the function $\rho_\perp^-(j)$ has the TAFF limit for $j\to 0$. The function $\rho_\perp^-(\tau)$ has the TAFF limit for $\tau\to 0$ if $p^{-1}j\cos\alpha \leqslant 1$ and/or $pj\sin\alpha \leqslant 1$, and a finite limit if $p^{-1}j\cos\alpha > 1$ and $pj\sin\alpha > 1$. The limit of the functions $\rho_\perp^-(j)$ and $\rho_\perp^-(\tau)$ for $j\to\infty$ and $\tau\to\infty$, respectively, is equal to $n\epsilon$. Unlike $\rho_\parallel^-$, the functions $\rho_\perp^-(j)$ and $\rho_\perp^-(\tau)$ do not change sign, since all the terms appear with the same sign in the magnetoresistivity $\rho_\perp^-$.

Let us consider the influence of the parameters p,k,ε, which characterize the bianisotropic pinning potential, on the observable magnetoresistivities. The parameters p and k specify the anisotropy of the potential, and the parameter ε the average concentration of pinning centers (recall that $\varepsilon_x=\varepsilon/k$, $\varepsilon_y=\varepsilon k$). In the functions $\rho_{\parallel,\perp}^-(j)$ an increase of the parameter p and decrease of the parameter k lead to an increase of the contribution of the odd component $\nu_x^-(f_x)$ and to a decrease of the contribution of the odd component $\nu_y^-(f_y)$ owing to the relative displacement of the functions ν_x and ν_y (the function ν_x is shifted to the right and ν_y is shifted to the left). In the limiting cases $p\gg 1, k\ll 1$ and $p\ll 1, k\gg 1$ the contributions from $\nu_x^-(f_x)$ and $\nu_y^-(f_y)$ are negligible. Figures 7 and 8 illustrate the current dependence of the magnetoresistivity $\rho_\parallel^-$ for a number of values of the parameters p and k. The influence of variations of the parameter p on the function $\rho_{\parallel,\perp}^-(\tau)$ is contained in a change of the arguments f_{Lx}, f_{Ly} of the functions ν_x, ν_y, and the influence of the parameter k is analogous to the case of the current dependences. The functions $\rho_\parallel^-(j)$ (see curve *3* in Fig. 8) and $\rho_\parallel^-(\tau)$ a double sign change is possible. This is explained by the fact that for $\alpha_1^* < \alpha < \alpha_2^*$, where a contribution to the resistance is given by both odd components ν_x^-, ν_y^-, there can exist an interval of currents and temperatures such that one of the components is dominant (in modulus) within that interval, while outside it the other component is dominant, so that their summation leads to a double sign change in the corresponding dependences. With increasing parameter ε the quantities ν_x and ν_y as functions of both j and τ are shifted rightward, and on that basis one can track the variation of the functions $\rho_{\parallel,\perp}^-(j,\tau)$. Figure 9 shows the dependence of the resistivity $\rho_\perp^-(j)$ for a number of values of ε.

We note that, according to formulas (23), the substitution $p\to 1/p$, $k\to 1/k$, and $\alpha\to 90°-\alpha$ reduces to a relabeling of the coordinates and, hence, to a symmetry of the layout of the $\rho_\parallel^-(j,\tau)$ curves for mutually reciprocal values of p and k and complementary angles. Therefore, upon this substitution the $\rho_\parallel^-(j,\tau)$ curves are symmetric about the line $\rho_\parallel^-(j,\tau)=0$, and the $\rho_\perp^-(j,\tau)$ curves coincides. The cases $p=1$ and $k=1$ are degenerate and give these types of symmetry for mutually reciprocal values of k and p, respectively, and complementary angles.

6. SCALING RELATIONS

Let us consider the scaling relations in this problem. We return to formulas of the general type (21), (22). Expressing the dimensionless Hall constant in terms of the observable magnetoresistivities $\rho_{\parallel,\perp}^{\pm}$, we obtain anisotropic scaling relations in two equivalent forms:

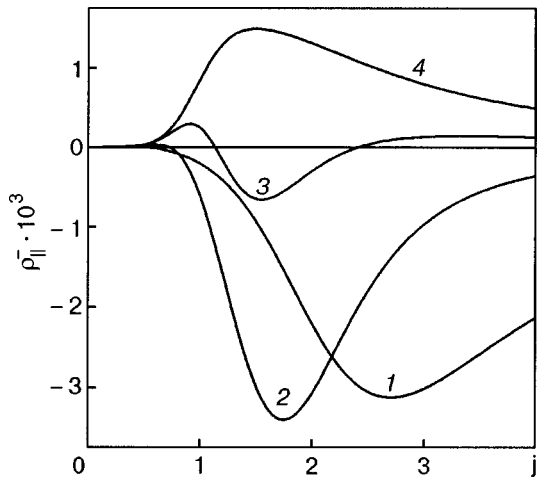

FIG. 8. The function $\rho_\parallel^-(j)$ for several values of the parameter k: 10 (*1*), 1 (*2*), 0.25 (*3*), and 0.1 (*4*) and $\varepsilon=0.001$, $\alpha=25°$, $\tau=0.1$, $\varepsilon=0.1$.

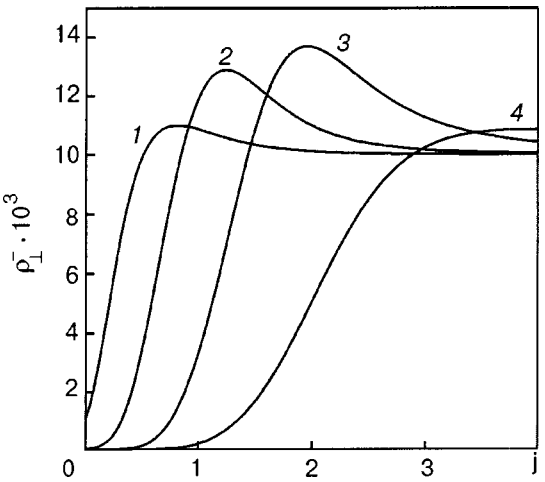

FIG. 9. The function $\rho_\perp(j)$ for several values of the parameter ε: 0.001 (*1*), 0.01 (*2*), 0.1 (*3*), and 1 (*4*) for $\epsilon=0.01$, $\alpha=25°$, $\tau=0.1$, $k=1$.

$$\begin{cases} \delta=\dfrac{\rho_\parallel^-\tan\alpha-\rho_\perp^-}{\nu_y'(j_x)\tilde{\nu}_x(j_y)\tan\alpha-\nu_x(j_y)\nu_y(j_x)}, \\ \delta=\dfrac{\rho_\parallel^-+\rho_\perp^-\tan\alpha}{\nu_x(j_y)\nu_y(j_x)\tan\alpha-\nu_x'(j_y)\tilde{\nu}_y(j_x)}, \end{cases} \tag{24}$$

and the functions ν appearing in these expressions are found by inverting Eqs. (21). Relations (24) are valid in the domain of applicability of formulas (21) and (22), i.e., for $\epsilon\ll 1$ and at angles α not close to $\alpha=0,\pi/2$, so that $\epsilon\ll\tan\alpha\ll\epsilon^{-1}$. Scaling relations (24) express the Hall constant in terms of the observable nonlinear magnetoresistivities $\rho_{\parallel,\perp}^{\pm}$. For example, by measuring all the magnetoresistivities $\rho_{\parallel,\perp}^{\pm}$, one can find the value of the Hall constant from the scaling relations (24). Alternatively, knowing the Hall constant and any three of the observable magnetoresistivities $\rho_{\parallel,\perp}^{\pm}$, one can recover the other. It is easily checked that in the particular case of uniaxial anisotropy ($\nu_y\equiv 1$) the first of the scaling relations (24) goes over to the relation obtained previously in Ref. 15 (formula (40) of that paper). We note that in the bianisotropic pinning model under discussion, scaling of the form $\rho_{xy}\propto\rho_{xx}^{\beta}$ ordinarily observed in the case of isotropic pinning is impossible, since the nonmonotonic function $\rho_\perp^-(j,\tau)$ and the monotonic function $\rho_\parallel^+(j,\tau)$ cannot be related by a power law.

Let us also consider the scaling in the X and Y geometries, in which $\mathbf{j}\|\mathbf{x}$ ($\alpha=\pi/2$) and $\mathbf{j}\|\mathbf{y}$ ($\alpha=0$). For these cases we obtain from formulas (15), (16), and (19)

$$\begin{aligned} &X \text{ geometry, } \alpha=\pi/2\text{: } \rho_{\parallel,X}^+=\nu_y(pj),\rho_{\perp,X}^- \\ &\qquad =n\varepsilon\nu_x[\varepsilon p^{-1}j\nu_y(pj)]\nu_y(pj), \\ &Y \text{ geometry, } \alpha=0\text{: } \rho_{\parallel,Y}^+=\nu_x(p^{-1}j),\rho_{\perp,Y}^- \\ &\qquad =n\varepsilon\nu_x(p^{-1})j)\nu_y[\varepsilon pj\nu_x(p^{-1}j)], \\ &\tan\Theta_H^X=\rho_{\perp,X}^-/\rho_{\perp,X}^+=n\varepsilon\nu_x[\varepsilon p^{-1}j\nu_y(pj)], \\ &\tan\Theta_H^Y=\rho_{\perp,Y}^-/\rho_{\parallel,Y}^+=n\varepsilon\nu_y[\varepsilon pj\nu_x(p^{-1}j)] \end{aligned} \tag{25}$$

and $\rho_{\parallel,X}^-=\rho_{\parallel,Y}^-=\rho_{\perp,X}^+=\rho_{\perp,Y}^+\equiv 0$, i.e., for a superconductor with anisotropic pinning the longitudinal odd $\rho_\parallel^-$ and transverse even $\rho_\parallel^+$ magnetoresistivities vanish in the X and Y geometries on account of the vanishing of the "tensor" (external) angle dependences. Formulas (25) for $\rho_\parallel^+$ and $\rho_\perp^-$ in the X and Y geometries are symmetric with respect to the transformations $\nu_y\leftrightarrow\nu_x$, $p\leftrightarrow p^{-1}$. The magnetoresistivities $\rho_\parallel^-$ in the X and Y geometries depend on the dynamics of vortices with respect to the systems of pinning centers along which the current is directed and are described by the functions ν_y and ν_x. The magnetoresistivities $\rho_\perp^-$ in the X and Y geometries arise because of the corresponding Magnus forces $f_{Mx}=n\epsilon p^{-1}j\nu_y(pj)$ and $f_{My}=n\epsilon pj\nu_x(p^{-1}j)$, which cause motion of the vortices in the direction of the current. Both the Magnus forces and the magnetoresistivities $\rho_\perp^-$ are proportional to the velocity of the vortices, and so they depend on the dynamics of the vortices with respect to the two systems of pinning centers. We note that at moderate currents $j\sim j_s^{x,y}$, which are actually attainable in experiment, $\nu_x[\epsilon p^{-1}j\nu y(pj)]\approx\nu_x(0)$, $\nu_y[\epsilon pj\nu_x(p^{-1}j)]\approx\upsilon_y(0)$ with an accuracy to quantities of order $\epsilon\nu_{x,y}'(0)\ll 1$. Consequently, to this accuracy $\tan\Theta_H^X\approx n\epsilon\nu_x(0)$, $\tan\Theta_H^Y\approx n\epsilon\nu_y(0)$, and the Hall angles $\Theta_H^{X,Y}$ are practically independent of the current density. Formulas (25) express the scaling relations between the magnetoresistivities $\rho_\parallel^+$ and $\rho_\perp^-$ observed in the X and Y geometries and the Hall constant ϵ and also enables one to recover the functions ν_x and ν_y from the observed $\rho_\parallel^+$ and $\rho_\perp^-$ in the X and Y geometries.

Let us discuss the question of stability of the measurements in the X and Y geometries, since in real samples the angle α cannot correspond precisely to the values $\alpha=0,\pi/2$ (see also Ref. 15). For finding the magnetoresistivity tensors near the X and Y geometries we use the results of the method proposed in Ref. 16 for solving the problem under consideration for arbitrary values of ϵ. In Ref. 16 it was shown that the components of the average velocity of the vortices are given by to $\langle v_x\rangle=\tilde{\nu}_x(\overline{F}_x)/\eta$, $\langle v_y\rangle=\tilde{\nu}_y(\overline{F}_y)/\eta$, where the forces $\overline{F}_x$ and $\overline{F}_y$ satisfy Eqs. (13). For $\epsilon\ll 1$ these equations are transformed to

$$\begin{aligned} \overline{F}_x&=F_{Lx}-n\varepsilon F_{Ly}\nu_y[F_{Ly}+n\varepsilon F_{Lx}\nu_x(\tilde{F}_x)], \\ \overline{F}_y&=F_{Ly}-n\varepsilon F_{Lx}\nu_x[F_{Lx}-n\varepsilon F_{Ly}\nu_y(\overline{F}_y)]. \end{aligned} \tag{26}$$

Let us consider the regions of angles near the X and Y geometries.

Near the X geometry ($\cot\alpha\ll\epsilon$)

$$\begin{aligned} \nu_y[F_{Ly}+n\varepsilon F_{Lx}\nu_x(\overline{F}_x)]&\approx\nu_y(F_{Ly})+\nu_y'(F_{Ly}) \\ &\quad\times(n\varepsilon F_{Lx}\nu_x(\overline{F}_x)). \end{aligned}$$

Neglecting the terms quadratic in ϵ, we obtain

$$\begin{aligned} \overline{F}_x^X&=F_{Lx}-n\varepsilon F_{Ly}\nu_y[F_{Ly}+n\varepsilon F_{Lx}\nu_x(\overline{F}_x)] \\ &\approx F_{Lx}-n\varepsilon F_{Ly}\nu_y(F_{Ly}), \\ \overline{F}_y^X&\approx F_{Ly}+n\varepsilon F_{Lx}\nu_x[F_{Lx}-n\varepsilon F_{Ly}\nu_y(F_{Ly})] \\ &\approx F_{Ly}+n\varepsilon F_{Lx}\nu_x(\overline{F}_x^X), \end{aligned}$$

and in dimensionless quantities

$$\begin{aligned} f_x^X&\approx np^{-1}j(\cos\alpha+n\varepsilon\nu_y(f_{Ly})\sin\alpha), \\ f_y^X&\approx npj(-\sin\alpha+n\varepsilon\nu_x(f_x^X)\cos\alpha). \end{aligned}$$

Using formula (26), we obtain the magnetoresistivity tensor near the X geometry:

$$\hat{\rho}_X=\begin{pmatrix} \nu_y(f_y^X) & -n\varepsilon\,\nu_x(f_x^X)\nu_y(f_{Ly}) \\ n\varepsilon\,\nu_x(f_x^X)\nu_y(f_{Ly}) & \nu_x(f_x^X) \end{pmatrix} \tag{27}$$

Similarly, near the Y geometry ($\tan\alpha \ll \epsilon$) we obtain the magnetoresistivity tensor $\hat{\rho}_Y$.

Finally, substituting the tensors $\hat{\rho}_X$ and $\hat{\rho}_Y$ into formulas (19), expanding $\rho_{\parallel,\perp}$ in powers of $\Delta\alpha=\pi/2-\alpha$ in the vicinity of $\alpha=\pi/2$ ($\cot\alpha \ll \epsilon\nu_y(pj)$) and in powers of α in the vicinity of $\alpha=0$ ($\tan\alpha \ll \epsilon\nu_x(p^{-1}j)$) to the first nonvanishing terms with allowance for the terms of first order in ϵ ($\epsilon \ll 1$), and separating the odd and even components, we obtain

$$\begin{aligned}
\rho^{-}_{\parallel,X} &= -n\epsilon pj\nu_x[\epsilon p^{-1}j\nu_y(pj)]\nu'_y(pj)\Delta\alpha,\\
\rho^{+}_{\perp,X} &= -\left\{\nu_y(pj)-\nu_x[\epsilon p^{-1}j\nu_y(pj)]-\epsilon p^{-1}j\nu'_x[\epsilon p^{-1}j\nu_y(pj)]\nu_y(pj)\right\}\Delta\alpha,\\
\rho^{-}_{\parallel,Y} &= n\epsilon p^{-1}j\nu'_x(p^{-1}j)\nu_y[\epsilon pj\nu_x(p^{-1}j)]\,\alpha,\\
\rho^{+}_{\perp,Y} &= \left\{\nu_x(p^{-1}j)-\nu_y[\epsilon pj\nu_x(p^{-1}j)]-\epsilon pj\nu_x(p^{-1}j)\nu'_y[\epsilon pj\nu_x(p^{-1}j)]\right\}\alpha,\\
\rho^{+}_{\parallel,X} &= \nu_y(pj)+\left\{\nu_x[\epsilon p^{-1}j\nu_y(pj)]-\frac{1}{2}pj[1+2\epsilon p^{-1}j\nu'_x[\epsilon p^{-1}j\nu_y(pj)]]\nu'_y(pj)-\nu_y(pj)\right\}(\Delta\alpha)^2,\\
\rho^{-}_{\perp,X} &= n\epsilon\nu_x[\epsilon p^{-1}j\nu_y(pj)]\nu_y(pj)+np^{-1}j\nu'_x[\epsilon p^{-1}j\nu_y(pj)](\Delta\alpha)^2\\
&\quad+\frac{1}{2}n\epsilon\left\{pj\nu_x[\epsilon p^{-1}j\nu_y(pj)]\nu'_y(pj)+p^{-2}j^2\nu''_x[\epsilon p^{-1}j\nu_y(pj)]\nu_y(pj)\right\}(\Delta\alpha)^2,\\
\rho^{+}_{\parallel,Y} &= \nu_x(p^{-1}j)+\left\{\nu_y[\epsilon pj\nu_x(p^{-1}j)]-\frac{1}{2}p^{-1}j\nu'_x(p^{-1}j)[1+2\epsilon pj\nu'_y[\epsilon pj\nu_x(p^{-1}j)]]-\nu_x(p^{-1}j)\right\}\alpha^2,\\
\rho^{-}_{\perp,Y} &= n\epsilon\nu_x(p^{-1}j)\nu_y[\epsilon pj\nu_x(p^{-1}j)]+npj\nu'_y[\epsilon pj\nu_x(p^{-1}j)]\,\alpha^2\\
&\quad+\frac{1}{2}n\epsilon\left\{p^{-1}j\nu'_x(p^{-1}j)\nu_y[\epsilon pj\nu_x(p^{-1}j)]+\frac{1}{2}p^2j^2\nu_x(p^{-1}j)\nu''_y[\epsilon pj\nu_x(p^{-1}j)]\right\}\alpha^2,
\end{aligned} \tag{28}$$

where a prime denotes the derivative: $\nu'(f)\equiv\partial\nu(f)/\partial f$. Formulas (28) for $\rho^{\pm}_{\parallel,\perp}$ at small deviations $\Delta\alpha$ and α from the X and Y geometries, like formulas (25), are symmetric with respect to the transformation $\nu_y\leftrightarrow\nu_x$, $p\leftrightarrow p^{-1}$. As formulas (28) show, the corrections of both first and second orders in $\Delta\alpha,\alpha$ exist only in the low-temperature region, where the nonlinear regimes are realized (we shall consider this case) and vanish when the temperature is raised. The magnetoresistivities $\rho^{-}_{\parallel}$ and $\rho^{+}_{\perp}$, which are equal to zero in the X and Y geometries, vary linearly in $\Delta\alpha$ and α at small deviations from those geometries. The magnetoresistivities $\rho^{-}_{\parallel}$ exist only in regions of nonlinearity of the functions $\nu_{y,x}$ (upon a deviation from the X and Y geometries, respectively) and are proportional to the factors $\nu_x(0)$, $\nu_y(0)\ll 1$, i.e., they are stable. The main contribution to the magnetoresistivity $\rho^{+}_{\perp}$ upon a deviation from the X and Y geometries at actually accessible values of the currents is given by terms $-\nu_y(pj)\Delta\alpha$ and $\nu_x(p^{-1}j)\alpha$, so that their stability is determined by the dynamical regime in regard to the pinning centers along which the current is directed in the X and Y geometries. The magnetoresistivities $\rho^{-}_{\parallel}$ and $\rho^{-}_{\perp}$ vary quadratically with respect to $\Delta\alpha$ and α from their values in the X and Y geometries. The relative deviations of the magnetoresistivities for $\rho^{+}_{\parallel,X}$ and $\rho^{+}_{\parallel,Y}$ are in order of magnitude

$$\Delta\rho^{-}_{\parallel,X}/\rho_{\parallel,X}+\simeq\left\{-\frac{1}{2}pj\nu'_y(pj)/\nu_y(pj)-1\right\}(\Delta\alpha)^2,$$

$$\Delta\rho^{+}_{\parallel,Y}/\rho^{+}_{\parallel,Y}\simeq\left\{-\frac{1}{2}p^{-1}j\nu'_x(p^{-1}j)/\nu_x(p^{-1}j)-1\right\}\alpha^2.$$

In the linear regime one has $\Delta\rho^{+}_{\parallel,X}/\rho^{+}_{\parallel,X}\simeq-(\Delta\alpha)^2$, $\Delta\rho^{+}_{\parallel,Y}/\rho^{+}_{\parallel,Y}\simeq-\alpha^2$. The relative deviations of the values of the magnetoresistivities for $\rho^{-}_{\perp,X}$ and $\rho^{-}_{\perp,Y}$ are in order of magnitude

$$\Delta\rho^{-}_{\perp,X}/\rho^{-}_{\perp,X}\simeq\frac{1}{2}pj[\nu'_y(pj)/\nu_y(pj)](\Delta\alpha)^2,$$

$$\Delta\rho^{-}_{\perp,Y}/\rho^{-}_{\perp,Y}\simeq\frac{1}{2}p^{-1}j[\nu'_x(p^{-1}j)/\nu_x(p^{-1}j)]\alpha^2$$

and exist only in regions of nonlinearity of the functions ν_y and ν_x. As in the case of the linear corrections, the corrections quadratic in $\Delta\alpha,\alpha$ to the magnetoresistivities $\rho^{+}_{\parallel}$ and $\rho^{-}_{\perp}$ at small deviations from the X and Y geometries are determined by the dynamics of the vortices with respect to the pinning centers parallel to the current in the respective geometries.

Formulas (28) for the observable magnetoresistivities $\rho^{\pm}_{\parallel,\perp}$ at small deviations of the angle α from the values $\alpha=0,\pi/2$ corresponding to the Y and X geometries can be used to find these deviations. Neglecting at first the small contributions quadratic in α and $\Delta\alpha=\pi/2-\alpha$ to the magnetoresistivities $\rho^{+}_{\parallel}$ and $\rho^{-}_{\perp}$, one can solve the scaling problem according to formulas (25), i.e., one can recover the value of

the constant ϵ and the functions ν_x and ν_y. Then, using formulas (28) for the magnetoresistivities $\rho_{\parallel}^{-}$ and $\rho_{\perp}^{+}$, which vanish in the Y and X geometries and are linear in α and $\Delta\alpha=\pi/2-\alpha$ at small deviations from those geometries, one can find the corresponding values of α and $\Delta\alpha$. The self-consistency of this scheme is checked by calculating the corrections quadratic in α and $\Delta\alpha$, which should be small relative to the main contribution in the Y and X geometries.

CONCLUSION

The odd resistive response due to the influence of the small isotropic Hall effect for a superconductor in the mixed state in the presence of two mutually orthogonal systems of unidirectional pinning centers has been studied in the framework of a planar stochastic model of bianisotropic pinning. Formulas for the observable odd longitudinal and transverse magnetoresistivities $\rho_{\parallel,\perp}^{-}(j,\tilde{T},\alpha)$ are obtained in this model on the basis of the Fokker–Planck equations in the noninteracting vortex approximation and to a first approximation in the small Hall constant. The two-dimensional bianisotropic pinning potential of general form (assumed to be additive and periodic in the anisotropy directions), which models two mutually orthogonal systems of unidirectional planar pinning centers, was made specific for the purpose of investigating the dependences of the magnetoresistivities $\rho_{\parallel,\perp}^{-}$ on all the (dimensionless) parameters of the problem—both on the external parameters j,τ,α, which characterize the current density, temperature, and current direction, and on the internal parameters p, ε, and k, which describe the intensity and anisotropy of the pinning potential itself, and on the dimensionless Hall constants ϵ.

The main features of the problem under study are the nonlinear, nonmonotonic behavior of the observed anisotropic magnetoresistivities as functions of the transport current density and temperature and the anisotropy of the critical current due to the anisotropic pinning. The nonlinearity of the vortex dynamics with respect to current is due to the nonlinear character of the dependence of the values of the potential barriers of the pinning centers on the external force acting on the vortices; the nonlinearity of the vortex dynamics with respect to temperature is due to the nonlinear temperature dependence of the probability that vortices will escape from the potential wells of the pinning centers. In the stochastic model of bianisotropic pinning investigated here, the principal nonlinear components are the probability functions for the vortices to overcome the potential barriers of the corresponding systems of pinning centers, $\nu_{x,y}(j,\tau,\alpha,p,\varepsilon,k)$, which describe the nonlinear (with respect to current and temperature) dynamics of the vortices relative to these systems of pinning centers. The investigated odd magnetoresistivities $\rho_{\parallel,\perp}^{-}(j,\tau)$ are linear combinations of the functions $\nu_{x,y}$ and their derivatives [see formulas (23)] and, hence, their properties are completely determined by the well-studied properties of the latter. The functions $\rho_{\parallel,\perp}^{-}(j,\tau)$ in the case of uniaxial anisotropic pinning, which is a particular case of bianisotropic pinning, were investigated in Ref. 15, but for arbitrary values of the Hall constant. A lucid quantitative and qualitative analysis of the functions $\rho_{\parallel,\perp}^{-}(j,\tau)$ has also been done with the aid of the dynamic state diagram of the vortex system on the j_xj_y plane. This diagram permits one to analyze how the vortex dynamics evolves upon changes in the current and temperature; this evolution determines the characteristic behavior and the existence regions of the functions $\rho_{\parallel,\perp}^{-}(j,\tau)$. It was shown that the nonlinear anisotropic properties of the magnetoresistivities $\rho_{\parallel,\perp}^{-}$ are naturally linked to the principal critical currents $j_c^{x,y}(\tau)$ and saturation currents $j_s^{x,y}(\tau)$, which form the state diagram of the system under study. Unlike the stochastic model of uniaxial anisotropic pinning studied previously,[15] where the critical current density j_c is indeed equal to zero for all directions, in the given model the anisotropic critical current exists for all directions. It should be noted that the functions $\rho_{\parallel}^{-}(j,\tau)$ can have a change of sign (even a double change), whereas the sign of $\rho_{\perp}^{-}(j,\tau)$ does not change; at moderate currents $j\lesssim j_s^{x,y}$ the Hall angles $\Theta_H^{X,Y}$ are practically independent of the current density.

We have discussed the scaling relations for the Hall conductivity in terms of the observed magnetoresistivities $\rho_{\parallel,\perp}^{\pm}$ (in the region of angles bounded by the condition $\epsilon\ll\tan\alpha\ll\epsilon^{-1}$), and we have examined the scaling and its stability in the basal X and Y geometries.

[a]E-mail: valerij.a.shklovskij@univer.kharkov.ua

[1] V. M. Vinokur, V. B. Geshkenbein, M. V. Feigel'man, and G. Blatter, Phys. Rev. Lett. **71**, 1242 (1993).
[2] Wu Liu, T. W. Clinton, and C. J. Lobb, Phys. Rev. B **52**, 7482 (1994).
[3] A. V. Samoilov, A. Legris, F. Rullier-Albenque, P. Lejay, S. Bouffard, Z. G. Ivanov, and L.-G. Johanson, Phys. Rev. Lett. **74**, 2351 (1995).
[4] T. W. Clinton, A. W. Smith, Qi Li, J. L. Peng, R. L. Greene, C. J. Lobb, M. Eddy, and C. C. Tsuei, Phys. Rev. B **52**, R7046 (1995).
[5] S. J. Hagen, C. J. Lobb, R. L. Greene, M. G. Forrester, and J. H. Kang, Phys. Rev. B **41**, 11630 (1990).
[6] Z. D. Wang, J. Dong, and C. S. Ting, Phys. Rev. Lett. **72**, 3875 (1994).
[7] A. A. Prodan, V. A. Shklovskij, V. V. Chabanenko, A. V. Bondarenko, M. A. Obolenskii, H. Szymczak, and S. Piechota, Physica C **302**, 271 (1998).
[8] A. Casaca, G. Bonfait, C. Dubourdieu, F. Weiss, and J. P. Senateur, Phys. Rev. B **59**, 1538 (1999).
[9] G. D'Anna, V. Berseth, L. Forro, A. Erb, and E. Walker, Phys. Rev. B **61**, 4215 (2000).
[10] N. B. Kopnin and V. M. Vinokur, Phys. Rev. Lett. **83**, 4864 (1999).
[11] É. B. Sonin and A. L. Kholkin, Fiz. Tverd. Tela. (St. Petersburg) **34**, 1147 (1992) [Phys. Solid State **34**, 610 (1992)].
[12] V. A. Shklovskij, Fiz. Nizk. Temp. **23**, 1134 (1997) [Low Temp. Phys. **23**, 853 (1997)].
[13] V. A. Shklovskij, Fiz. Nizk. Temp. **25**, 153 (1999) [Low Temp. Phys. **25**, 109 (1999)].
[14] Y. Mawatari, Phys. Rev. B **56**, 3433 (1997).
[15] V. A. Shklovski (Shklovskij), A. A. Soroka, and A. K. Soroka, Zh. Éksp. Teor. Fiz. **116**, 2103 (1999) [JETP **89**, 1138 (1999)].
[16] V. A. Shklovskij, Phys. Rev. B **65**, 092508 (2002).
[17] Y. Mawatari, Phys. Rev. B **59**, 12033 (1999).
[18] V. A. Shklovskij and A. A. Soroka, Fiz. Nizk. Temp. **28**, 365 (2002) [Low Temp. Phys. **28**, 254 (2002)].
[19] V. A. Shklovskij and A. A. Soroka, Fiz. Nizk. Temp. **28**, 449 (2002) [Low Temp. Phys. **28**, 312 (2002)].
[20] S. Fleshler, W.-K. Kwok, U. Welp, V. M. Vinokur, M. K. Smith, J. Downey, and G. W. Crabtree, Phys. Rev. B **47**, 14448 (1993).
[21] A. K. Niessen and C. H. Weijsenfeld, J. Appl. Phys. **40**, 384 (1969).
[22] V. V. Chabanenko, A. A. Prodan, V. A. Shklovskij, A. V. Bondarenko, M. A. Obolenskii, H. Szymczak, and S. Piechota, Physica C **314**, 133 (1999).

[23] H. Pastoriza, S. Candia, and G. Nieva, Phys. Rev. Lett. **83**, 1026 (1999).
[24] J. Z. Wu and W. K. Chu, Phys. Rev. B **49**, 1381 (1994).
[25] G. Koren, E. Polturak, N. Levy, D. Deutscher, and N. D. Zakharov, Appl. Phys. Lett. **73**, 3763 (1998).
[26] A. Hoffmann, P. Prieto, and I. K. Schuller, Phys. Rev. B **61**, 6958 (2000).
[27] M. J. Van Bael, K. Temst, V. V. Moshchalkov, and Y. Bruynseraede, Phys. Rev. B **59**, 14674 (1999).
[28] G. Blatter, M. V. Feigelman, V. B. Geshkenbein, A. I. Larkin, V. M. Vinokur, Rev. Mod. Phys. **66**, 1125 (1994).

Translated by Steve Torstveit

LOW-TEMPERATURE MAGNETISM

Kinetic properties and magnetic susceptibility of $La_{0.9}Sr_{0.1}MnO_3$ under hydrostatic pressure

E. S. Itskevich, V. F. Kraidenov, A. E. Petrova,* V. A. Ventcel', and A. V. Rudnev

L. F. Vereshchagin Institute of High Pressure Physics, 142090 Troitsk, Moscow District, Russia
(Submitted June 10, 2002; revised July 8, 2002)
Fiz. Nizk. Temp. **29**, 39–46 (January 2003)

The magnetic susceptibility χ, thermopower α, and electrical resistivity ρ of single-crystal samples of the manganite $La_{1-x}Sr_xMnO_3$ with $x=0.1$ are measured in the temperature range 80–300 K at pressures up to 10 kbar. The thermopower $\alpha(T)$ is positive, with a domelike shape of the curve, and decreases with increasing pressure. The $\chi(T)$ and $\rho(T)$ curves are found to have features at $T\approx 95$, 120, and 135 K. The feature at $T_{OO}\approx 95$ K is attributed to orbital ordering, and that at $T_{CA}\approx 135$ K to a canted antiferromagnet$\leftrightarrow$paramagnet transition. The physical cause of the feature at $T_M=120$ K is discussed. The transition temperatures increase with increasing pressure at rates of $\partial T_{CA}/\partial P=0.43$ K/kbar and $\partial T_M/\partial P=0.57$ K/kbar. A weak feature is detected on the $\rho(T)$ and $\alpha(T)$ curves at $T=225-235$ K. © *2003 American Institute of Physics.* [DOI: 10.1063/1.1542374]

Complex oxides of manganese with the perovskite crystal structure, which exhibit colossal magnetoresistance (CMR) and have a number of interesting and unusual physical properties (charge and orbital ordering, quantum phase transitions) are attracting interest in connection with the possibility of their practical application. Their crystal structure is similar to that of the high-T_c superconducting (HTSC) oxides of copper. The main similarity of the manganites and cuprates is the mechanism of doping by divalent metals, in particular La, which substitute for the trivalent rare-earth ion, causing the system to acquire new properties.[1] By analogy with HTSCs it can be assumed that the characteristic feature of the layered perovskite manganites is the two-dimensional character of the conduction in the MnO_2 plane and a strong interaction of the two-dimensional charge carriers with optical phonons.

The results of different experimental studies on these materials show much disagreement. This is explained by the strong dependence of the physical parameters of metal oxides on the degree of doping, stoichiometry, and structural defects.

Interest in the compound with $x=0.1$ in the $La_{1-x}Sr_xMnO_3$ series is dictated by the fact that this Sr concentration corresponds to the lower edge of the concentration region $x=0.1-0.15$ in which the main low-temperature state is a ferromagnetic insulator (FMI). For $0<x<0.1$, canted antiferromagnetism (CAF) is realized. At the other end of this region, for $x\geqslant 0.16$, the main state is a ferromagnetic metal (FMM). According to the phase diagram of $La_{1-x}Sr_xMnO_3$ (Ref. 2) and the data of Refs. 3–5, a sample with $x=0.1$ undergoes three phase transitions as the temperature is lowered.

1. At $T=T_s=320$ K one observes a structural transition of the orthorhombic phase O to an orthorhombic phase O' with Jahn–Teller (JT) distortions ($O\rightarrow O'$). Here the sample remains in the paramagnetic insulator (PMI) state.

2. At $T=T_{CA}\approx 150$ K a magnetic transition from the paramagnetic phase to a phase of canted antiferromagnetism occurs, and in many papers[6–10] the CAF state is said to be unstable and accompanied by phase separation into ferromagnetic polarons (droplets) in an antiferromagnetic matrix.

3. At $T=T_{OO}\approx 95-105$ K a structural transition to a pseudocubic phase O^* is observed ($O'\rightarrow O^*$), with a simultaneous magnetic transition to the FMI state. This is accompanied by new orbital and, possibly, charge ordering brought about by superexchange.

The physical properties of $La_{1-x}Sr_xMnO_3$ have been investigated in many studies: the magnetic susceptibility χ in Refs. 2, 5, 11, and 12, the resistivity ρ in Refs. 2–4, the magnetization **M** in Refs. 4 and 11–13, the conductivity $\sigma(\omega)$ and dielectric permittivity $\varepsilon(\omega)$ in the submillimeter and optical frequency ranges in Refs. 11, 12, and 14–16, and the sound velocity V_t in Ref. 17.

An important role in understanding the mechanisms governing the behavior of manganites is played by studies under pressure. We know of only one study of $La_{0.9}Sr_{0.1}MnO_3$ under pressure, and that was done at pressures up to 8.8 kbar.[4] The values found in that study for the shifts of the phase transitions under pressure, 2.3 K/kbar for $T_{CA}(T_C)$ and 2.5 K/kbar for T_{OO}, obtained on the basis of electrical resistance measurements under pressure, are close to the values which we found in Ref. 18 for $La_{1-x}Sr_xMnO_3$ samples with a higher Sr concentration ($x=0.125$). Since the sample with $x=0.1$ is found at the boundary with the AF region, this coincidence seems strange and needs additional verification. The goal of the present study was to obtain additional information about the mechanism of the magnetic phase transitions in a comparative study of the kinetic and magnetic properties of $La_{1-x}Sr_xMnO_3$ under pressure. For this we made measurements of the magnetic susceptibility χ, resis-

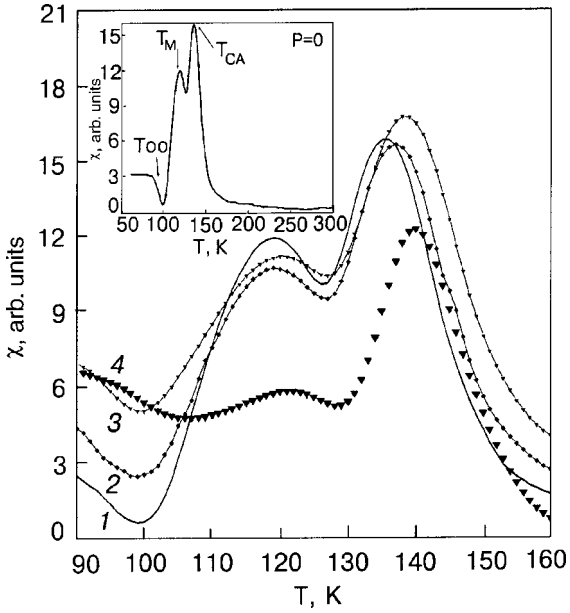

FIG. 1. Temperature dependence of the magnetic susceptibility of $La_{0.9}Sr_{0.1}MnO_3$ at pressures P [kbar]: 0 (*1*), 4.3 (*2*), 6.2 (*3*), 8 (*4*). The average values of the pressures for the temperature interval corresponding to the phase transitions are indicated. The inset shows a plot of $\chi(T)$ for $P=0$.

tivity ρ, and thermopower α in the temperature range 80–300 K at hydrostatic pressures of up to 10 kbar.

SAMPLES

Single-crystal samples of $La_{1-x}Sr_xMnO_3$ with $x=0.1$ were cut from a cylindrical bar grown by the zone-melting method with radiant heating,[19] with the axis of the bar in the [100] direction of the crystal.

MAGNETIC SUSCEPTIBILITY

The magnetic susceptibility χ was measured by a modulational method in a 19 Hz alternating current and with a magnetic field amplitude of ≈ 10 Oe.[20] The modulating and receiving coils were placed inside the high-pressure chamber. The pressure was measured by a Manganin manometer in the whole temperature range as the sample was cooled at a rate of 0.3–0.5 K/min.

Figure 2 shows the temperature dependence of the magnetic susceptibility at different pressures, and the inset shows the $\chi(T)$ curve at atmospheric pressure. The growth of the susceptibility on cooling from room temperature begins at $T\sim 160$ K, and the $\chi(T)$ curve has two maxima at temperatures of 135 and 119 K. The first maximum (T_{CA}) can be attributed to a phase transition from the paramagnetic insulator to a canted antiferromagnet, and the second (T_M) may be due to various causes which will be considered below. Near 100 K one observes a minimum with a subsequent growth and an inflection point at 95 K. This is a region of orbital ordering (T_{OO}) and also of structural ($O'\rightarrow O^*$) and magnetic (CAF→FMI) transitions. With increasing pressure all of the singular points shift to higher temperatures.

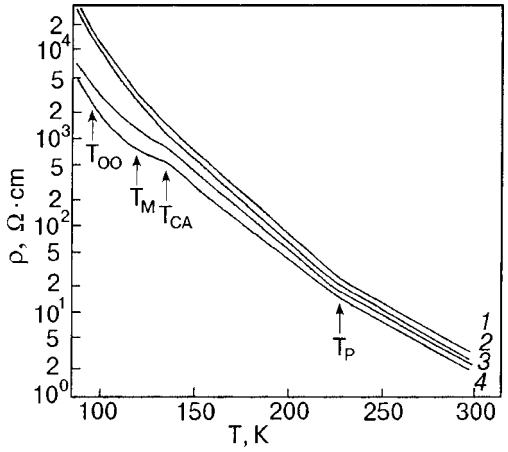

FIG. 2. The temperature dependence of the resistivity of $La_{0.9}Sr_{0.1}MnO_3$ at pressures P [kbar]: 0 (*1*), 5.3 (*2*), 7.7 (*3*), and 9.9 (*4*). The pressure values correspond to room temperature.

RESISTIVITY

The sample used for the resistivity measurements was a cylinder 5 mm in diameter and 7 mm in height. The measurements of ρ were done by the standard four-contact method. The contacts were prepared using Ag paste. The distance between potential leads was 3.5 mm. The measuring current did not exceed 100 μA. The resistivity at room temperature and atmospheric pressure was $\rho_{300}=4.0\ \Omega\cdot$cm.

The hydrostatic pressures were produced in a steel fixed-pressure chamber with an inner channel 12 mm in diameter.[21] The pressure medium used was PES-1 silicone liquid.

Figure 2 shows a semilogarithmic plot of $\rho(T)$ for different pressures. There are no regions with $d\rho/dT>0$. However, one can clearly see a tendency toward the appearance of such segments as the pressure is raised. Except for the region $T\approx 100-140$ K the $\ln\rho(T)$ curves are approximated by straight lines with kinks at the characteristic phase transition points: $T\approx 100$, 120, 136, and 225 K. With increasing pressure the resistivity ρ decreases and the points at which the kinks occur shift to higher temperatures. We associate the following phase transitions to these characteristic points in order of decreasing temperature: 1) $T_p\approx 225-235$ K—a transition within a paramagnetic insulator phase with the O' lattice, possibly due to diffusion of vacancies and ordering of the structure; 2) $T_{CA}\approx 136$ K—paramagnetic insulator → canted antiferromagnet, in which the distorted O' lattice and the insulator state are preserved; phase separation into ferromagnetic polarons (ferrons) and an AF matrix is not ruled out; 3) $T_M\approx 120$ K—a phase transition due either to "freezing" of the polarons and the formation of a spin glass[5] or to a change in the lattice parameters; 4) $T_{OO}\approx 100$ K—a structural transition $O'\rightarrow O^*$, accompanied by a magnetic transition to a ferromagnetic insulator state with orbital ordering and possible charge ordering of the type given in Ref. 22.

Figure 3 shows the pressure dependence of the phase transition temperatures T_{CA}, T_M, and T_{OO}, obtained from resistivity measurements and from magnetic susceptibility measurements. The averaged rates of change with pressure obtained from the ρ and χ measurements are $\partial T_{CA}/\partial P=0.43$ K/kbar and $\partial T_M/\partial P=0.57$ K/kbar.

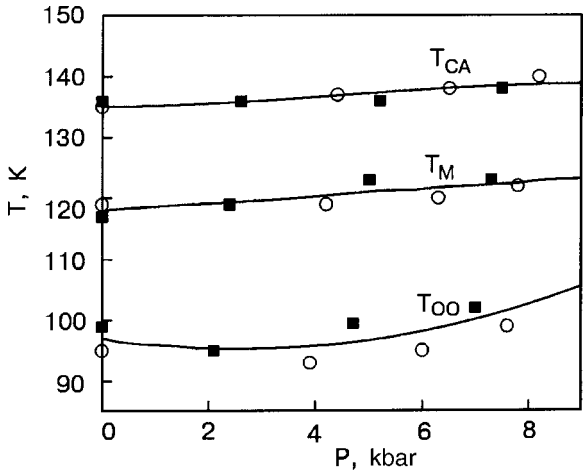

FIG. 3. Dependence of the critical temperature T_{CA}, T_M, and T_{00} on pressure for $La_{0.9}Sr_{0.1}MnO_3$, obtained from measurements of the resistivity (■) and magnetic susceptibility (○). The values of the pressures are given with allowance for the pressure drop as the temperature is lowered.

To monitor the stability of the resistivity in time at a pressure of 5.3 kbar we measured two $\rho(T)$ curves at an interval of 15 days. It was found that a hold under pressure decreases ρ. The observed decrease in ρ was largest (over 20%) in the room-temperature region and fell to zero for $T<130$ K.

THERMOPOWER

The thermopower measurements were made in the dynamic regime during cooling and heating of the high-pressure chamber by a modified form of the technique set forth in Ref. 23, which has previously been used successfully for measurements of α in metals, HTSCs, and manganites. Figure 4 shows the temperature dependence of the thermopower α at different pressures. One can discern several characteristic features on all the curves.

—At all pressures the curves have a domelike shape with a maximum at a temperature $T_{\max}\approx 185-190$ K.

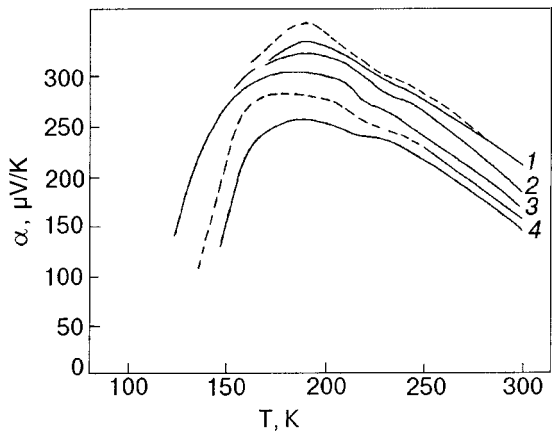

FIG. 4. Temperature dependence of the thermopower of $La_{0.9}Sr_{0.1}MnO_3$ at pressures P [kbar]: 0 (*1*), 5.3 (*2*), 7.7 (*3*), 9.9 (*4*). The solid curves were obtained on cooling, the dashed curves on heating. The pressures correspond to room temperature.

—The thermopower falls off with increasing pressure: at the maximum of α it decreases from 350 μV/K at $P=0$ to 250 μV/K at $P\approx 10$ kbar.

—For $T>T_{\max}$ the thermopower decreases almost linearly up to room temperature at a rate of ≈ 1.3 $\mu V/K^2$.

—For $T<T_{\max}$ the thermopower decreases very sharply with decreasing temperature. Measurements of α in this region are difficult on account of the high resistivity of the sample and are restricted to temperatures not lower than $T\approx 120-150$ K.

—In the temperature region 230–240 K the same feature as on the curves of $\ln\rho(T)$ is observed at all pressures.

—In the cooling–heating cycle the values of α exhibited substantial hysteresis, especially noticeable at $T\leqslant 220$ K. Repeated cooling from room temperature gives values of the thermopower $\sim 10\%$ higher than the previous measurement. This is seen on the $\alpha(T)$ curves in Fig. 4 at pressures of $P=0$ and ≈ 10 kbar.

—The value of α at $T=300$ K decreased by $\sim 20\%$ during a 7-day hold at a pressure of 10 kbar.

DISCUSSION OF THE RESULTS

The influence of pressure on the manganites can be reduced to three main factors:

1) pressure decreases the distance between atoms $d_{\text{Mn-O}}$, increasing the overlap of the orbitals and the hopping probability t_{ij} and causing broadening of the conduction band W ($\partial d_{\text{Mn-O}}/\partial P<0$; $\partial W/\partial P>0$);[24,25]

2) pressure causes an increase of the geometric angle θ in the Mn–O–Mn chain,[24,25] which again leads to an increase of the temperature t_{ij} and broadening of the conduction band $W\sim|\cos\theta|/d^{3.5}$ ($\partial\theta/\partial P>0$; $\partial W/\partial P>0$);

3) pressure decreases the coupling coefficient α_0 of the electron–phonon interaction due to the JT polarons ($d\alpha_0/dP<0$; $\partial\ln T_C/\partial P>0$),[26,27] where T_C is the Curie temperature.

The relative contribution of these factors to the change of the Curie temperature T_C of manganites under pressure was studied in Refs. 24 and 27. On the basis of the experimental data on the relative change under pressure of the distance $d_{\text{Mn-O}}$ ($k_d=-2.32\times10^{-5}$ kbar^{-1}) and angle θ ($k_\theta=(8.5-16)\times10^{-5}$ kbar^{-1}) obtained in Ref. 24 on a large number of oxides $L_{2/3}A_{1/3}MnO_3$ (L=La, Pr; A=Ca, Sr, Ba), the theoretical estimate $\partial\ln T_C/\partial P=\partial\ln W/\partial P\approx 4\times10^{-4}$ kbar^{-1} was made in Ref. 27. However, experiments on the manganites $(La,Y)_{0.7}Ca_{0.3}MnO_3$ (Ref. 27) and $La_{1-x}Sr_xMnO_3$ with $x=0.125$ (Refs. 18 and 28) and $x=0.1$ (Ref. 4) give an average value $\partial T_C/\partial P\approx 2$ K/kbar and, hence, $\partial\ln T_C/\partial P\approx 2\times10^{-2}$ kbar^{-1}. This is more than an order of magnitude higher than the theoretical estimate, which takes into account the pressure dependence of only the parameters $d_{\text{Mn-O}}$ and θ. Therefore, as was proposed in Ref. 27, it is necessary to take into account a third factor, i.e., the electron–lattice (polaron) coupling and its pressure dependence. The lifting of the degeneracy of the ground state e_g of the electrons on account of the Jahn–Teller effect leads to local deformations of the lattice around these electrons and to the formation of so-called JT polarons. The effective conduction band of these polarons has the form

$$W_{\text{eff}} = W \exp(-2\alpha_0). \quad (1)$$

In the case of strong Hund coupling ($J_H \gg W_{\text{eff}}$) one has $T_C \sim W_{\text{eff}}$, and

$$\partial \ln T_C / \partial P = \partial \ln W / \partial P - 2\partial \alpha_0 / \partial P. \quad (2)$$

According to estimates,[27] $\partial \alpha_0 / \partial P = -(1-2) \times 10^{-2}$ kbar^{-1}. Thus the contribution of the change of the energy of the polaronic coupling to the increase of the temperature T_C under pressure is an order of magnitude larger than the contributions due to the change of the distance $d_{\text{Mn-O}}$ and angle θ ($\approx 4 \times 10^{-4}$ kbar^{-1}). Acting in the same direction, these three factors provide a good correlation of the calculated estimates and the experimental results for the dependence $\partial \ln T_C / \partial P$ ($\sim 10^{-2}$ kbar^{-1}).

It follows from Refs. 18 and 28 that in a $La_{1-x}Sr_xMnO_3$ sample with $x = 0.125$ the characteristic temperatures T_C, T_{OO} (T_{CO}), and T_M vary with pressure at close rates ~ 2 K/kbar. This is evidence that the same physical cause underlies these changes. A similar closeness of the rates of change of the characteristic temperatures (T_{char}) T_{CA}, T_{OO}, and T_M (0.4–0.6 K/kbar) is also observed for the $La_{1-x}Sr_xMnO_3$ sample with $x = 0.1$, only they are 4–5 times smaller than for the sample with $x = 0.125$. This leads to a value $\partial \ln T_{\text{char}} / \partial P \approx 5 \times 10^{-3}$ kbar^{-1} in the samples studied; in our view, this can be explained by two causes. With decreasing x in the $La_{1-x}Sr_xMnO_3$ system the value of α_0 increases from 0.07 for $x = 0.15$ to $\alpha_0 = 0.19$ for $x = 0.1$.[26] This is due to the growth of the JT distortions of the lattice with decreasing x. One can surmise a strong drop in $\partial \alpha_0 / \partial P$ for small x. However, we think it is more realistic to assume, as was done in Ref. 25, that the low value of $\partial T_N / \partial P \sim 0.3$ K/kbar (T_N is the Néel temperature) observed in $LaMnO_3$ to 60 kbar is explained by strong localization of the carriers and the absence of double exchange even at such a pressure. The low values of the derivatives $\partial T_N / \partial P$ are also obtained for other AF insulators: $CaMnO_3$ (0.41 K/kbar), $YCrO_3$ (0.38 K/kbar), and $LaTiO_3$ (0.23 K/kbar). However, with doping and the appearance of double exchange and ferromagnetism the values of the derivatives $\partial T_C / \partial P$ in manganites increase to 1.5–2 K/kbar. This is apparently due to the strong dependence of the double exchange on pressure. In the manganites that we studied, which are found near the boundary of the AF region, the double exchange is still very small.

The appreciable difference in the values obtained for the characteristic temperatures and their pressure derivatives in the present study and in Ref. 4 and also the increased value of ρ_{300} in comparison with Ref. 3 made it necessary to check the stoichiometric composition of the samples. An iodometric analysis of the samples for their oxygen concentration gave a value of 2.995 ± 0.005 oxygen atoms per atom of manganese.

The disparity in the temperature dependence of the kinetic parameters and the phase transition temperatures according to different investigators for samples of the same composition is due to different conditions of chemical synthesis, which determines the stoichiometric composition of these samples.[29] At low doping levels large accumulations of vacancies can form at the La and Sr sites and/or Mn sites. In the first case there is an increase in the hole concentration, which facilitates double exchange and is analogous to an increase in the Sr concentration. In the second case, changes can be localized in the vacant sites of the metal, causing a displacement of the oxygen atoms; this is similar to an increase in the JT distortions of the lattice. A thermogravimetric study done in Ref. 29 on samples with $x = 0.1$ and which, like ours, did not have a segment with $\partial \rho / \partial T > 0$ on the $\ln \rho(T)$ curve, gave a value of 3.002 ± 0.002 oxygen atoms per manganese atom. Since in these manganites the oxygen concentration cannot be greater than 3, this number indicates the nearly complete absence of vacancies in the La, Sr, and Mn sites. We therefore concluded that the discrepancies in the data are due either to the presence of dislocations in our samples or to a nonstoichiometric composition and the presence of vacancies in the crystals of other authors.

Studies of $La_{1-x}Sr_xMnO_3$ at frequencies in the submillimeter region, 100–1100 GHz,[15] for values $x = 0.1$—0.175 in the temperature range 10–300 K the transport of charge (conductivity) is effected mainly by localized carriers, even in those regions where $d\rho / dT > 0$. As a rule, satisfaction of this inequality is indicative of the presence of metallic conductivity. It turned out that the charge carriers in this range of x and temperatures are still strongly coupled to the lattice. This strong localization of carriers should invariably manifest itself in the temperature dependence of $\rho(T)$ obtained in direct current. In the whole temperature range at all pressures we did not observe the segment with decreasing resistivity which was described in Refs. 2–4—we observed only a tendency toward the appearance of such a region at $T < T_{CA}$ with increasing pressure (Fig. 2). To elucidate the nature of the conductivity and the degree of localization of the charge carriers we constructed plots of $\ln \rho = f(1/T^4)$ and $\ln \rho = f(1/T)$ (Fig. 5) for the maximum pressure of 10 kbar. In the case of hopping conductivity with a variable hopping length one has

$$\rho = \text{const} \cdot \exp[(T_0 / T)^{1/4}], \quad (3)$$

where T_0 is a characteristic temperature.

However, if thermally activated hops occur only between nearest neighbors (Miller–Abrahams conductivity) or if there is thermal excitation of carriers from a localized Fermi level to the conduction edge, then

$$\rho = \text{const} \cdot \exp(E / T), \quad (4)$$

where E is the energy difference of the two states.[30] The first type of dependence is shown in Fig. 5a. One observes two rectilinear segments: one in the low-temperature (LT), FM insulator region ($T \approx 90$–110 K) and the other in the high-temperature (HT), PM insulator region ($T \approx 185$–300 K). This is evidence of hopping conductivity with a variable hopping length in these temperature regions. Figure 5b shows the second type of dependence, $\ln \rho = f(1/T)$. In the high-temperature region the curve is nonlinear, but in the low-temperature region a good linear approximation is observed. However, the thermal excitation of carriers is more probable in the HT region than in the LT region. It may be that the linear approximation is explained by the small size of the LT region (~ 15 K). Moreover, the start of the linear dependence (~ 108 K) is shifted with respect to the tempera-

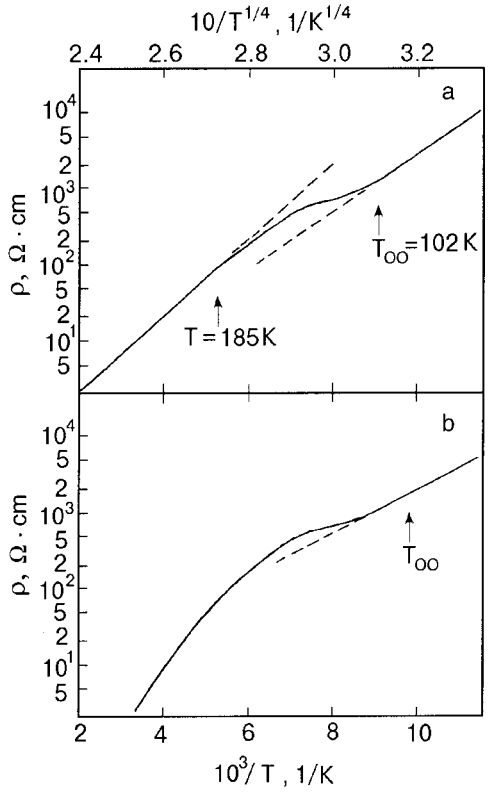

FIG. 5. Temperature dependence of the resistivity of $La_{0.9}Sr_{0.1}MnO_3$ at a pressure $P=9.9$ kbar: $\rho=f(1/T^{1/4})$ (a); $\rho=f(1/T)$ (b). The pressure corresponds to room temperature.

ture T_{OO} by ~ 6 K. All these factors suggest that the thermal excitation hypothesis be rejected in favor a hopping mechanism with a variable hopping length.

It is of interest to examine the deviation of the temperature dependence of the resistivity from formula (3) in the region 100–185 K in relation to the temperature $T_{\max} \approx 185-190$ K at which the thermopower $\alpha(T)$ reaches its maximum. To within the experimental accuracy, both of the characteristic points, $T_{\max}$ and the boundary of the HT region, are nearly independent of pressure. When the temperature is decreased below ~ 185 K, a sharp decrease of the thermopower and a slowing of the rate of increase of the resistivity are observed. This indicates that a new mechanism, tending to increase the conductivity, comes into play at that temperature. We are inclined to attribute it to the appearance of FM clusters and double exchange. This mechanism will remain present as the temperature is decreased to T_{OO}, when the sample passes completely into the orbitally ordered FMI state.

From the plots of $\ln\rho=f(1/T^{1/4})$ we determined the phase transition T_0 for all pressures. The values of T_0 at atmospheric pressure for the LT ($T_0^{(lt)}=1.3\times10^8$ K) and HT ($T_0^{(ht)}=2.32\times10^8$ K) regions correlate with the data of Refs. 2 and 31. The characteristic temperature T_0, which determines the slope of the straight lines in Fig. 5a, depends on the state of the sample. On the high-temperature part of the graph the sample is found in the PMI state, and on the low-temperature part, in the FMI state. The fact that $T_0^{(lt)}<T_0^{(ht)}$ is apparently explained by the fact that the scattering of the carriers on the ordered spins in the FMI state is less than the scattering on the disordered spins in the PMI state. The pressure dependence of the temperature T_0 from samples with $x=0.1$ in the LT and HT regions is of an irregular character, but, on average, T_0 decreases with increasing pressure.

As to the anomalies of ρ and χ at the temperature $T_M \approx 120$ K there is as yet no unanimity of opinion. In Ref. 5 it is attributed to the formation of a spin glass. That conclusion was reached on the basis of an observation of a shift of the maximum of the magnetic susceptibility at 120 K to higher temperatures as the frequency of the modulating field was increased. We have conducted a similar experiment, varying the modulation frequency from 19 Hz to 10 kHz, and detected no such effect. We are inclined to regard the phase transition point at $T_M \approx 120$ K observed in the measurements of ρ and χ as being due not to the formation of a spin glass[5] but to a transition from a mixture of two phases O' and O^*, which, according to neutron diffraction studies,[29] coexist in a narrow temperature interval 120–140 K, to a single structural phase O^*.

The general form of the temperature dependence of the thermopower $\alpha(T)$ for $La_{1-x}Sr_xMnO_3$ with $x=0.1$ has been encountered previously for other perovskite structures. A similar character of the $\alpha(T)$ curve, with a broad maximum (hump) in the region 160–190 K, was observed by the authors previously in HTSC yttrium and mercury cuprates in the normal state. In the compound $YBa_2Cu_3O_{6.4}$ a value $T_{\max} \approx 190$ K was obtained.[32] In mercury cuprates the value of $T_{\max}$ increases with increasing number of CuO_2 planes, from 165 K for Hg-1223 to 195 K for Hg-1245.[33] The manganites and HTSC cuprates both have the perovskite structure, and the optical frequencies of their phonon spectra are close: 160–600 cm^{-1}. An attempt to explain the appearance of the broad maximum on the $\alpha(T)$ curves in HTSC cuprates as being due to a strong electron–lattice interaction and the formation of vibrons (correlated polaron theory) was made in Ref. 34. However, the real change of T_c, $\alpha_{\max}$, and $T_{\max}$ under pressure in the yttrium cuprates in many cases differs from the theory even in sign. But the great similarity of the behavior of $\alpha(T)$ in HTSC cuprates and manganites, in both of which the charge carriers are small and strongly localized, suggests that the explanation for this nevertheless lies in the strong electron–lattice interaction.

The anomalies which we have observed in experiments on the resistivity and thermopower in the region 220–235 K have also been observed in measurements on the propagation of sound with a frequency of 770 MHz in $La_{1-x}Sr_xMnO_3$ samples with $x=0.175$.[35] Since in the case which we investigated the transition occurs to the paramagnetic insulator phase, while in Ref. 35 it occurred to the ferromagnetic metal phase, this transition is most likely due to structural changes, e.g., to a decrease of the JT deformations of the lattice, and not to magnetic transformations.

CONCLUSIONS

1. The temperature dependence of the resistivity and magnetic susceptibility of a $La_{0.9}Sr_{0.1}MnO_3$ sample in the temperature region 90–300 K and at pressures up to 10 kbar has been found to exhibit features at $T \approx 100$, 120, and 135

K, which are identified as phase transition points. The temperature dependences of the resistivity and thermopower have an anomaly at $T \approx 220$ K.

2. In the temperature range 90–300 K the resistivity has a semiconductor trend.

3. In the temperature regions 90–110 and 185–300 K the conductivity is due to hops of the carriers with a variable hopping length.

4. The thermopower in the measured temperature range 150–300 K is positive and has a domelike shape with a maximum at a temperature $T_{\max} \approx 195$ K. The absolute value of α in this temperature interval decreases with increasing pressure $(\partial\alpha/\partial P < 0)$.

5. With increasing pressure all of the temperature points except the temperature T_p shift to higher temperatures, at rates of $\partial T_{CA}/\partial P = 0.43$ K/kbar and $\partial T_M/\partial P = 0.57$ K/kbar. These low rates apparently are evidence of a weak role of double exchange in the samples studied. The temperature T_p, which lies in the region 225–250 K, is apparently due to some structural transition, and it shifts to lower temperatures as the pressure is raised.

6. We obtained no evidence that the anomaly observed on the $\rho(T)$ and $\chi(T)$ curves at $T \approx 120$ K is due to the formation of a spin glass.

The authors thank the A. M. Abakumov Chemistry Department at Moscow State University for doing the iodometric analysis of the samples.

This study was supported by Grant No. 00-02-16019 of the Russian Foundation for Basic Research, the HTSC Program of the Russian Federation, and a grant from INTAS (Project No. 99.1136).

*E-mail: apetrova@ns.hppi.troitsk.ru

[1] L. P. Gor'kov, Usp. Fiz. Nauk **168**, 6,665 (1998).
[2] M. Paraskevopoulos, F. Mayr, J. Hemberger, A. Loidl, R. Heichele, D. Maurer, V. Muller, A. A. Muchin, and A. M. Balbashov, J. Phys.: Condens. Matter **12**, 3993 (2000).
[3] A. Urushibara, Y. Moritomo, T. Arima, A. Asamitsu, G. Kido, and Y. Tokura, Phys. Rev. B **51**, 14103 (1995).
[4] R. Senis, V. Laykhin, B. Martinez, J. Fontcuberta, X. Obradors, A. A. Arsenov, and Y. M. Mukovskii, Phys. Rev. B **57**, 14680 (1998).
[5] V. Skumryev, J. Nogues, J. S. Munoz, B. Martinez, R. Senis, J. Fortcuberta, L. Pinsard, A. Revcolevschi, and Y. M. Mukovskii, Phys. Rev. B **62**, 3879 (2000).
[6] É. L. Nagaev, JETP Lett. **8**, 297 (1967); Zh. Éksp. Teor Fiz. **54**, 228 (1968) [Sov. Phys. JETP **27**, 122 (1968)].
[7] É. L. Nagaev, JETP Lett. **16**, 394 (1972); V. A. Kashin and É. L. Nagaev, Zh. Éksp. Teor Fiz. **66**, 2105 (1974) [Sov. Phys. JETP **39**, 1036 (1974)]
[8] É. L. Nagaev, Usp. Fiz. Nauk **166**, 833 (1996).
[9] A. Moreo, S. Yunoki, and E. Dagotto, Science **283**, 2034 (1999).
[10] M. Yu. Kagan and K. I. Kugel', Usp. Fiz. Nauk **171**, 577 (2001).
[11] A. A. Mukhin, V. Yu. Ivanov, V. D. Travkin, S. P. Lebedev, A. Pimenov, A. Loidl, and A. M. Balbashov, JETP Lett. **68**, 356 (1998).
[12] M. Paraskevopoulos, F. Mayr, C. Hartinger, A. Pimenov, J. Hemberger, P. Lunkenheimer, A. Loidl, and A. A. Muchin, and V. Yu. Ivanov, J. Magn. Magn. Mater. **211**, 118 (2000).
[13] K. Glosh, R. L. Green, S. E. Lofland, S. M. Bhagat, S. G. Karabashev, D. A. Shulyatev, A. A. Arsenov, and Y. M. Mukovskii, Phys. Rev. B **58**, 8206 (1998).
[14] V. Yu. Ivanov, V. D. Travkin, A. A. Muchin, S. P. Lebedev, A. A. Volkov, A. Pimenov, A. Loidl, A. M. Balbashov, and A. V. Mozhaev, J. Appl. Phys. **83**, 7180 (1998).
[15] A. Pimenov, C. Hartinger, A. Loidl, A. A. Muchin, V. Yu. Ivanov, and A. M. Balbashov, Phys. Rev. B **59**, 12419 (1999).
[16] Y. Okimoto, T. Katsufuji, T. Arima, and Y. Tokura, Phys. Rev. B **55**, 4206 (1997).
[17] Yu. P. Gaĭdukov, N. P. Danilova, A. A. Mukhin, and A. M. Balbashov, JETP Lett. **68**, 153 (1998).
[18] A. E. Petrova, E. S. Itskevich, V. A. Ventcel', V. F. Kraidenov, and A. V. Rudnev, Fiz. Nizk. Temp. **27**, 1123 (2001) [Low Temp. Phys. **27**, 831 (2001)].
[19] A. M. Balbashov, S. G. Karabashev, Ya. M. Mukovskii, and S. A. Zverkov, J. Cryst. Growth **167**, 365 (1996).
[20] A. G. Budarin, V. A. Ventcel', O. A. Voronov, and A. V. Rudnev, Izmer. Tekh. **4**, 66 (1982).
[21] E. S. Itskevich, Prib. Tekh. Éksp. **4**, 148 (1963).
[22] Y. Yamada, O. Hino, S. Nohdo, R. Kanao, T. Inami, and S. Katano, Phys. Rev. Lett. **77**, 904 (1996); Y. Yamada, J. Suzuki, K. Oikawa, S. Katano, and J. A. Fernández-Baca, Phys. Rev. B **62**, 11600 (2000).
[23] S. L. Bud'ko, A. G. Gapotchenko, E. S. Itskevich, and V. F. Kraĭdenov, Prib. Tekh. Éksp. **5**, 189 (1986).
[24] P. G. Radaelli, G. Iannone, M. Marezio, H. Y. Hwang, S. W. Cheong, J. D. Jorgensen, and D. N. Argyriou, Phys. Rev. B **56**, 8265 (1997).
[25] L. Pinsard-Gaudart, J. Rodriguez-Carvajal, A. Daoud-Aladine, J. Goncharenko, M. Medarde, R. I. Smith, and A. Revcolevschi, Phys. Rev. B **64**, 064426 (2001).
[26] Guo-Meng Zhao, K. Conder, H. Keller, and K. A. Muller, Nature (London) **381**, 676 (1996).
[27] V. Laukhin, J. Fontcuberta, J. L. Garcia-Munoz, and X. Obradors, Phys. Rev. B **56**, R10009 (1997).
[28] E. S. Itskevich and V. F. Kraĭdenov, Fiz. Tverd. Tela (St. Petersburg) **43**, 1220 (2001) [Phys. Solid State **43**, 1267 (2001)].
[29] B. Dabrowski, X. Xiong, Z. Bukowski, R. Dybzinski, P. W. Klamut, J. E. Siewenie, O. Chmaissem, J. Shaffer, C. W. Kimball, J. D. Jorgensen, and S. Short, Phys. Rev. B **60**, 7006 (1999).
[30] N. F. Mott and E. A. Davis, *Electronic Processes in Non-Crystalline Materials*, Clarendon Press, Oxford (1971), Mir, Moscow (1982).
[31] J. Fontcuberta, B. Martínez, A. Seffar, S. Pinol, J. L. García-Múñoz, and X. Obradors, Phys. Rev. Lett. **76**, 1122 (1996).
[32] V. F. Kraidenov and E. S. Itskevich, Fiz. Nizk. Temp. **22**, 1028 (1996) [Low Temp. Phys. **22**, 784 (1996)].
[33] E. S. Itskevich, V. F. Kraĭdenov, and I. G. Kuzemskaya, Zh. Éksp. Teor Fiz. **118**, 647 (2000) [JETP **91**, 502 (2000)].
[34] J. B. Goodenough and J. S. Zhou, Phys. Rev. B **49**, 4251 (1994); J. S. Zhou and J. B. Goodenough, Phys. Rev. B **51**, 3104 (1995).
[35] Kh. G. Bogdanova, A. R. Bulatov, V. A. Golenishchev-Kutuzov, and M. M. Shakirzyanov, Fiz. Tverd. Tela (St. Petersburg) **43**, 1512 (2001) [Phys. Solid State **43**, 1572 (2001)].

Translated by Steve Torstveit

ELECTRONIC PROPERTIES OF METALS AND ALLOYS

Electronic structure and magneto-optical Kerr effect in $UCuAs_2$

V. N. Antonov[a),b)] and B. N. Harmon

Ames Laboratory, Iowa State University, Iowa, 50011

O. Horpynyuk

Institute of Metal Physics, 36 Vernadsky St., Kiev 03142, Ukraine

A. N. Yaresko

Max-Planck Institute for the Chemical Physics of Solids Nöthnitzer Str. 40, D-01187 Dresden, Germany

(Submitted June 17, 2002; revised July 30, 2002)
Fiz. Nizk. Temp. **29**, 47–52 (January 2003)

The optical and magneto-optical (MO) spectra of the ternary compound $UCuAs_2$ are investigated theoretically from first principles, using the fully relativistic Dirac linear-muffin-tin-orbital band structure method. The electronic structure is obtained with the local spin-density approximation (LSDA), as well as with the so-called LSDA+U approach. Better agreement between the theoretically calculated and the experimentally measured MO Kerr spectra is found with the LSDA+U approximation. The origin of the Kerr rotation in the compound is examined. © *2003 American Institute of Physics.* [DOI: 10.1063/1.1542375]

1. INTRODUCTION

Determination of the energy band structure of solids is a many-body problem. Band theory (a mean-field theory for treating this problem) in the framework of the local spin-density approximation (LSDA) has been successful for many kinds of materials and has become an exceptionally valuable tool for first-principles calculations in solid state physics. However, there are some systematic errors which have been observed when using the LSDA. In particular, the LSDA fails to describe the electronic structure and properties of $4f$ and some $5f$ electron systems in which the on-site Coulomb interaction among the electrons is strong. A wide variety of physical properties arise from the correlations among f electrons in these materials: metal—insulator transitions, valence fluctuations in the Kondo effect, heavy fermion behavior, superconductivity, and so on. Such materials are called strongly correlated electron systems. Many new concepts for addressing these phenomena have been proposed, and this is a field of very active research.

Actinide compounds occupy an intermediate position between itinerant $3d$ and localized $4f$ systems,[1,2] and one of the fundamental questions concerning actinide materials is whether their $5f$ states are localized or itinerant. This question is most frequently answered by comparison between experimental spectroscopies and the different theoretical descriptions. Indeed, recent progress in first-principles calculations of optical spectra illustrates that optical and magneto-optical (MO) spectra are developing into a powerful tool for tracing the electronic structure of actinide compounds. Both spectra depend quite sensitively on the underlying electronic structure, and can be utilized to assess the degree of localization of the $5f$ electrons. The basic supposition is that optical and MO spectra calculated with itinerant and localized electron models are sufficiently different and accurate that comparison with experimental spectra allows a meaningful assessment of the localization.

There are quite a few first-principles calculations of the MO spectra of uranium compounds.[3–8] The MO spectra of such compounds as UAsSe (Ref. 5) and U_3P_4 (Refs. 6 and 8) are well described in the LSDA, and we can conclude that they have at least partially itinerant electron behavior. On the other hand, the MO spectra in US, USe, and UTe can be well described only in the LSDA+U approximation,[7] supporting the localized description for their $5f$ electrons.

In our previous paper[9] we reported the theoretically calculated MO spectra of $UCuP_2$. Within a bandlike description of the $5f$ electrons, good agreement with the measured MO spectra was obtained. In this work we present a detailed theoretical investigation of the electronic structure and MO Kerr properties of the $UCuAs_2$ compound. The nearest-neighbor distance between uranium atoms is increased from 3.80 Å in $UCuP_2$ to 3.95 Å in $UCuAs_2$, and one would therefore expect an increase of the $5f$ localization in going from $UCuP_2$ to $UCuAs_2$.

Experimental measurements of MO spectra in $UCuAs_2$ were reported by Schoenes *et al.* in Ref. 10. It was found that the MO Kerr rotation in the ferromagnetic phase reaches a value as high as 1.75° at 1.2 eV. The Kerr ellipticity of $UCuAs_2$ has a maximum value of 1.1° at 2.3 eV.[10]

This paper is organized as follows. The computational details are given in Sec. 2. Section 3 presents the theoretical electronic structure and MO spectra of $UCuAs_2$. The results are then compared to the experimental data. Finally, the results are summarized in Sec. 4.

2. CRYSTAL STRUCTURE AND COMPUTATIONAL DETAILS

$UCuAs_2$ belongs to tetragonal As–Cu–Si–Zr crystal structure with the space group $P4/nmm$ (No. 129) with U at the $2c$ position, Cu at the $2b$ position, and As at the $2a$ and $2c$ positions. The lattice constants are $a=3.951$ Å, $c=9.558$ Å.[11] The unit cell of $UCuAs_2$ contains 8 atoms.

The details of the computational method are described in our previous paper,[9] and here we only mention several aspects. Self-consistent energy band-structure calculations of $UCuAs_2$ were performed by means of the fully relativistic, spin-polarized linear-muffin-tin-orbital (SPR LMTO) method using the atomic sphere approximation with combined corrections included.[12–16] The LSDA part of the energy band-structure calculations was based on the spin-density-functional theory with von Barth–Hedin parametrization[17] of the exchange-correlation potential. The **k**-space integrations were performed with the improved tetrahedron method[18] and the charge was obtained self-consistently with 270 irreducible **k** points. The basis consisted of U *s, p, d, f* and *g*; Cu *s, p, d* and *f*; As *s, p* and *d* LMTOs. We mention, lastly, that the Kramers–Kronig transformation was used to calculate the dispersive parts of the optical conductivity from the absorptive parts.

The application of standard LSDA methods to *f*-shell systems meets with problems in most cases because of the correlated nature of the *f* electrons. To account better for the on-site *f*-electron correlations, we have adopted as a suitable model Hamiltonian that of the LSDA+U approach.[19] The main idea is the same as in the Anderson impurity model:[20] the separate treatment of localized *f* electrons for which the Coulomb $f-f$ interaction is taken into account by a Hubbard-type term in the Hamiltonian $1/2U\sum_{i\neq j} n_i n_j$ (n_i are *f*-orbital occupancies), and delocalized *s, p, d* electrons for which the local density approximation is regarded as sufficient.

Let us consider the *f* ion as an open system with a fluctuating number of *f* electrons. The formula for the Coulomb energy of $f-f$ interactions as a function of the number of *f* electrons N given by the LSDA is $E=UN(N-1)/2$. If we subtract this expression from the LSDA total energy functional, add a Hubbard-like term and take into account the exchange interaction, we obtain the following functional [19]:

$$E=E_{LSDA}+\frac{1}{2}U\sum_{m,m',\sigma} n_{m\sigma}n_{m'-\sigma} + \frac{1}{2}(U-J)\sum_{m\neq m',m',\sigma} n_{m\sigma}n_{m'\sigma}-\text{d.c.}, \quad (1)$$

where

$$\text{d.c.}=U\frac{N(N-1)}{2}-\frac{JN^{\uparrow}(N^{\uparrow}-1)}{2}-\frac{JN^{\downarrow}(N^{\downarrow}-1)}{2},$$

N is the total number of localized *f* electrons, $N^{\uparrow}$ and $N^{\downarrow}$ are the number of *f* electrons with spin up and spin down, respectively, U is the screened Coulomb parameter, and J is the exchange parameter.

The orbital energies ε_i are derivatives of (1) with respect to the orbital occupations n_i:

$$\varepsilon_i=\frac{\partial E}{\partial n_i}=E_{LSDA}+(U-J)\left(\frac{1}{2}-n_i\right) =E_{LSDA}+U_{\text{eff}}\left(\frac{1}{2}-n_i\right). \quad (2)$$

This simple formula gives the shift of the LSDA orbital energy $-U_{\text{eff}}/2$ for occupied *f* orbitals ($n_i=1$) and $+U_{\text{eff}}/2$ for unoccupied *f* orbitals ($n_i=0$). A similar formula is found for the orbital-dependent potential $V_i(\mathbf{r})=\delta E/\delta n_i(\mathbf{r})$, where the variation is taken not on the total charge density $\rho(\mathbf{r})$ but on the charge density of a particular ith orbital $n_i(\mathbf{r})$:

$$V_i(\mathbf{r})=V_{LSDA}(\mathbf{r})+U_{\text{eff}}\left(\frac{1}{2}-n_i\right). \quad (3)$$

The advantage of the LSDA+U method is the ability to treat *simultaneously* delocalized conduction band electrons and localized *f* electrons in the same computational scheme. With regard to these electronic structure calculations, we mention that the present approach is still essentially a single-particle description, even though intra-atomic *f* Coulomb correlations are explicitly taken into account.

3. RESULTS AND DISCUSSION

The uranium pnictide ternary compounds with copper or nickel crystallize in a high-symmetry structure: $UCuP_2$, $UCuAs_2$, $UNiAs_2$ are tetragonal[21] and UCu_2P_2 and UCu_2As_2 are hexagonal.[22] The U–Cu ternaries order ferromagnetically, in contrast to the U–Ni ternaries, which are all antiferromagnets.[23] The magnetic ordering temperatures are among the highest known so far for uranium compounds, reaching 216 K for UCu_2P_2 (Ref. 24). The magnetic and transport properties of $UCuAs_2$ were investigated by Kaszorowski *et al.*[25] on single-crystal specimens. They found that the compound is a ferromagnet below 131 K with a spontaneous magnetic moment of 1.27 μ_B per U atom, and in the magnetically ordered region it exhibits large magnetocrystalline anisotropy constants. The electrical resistivity of $UCuAs_2$ at low temperature behaves as T^2, while in the temperature range above T_C the observed negative slope of $\rho(T)$ may point to Kondo lattice behavior.[25]

The energy dependence of the Kerr rotation and ellipticity of $UCuAs_2$ have been measured by Schoenes *et al.*[10] The measurements were made on a natural grown surface perpendicular to the *c* axis in the energy range 0.55 to 5 eV and at temperatures down to 2 K in an external magnetic field up to 10 T. Although $UCuAs_2$ has lower uranium concentration in comparison with the UX and U_3X_4 (X=P, As) compounds, its Kerr rotation reaches 1.75° (Ref. 10), which is the largest among these compounds.

The fully relativistic spin-polarized total and partial density of states (DOS) of ferromagnetic $UCuAs_2$ calculated in the LSDA approximation is shown in Fig. 1. The energy bands in the lowest region between −13.6 and −7.5 eV have mostly As *s* character, with some amount of U and Cu *spd* character mixed in. The energy bands between −7.5 and −1.0 eV are As $4p$ states strongly hybridized with the Cu $3d$ and U $6d$ states. There is a small energy gap between As *s* and *p* states. The Cu $3d$ states are fully occupied and situated around 5.0 eV below the Fermi level. The highest region

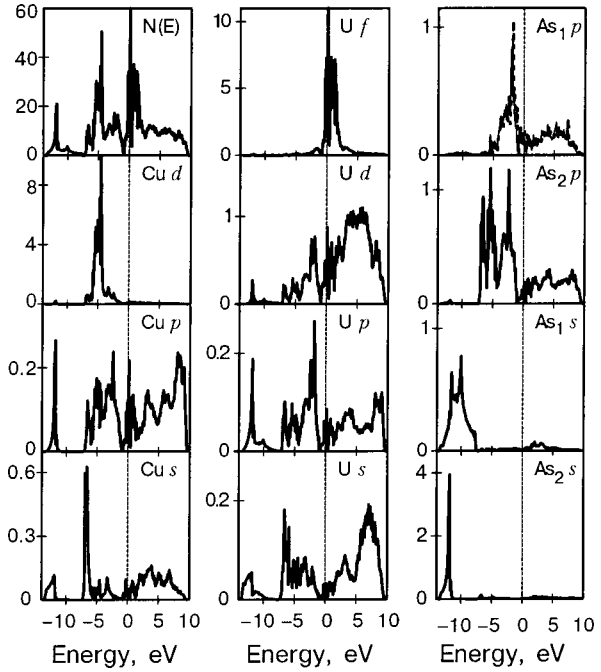

FIG. 1. Fully relativistic, spin-polarized total [in states/(unit cell·eV)] and partial densities of state [in states/(atom·eV)] calculated for $UCuAs_2$ in the LSDA approximation.

above the Fermi energy can be characterized by antibonding U $6d$ states. The U $5f$ energy bands in LSDA are located above and below E_F at about -0.5 to 1.5 eV. It is interesting to note that the $4p$ partial densities of states for As_1 and As_2 sites differ from each other significantly. This reflects the different geometrical positions of the two arsenic atoms. The plane with As_1 atoms is situated between uranium planes, whereas the plane with As_2 atoms is between uranium and copper planes. The As_1 atoms have as neighbors four As_1 atoms at 2.794 Å distance and four uranium atoms at 2.981 Å. On the other hand, the As_2 atoms have four Cu neighbor atoms at 2.513 Å distance and four uranium atoms at 2.965 Å. As a result, the $4p$ partial density of states for the As_1 site has one peak structure for occupied states, reflecting strong hybridization between the As_1 $3p$ and U $6d$ states, whereas the $4p$ partial density of states for the As_2 site has two additional peaks at -6.5 to 5 eV due to the hybridization of As_2 $3p$ states with Cu $3d$ states.

In our LSDA$+U$ band structure calculations we started the fully consistent iterations from a $5f^2$ configuration for the U^{4+} ion with two on-site $5f$ levels shifted downward by $U_{\text{eff}}/2$ and twelve levels shifted upwards by this amount. The energies of occupied and unoccupied $5f$ levels are separated by approximately U_{eff}. The Coulomb repulsion U_{eff} strongly influences the U $5f$ electronic states in $UCuAs_2$. The U $5f$ partial density of states calculated in the LSDA and LSDA $+U$ approximations are presented in Fig. 2.

After consideration of the above band structure properties we turn to the MO spectra. In Fig. 3 we show the calculated and experimental[10] MO Kerr rotation and ellipticity spectra of the $UCuAs_2$ compound. Better agreement between the calculated and the experimentally measured MO Kerr spectra was found when we used the LSDA$+U$ approximation. The prominent peak at 1.2 eV in the Kerr rotation spectrum originates mostly from U $5f \rightarrow 6d$ interband transitions. The interband transitions from Cu $3d$ to U $5f$ bands start above 4 eV. The LSDA calculations produce a two-peak

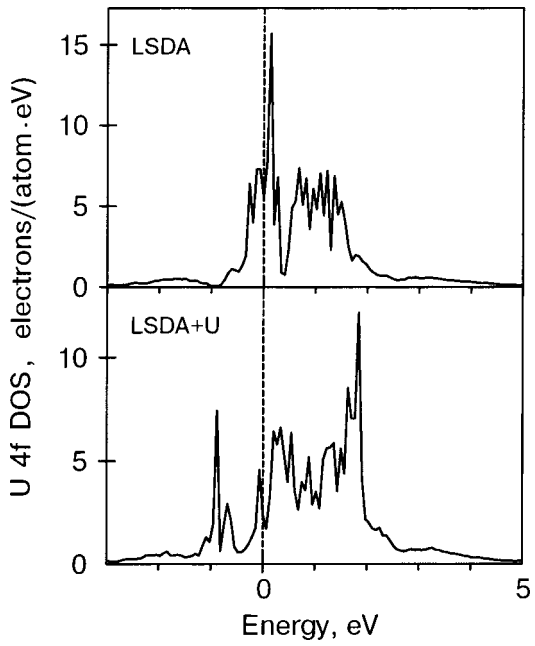

FIG. 2. Fully relativistic, spin-polarized U partial $5f$ densities of states calculated for $UCuAs_2$ in the LSDA and LSDA$+U$ approximations.

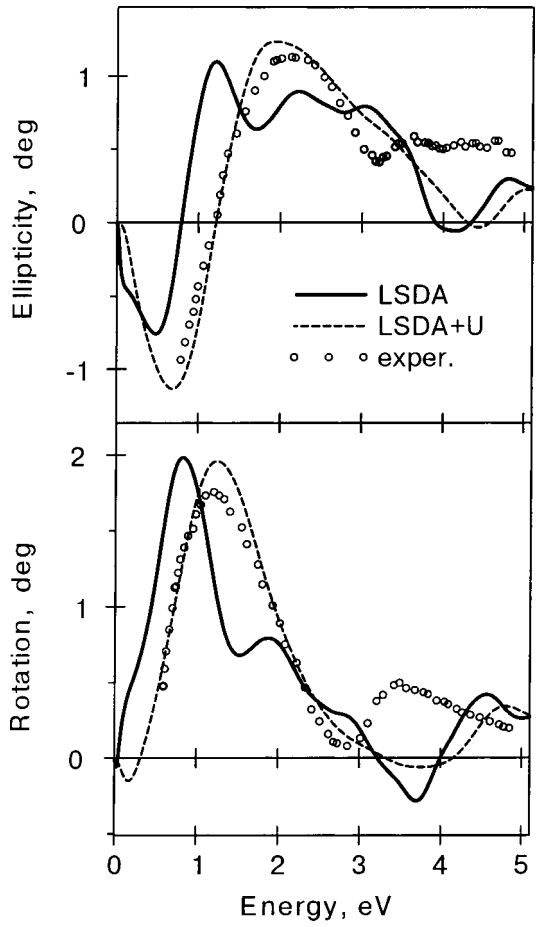

FIG. 3. Calculated and experimental Kerr ellipticity (ε_K) and Kerr rotation (θ_K) spectra of $UCuAs_2$. The experimental data are those of Ref. 10.

TABLE I. The experimental and LSDA calculated spin, orbital and total magnetic moments (in μ_B) of $UCuAs_2$. The experimental datum is from Ref. 10.

Atom	LSDA			LSDA + U			Experiment
	M_s	M_l	M_{total}	M_s	M_l	M_{total}	
U	−1.677	2.318	0.641	−2.135	4.123	1.988	1.27
Cu	−0.020	−0.002	−0.022	−0.017	−0.002	−0.019	
As_1	−0.003	0.002	−0.001	0.003	0.005	0.008	
As_2	−0.010	−0.018	−0.028	−0.008	−0.016	−0.024	

structure with the largest peak situated at 0.9 eV. The Coulomb repulsion U_{eff} shifts the energies of occupied $5f$ levels downwards and unoccupied ones upwards (Fig. 2); as a result, the LSDA+U calculations correctly produce the shape and energy position of the prominent peak in both the Kerr rotation and ellipticity spectra (Fig. 3). On the other hand, the theory, both in the LSDA and LSDA+U approximations, produces a blue energy shift by about 1 eV in the position of the local minimum and second high-energy peak in the Kerr rotation and ellipticity spectra in comparison with the experiment.

Table I presents a comparison between the calculated and experimental magnetic moments in $UCuAs_2$. The LSDA total magnetic moment on uranium in $UCuAs_2$ is only 0.641 μ_B (Table I) (with spin moment -1.677 μ_B and orbital moment 2.318 μ_B), which is considerably smaller than the experimental moment of about 1.27 μ_B.[10] The calculated moment is dominated by $5f$ states: the $5f$ components of the spin and orbital moment are -1.569 μ_B and 2.283 μ_B, respectively. It is a well-known fact, however, that within the LSDA the total magnetic moment of uranium compounds in general comes out too small.[26–30] Corrections which simulate Hund's second rule interactions in solids, describing orbital correlations absent in the homogeneous electron gas, such as the orbital polarization, are needed to bring the magnetic moment into better agreement with experiment.[27–30] On the other hand, our LSDA+U calculations overestimate the total magnetic moment in $UCuAs_2$ compound (Table I). We should mentioned that it is still not clear how to choose the projections m_l of the orbital momentum onto the spin direction if we have more than one occupied state. From total energy calculations we found that the U^{4+} ground state corresponds to values of the projection of the orbital momentum onto the spin direction equal to $m_l=-3$ and -2, in accordance with all three Hund's rules. The value of the magnetic moment and MO spectra depends strongly on the m_l, and it may be better to regard the values of the m_l as parameters and try to specify them from comparison of the calculated physical properties with experiment. We performed calculations for every possible combination of the m_l and found that the best agreement between the calculated and measured MO spectra can be achieved with $m_l=-3$ and -2 for U^{4+} in $UCuAs_2$ (in accordance with Hund's rules and total energy calculations). These values give the magnetic moments presented in Table I. On the other hand, the theoretically calculated magnetic moments are in better agreement with the experiment for $m_l=\pm 2$ (total magnetic moment at the U site equal to 1.029 μ_B, with spin and orbital magnetic moments equal to -1.144 and 2.173 μ_B, respectively). Evaluation of the correct magnetic moment in this compound needs further theoretical investigation.

4. SUMMARY

The spectral behavior of the MO Kerr spectra in $UCuAs_2$ is better described by LSDA+U band-structure theory than by the LSDA. This fact indicates that the U $5f$ electrons in the ternary $UCuAs_2$ are likely to be partly localized, in contrast to $UCuP_2$, where the U $5f$ electrons are itinerant.[19] This supports the conclusion drawn early by Schoenes *et al.*[10] that the localization of the f states is increased in going from $UCuP_2$ to $UCuAs_2$.

[a]E-mail: antonov@ameslab.gov; anton@imp.kiev.ua
[b]Permanent address: Institute of Metal Physics, 36 Vernadsky St., Kiev 03142, Ukraine

[1] J. D. Becker, J. M. Wills, L. Cox, and B. R. Cooper, Phys. Rev. B **54**, 17265R (1996).
[2] L. M. Sandratskii and J. Kübler, Phys. Rev. B **55**, 11395 (1997).
[3] T. Kraft, P. M. Oppeneer, V. N. Antonov, and H. Eschrig, Phys. Rev. B **52**, 3561 (1995).
[4] B. R. Cooper, S. P. Lim, I. Avgin, Q. G. Sheng, and D. L. Price, J. Phys. Chem. Solids **56**, 1509 (1995).
[5] P. M. Oppeneer, M. S. S. Brooks, V. N. Antonov, T. Kraft, and H. Eschrig, Phys. Rev. B **53**, 10437R (1996).
[6] J. Köhler, L. M. Sandratskii, and J. Küber, Phys. Rev. B **55**, 10153R (1997).
[7] P. M. Oppeneer, V. N. Antonov, A. Ya. Perlov, A. N. Yaresko, T. Kraft, and H. Eschrig, Physica B **230–232**, 544 (1997).
[8] V. N. Antonov, B. N. Harmon, A. N. Yaresko, and A. Ya. Perlov, Phys. Rev. B **59**, 14571 (1999).
[9] O. Horpynyuk, V. V. Nemoshkalenko, V. N. Antonov, B. N. Harmon, and A. N. Yaresko, Fiz. Nizk. Temp. **28**, 745 (2002) [Low Temp. Phys. **28**, 533 (2002)].
[10] J. Schoenes, P. Fumagalli, H. Rüegsegger, and D. Kaczorowski, J. Magn. Magn. Mater. **81**, 112 (1989).
[11] P. Villars and L. D. Calvert, *Pearson's Handbook of Crystallographic Data for Intermetallic Phases*, ASM International, Materials Park (1991).
[12] H. Ebert, Phys. Rev. B **38**, 9390 (1988).
[13] O. K. Andersen, Phys. Rev. B **12**, 3060 (1975).
[14] V. V. Nemoshkalenko, A. E. Krasovskii, V. N. Antonov, Vl. N. Antonov, U. Fleck, H. Wonn, and P. Ziesche, Phys. Status Solidi B **120**, 283 (1983).
[15] V. N. Antonov, A. Ya. Perlov, A. P. Shpak, and A. N. Yaresko, J. Magn. Magn. Mater. **146**, 205 (1995).
[16] V. V. Nemoshkalenko and V. N. Antonov, *Computational Methods in Solid State Physics*, Gordon and Breach, London (1998).
[17] U. von Barth and L. A. Hedin, J. Phys. C: Solid State Phys. **5**, 1692 (1972).
[18] P. E. Blöchl, O. Jepsen, and O. K. Andersen, Phys. Rev. B **49**, 16223 (1994).
[19] V. I. Anisimov, J. Zaanen, and O. K. Andersen, Phys. Rev. B **44**, 943 (1991).

[20] P. W. Anderson, Phys. Rev. **124**, 41 (1961).
[21] Z. Zolnierek, D. Kaczorowski, and R. Troc, J. Less-Common Met. **128**, 265 (1987).
[22] Z. Zolnierek, H. Nöel, and D. Kaczorowski, J. Less-Common Met. **132**, 265 (1987).
[23] W. Reim and J. Schöenes, in *Ferromagnetic Materials*, edited by E. P. Wohlfarth and K. H. J. Buschow. North-Holland, Amsterdam (1990), Vol. 5, p. 133.
[24] Z. Zolnierek, D. Kaczorowski, R. Troc, and H. Nöel, J. Less-Common Met. **121**, 193 (1986).
[25] D. Kaczowski, R. Troc, and H. Noöl, J. Phys.: Condens. Matter **3**, 4959 (1991).
[26] M. S. S. Brooks and B. Johansson, in *Handbook of Magnetic Materials*, edited by K. H. J. Buschow, North-Holland, Amsterdam (1993), Vol. 7, p. 139.
[27] M. S. S. Brooks, Physica B **130**, 6 (1985).
[28] O. Eriksson, M. S. S. Brooks, and B. Johansson, Phys. Rev. B **41**, 7311 (1990).
[29] L. Severin, M. S. S. Brooks, and B. Johansson, Phys. Rev. Lett. B **71**, 3214 (1993).
[30] Mavromaras, L. Sandratskii, and J. Kübler, Solid State Commun. **106**, 115 (1998).

This article was published in English in the original Russian journal. Reproduced here with stylistic changes by AIP.

Acoustoelectric conversion at a metal boundary. Taking the surface scattering of carriers into account

V. M. Gokhfeld*

A. A. Galkin Donetsk Physicotechnical Institute, ul. R. Lyuksemburg 72, 83114 Donetsk, Ukraine
(Submitted July 22, 2002)
Fiz. Nizk. Temp. **29**, 53–57 (January 2003)

The electric potential arising at a metal surface deformed by ultrasound is calculated for the diffuse reflection of conduction electrons by the surface. The frequency dependence obtained for the conversion coefficients (in the case of both a free and a fixed sample boundary) are compared with the results of a simplified theory which assumes specular reflection of the carriers by the surface. © *2003 American Institute of Physics.* [DOI: 10.1063/1.1542376]

INTRODUCTION

Low-temperature measurements of the electric potential arising on a metal surface when a longitudinal sound wave is incident on it (from the opposite face of the sample) were reported in Refs. 1 and 2.[1)]

The effect is linear in the interaction of electrons with crystal lattice vibrations and can be used for a comparative estimate of the constants characterizing the deformation potential in different metals, including the new ''synthetic'' conductors.[3] However, the theoretical analysis in Refs. 1 and 2 presupposes that the crystal has an ideal boundary that reflects conduction electrons specularly, and that makes it difficult to compare the data for different samples in a meaningful way. In real crystals there is always scattering (stronger or weaker) of charge carriers by defects of the boundary, and its role in surface phenomena is hard to assess on general considerations: for example, for the skin effect and cyclotron resonance it is not very important,[4,5] whereas in the conductivity of thin films or in the static skin effect in a magnetic field it can change the order of magnitude of the observable quantities.[6,7] Therefore, although the agreement of the theoretical and experimental data in Ref. 2 turned out to be acceptable, it is important to explore even the tendency of an influence of surface relaxation of carriers on the effect under discussion. With this goal, in the present study we have undertaken a calculation of acoustoelectric conversion in a metal in the case of strong, ''diffuse'' surface scattering of electrons, a completely isotropic distribution of reflected particles. As in Ref. 2, we assume that the sample is thick with respect to the sound wavelengths $2\pi s/\omega$ and the carrier mean free path $l=v_F\tau$, so that the mathematical problem is formulated for a conducting half space ($x\geqslant 0$) with a specified field of harmonic longitudinal strains $u'(x)$ in it.[2)] We chose the Wiener–Hopf method for solving this problem.

CONVERSION COEFFICIENTS

Since we are talking about ultrasonic frequencies, certainly much lower than the plasma frequency of a ''good'' metal, the latter can to good accuracy be assumed electrically neutral, so that the electric potential $\varphi(x)$ should be determined from the condition

$$\langle\psi\rangle\equiv 2(2\pi h)^{-3}\int \psi dS_F/v=0.$$

The distribution function of nonequilibrium carriers ψ satisfies the kinetic equation

$$v_x(\psi-e\varphi)'-i\tilde{\omega}\psi=-i\omega\Lambda u', \tag{1}$$

where $\mathbf{v}$ is the velocity of an electron on the Fermi surface S_F, $\tilde{\omega}\equiv\omega+i/\tau$, where τ is the relaxation time characterizing the bulk scattering of carriers, and $\Lambda(\mathbf{p})$ is the xx component of the (reduced) deformation potential tensor; in the case when the carriers have a quadratic dispersion relation it can be written in the form $\Lambda(v_x)=L(3v_x^2/v_F^2-1)$ (see Ref. 8).

Introducing $\alpha\equiv i\tilde{\omega}/|v_x|$ and solving equation (1) for the function $\Psi\equiv\chi-e\varphi$, we have

$$\Psi_>(x)=\Psi_>(0)e^{\alpha x}+\int_0^x dy e^{\alpha(x-y)}\alpha \times\left(e\varphi(y)-\frac{\omega}{\tilde{\omega}}\Lambda u'(y)\right),$$

$v_x>0$;

$$\Psi_<(x)=\int_x^\infty dy e^{\alpha(y-x)}\alpha\left(e\varphi(y)-\frac{\omega}{\tilde{\omega}}\Lambda u'(y)\right),\quad v_x<0. \tag{2}$$

In the case of diffuse surface scattering one should set $\Psi_>(0)=\text{const}$, and from the condition of electrical neutrality we obtain the following integral equation for the potential $\varphi(x)$:

$$\varphi(x)\langle 1\rangle-+\left\langle\int_0^\infty dy e^{\alpha|x-y|}\alpha\left(\varphi(y)-\frac{\omega\Lambda}{\tilde{\omega}e}u'(y)\right)-Ce^{\alpha x}\right\rangle=0. \tag{3}$$

The Fourier transforms of the kernels of equation (3) (divided by the energy density of states $\langle 1\rangle$) are easily calculated as

$$K_1(k)=\frac{k_0}{2k}\ln\frac{k_0-k}{k_0+k};$$

$$K_2(k)=\frac{\omega L}{\tilde{\omega}e}\left(1+(1+K_1)\left(3\frac{k_0^2}{k^2}-1\right)\right);\quad k_0\equiv\frac{\tilde{\omega}}{v_F}. \tag{4}$$

However, Eq. (3) is specified only on the semiaxis $x\geqslant 0$, and for the Fourier transformation one should, using the Wiener–Hopf method (see, e.g., Ref. 9), extend the definition of the functions appearing in it to negative values of x by introducing step functions containing the Heaviside θ function

$$\varphi_+(x)\equiv\theta(x)\frac{\tilde{\omega}e}{\omega L}\varphi(x),\varphi_-(x)\propto\theta(-x),$$

continuing the free term in an odd way for $x<0$ and choosing the following function as a new, more convenient kernel:

$$K(k)\equiv\left(1-3\frac{k_0^2}{k^2}\right)(1+K_1(k)). \tag{5}$$

In the k representation we obtain the functional equation

$$\left(ik\frac{C_1+ik\varphi_+(k)}{k^2-3k_0^2}-D_+(k)\right)K(k)=\varphi_-(k)-D_+(k), \tag{6}$$

where C_1 is a constant proportional to C, and

$$D_+(k)=\frac{q^2u_0-iku_0'}{\overline{k^2}-q^2} \tag{7}$$

is the transform of the harmonic elastic deformation field

$$D_+(x)\equiv\theta(x)(u_0'\cos(qx)-qu_0\sin(qx))$$

in a semi-infinite sample with specified boundary values of the displacements u_0 and their derivatives u_0', $q\equiv\omega/s$ is the wave number, s is the speed of sound, and $\overline{k}=k-i0$.

Then in the Wiener–Hopf method the Fourier transform of the kernel, $K(k)$, is separated into factors $K_+(k)$ and $K_-(k)$, which are regular and do not have zeros in the lower and upper halves of the complex k plane, respectively, and these regions overlap in a strip covering the whole real axis.[3)]

As a result, Eq. (6) can be written in the form of an equality of two expressions which also have such properties and, consequently, are the analytic continuations of each other.[4)]

In other words, the two of them equal an entire function, in this case a polynomial, the coefficients of which can be determined by using the asymptotic expressions and particular values of the functions appearing in (6). In particular, in Eqs. (4)–(6) obviously imply that $\lim_{k\to 0}\varphi_-=0$, i.e., the auxiliary function $\varphi_-(x)$ is on average equal to zero.

In principle the problem can be solved for a general mechanical boundary condition, but for the sake of simplicity we shall consider only the extremal cases of a fixed and a free boundary. In the first of these cases $u_0=0$ (see (7)), and for the reduced functions $\Phi_\pm(k)\equiv(u_0')^{-1}\varphi_\pm(k)$ equation (6) takes the form

$$\left(\frac{C_2+ik\Phi_+}{k-k_0\sqrt{3}}(\overline{k^2}-q^2)-k+k_0\sqrt{3}\right)K_+(k)$$
$$=\left(1+\Phi_-\frac{\overline{k^2}-q^2}{ik}\right)\frac{k+k_0\sqrt{3}}{K_-(k)}=qB_0+kB_1. \tag{8}$$

The polynomial here should be such a one, since for $k\to 0$ the left-hand side goes to a constant $C_2q^2/k_0\sqrt{3}+k_0\sqrt{3}$, and for $k\to\infty$ the limits of the functions $ik\Phi_+(k)$ and $ik\Phi_-(k)$ are finite (and equal to the boundary values of the originals $\Phi_+(x)$ and $-\Phi_-(x)$). Further, the function $\Phi_-(k)$ by definition is regular at the points $k=\pm q-i0$, so that the coefficients on the right-hand side of (8) are equal to

$$B_0=A(a)+S(a)\sqrt{3}/a;\quad B_1=S(a)+A(a)\sqrt{3}/a,$$

where we have introduced the dimensionless variable $z\equiv k/k_0$, the frequency-dependent parameter

$$a(\omega\tau)\equiv\frac{q}{k_0}\equiv\frac{v_F}{s}\frac{\omega\tau}{\omega\tau-i}, \tag{9}$$

and (taking into account the parity of the kernel) the functions

$$A(z)\equiv[K_+(z)-K_-(z)]/2zK(z);$$
$$S(z)\equiv[K_+(z)+K_-(z)]/2K(z). \tag{10}$$

As a result, the Fourier transform of the solution is given by the expression

$$ik\Phi_+(k)=\frac{k-k_0\sqrt{3}}{\overline{k^2}-q^2}\left(\frac{qB_0+kB_1}{K_+(k)}-k-k_0\sqrt{3}\right)-C_2 \tag{11}$$

with the coefficients B_0, B_1, and C_2 already defined; its limit for $k\to\infty$, as is known, gives the boundary value of the original $\Phi_+(x\to+0)$.[5)]

Returning to the initial unknown function $\varphi(k)$, we obtain the desired potential of the deformed surface of the sample; it can be written in the form

$$e\varphi_{\text{fix}}(+0)=u_0'L\frac{s}{v_F}F(a),$$
$$F(a)\equiv(3/a-a)(1-S(a)). \tag{12}$$

Now let the boundary of the sample be free, $u_0'=0$ [see (7)]. We shall omit the manipulations, which are analogous to those given above, and just write the result:

$$e\varphi_{\text{free}}(+0)=iqu_0L\frac{s}{v_F}G(a),$$
$$G(a)\equiv(a^2-3)A(a)+3A(0). \tag{13}$$

The factors F and G can be called the reduced coefficients of conversion of the elastic field into the electric potential measured at the boundary of the metal. At a fixed sound intensity in the sample it is those factors that, through the parameter $a(\omega\tau(T))$ [see (9)], determine the frequency dependence and temperature dependence of the effect. However, the results (12) and (13) as yet have a formal character: it is necessary to calculate the quantities $A(0)$, $A(a)$, and $S(a)$ [see (10)]. For this we can use the standard general procedure of factorization of the kernel;[9] however, the integral formulas thus obtained are rather complicated and are really only usable for numerical calculations. Nevertheless, in the limiting cases characterized by small and large absolute values of the parameter a it turns out to be possible to do a direct factorization of the limiting expressions for the

function $K(k)$; that makes it possible to calculate the asymptotic expressions for the surface potential $\varphi_{\text{fix}}(+0)$ and $\varphi_{\text{free}}(+0)$ at low and high frequencies.

ASYMPTOTIC FACTORIZATION

Let us first consider the so-called local limit $|a| \ll 1$ $(ql \ll 1)$. Using the series expansion of the function (5), for small values of the argument we write it in the required form:

$$K(z) \cong 1 + \frac{4}{15} z^2 + \ldots = \prod_{\pm} \left(1 \pm \frac{2i}{\sqrt{15}} z \right) \equiv K_+(z) K_-(z),$$

where the signs are chosen such that (by definition) the root of $K_+(k)$ lies in the upper half of the k plane and that of $K_-(k)$ in the lower half. In this case the values sought for the functions in (10) are

$$A(0) = 2i/\sqrt{15};$$

$$A(a) \cong A(0)(1 - 4a^2/15);$$

$$S(a) \cong 1 - 4a^2/15. \tag{15}$$

The approximate factorization of the kernel is just as obvious at large arguments: with an accuracy up to corrections $\propto z^{-2}$ we can write

$$K(z) \cong \left(1 + \frac{\ln(1-z)}{2z} \right) \left(1 - \frac{\ln(1+z)}{2z} \right) \equiv K_+(z) K_-(z)$$

[see Eqs. (4) and (5)], so that in the nonlocal limit for $|a| \gg 1$ $(ql \gg 1)$ we have

$$S(a) \cong 1 - \frac{1}{4a} \ln \frac{1-a}{1+a}; \quad A(a) \cong \frac{1}{4a^2} \ln(1-a^2). \tag{16}$$

RESULTS AND DISCUSSION

Substituting (15) into the general formulas (12) and (13), we find in the local range

$$F(a) \cong \frac{4}{5} a; G(a) \cong \frac{6}{5} \sqrt{\frac{3}{5}} i a^2, |a| \equiv \left| \frac{v_F}{s} \frac{\omega\tau}{\omega\tau + i} \right| \ll 1. \tag{17}$$

At the same sound intensity in the sample, i.e., at comparable absolute values of u_0' and qu_0, the second term contains an additional small factor $ia \approx ql$: in the low-frequency region the potential of the fixed boundary is much higher than that of the free boundary.

In the nonlocal region of frequencies formulas (12), (13), and (16) imply that

$$F(a) \cong \frac{1}{4} \ln \frac{1+a}{1-a}; \quad G(a) \cong \frac{\ln(1-a^2)}{4} - 2i \sqrt{\frac{3}{5}},$$

$$|a| \gg 1. \tag{18}$$

Here, on the contrary, at sufficiently large $|a|$ the conversion coefficient is much larger (in modulus) for the case of a free boundary (see Fig. 1). Consequently, in the general case, i.e., at finite values of the ratio $|qu_0/u_0'|$, which characterizes the degree of mobility of the boundary, with increasing value of that ratio the effect should become weaker at low frequencies and stronger at high frequencies.

Let us compare these asymptotic expressions with the results obtained[1,2] in neglect of the surface scattering of carriers.[6)]

In our present notation they have the form

$$F_0(a) = \frac{a}{1 - K_1(a)} + \frac{3}{a} - a;$$

$$G_0(a) = \int_1^\infty \frac{4a^2}{a^2 - z^2} \frac{z\,dz}{\left(2z + \ln \dfrac{z-1}{z+1} \right)^2 + \pi^2}. \tag{19}$$

At small $|a|$ the conversion coefficients are approximately equal to $F_0 \cong (4/5)a$ for a fixed boundary and $G_0 \cong -0.345a^2$ for a free boundary, i.e., they coincides "functionally" with the asymptotic expression (17); however, in the latter case the numerical coefficient in (17) differs significantly in modulus (0.93) and phase.

The high-frequency asymptotic forms of expressions (19) are

$$F_0(a) \cong \frac{1}{2} \ln \frac{1+a}{a-a} \approx -\frac{i\pi}{2}$$

and

$$G_0(a) \cong \frac{1}{2} \ln(1-a^2) \approx \frac{i\pi}{2} + \ln|a| (|a| \gg 1);$$

for $|a| \to \infty$ this would be double the corresponding "diffuse" coefficients (18).

Thus we can conclude that for both types of mechanical boundary conditions considered, taking the surface scattering of electrons into account does not *qualitatively* alter the char-

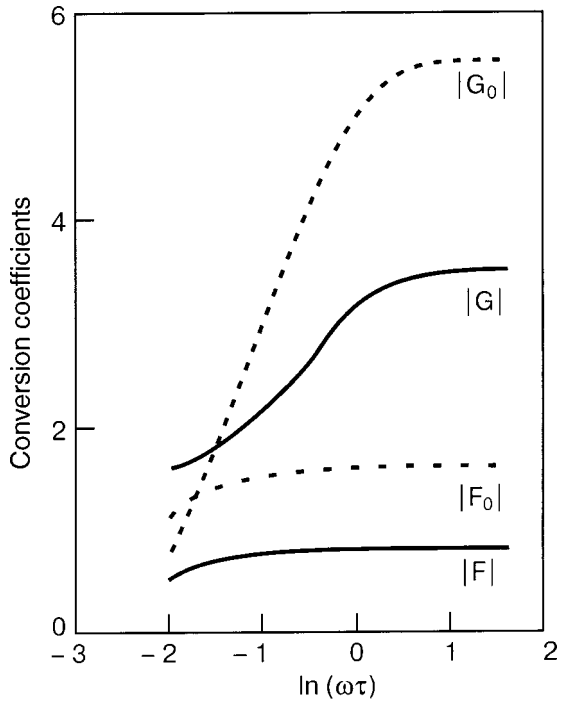

FIG. 1. Comparison (in absolute value) of the high-frequency dependences of the conversion coefficients in the case of diffuse (—) and specular (---) reflection of carriers by the surface of the sample. F corresponds to a fixed surface, and G to a mechanically free surface; $\omega\tau \gg s/v_F$; the parameter $s/v_F = 0.005$.

acter of the frequency dependence of the absolute values of the conversion coefficients (Fig. 1). Nevertheless, *numerically* the effect should be noticeably increased (in the case of a free boundary) at low frequencies and decreased (in both cases) at high frequencies in comparison with the ideal situation of specular surface reflection of carriers. This agrees with the tendency observed in Ga at $\omega\tau\sim 5$: ''The maximum response at a fixed excitation power could be attained only for freshly ground surfaces; prolonged storage of a sample led to a falloff of the signal amplitude, apparently because of diffusion of impurities into the subsurface region.'' [2]

In addition, for a free boundary the conversion coefficients (G) in (17) and (18) differ in phase from the corresponding asymptotic behavior of the ''specular'' expression (19), i.e., surface scattering, generally speaking, has an influence on the phase relations between the acoustic oscillations and the electrical oscillations engendered by them.

The author is grateful to V. G. Peschanskii and V. D. Fil for fruitful discussions which stimulated this study.

[1)]The potential difference was measured by a contact method or a capacitive coupling between the ''acoustic spot'' on the surface of the sample and points far from it, where there was no deformation.

[2)]The common temporal factor $\exp(-i\omega t)$ is omitted here and below.

[3)]As we see from Eq. (4), the function (5) is even in the complex k plane with branch cuts along the rays $k=\pm k_0 y$, $1\leqslant y<\infty$; it is regular and does not have zeros in the strip $|\mathrm{Im}\, k|<1/l$, and it approaches 1 at both large and small values of k.

[4)]The first and second parts of (8) are simultaneously analytical in the strip $-l^{-1}<\mathrm{Im}\, k<+0$.

[5)]As we see from Eq. (11), the electric field distribution in a finite sample is nontrivial: as in the ''specular'' case, in addition to a term similar to the elastic field (the ''acoustic'' pole) there is a nonlocal part associated with the branch point $k=k_0$ of the function K_+. This is the contribution of the ballistic motion of the carriers, which can be observed in hf pulse experiments as a precursor of the signal proportional to $u'(x)$ (see Ref. 1). However, in the present paper we are interested only in the value of the potential at the surface, measured in an effectively monochromatic regime.

[6)]In the approach adopted in the present paper, those results are obtained when the ''specular'' boundary condition $\Psi_>(0)=\Psi_<(0)$ is substituted into (2). Then the integral equation of electrical neutrality has a more symmetric form than (3), and after even continuation of the functions and kernels to the semiaxis $x<0$ it can be solved directly by the Fourier method.

*E-mail: gokhfeld@host.dipt.donetsk.ua

[1] V. M. Gokhfeld and V. D. Fil, Fiz. Tekh. Vysokikh Davlenii **11**, No. 4, 76 (2001).
[2] Yu. A. Avramenko, E. V. Bezuglyi, N. G. Burma, V. M. Gokhfeld, I. G. Kolobov, V. D. Fil, and O. A. Shevchenko, Fiz. Nizk. Temp. **28**, 469 (2002) [Low Temp. Phys. **28**, 328 (2002)].
[3] J. Vosnitza, *Fermi Surfaces of Low-Dimensional Organic Metals and Superconductors*, Vol. 134 of Springer Tracts of Modern Physics (1996).
[4] G. E. Reuter and E. H. Sondheimer, Proc. R. Soc. London, Ser. A **195**, 336 (1948).
[5] L. E. Hartmann and J. M. Luttinger, Phys. Rev. **151**, 430 (1966).
[6] K. Fuchs, Proc. Cambridge Philos. Soc. **34**, 100 (1938).
[7] V. G. Peschanskiĭ, JETP Lett. **7**, 375 (1968).
[8] V. M. Kontorovich, Usp. Fuz. Nauk **142**, 265 (1984) [Sov. Phys. Usp. **27**, 134 (1984)].
[9] B. Noble, *Methods Based on the Wiener-Hopf Technique*, Pergamon Press, Oxford (1958), IL, Moscow (1962).

Translated by Steve Torstveit

LOW-DIMENSIONAL AND DISORDERED SYSTEMS

Single-particle scenario of the metal–insulator transition in two-dimensional systems at $T=0$

Yu. V. Tarasov

Institute of Radio Physics and Electronics, National Academy of Sciences of Ukraine, ul. akad. Proskury 12, 61085 Kharkov, Ukraine

(Submitted May 6, 2002; revised July 30, 2002)
Fiz. Nizk. Temp. **29**, 58–70 (January 2003)

The conductance of disordered electron systems of finite size is calculated by reducing the initial dynamical problem of arbitrary dimensionality to strictly one-dimensional problems for single-particle mode propagators. It is shown that the metallic ground state of two-dimensional conductors, considered as a limiting case of three-dimensional quantum waveguides, is due to their multimode nature. As the thickness of the waveguide is decreased, e.g., with the aid of a ''pressing'' potential, the electron system undergoes a sequence of continuous quantum phase transitions involving a discrete change in the number of extended modes. The closing of the last current-carrying mode is interpreted as a phase transition of the electron system from the metallic to an insulator state. The results agree qualitatively with the observed ''anomalies'' of the resistance of various two-dimensional electron and hole systems. © *2003 American Institute of Physics.* [DOI: 10.1063/1.1542377]

1. INTRODUCTION

The problem of electron transport in disordered conductors has attracted research interest for many years, both on account of its importance in connection with applications and because of the intriguing complexity of the fundamental problems that arise in this area. One such problem, which has yet to be solved unambiguously, is to explain the nature of an unusual phenomenon observed in two-dimensional electron and hole systems, which many investigators interpret as a metal–insulator transition (MIT) caused by disorder. The unusual behavior of the conductance of planar heterostructures in experimental observations (see the vast bibliography in Ref. 1) is clearly at odds with the widely held conviction that in two-dimensional (2D) systems, as in one-dimensional (1D) systems, a metallic ground state cannot exist in the presence of even arbitrarily small disorder.[2] This point of view still remains prevalent, even though, to accommodate the experimental facts, the one-parameter scaling approach[2] has already been subjected to both a partial refinement[3,4] and a radical revision.[5]

There have been repeated attempts to explain the ''anomalous'' metallic behavior of 2D systems in the low-temperature region by invoking various physical hypotheses. Among them are the onset of a conducting phase in highly dilute electron systems,[6,7] non-Fermi-liquid behavior of such systems,[8] the possibility of a superconducting state of a 2D electron gas with interaction,[9,10] temperature-dependent screening of impurity scattering,[11,12] and others. However, the fundamental issue of whether the observed anomalies of the resistance are a manifestation of a true quantum phase transition[13] or whether they can be explained in the framework of the conventional theory of disordered systems[14] remains an open question.

In the present paper we propose a model for explaining the observed effects. It is in essence a realization of the concept of quantum dephasing of the electronic states as a result of their interaction with a certain ''dephasing environment,'' the state of which is not determined in the course of the experiment.[15] It is ordinarily assumed that the loss of coherence by the electrons in conductors with a *static* disorder is due to conventional truly inelastic interaction processes (electron–phonon, electron–electron, etc.), so that the dephasing frequency due to these types of interactions tends toward zero as the temperature is lowered. However, publications over the past few years show a lack of agreement as to the physical nature of the dephasing environment.[16] Most often a quasi-elastic electron–electron interaction is considered to be the main mechanism for dephasing of the initially coherent (presumably localized) electronic states, since the ''anomalous'' behavior of the resistance is registered mainly in 2D systems of low density ($r_s \gtrsim 10$, where $r_s = E_{e-e}/E_F$ is the ratio of the Coulomb energy of the electrons to their Fermi energy). However, the role of this interaction is interpreted differently in different theories—both as promoting localization[17,18] and as preventing its appearance.[6,7,19]

Meanwhile, it was shown in Refs. 20 and 21 that dephasing of quantum states classified with allowance for the finiteness of a real dynamical system can be brought about not only by inelastic processes but also by scattering on static inhomogeneities. For proof, a mode representation of the single-particle propagators was used,[20,21] which is best suited for analyzing *open* quantum systems of a waveguide configuration. An important fact here is that in reference to electrons in solids the mode states are *collective* and therefore well suited for describing a highly correlated systems of current carriers. The correlated nature of that system, even be-

fore the Coulomb interaction is taken into account, is built in from the start in the Green's function formalism, which explicitly incorporates the Pauli principle.[22]

It was shown in Refs. 20 and 21 that in 2D conductors that are not too narrow, when more than one extended mode is present (or, in other words, when there is more than one open quantum channel), the scattering between such modes, if it is not suppressed by virtue of some special conditions, will lead to dephasing of the coherent modes states and prevent their interference localization. Here the role of the dephasing environment for each of the channels is played by the set of all the other open channels of that conductor. If intermode scattering is absent, as is the case for conductors which are randomly layered in the current direction, then Anderson localization of the electronic states arises in each of the channels independently. This results in an exponential decrease of the conductance with increasing length of the conductor when the latter exceeds a value of the order of $N_c\ell$, where N_c is the number of open channels and ℓ is the quasi-classical mean free path of the electrons, which is well known in the theory of quasi-one-dimensional conductors.[23–26]

Although the results of Refs. 20 and 21 imply that the metallic ground state of a two-dimensional statically disordered systems should not be regarded as an anomalous effect, the mechanism of the transition of 2D systems from the conducting to the insulating state, which observed in numerous experiments, was not identified in those papers. To elucidate the physical nature of the metal–insulator transition in planar structures, in the present paper (a brief version of which was published previously in Ref. 27) we propose to adapt the formulation of the problem to the real conditions of the experiment by extending the method of Refs. 20 and 21, which was developed previously for strictly two-dimensional open systems, to systems of higher dimensionality. This is motivated by the fact that in practice, 2D systems are most often formed by using subsurface potential wells of finite width, created either by applying an external ''pressing'' electric field or by means of a contact potential difference.

2. CHOICE OF MODEL AND STATEMENT OF THE PROBLEM

Conductors of reduced dimensionality (one-dimensional and two-dimensional) serve as a mathematical idealization of real physical objects which are three-dimensional in a geometric sense. Potential wells formed by the bending of the energy bands in a contact region between different materials (see, e.g., Fig. 1a) form a subsurface quantum waveguide of finite width, the *two-dimensional* density of current carriers in which is ordinarily varied by means of an external potential Φ_d (depletion voltage) or by a capacitive effect. The shape of the subsurface wells (in the majority of cases it is close to triangular)[19,28] is not of fundamental importance for their main function—restricting the electron transport in the direction perpendicular to the heterointerface. Therefore, in this paper we will simplify the calculations by considering a model planar conductor in the form of a rectangular three-dimensional ''electron waveguide'' having rigid side walls (Fig. 1b) and occupying the spatial region

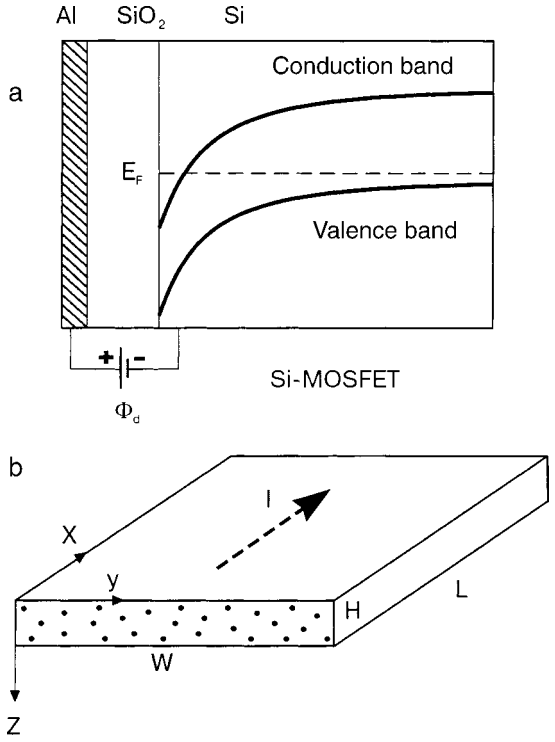

FIG. 1. Real (a) and model (b) configurations of a two-dimensional conducting system.

$$x\in(-L/2,L/2),\quad y\in[-W/2,W/2],\quad z\in[-H/2,H/2]. \tag{1}$$

The length L of the conductor and the width W and thickness H of the waveguide will be treated as arbitrary.

From linear response theory[29] the dimensionless (in units of $e^2/\pi\hbar$) static conductance $g(L)$ at $T=0$ is expressed as follows in terms of the single-particle electron propagators:

$$g(L)=\frac{2}{L^2}\int\int d\mathbf{r}d\mathbf{r}'\frac{\partial}{\partial x}[G^A(\mathbf{r},\mathbf{r}')-G^R(\mathbf{r},\mathbf{r}')]$$

$$\times\frac{\partial}{\partial x'}[G^A(\mathbf{r}',\mathbf{r})-G^R(\mathbf{r}',\mathbf{r})]. \tag{2}$$

Here $G^{R,A}(\mathbf{r},\mathbf{r}')$ are the retarded (R) and advanced (A) Green's functions of the electrons, and the integration is over the spatial region (1) occupied by the waveguide. In the model of an isotropic Fermi liquid when units such that $\hbar=2m=1$, where m is the effective mass of the electrons) are used, the retarded propagator, from which we shall henceforth drop the superscript R, satisfies the equation

$$[\Delta+k_F^2+i0-V(\mathbf{r})]G(\mathbf{r},\mathbf{r}')=\delta(\mathbf{r}-\mathbf{r}'). \tag{3}$$

Here Δ is the three-dimensional Laplacian, k_F is the Fermi wave number, $V(\mathbf{r})$ is a static random potential characterized by a zero mean value $\langle V(\mathbf{r})\rangle=0$ and a binary correlation function $\langle V(\mathbf{r})V(\mathbf{r}')\rangle=\mathcal{Q}\mathcal{W}(\mathbf{r}-\mathbf{r}')$. The function $\mathcal{W}(\mathbf{r})$ is assumed to be normed to unity and to fall off over a characteristic scale r_c (the correlation radius). To simplify the formulas below, we restrict discussion to a correlation function of a somewhat less general form, viz.,

$$\langle V(\mathbf{r})V(\mathbf{r}')\rangle=\mathcal{Q}\mathcal{W}(x-x')\delta(\mathbf{r}_\perp-\mathbf{r}'_\perp),\quad \mathbf{r}_\perp=(y,z), \tag{4}$$

which clearly should not affect the results materially.

The solution of equation (3) requires specifying suitable boundary conditions. The side boundaries, which are impermeable to electrons, can be characterized by a real impedance, a particular case of which leads to the Dirichlet conditions

$$G(\mathbf{r},\mathbf{r}')\Big|_{\substack{y=\pm W/2\\ z=\pm H/2}}=0. \tag{5}$$

At the same time, being joined at the points $x=\pm L/2$ to equilibrium ''reservoirs,'' the conductor is an *open* system, and this has two important consequences. First, in Kubo theory the chemical potentials of the massive contacts are assumed to be identical. Therefore, the chemical potential of the conductor connecting them (or, in the conducting phase, the Fermi energy of the electrons in it) can be assumed to be independent of the geometric parameters of the quantum waveguide, and everywhere below we set $k_F=\text{const}$. Second, the openness of the ends of the waveguide makes for a *complex* characteristic of the impedance of the contact regions, and because of this the differential operation in Eq. (3) when applied to system (1) is non-Hermitian.

A method of solving such a non-Hermitian problem in the case of two dimensions was proposed in Refs. 20 and 21. An important step in it is the transition from one initially multidimensional stochastic problem to an infinite system of strictly one-dimensional problems (which are in general non-Hermitian) for the mode Fourier components of the propagator $G(\mathbf{r},\mathbf{r}')$. Below we set forth in more detail the key elements of the technique of Refs. 20 and 21 as applied to the waveguide system under study.

3. REDUCTION TO ONE DIMENSION

3.1. General scheme

The proposed algorithm for the reduction of the multidimensional problem (3) to a system of strictly one-dimensional boundary-value problems will be applied to open systems with arbitrary waveguide configurations and with arbitrary levels of disorder. The first step is to change to a mode representation of the electron propagators. In the case of the waveguide illustrated in Fig. 1b, one changes to this representation by expanding in a complete orthonormalized set of eigenfunctions $|\mathbf{r}_\perp;\boldsymbol{\mu}\rangle$ of the transverse Laplacian operator. This set is made up of ordinary trigonometric functions; for configuration (1) and boundary conditions (5), these functions have the form

$$|\mathbf{r}_\perp;\boldsymbol{\mu}\rangle=\frac{2}{\sqrt{WH}}\sin\left[\left(\frac{y}{W}+\frac{1}{2}\right)\pi n\right]\sin\left[\left(\frac{z}{H}+\frac{1}{2}\right)\pi m\right], \tag{6}$$

where $\boldsymbol{\mu}=(n,m)$ is a vector mode index ($n,m\in\mathcal{N}$). Using the functions (6), one transforms Eq. (3) into a system of coupled equations for the mode components of the Fourier function $G(\mathbf{r},\mathbf{r}')$:

$$\left[\frac{\partial^2}{\partial x^2}+\kappa_{\boldsymbol{\mu}}^2+i0-V_{\boldsymbol{\mu}}(x)\right]G_{\boldsymbol{\mu}\boldsymbol{\mu}'}(x,x')$$

$$-\sum_{\boldsymbol{\nu}\neq\boldsymbol{\mu}}U_{\boldsymbol{\mu}\boldsymbol{\nu}}(x)G_{\boldsymbol{\nu}\boldsymbol{\mu}'}(x,x')=\delta_{\boldsymbol{\mu}\boldsymbol{\mu}'}\delta(x-x'). \tag{7}$$

In Eq. (7) the parameter

$$\kappa_{\boldsymbol{\mu}}^2=k_F^2-(\pi n/W)^2-(\pi m/H)^2 \tag{8}$$

has the meaning of the unperturbed longitudinal energy of the mode $\boldsymbol{\mu}$. The potential matrix $\|U_{\boldsymbol{\mu}\boldsymbol{\mu}'}\|$ is made up of the functions

$$U_{\boldsymbol{\mu}\boldsymbol{\mu}'}(x)=\sum_S d\mathbf{r}_\perp|\mathbf{r}_\perp;\boldsymbol{\mu}\rangle V(\mathbf{r})\langle\mathbf{r}_\perp;\boldsymbol{\mu}'|, \tag{9}$$

where the integration is done over the transverse cross section S of the conductor. The diagonal elements of this matrix, $V_{\boldsymbol{\mu}}(x)\equiv U_{\boldsymbol{\mu}\boldsymbol{\mu}}(x)$ are the Fourier components of the potential $V(\mathbf{r})$ due to the intramode scattering of quantum particles, and the off-diagonal elements are those due to the intermode scattering. The reason for separating off the terms with the ''intramode'' potentials from the terms with the ''intermode'' potentials $U_{\boldsymbol{\mu}\boldsymbol{\nu}}(x)$ ($\boldsymbol{\nu}\neq\boldsymbol{\mu}$) in Eq. (7) is to avoid singularities later on when constructing a perturbation theory (see Ref. 21).

The initial problem, reformulated into a system of one-coordinate differential equations (7) cannot, of course, be considered to be one-dimensional, because of the entanglement of all the mode components of the Green's matrix $\|G_{\boldsymbol{\nu}\boldsymbol{\mu}}\|$. With the goal of reducing Eq. (3) to a system of *independent* one-dimensional equations, we introduce as a first step the auxiliary mode propagators, which take into account the scattering on only the intramode potentials:

$$\left[\frac{\partial^2}{\partial x^2}+\kappa_{\boldsymbol{\mu}}^2 i0-V_{\mu}(x)\right]G_{\boldsymbol{\mu}}^{(V)}(x,x')=\delta(x-x'). \tag{10}$$

For the ''trial'' Green's functions $G_{\boldsymbol{\mu}}^{(V)}(x,x')$ the condition that the quantum waveguide is open at the ends $x=\pm L/2$ can be formulated as Sommerfeld radiation conditions,[30,31] which in the case of an ideal (not conducive to scattering) contact of a conductor with the leads has the form

$$\left(\frac{\partial}{\partial x}\mp i\kappa_{\boldsymbol{\mu}}\right)G_{\boldsymbol{\mu}}^{(V)}(x,x')\Big|_{x=\pm L/2}=0,\quad x'\in(-L/2,L/2). \tag{11}$$

Assuming that the solution of the problem (10), (11) is known, we change from the differential equation (7) to an integral equation:

$$G_{\boldsymbol{\mu}\boldsymbol{\mu}'}(x,x')=G_{\boldsymbol{\mu}}^{(V)}(x,x')\delta_{\boldsymbol{\mu}\boldsymbol{\mu}'}$$

$$+\sum_{\boldsymbol{\nu}\neq\boldsymbol{\mu}}dx_1,R_{\boldsymbol{\mu}\boldsymbol{\nu}}(x,x_1)G_{\boldsymbol{\nu}\boldsymbol{\mu}'}(x_1,x'), \tag{12}$$

whose kernel

$$R_{\boldsymbol{\mu}\boldsymbol{\nu}}(x,x')=G_{\boldsymbol{\mu}}^{(V)}(x,x')U_{\boldsymbol{\mu}\boldsymbol{\nu}}(x') \tag{13}$$

contains only intermode harmonics of the scattering potential. From system (12) all of the off-diagonal elements of the matrix $\|G_{\boldsymbol{\nu}\boldsymbol{\mu}}\|$ can be expressed in terms of the corresponding

diagonal elements $G_{\mu\mu}$ with the aid of a certain linear operator $\hat{K}$, which is defined on the coordinate–mode space $M=\{x,\nu\}$,

$$G_{\nu\mu}(x,x')=\int_L dx_1,\ K_{\nu\mu}(x,x_1)G_{\mu\mu}(x_1,x'),\quad \nu\neq\mu. \tag{14}$$

The matrix elements $K_{\nu\mu}(x,x')$ can be found from the Lippmann–Schwinger equation:[32]

$$K_{\nu\mu}(x,x')=R_{\nu\mu}(x,x') + \sum_{\nu_1\neq\mu}\int_L dx_1 R_{\nu\nu_1}(x,x_1)K_{\nu_1\mu}(x_1,x'), \tag{15}$$

the solution of which in operator form $\hat{K}=(1-\hat{R})^{-1}\hat{R}$ is expressed in terms of the operator $\hat{R}$, which is represented on M by the matrix elements (13).

We note that since the sums (12) and (15) do not contain terms with the mode index μ, the operator $\hat{R}$ can be interpreted as the intermode scattering operator, which operates in a reduced coordinate–mode space $\overline{M}_\mu$ containing all the modes of the quantum waveguide except μ. The presence of the mode index μ in the kernel of the integral operator (14) and in other cases when necessary will be provided by the projection operator $\mathbf{P}_\mu$, the action of which is to assign the fixed value μ to the nearest mode index of an arbitrary operator standing next to it (either to the left or right).

Assuming that $\mu'=\mu$ in Eq. (7) and substituting the intermode propagators in the form (14), we finally arrive at a closed *one-dimensional* differential equation for the diagonal propagator $G_{\mu\mu}(x,x')$:

$$\left[\frac{\partial^2}{\partial x^2}+\kappa_\mu^2+i0-V_\mu(x)-\hat{\mathcal{T}}_\mu\right]G_{\mu\mu}(x,x')=\delta(x-x'). \tag{16}$$

Here, together with the *local* intramode potential $V_\mu(x)$, there has arisen an effective *nonlocal* (operator in x space) potential

$$\hat{\mathcal{T}}_\mu=\mathbf{P}_\mu\hat{\mathcal{U}}(1-\hat{R})^{-1}\hat{R}\mathbf{P}_\mu=\mathbf{P}_\mu\hat{\mathcal{U}}(1-\hat{R})^{-1}\mathbf{P}_\mu, \tag{17}$$

where $\hat{U}$ is the intermode potential operator, which is defined on $\overline{M}_\mu$ by the matrix elements

$$|x,\mu\rangle\hat{\mathcal{U}}\langle x'\nu|=U_{\mu\nu}(x)\,\delta(x-x'). \tag{18}$$

Strictly speaking, the potential $\hat{\mathcal{T}}_\mu$, like $V_\mu(x)$, is *intramode* in the sense that both the initial and final states of the scattering on it belong to the mode μ. However, it effectively also takes *intermode* scattering into account, and exactly, in any order of perturbation theory. From the structure of expression (17) it is seen that scattering on the potential operator $\hat{\mathcal{T}}_\mu$ can be interpreted as occurring via intermediate "trial" modes states described by the propagators $G_\nu^{(V)}(x,x')$ with $\nu\neq\mu$. Therefore, in what follows we shall by convention call the potential $\hat{\mathcal{T}}_\mu$ as the intermode potential. From a mathematical standpoint it is none other than the T matrix, well known in the quantum theory of scattering.[32,33]

In the finishing stage of the procedure of reducing the multidimensional problem of the conductance of system (1) to a one-dimensional problem (16), we express the conductance (2) directly in terms of the function $G_{\mu\mu}(x,x')$. Expanding the electron propagators in the eigenfunctions (6), we separate out two terms in expression (2). In the first, which we shall refer to below as the "diagonal" conductance and denote it as $g^{(d)}(L)$, we group together those terms of the expansion which from the beginning contain the diagonal mode propagators $G_{\mu\mu}$. In the second term, the "off-diagonal" conductance $g^{(nd)}(L)$, we combine all the remaining terms of the expansion, which contain mode components $G_{\nu\mu}$ with $\nu\neq\mu$. Taking relation (14) into account along with the fact that the retarded and advanced Green's functions of the evanescent modes ($\kappa_\mu^2<0$) in the case of weak scattering can be considered to be real-valued (see formula (23) in the next Section), the aforementioned conductance terms can be written in the form

$$g^{(d)}(L)=-\frac{4}{L^2}\overline{\sum_\mu}\int\int_L dx\,dx'\,\frac{\partial G_{\mu\mu}(x,x')}{\partial x}\,\frac{\partial G'_{\mu\mu}(x,x')}{\partial x'}; \tag{19a}$$

$$g^{(nd)}(L)=-\frac{4}{L^2}\overline{\sum_{\substack{\mu,\nu\\ \nu\neq\mu}}}\int\int\int\int_L dx_1\ldots dx_4\frac{\partial K_{\nu\mu}(x_1,x_2)}{\partial x_1} \times G_{\mu\mu}(x_2,x_4)K^*_{\nu\mu}(x_1,x_3)\frac{\partial G^*_{\mu\mu}(x_3,x_4)}{\partial x_4}. \tag{19b}$$

Here and below a bar over a summation sign means that the summation is only over *extended* modes with $\kappa_\mu^2>0$.

3.2. Weak scattering approximation

In view of the statistical formulation of the problem, an important auxiliary element of the technique used, the trial Green's function $G_\mu^{(V)}(x,x')$, can be considered to be determined exactly if all of its mathematical moments $\langle[G_\mu^{(V)}(x,x')]^p\rangle$, $p\in\mathcal{N}$, have been found. For highly disordered systems this can be done only by numerical methods. However, if the scattering on the potential $V(\mathbf{r})$ is weak, then by using the technique described in Ref. 21, which allows one to take into account multiple scattering in the 1D stochastic problem (10), (11), these moments can be found analytically. The criterion of weak scattering is expressed as a system of inequalities

$$k_F,\quad \mathbf{r}_c\ll\ell, \tag{20}$$

where ℓ denotes the Born mean free path of the electrons. In the particular case of a strictly white-noise potential, when $\mathcal{W}(x)=\delta(x)$ in (4), this length is equal to $4\pi/Q$. When conditions (20) are satisfied, the calculation of the desired moments for extended modes gives

$$\left\langle[G_\mu^{(V)}(x,x')]^p=\left(\frac{-i}{2\kappa_\mu}\right)^p\exp\left[ip\kappa_\mu|x-x'|\frac{p}{2} \times\left(\frac{p}{L_f^{(V)}(\mu)}+\frac{1}{L_b^{(V)}(\mu)}\right)|x-x'|\right]. \tag{21}$$

Here $L_{f,b}^{(V)}(\boldsymbol{\mu})$ are the forward (f) and backward (b) scattering lengths of mode $\boldsymbol{\mu}$ on the intermode potential $V_{\boldsymbol{\mu}}(x)$:

$$L_f^{(V)}(\boldsymbol{\mu})=\frac{4S}{9\mathcal{Q}}(2\kappa_{\boldsymbol{\mu}})^2,$$

$$L_b^{(V)}(\boldsymbol{\mu})=\frac{4S}{9\mathcal{Q}}\frac{(2\kappa_{\boldsymbol{\mu}})^2}{\tilde{\mathcal{W}}(\kappa_{\boldsymbol{\mu}})},$$

where $\tilde{\mathcal{W}}(\kappa_{\boldsymbol{\mu}})$ is the Fourier transform of the function $\mathcal{W}(x)$. As to the inhomogeneous (evanescent) modes with $\kappa_{\boldsymbol{\mu}}^2<0$, for them one can neglect the potential $V_{\boldsymbol{\mu}}(x)$ in (10) in the case of weak scattering, and consider only the unperturbed solution:

$$G_{\boldsymbol{\mu}}^{(V)}(x,x')=-\frac{1}{2|\kappa_{\boldsymbol{\mu}}|}\exp(-|\kappa_{\boldsymbol{\mu}}||x-x'|). \tag{23}$$

The functional structure of the T matrix (17) and, accordingly, of Eq. (16) under condition (20) is substantially simplified. A direct calculation with the use of (13) and (21) shows that the norm of the operator $\hat{R}$ on a space of basis functions $\exp(i\kappa_{\boldsymbol{\mu}}x)$ is estimated by the following parameter

$$\|\hat{R}\|^2\sim\frac{1}{\kappa_{\boldsymbol{\mu}}\ell}. \tag{24}$$

This allows one to replace the operator $\hat{K}$ defined in (15) by its approximate value $\hat{K}\approx\hat{R}$. As a result, potential (17) takes the form

$$\hat{\mathcal{T}}_{\boldsymbol{\mu}}=\mathbf{P}_{\boldsymbol{\mu}}\hat{\mathcal{U}}\hat{\mathcal{G}}^{(V)}\hat{\mathcal{U}}\mathbf{P}_{\boldsymbol{\mu}}, \tag{25}$$

where the operator $\hat{\mathcal{G}}^{(V)}$ is defined on $\overline{M}_{\boldsymbol{\mu}}$ by the matrix elements

$$|x,\boldsymbol{\nu}\rangle\hat{\mathcal{G}}^{(V)}(x',\boldsymbol{\nu}'|=G_{\boldsymbol{\nu}}^{(V)}(x,x')\delta_{\boldsymbol{\nu}\boldsymbol{\nu}'}. \tag{26}$$

An analogous replacement of the exact matrix elements of the operator $\hat{K}$ in (19b) by their approximate values allows one to conclude that in the case of weak scattering the off-diagonal part of the conductance $g^{(nd)}(L)$ is parametrically small in comparison with its diagonal part $g^{(d)}(L)$. Further confirmation of the correctness of such an estimate is provided by the result of a numerical calculation of the two conductance terms. When this circumstance is taken into account, we can confine our analysis to only the term in (19a), assuming $g(L)\approx g^{(d)}(L)$.

4. ANALYSIS OF THE SPECTRUM OF MODE STATES

In contrast to the initial potential $V(\mathbf{r})$ and, accordingly, its mode components in Eq. (7), the effective potential $\hat{\mathcal{T}}_{\boldsymbol{\mu}}$ has a nonzero mean. For application to a perturbation theory in this potential, we separate it into its averaged and fluctuating parts, $\langle\hat{\mathcal{T}}_{\boldsymbol{\mu}}\rangle$ and $\Delta\hat{\mathcal{T}}_{\boldsymbol{\mu}}-\langle\hat{\mathcal{T}}_{\boldsymbol{\mu}}\rangle$. As the zeroth approximation for the mode propagator $G_{\boldsymbol{\mu}\mu}(x,x')$, we consider the Green's function of the equation

$$\left[\frac{\partial^2}{\partial x^2}+\kappa_{\boldsymbol{\mu}}^2+i0-\langle\hat{\mathcal{T}}_{\boldsymbol{\mu}}\rangle\right]G_{\boldsymbol{\mu}\boldsymbol{\mu}}^{(0)}(x,x')=\delta(x-x'), \tag{27}$$

which differs from (16) by the absence of fluctuating potentials. In determining the action of the operator $\langle\hat{\mathcal{T}}_{\boldsymbol{\mu}}\rangle$ on the function $G_{\boldsymbol{\mu}\boldsymbol{\mu}}^{(0)}(x,x')$, it is an important circumstance that for a waveguide with ''rigid'' side walls there is no correlation of the intermode and intramode scattering:

$$\langle U_{\boldsymbol{\mu}\boldsymbol{\nu}}(x)V_{\boldsymbol{\nu}}(x')\rangle=0. \tag{28}$$

As a consequence of this, the potential (25) upon averaging is transformed from an operator equation to an effectively local equation. It was shown in Ref. 21 that its operation reduces to a renormalization of the mode energy $\kappa_{\boldsymbol{\mu}}^2$ by the mass operator $\Sigma(\kappa_{\boldsymbol{\mu}})=\Delta\kappa_{\boldsymbol{\mu}}^2+i/\tau_{\boldsymbol{\mu}}^{(\varphi)}$:

$$(\langle\hat{\mathcal{T}}_{\boldsymbol{\mu}}\rangle\hat{G}_{\boldsymbol{\mu}\boldsymbol{\mu}}^{(0)}(x,x')=-\Sigma(\kappa_{\boldsymbol{\mu}})G_{\boldsymbol{\mu}\boldsymbol{\mu}}^{(0)}(x,x'). \tag{29}$$

Applying to the system under study the calculation procedure set forth in Ref. 21, we find

$$\Delta\kappa_{\boldsymbol{\mu}}^2\frac{\mathcal{Q}}{S}\sum_{\boldsymbol{\nu}\neq\boldsymbol{\mu}}\mathcal{P}\int_{-\infty}^{\infty}\frac{dq}{2\pi}\frac{\tilde{\mathcal{W}}(q+\kappa_{\boldsymbol{\mu}})}{q^2-\kappa_{\boldsymbol{\nu}}^2}, \tag{30a}$$

$$\frac{1}{\tau_{\boldsymbol{\mu}}^{(\varphi)}}=\frac{\mathcal{Q}}{4S}\overline{\sum_{\boldsymbol{\nu}\neq\boldsymbol{\mu}}}\frac{1}{\kappa_{\boldsymbol{\nu}}}[\tilde{\mathcal{W}}(\kappa_{\boldsymbol{\mu}}-\kappa_{\boldsymbol{\nu}})+\tilde{\mathcal{W}}(\kappa_{\boldsymbol{\mu}}+\kappa_{\boldsymbol{\nu}})]. \tag{30b}$$

The integral in (30a) is understood in the principal value sense.

The absolute value of the mass operator (30) does not depend substantially on the number of open channels in the conductor. For any $N_c>1$ the estimate $\Delta\kappa_{\boldsymbol{\mu}}^2\sim 1/\tau_{\boldsymbol{\mu}}^{(\varphi)}\sim k_F/\ell$ is valid, and that allows one to neglect the renormalization of the velocity due to the term in (30a) for almost all of the modes. At the same time, the width of the mode levels is of critical importance for analysis of the electron dynamics. The frequency (30b) saturates rapidly with increasing N_c and ceases to depend on the mode index. In particular, in the model of point scatterers the asymptotic behavior of this frequency for $N_c\gg 1$ has the form

$$\frac{1}{\tau_{\boldsymbol{\mu}}^{(\varphi)}}\approx\frac{\mathcal{Q}k_F}{4\pi}=\frac{k_F}{\ell}. \tag{31}$$

We note that in formula (30b), unlike (30a), the summation is only over extended modes of the quantum waveguide which are different from the mode $\boldsymbol{\mu}$ in question. For a single-channel conductor, where only the lowest mode $\boldsymbol{\mu}_1=(1,1)$ is nonlocal, the term (30b) is absent.

The imaginary part of the mass operator (30) can be interpreted as being the result of a dephasing of the coherent mode states. It follows from the structure of expression (30b) that for an arbitrary mode $\boldsymbol{\mu}$ the cause of the dephasing is the cyclic (''reentrant'') scattering of electrons exclusively via nonlocal intermediate modes if such modes exist in the system under study. In such an interpretation, for each of the current-carrying modes one would be justified in treating all the other extended modes of the same conductor as a sort of ''dephasing environment,'' the interaction with which is brought about by means of intermode scattering on the potential $V(\mathbf{r})$. Although in terms of the one-electron energy the scattering on static inhomogeneities is elastic (for $T=0$ this energy is always the Fermi energy), the *many-particle* mode states are characterized by different (longitudinal) energies. This allows one to consider the virtual intermode transitions ''hidden'' in the $\mathcal{T}$ matrices (17) and (25) as effec-

tively inelastic, thereby upholding the traditional point of view that attributes the dephasing of the quantum states exclusively to inelastic scattering processes.

We note that intermode scattering by strongly localized *evanescent* intermediate modes alone (single-mode conductor) will not lead to dephasing. An appreciable dephasing effect appears in the scattering of electrons via substantially nonlocal extended modes, as is possible, of course, if there are at least two of them. From this we can conclude that for an interference type of Anderson localization an important factor is that not only the temporal coherence but also the spatial coherence is preserved in the scattering.

The influence of the fluctuational potentials $V_{\mu}(x)$ and $\Delta\hat{\mathcal{T}}_{\mu}$ on the mode levels can be analyzed by estimating the corresponding Born scattering frequencies $1/\tau_{\mu}^{(V)}$ and $1/\tau_{\mu}^{(V)}$. With allowance for the structure of operator (25) and the result (31), we have

$$\frac{\tau_{\mu}^{(\varphi)}}{\tau_{\mu}^{(V)}}\sim[k_F\mathbf{r}_c N_c\cos^2\theta_{\mu}]^{-1}, \tag{32a}$$

$$\frac{\tau_{\mu}^{(\varphi)}}{\tau_{\mu}^{(\mathcal{T})}}\sim\frac{\tau_{\mu}^{(\varphi)}}{\tau_{\mu}^{(V)}}\times\begin{cases}L/\ell, & L<\ell,\\ N_{\mathrm{loc}}^{(s)}, & L>l.\end{cases} \tag{32b}$$

Here θ_{μ} is the "slip" angle of the mode $\boldsymbol{\mu}$ ($\cos\theta_{\mu}=|K_{\mu}|/k_F$); and $N_{\mathrm{loc}}^{(s)}\leqslant N_c$ is the number of "bare" mode states, determined by Eq. (10), whose localization length $4L_b^{(V)}(\boldsymbol{\mu})$ does not exceed the length L of the conductor.

Since in real materials the relation $k_F r_c\geqslant 1$ is usually satisfied, it is easily inferred from (32) that the influence of the potential $V_{\mu}(x)$ on the dynamics of electrons in multimode systems is negligible. The same is also true of the potential $\Delta\hat{\mathcal{T}}_{\mu}$ if the length of the conductor obeys $L\ll N_c\ell$. A more careful analysis, carried out in Ref. 21, showed that scattering on this potential (substantially nonlocal for $N_c>1$) has a weak effect on the conductance even for $L\gg N_c\ell$. This seems quite natural if it is taken into account that the scattering on the potential $\Delta\hat{\mathcal{T}}_{\mu}$ is of a "reentrant" character. From the standpoint of perturbation theory this implies that by means of the operator $\Delta\hat{\mathcal{T}}_{\mu}$ the scattering on the intermode potentials $U_{\mu\nu}(x)$ is taken into account to higher order than in the calculation of the mass operator (30).

Returning to the bare intramode potential $V_{\mu}(x)$, we should stress that the scattering on on it under condition (20) breaks the spatial coherence of the mode slightly, and it must therefore be taken into account with special accuracy. For $N_c\gg 1$ this scattering leads to small weak-localization corrections to the conductance, which are not being taken into account in this paper. The role of these corrections clearly grows with decreasing number of conducting channels, but even for $N_c\sim 1$ they do not qualitatively alter the result obtained in the kinetic approximation. The potential $V_{\mu}(x)$ has a governing influence on the spectrum of electronic states only in *single-mode* conductors, which we shall discuss in more detail in the next Section.

5. DEPENDENCE OF THE CONDUCTANCE ON THE SHAPE OF THE CONDUCTOR

The mode spectrum of the current carriers, together with the energy of the electrons, is determined by the structure of the confining potential—in the model considered here, by the geometry of the sample. If the conductance of a bulk conductor varies with the dimensions of the sample in accordance with the classical Ohm's law, then when any of these dimensions becomes comparable to the microscopic lengths of the system, the quantization of the spectrum becomes extremely important and can radically alter the classical behavior of the conductance. Let us consider some limiting cases in which the size quantization influences the character of the electron transport in substantially different ways.

5.1. Multimode conductors

If the configuration of the confining potential and electron energy are such that there is more than one conducting channel in the system, the exact Green's function $G_{\mu\mu}(x,x')$, as follows from (32), is well approximated by the function $G_{\mu\mu}^{(0)}(x,x')$ in the region $L\ll N_c\ell$. But even for $L>N_c\ell$, as was shown in Ref. 21, replacing the exact propagator in (19a) by its approximate value from Eq. (27) is justified in view of the configurational averaging. The solution of equation (27) satisfying radiation boundary conditions at the open end of the conductor has the form

$$G_{\mu\mu}^{(0)}(x,x')=\frac{1}{2i\kappa_{\mu}}\exp\{i\kappa_{\mu}-1/l_{\mu}^{(\varphi)}]|x-x'|\}. \tag{33}$$

Here $l_{\mu}^{(\varphi)}=2\kappa_{\mu}\tau_{\mu}^{(\varphi)}$ is the extinction length (or, equivalently, the dephasing length) of the mode $\boldsymbol{\mu}$ due to incoherent intermode scattering. The substitution of (33) into (19a) gives the following expression for the average conductance:

$$\langle g(L)\rangle=\overline{\sum_{\mu}}\frac{l_{\mu}^{(\varphi)}}{L}\left[1-\frac{l_{\mu}^{(\varphi)}}{L}\exp\left(-\frac{L}{l_{\mu}^{(\varphi)}}\right)\sinh\frac{L}{l_{\mu}^{(\varphi)}}\right]. \tag{34}$$

In the case of a large number of channels ($N_c\gg 1$) the replacement of the sum (34) by an integral allows one to obtain simple limiting formulas for the conductance in those regions which correspond to the classical ballistic ($L\ll\ell$) and diffusive ($L\gg\ell$) electron transport:

$$\langle g(L)\rangle\approx N_c, \quad L\ll\ell, \tag{35a}$$

$$\langle g(L)\rangle\approx\frac{4}{3}\frac{N_c\ell}{L}, \quad L\ll\ell. \tag{35b}$$

In the ballistic limit (35a) the conductance as a function of the electron energy and the transverse dimensions of the quantum waveguide has a stepped structure, the height of the steps being exactly equal to the quantum of conductance $G_0=e^2/\pi\hbar$ (recall that for bulk conductors $N_c=[k_F^2S/4\pi]$, where $[\ldots]$ denotes the integer part of the number in brackets). As one goes from the ballistic to the diffusive regime ($\ell\ll L$) the conductance asymptotically approaches the classical value (35b), which is known from kinetic theory. Here the stepped structure of the conductance is formally preserved, but the height of the steps decreases in proportion to the ratio ℓ/L. The dependence of the average conductance (34) on the length of the quantum waveguide is presented in

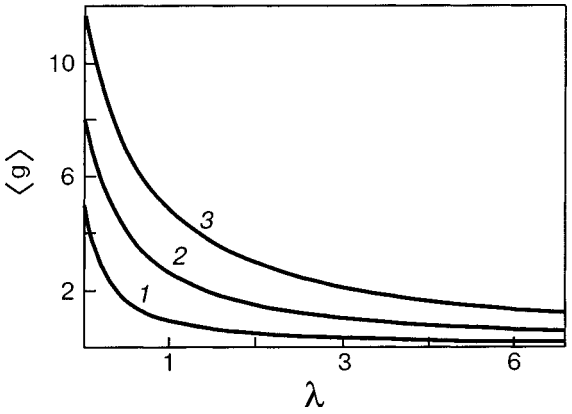

FIG. 2. Conductance (34) as a function of the dimensionless length $\lambda = L/\ell$ for conductors with different numbers of open channels N_c: 5 (*1*), 8 (*2*), and 12 (*3*).

Fig. 2. The curves correspond to different numbers of open channels, but in the region $L/\ell > 1$, they all exhibit identical ''Ohmic'' behavior.

It is important that the diffusive character of the conductance (formula (35b)) is preserved not only in the region of lengths $\ell \ll L \ll N_c\ell$ in which the electron transport is traditionally considered to be diffusive, but also for $L > N_c\ell$. The theory of quasi-one-dimensional (Q1D) conductors[23–26] predicts that at such lengths $\langle g(L)\rangle \propto \exp(-L/N_c\ell)$, from which it is concluded that Anderson localization of all the electronic states obtains in such conductors, regardless of the energy.

The reason for the disagreement of the result (35b) with the predictions of the theory of Q1D localization is due to dephasing of the *mode* electronic states arising because of the quasielasticity of the intermode scattering. From a mathematical standpoint the inelasticity is due to the absence of the ''rotational symmetry'' in the *channel* space which was explicitly used in the derivation of the equations of that theory.[24–26] If all of the unperturbed mode energies in (7) could formally be set equal (''symmetric'' channels), then the mass operator (30) would turn out to be real. This, in turn, would mean that in the presence of weak scattering the coherence of the mode electronic states would essentially be preserved. The average conductance in the region $L > N_c\ell$ in this case would actually depend exponentially on the length of the conductor, in complete agreement with the results of the theory of Refs. 23–26.

In contrast to the model channel-symmetric systems, in real Q1D conductors all the channels (waveguide modes) are characterized by *different* longitudinal energies (8), although the one-electron energy at $T=0$ is, of course, maintained at the Fermi energy. However, since the theory presented here is based not on the single-particle energies but on the mode energies of the electron system, the inelasticity of intermode scattering cannot be eliminated even for a static scattering potential. This inelasticity manifests itself in finiteness of the spatial scale of the damping of the mode propagators (33); from a physical standpoint this corresponds to incoherent intrachannel electron transport. It follows from Eq. (31) that all the modes without exception the coherence lengths do not exceed the electron mean free path ℓ in order of magnitude.

The effective inelasticity of the interchannel scattering in real conductors can be eliminated by assuming that all the matrix elements (9) are equal to zero for $\boldsymbol{\mu} \neq \boldsymbol{\mu}'$. For a (quasi-)two-dimensional conductor of finite thickness this can be accomplished by choosing a model for the random potential which depends only on the coordinates along the direction of the current (a randomly stratified system). Such a model was considered in Ref. 34, where the origin of the ''stratified'' (and, hence, localizing) random potential was attributed to long-range charged centers distributed randomly outside the quantum waveguide. The delocalizing mode mixing of the electrons in Ref. 34 came about not because of intermode impurity scattering but because of an external magnetic field oriented parallel to the surface of the Q2D conductor.

5.2. Anderson localization in single-mode conductors

If the parameters of the electron system admit the existence of only one open channel, then all of the other modes of the quantum waveguide will be evanescent and highly localized with respect to the coordinate x. In that case the potential $\hat{T}_{\boldsymbol{\mu}}$, like $V_{\boldsymbol{\mu}}(x)$, is real and local. Because of this, perturbation theory in the form used above is no longer constructive, since weak scattering, including intermode scattering, does not substantially disrupt the coherence of the single extended mode. A calculation of the conductance in that situation requires the use of methods that permit one to take into account the interference of multiply scattered quantum waves, e.g., such as those which were used in Refs. 35 and 36 in calculating the conductivity of 1D disordered conductors.

In Refs. 37 and 38, with the use of a weak-scattering resonance method, equivalent to the methods of Refs. 35 and 36, we obtained a general expression for the statistical moments of the conductance of single-mode conductors of finite length in the situation where the disorder is caused not by bulk inhomogeneities but by roughness of the side walls of the conductor. That problem, although it is substantially different physically from the problem of bulk scattering, is completely analogous to the problem solved in the present paper from the standpoint of the mathematical formalism used. In its single-mode version the difference is manifested only in the concrete form of the scattering lengths, which in the case of inhomogeneities of a surface nature are complicated nonlocal expressions which differ from (22). Applying the technique described in Refs. 37 and 38 to the present problem, we obtain for a single-mode conductor with bulk disorder

$$\langle g^n(L)\rangle = \frac{4}{\sqrt{\pi}}\left[\frac{L_b^{(V)}(\boldsymbol{\mu}_1)}{L}\right]^{3/2}\exp\left[-\frac{L}{4L_b^{(V)}(\boldsymbol{\mu}_1)}\right] \times \int_0^\infty \frac{z\,dz}{\cosh^{2n-1}z}\exp\left[-z^2\frac{L_b^{(V)}(\boldsymbol{\mu}_1)}{L}\right] \times \int_0^z dy\,\cosh^{2(n-1)}y. \tag{36}$$

We can conclude from Eq. (36) that in the one-channel case only two regimes of electron transport are distinguished—ballistic and ''localized''—the diffusive

transport regime is absent. The corresponding limiting expressions for the average conductance have the form

$$\langle g(L)\rangle \approx \begin{cases} 1-4L/\xi_1, & L/\xi_1 \ll 1, \\ (\pi^{5/2}/16)(\xi_1/L)^{3/2}\exp(-L/\xi_1), & L/\xi_1 \gg 1, \end{cases} \tag{37}$$

where $\xi_1 = 4L_b^{(V)}(\boldsymbol{\mu}_1)$ is the one-dimensional localization length of the harmonic $\boldsymbol{\mu}_1$ in reference to the *collective* ''backscattering'' of electrons on the bare intramode potential $V_{\boldsymbol{\mu}_1}(x)$.

5.3. Metal–insulator transition as a quantum phase transition

The conductance (37) demonstrates a localized character of electron transport in a single-mode quantum waveguide, in agreement with the known results of a spectral analysis of one-dimensional disordered systems.[39] This fact in itself is an indication that it is in principle possible for a bounded electron system to undergo a transition from the conducting to the insulating state under the influence of geometric factors alone, at a fixed level of disorder. The one-dimensional localization (of the Anderson type) in linear systems is universal in the sense that in the 1D random potential all the electronic states, regardless of energy, are exponentially localized. At the same time, in a certain sense this localization can be regarded as weak. With decreasing level of disorder the length ξ_1 increases without bound, and in comparatively pure conductors, even very long ones, the collective transport of electrons can actually remain close to ballistic.

The approach proposed in this paper allows one to explain the observed transition of an electron system from the conducting state to the insulating state even for samples of mesoscopic length, and independently of the degree of their structural disorder. With decreasing transverse dimensions the conductor ultimately must pass into a ''cutoff'' waveguide regime, where all the modes in it become evanescent, each localized on a scale of its wavelength $|\kappa_{\boldsymbol{\mu}}|^{-1}$, which in the framework of the calculational technique used here is considered to be microscopic. In this ''size-localized'' regime the conductance falls off sharply relative to its value (37) in the marginal single-mode state of the quantum system, and to parametric accuracy it can be assumed equal to zero.

It is essential that the mode structure of the conductor illustrated in Fig. 1b can be altered by changing only one of its transverse dimensions while keeping the other one constant. It is seen from Eq. (8) that even at a very large width W the quantum waveguide can be brought to a cutoff regime by decreasing only its thickness H. In real planar structures this is accomplished by increasing the externally applied pressing potential (see Fig. 1a) or by a capacitive influence on the heterocontact region.

Figure 3 shows the results of a numerical calculation of the dependence of the conductance (34) on the thickness of the conductor at a fixed value of its width. Curve *1* corresponds to the ballistic limit $\ell/L \to \infty$, and curves *2* and *3* to finite values of this ratio. The ballistic conductance is ideally quantum, with a value of the jump equal to the quantum G_0. The peculiar modulation of curve *1* is due to the quantum

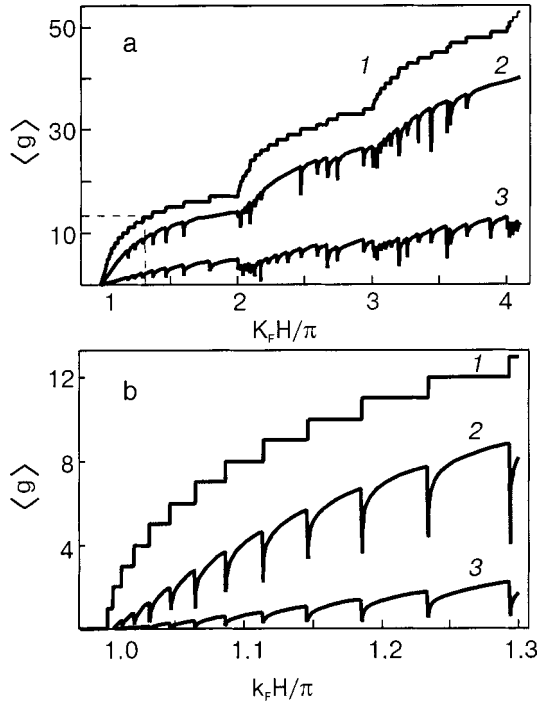

FIG. 3. Dependence of the dimensionless conductance on the thickness of a quantum waveguide at a fixed width ($k_F W/\pi = 20.5$) and different values of the diffusion parameter $\lambda = L/\ell$: 0 (*1*), 0.5 (*2*), and 5 (*3*).

waveguide model used (see Fig. 1b), the spectrum (8) of which dictates the opening and closing of conducting channels at nonequidistant points in H.

As the disorder increases (curves *2* and *3*), the jumps of the conductance decrease in size, and the shape of the steps becomes smoothened. In the neighborhood of the points of opening (closing) of quantum channels one should observe substantial dips in the conductance. The shape of these dips is clearly seen in Fig. 3b, where the curves in the region indicated in Fig. 3a are shown on an enlarged scale. The relatively smooth decrease of the conductance as the point of closing of the next channel is approached from the side of larger values of H is due to growth of the density of states of the *slow* marginal mode $\boldsymbol{\mu}_m$ and, accordingly, to a transition of electrons from the faster open modes into it. The dephasing frequencies of the latter [formula (30b)] have square-root singularities at the critical points ($\kappa_{\boldsymbol{\mu}_m} = 0$), and that is reflected in the destructive reduction of the mode propagators (33) in the vicinity of the critical points.

Analogous dips were observed in a numerical analysis of the optical conductance of waveguide systems in Ref. 40, using the Landauer approach. However, the dips in Ref. 40 had a comparatively symmetric shape with respect to the points at which the extended modes vanish, whereas in Fig. 3 their shape has a pronounced asymmetry. This asymmetry is due to the circumstance that in the derivation of formula (34) in approximation (20) we neglected the contribution of the evanescent modes to the conductance and were therefore not studying the *tunneling* part of the conductance, which is due to those modes. For a marginal mode this is not fully justified, since in the vicinity of a critical point the condition of weak scattering is violated, and the propagator of such a

mode immediately after its closing is, strictly speaking, not equal to expression (23).

The curves shown in Fig. 3 demonstrate the sequence of quantum phase transitions[13] occurring in the electron system upon a change of its confining potential. At the critical points the conductance changes in a jumplike manner, and the role of the correlation length in the electron system in the vicinity of these points is played by the wavelength of the marginal mode, which is proportional to its density of states.

The leftmost phase transition, clearly seen in Fig. 3b, is a transition of the electron system from the conducting phase to an insulating state. In the metallic phase in the immediate vicinity of the transition the value of the conductance in the ideal ballistic situation is equal to the quantum G_0. This corresponds approximately to the values observed in the neighborhood of the so-called separatrix—a line which nominally divides the set of experimental curves of the T dependence of the resistance into subsets pertaining to the insulating and conducting phases of 2D systems.[1]

In the majority of experimental papers the spectral classification of two-dimensional systems is done on the basis of data on the temperature and magnetic-field dependences of their resistance. A detailed analysis of the effects due to the magnetic field is the subject of a separate paper. As to the temperature dependence of the resistance of two-dimensional systems, a number of qualitative conclusions can be reached already on the basis of the above-described features of the quantum transport in planar structures.

First, we note that the transition from the ''metallic'' conductance (34), (35) to the small value it has in the localized (0-mode) phase inevitably occurs via a single-mode state of the electron system, which, in spite of the macroscopic width of the quantum waveguide, behaves as effectively one-dimensional. For one-dimensional systems it has been predicted previously that the conductance depends monotonically on temperature, in Ref. 36 for the case $T\tau \gg 1$ and in Ref. 41 for $T\tau \ll 1$. For 2D systems, the resistance measured near the separatrix on the metallic side[1] actually varies nonmonotonically with temperature.

The weak temperature dependence of the separatrix itself can also be explained if one considers that the wavelength of the last of the extended modes increases without bound as the point of its closing is approached, and it becomes large compared to the wavelength of thermal phonons, whereupon the interaction of the mode with the phonon subsystem of the crystal naturally becomes ineffective.

Finally, deep in the insulating phase, when all the electronic modes have become evanescent and, hence, highly localized, it is natural to expect that the resistance will exhibit the temperature dependence that follows from the hopping theory of percolation.[42] This is the type of temperature dependence that is observed in two-dimensional systems found in the insulating phase.[1,43]

CONCLUDING REMARKS

The main goal of the present study was to develop a single-particle field model of the transition of a two-dimensional electron system from the insulating state (prescribed by the scaling theory of localization) to the metallic phase observed experimentally. The essence of the proposed approach is that systems which from the experimental standpoint are completely two-dimensional should be treated as the limiting case of *three-dimensional* quantum waveguides to more fully take into account the quantum character of the electron system.

We note that the procedure of reducing multidimensional dynamical problems to one-dimensional problems, which is a part of the analytical technique used, has also been applied to systems originally regarded as strictly two-dimensional.[20,21] However, for such systems it is hard to consider the possibility of a transition from the metallic to the insulating state in the framework of the approach developed, since the single-mode state of 2D electrons is usually associated not with macroscopic conductors but with quantum wires.

Nevertheless, a macroscopic two-dimensional quantum waveguide, if it is considered as ''flattened'' three-dimensional one, is fully capable of being found in the single-mode, and even in the cutoff, 0-mode state. In this connection one quite naturally wonders which electron systems are reasonably classified as two-dimensional and which ones are not. And, specifically, how do non-one-dimensional electron systems differ fundamentally from three-dimensional systems from the standpoint of their transport properties?

From the numerical and analytical results presented in this paper it is impossible to establish objective criteria for differentiating 2D and 3D systems. Only the conductance of the *diffusion* type, characteristic for *non-one-dimensional* systems, and the ''localized'' conductance of single-mode conductors and 0-mode (insulating) systems are fundamentally different. Since two-dimensional and three-dimensional transport problems reduce to a one-dimensional problem in the mode representation in an identical way, one is forced to conclude that a rational classification of nonballistic systems of the Fermi type should be done not on the basis of their formal geometric structure but according to the mode content. From the this standpoint disordered systems with more than one extended mode, in which a diffusive transport of quasiparticles is realized, so that their single-particle spectrum has a continuous component, are substantially different from the class of localized systems. The latter, in turn, include single-mode systems, which are characterized by localization of an Anderson nature (strong or weak, depending on the degree of disorder) and 0-mode systems, the localization of the states in which is not due to disorder and/or interaction but rather to the size-quantization of the spectrum of the current carriers.

[1] E. Abrahams, S. V. Kravchenko, and M. P. Sarachik, Rev. Mod. Phys. **72**, 251 (2001).
[2] E. Abrahams, P. W. Anderson, D. C. Licciardello, and T. V. Ramakrishnan, Phys. Rev. Lett. **42**, 673 (1979).
[3] M. Shreiber and M. Ottomeier, J. Phys.: Condens. Matter **4**, 1959 (1992).
[4] V. Dobrosavljević, E. Abrahams, and E. Miranada, and S. Chakravarty, Phys. Rev. Lett. **79**, 455 (1997).
[5] Z. Ye, Chin. J. Phys. **39**, L207 (2001); *idem* cond-mat/0106481.
[6] A. M. Finkel'stein, Z. Phys. B: Condens. Matter **56**, 189 (1984).
[7] C. Castellani, C. D. Di Castro, and P. A. Lee, Phys. Rev. B **57**, R9381 (1998).
[8] S. Chakravarty, L. Yin, and E. Abrahams, Phys. Rev. B **58**, R559 (1998).
[9] D. Belitz and T. R. Kirkpatrick, Phys. Rev. B **58**, 8214 (1998).

[10] J. S. Takur and D. Neilson, Phys. Rev. B **58**, 13717 (1998).
[11] T. M. Klapwijk and S. Das Sarma, Solid State Commun. **110**, 581 (1999).
[12] S. Das Sarma and E. H. Hwang, Phys. Rev. Lett. **84**, 5596 (2000).
[13] S. L. Sondhi, S. M. Girvin, J. P. Carini, and D. Shahar, Rev. Mod. Phys. **69**, 315 (1997).
[14] P. A. Lee and T. V. Ramkrishnan, Rev. Mod. Phys. **57**, 287 (1985).
[15] P. Mohanty, Physica B **280**, 446 (2000); *idem* cond-mat/9912263.
[16] I. L. Aleiner, B. L. Altshuler, and M. E. Gershenson, Waves Random Media **9**, 201 (1999).
[17] B. L. Altshuler, A. G. Aronov, and P. A. Lee, Phys. Rev. Lett. **44**, 1288 (1980).
[18] B. Tanatar and D. M. Ceperley, Phys. Rev. B **39**, 5005 (1989).
[19] D. Belitz and T. R. Kirkpatrick, Rev. Mod. Phys. **66**, 261 (1994).
[20] Yu. V. Tarasov, J. Phys.: Condens. Matter **11**, L437 (1999).
[21] Yu. V. Tarasov, Waves Random Media **10**, 395 (2000).
[22] F. Mancini and A. Avella, cond-mat/0006377.
[23] K. B. Efetov, Adv. Phys. **32**, 53 (1983).
[24] O. N. Dorokhov, Solid State Commun. **51**, 381 (1984).
[25] O. N. Dorokhov, Phys. Rev. B **37**, 10526 (1988).
[26] P. A. Mello, P. Pereyra, and N. Kumar, Ann. Phys. **181**, 290 (1988).
[27] Yu. V. Tarasov, J. Phys.: Condens. Matter **14**, L357 (2002); *idem* cond-mat/0203507.
[28] M. P. Sarachik and S. V. Kravchenko, Proc. Natl. Acad. Sci. U.S.A. **96**, 5900 (1999); *idem* cond-mat/9903292.
[29] R. Kubo, J. Phys. Soc. Jpn. **12**, 570 (1957).
[30] F. G. Bass and I. M. Fuchs, *Wave Scattering from Statistically Rough Surfaces*, Pergamon Press, Oxford (1978), Nauka, Moscow, (1972).
[31] V. S. Vladimirov, Uravneniya matematicheskoĭ fiziki, Nauka, Moscow, (1967).
[32] J. R. Taylor, *Scattering Theory. The Quantum Theory on Nonrelativistic Collisions*, Wiley, New York (1972), Mir, Moscow, (1975).
[33] R. Newton, *Scattering Theory of Waves and Particles*, McGraw-Hill, New York (1968), Mir, Moscow, (1969).
[34] J. S. Meyer, V. I. Fal'ko, and B. L. Altshuler, in *Strongly Correlated Fermions and Bosons in Low-Dimensional Disordered Systems*, I. V. Lerner, B. L. Altshuler, V. I. Fal'ko, and T. Giamarchi (eds.), Vol. 72 of NATO Science Series II: Mathematics, Physics and Chemistry, Kluwer Academic Publishers (2002), p. 117; *idem* cond-mat/0206024.
[35] V. L. Berezinskiĭ, Zh. Éksp. Teor. Fiz. **65**, 1251 (1973) [Sov. Phys. JETP **38**, 620 (1974)].
[36] A. A. Abrikosov and I. A. Ryzhkin, Adv. Phys. **27**, 147 (1978).
[37] N. M. Makarov and Yu. V. Tarasov, J. Phys.: Condens. Matter **10**, 1523 (1998).
[38] N. M. Makarov and Yu. V. Tarasov, Phys. Rev. B **64**, 235306 (2001).
[39] I. M. Lifshits, S. A. Gredeskul, and L. A. Pastur, *Introduction to the Theory of Disordered Systems*, Wiley, New York (1982), Nauka, Moscow, (1982).
[40] P. García-Mochales and P. Serena, N. García, and J. L. Costa-Krämer, Phys. Rev. B **53**, 10268 (1996).
[41] Yu. V. Tarasov, Phys. Rev. B **45**, 8873 (1992).
[42] B. I. Shklovskiĭ and A. L. Efros, *Electronic Properties of Doped Semiconductors*, Springer-Verlag, New York (1984), Nauka, Moscow, (1979).
[43] W. Mason, S. V. Kravchenko, G. E. Bowker, and J. E. Furneaux, Phys. Rev. B **52**, 7857 (1995).

Translated by Steve Torstveit

Mechanism of vortex switching in magnetic nanodots under a circular magnetic field. II. Dynamics of a spin plaquette containing a vortex

A. S. Kovalev* and J. E. Prilepsky

B. Verkin Institute for Low Temperature Physics and Engineering, National Academy of Sciences of Ukraine, pr. Lenina 47, 61103 Kharkov, Ukraine

(Submitted June 20, 2002)
Fiz. Nizk. Temp. **29**, 71–83 (January 2003)

For a theoretical explanation of the mechanism of switching of the polarization of magnetic vortices in an external circular magnetic field, a small spin plaquette in a vortex configuration is considered. An analytical investigation of the initial (linear) stage of the vortex switching process is carried out. The analytical results obtained confirm the data of a numerical calculation of the plaquette dynamics. Both the numerical simulation and an analytical treatment of the initial stage of activation show the importance of taking the azimuthal modes of the system into account. It is at the frequencies of these modes that the most rapid growth of the vortex energy and the total intraplane projection of the magnetization occur. Increasing the amplitude of these modes leads to parametric excitation of a low-frequency symmetric mode, and that causes vortex switching. The results provide a qualitative explanation of the data of a numerical simulation of vortex switching in large magnetic systems and can be used in experiments on the directed influencing of the polarization of vortices in magnetic nanodots. [DOI: 10.1063/1.1542378]

INTRODUCTION

In recent years a new kind of object has been attracting heightened interest among physicists—magnetic particles of small size, from hundreds of nanometers to several magnetic atoms and referred to variously as magnetic nanodots, magnetic clusters, and magnetic molecules.[1–4] By now there has been direct experimental confirmation that magnetic nanodots contain magnetic vortices—topological excitations close in nature to Pitaevskiĭ vortices in superfluid liquids and hydrodynamic vortices in two-dimensional incompressible liquids.[1,2] In the case of easy-plane magnetic anisotropy, the magnetization in a magnetic vortex rotates by an angle of 2π in passing around the center of the vortex.[5–10] In a number of cases the presence of a nonzero component of the magnetization in the direction perpendicular to the easy plane—''polarization'' of the vortex—has been observed experimentally.[1,2] This polarization can have opposite signs and is characterized by a topological index $p=\pm 1$ (see Refs. 10–12). In real discrete systems this index is not a true topological charge and can vary under the influence of temperature[11] or a circular[12] or constant field perpendicular to the plane of the nanodot.[2] The possibility of directed change of the polarization of a vortex is especially important when one considers that nanodots containing vortices of different polarity might, in principle, be used in the future as memory elements in high-density data storage media.

Changing the polarization of a vortex in a circular field was studied by numerical simulation in Ref. 12, where it was shown that the vortex switching process has a resonance character and is asymmetric with respect to a change in sign of the frequency of the applied field (the direction of its rotation). Part I of this paper[10] included a critique of the analytical part of Ref. 12, and it was shown that the scenario proposed by the authors of Ref. 12 does not explain the asymmetry of the vortex switching process with respect to the direction of rotation of the field. We showed that the the process of excitation of a nanodot in a vortex configuration is of a complex character and requires that several eigenmodes of the system be included in the treatment, chief among which are the so-called first azimuthal modes, associated with the rotation of spin waves around the center of the vortex. However, the simplified model used by the present authors in Ref. 10 did not permit explanation of the asymmetry of the process upon a change in frequency.

In the present paper, which is a continuation of Ref. 10, we consider the dynamics of a small ''magnetic plaquette'' (magnetic cluster) of several coordination spheres of the magnetic lattice in a vortex configuration under the influence of a spatially uniform rotating external field, but we have taken into account the magnon eigenmodes of the system in the presence of a vortex. Classification of the magnon eigenmodes of such plaquettes in a vortical state has been carried out previously by the authors in Refs. 13 and 14, where it was shown that the spectra of such a system have a complete qualitative similarity to the low-frequency part of the spectra of the large-radius systems discussed in Part I.[10] Our numerical calculations confirm the results of the qualitative analytical treatment of the problem of the change of polarity of a vortex in an external circular field.

The results of the present paper for a small magnetic plaquette, together with the results obtained in Part I[10] for a nanodot of finite size, give a complete qualitative description of the scenario of vortex switching in a circular magnetic field.

1. MODEL AND STATEMENT OF THE PROBLEM

Let us consider the spin dynamics of the small plaquette shown in Fig. 1, in a vortex configuration with fixed bound-

ary spins. Such boundary conditions can be explained by the presence of an additional strong surface anisotropy, which orders the boundary spins perpendicular to the surface of a small magnetic particle, or by an influence exerted on the surface spins by the matrix surrounding this particle. The equations of spin dynamics—the Landau–Lifshitz equations (LLEs)—with the circular magnetic field $\mathbf{h}=h(\cos\omega t, \sin\omega t,0)$ are written in general form as[10]

$$\frac{d\varphi_n}{dt}=\sum_{\delta}\left(\frac{m_{\perp\delta}}{m_{\perp n}}[m_n\cos(\varphi_n-\varphi_{n+\delta})-\gamma\sin(\varphi_n-\varphi_{n+\delta})]-\lambda m_{n+\delta}\right)+h\frac{m_n}{m_{\perp n}}\cos(\varphi_n-\omega t), \quad (1)$$

$$\frac{dm_n}{dt}=\sum_{\delta}\ (-m_{\perp n}m_{\perp n+\delta}[\gamma m_n\cos(\varphi_n-\varphi_{n+\delta})+\sin(\varphi_n-\varphi_{n+\delta})]+\gamma\lambda m_{\perp n}^2 m_{n+\delta})-hm_{\perp n}\sin(\varphi_n-\omega t), \quad (2)$$

where we have used the notation from Part I of this paper: $m_n=S_n^z$ is the z projection of the spin onto the "hard" axis, $\varphi_n=\tan^{-1}(S_n^y/S_n^x)$ is the azimuthal angle of the spin, $J=1$, and

$$m_{\perp n}\equiv\sqrt{1-m_n^2}.$$

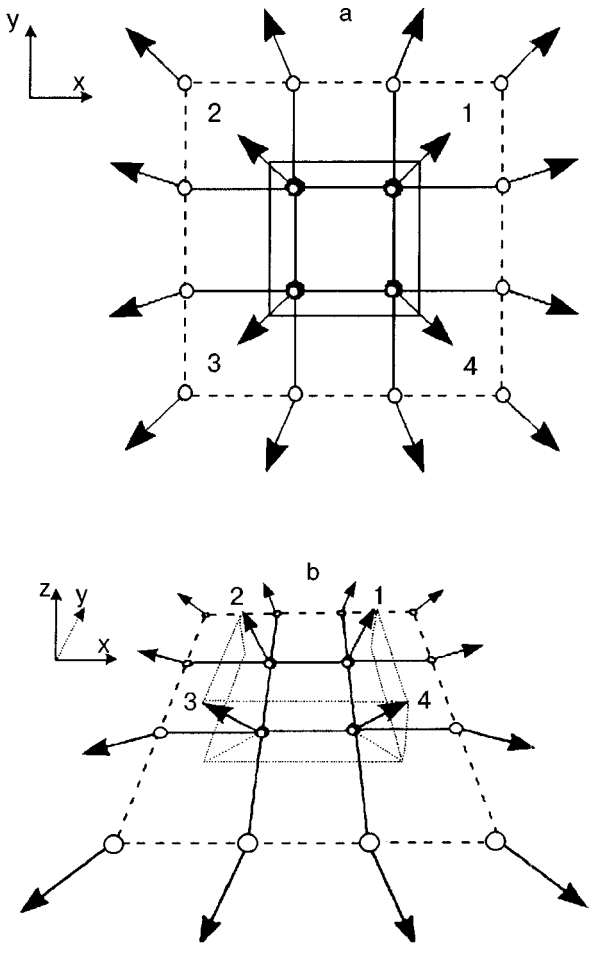

FIG. 1. Configuration of a spin plaquette corresponding to an in-plane (a) and out-of-plane (b) vortex. The dark circlets from the first coordination sphere denote the mobile spins (*1,2,3,4*).

The smallness of the damping coefficient for a plaquette is determined by the inequality $\gamma\ll 1$, since the eigenmode frequencies in this case are of the order of unity.

The magnetic structure and property of the spectrum of the plaquette systems illustrated in Fig. 1 were considered previously in Refs. 13 and 14, in which it was shown that the classification of vortex states of such systems (the existence of an in-plane (IP) vortex configuration in the case of strong anisotropy and an out-of-plane (OP) vortex configuration at values of the anisotropy parameter close to unity) is analogous to that in systems of large size,[15,16] and the spectrum of excitations of such small plaquettes has a qualitative similarity with the low-frequency part of the spin-wave spectrum in systems of large size with the corresponding boundary conditions (see Refs. 17 and 18). In the plaquette considered, the four spins of its inner (first) coordination sphere can change their orientation, while the spins of the second and third coordination spheres are fixed in the position corresponding to the equilibrium configuration of the in-plane vortex. The vortex state for such a plaquette, thanks to the fixing of the outer spins, is the ground state and is determined by the following system of static equations for the four mobile spins with indices $n=1,2,3,4$:

$$\sum_{\delta}\ m_{\perp n}m_{\perp n+\delta}\sin(\varphi_n-\varphi_{n+\delta})=0, \quad (3)$$

$$\sum_{\delta}\left[\lambda m_{n+\delta}-m_n\frac{m_{\perp n+\delta}}{m_{\perp n}}\cos(\varphi_n-\varphi_{n+\delta})\right]=0, \quad (4)$$

where the summation is over nearest neighbors, with indices $n+\delta$. The state of the 12 boundary spins is fixed and is determined by the values $m\equiv 0$ and $\varphi=\Phi_0$, $\pi/4$, $\pi/2-\Phi_0$, $\pi/2+\Phi_0$, $3\pi/4\ldots$, where $\Phi_0=(1/2)\sin^{-1}(\sqrt{3}-1)$. Here the IP vortex configuration corresponds to the solution for four mobile spins $\varphi_n^0=\pi/4+\pi n/2$, $m_n^0\equiv 0$, $n=1-4$, which is stable in the interval of values of the anisotropy parameter $0\leqslant\lambda\leqslant\lambda_c=\cos(\pi/4-\Phi_0)=\sqrt{\sqrt{3}/2}\approx 0.93$. We note that the difference of the critical value λ_c from the value for systems of large size ($\lambda_c\approx 0.72$ for a square lattice[15]) is insubstantial and is due to the fact that for systems of small size, this quantity depends considerably on the configuration of the system itself and the fixed configuration of the boundary spins.[14,15] By varying Φ_0, one can also vary the value of λ_c.

For weak easy-plane anisotropy less than the critical value ($\lambda>\lambda_c$) another vortex configuration—OP, in which the spin at the center of the vortex sticks out of its plane—is stable. The static distribution of the the directions of the mobile spins for an OP configuration is given by the following expressions: $\varphi_n^0=\pi/4+\pi n/2$, as for the IP configuration, and for the z projection

$$m_n^0=m=p\sqrt{1-(\lambda_c/\lambda)^2}, \quad (5)$$

where $p=\pm 1$ is the polarization of the vortex. After linearization of the system of equations (1), (2) for the four mobile spins with respect to small time-dependent corrections μ and ν to the vortex solution, $m_n(t)=\mu_n(t)+m_n^0$, $\varphi_n(t)=\nu_n(t)+\varphi_n^0$, we obtain for μ and ν a system of eight first-order differential equations:

$$\frac{d\nu_n}{dt}=\sum_{\delta}\left(\mu_n\frac{m_{\perp n+\delta}}{m_{\perp n}^3}\cos(\varphi_{n+\delta}^0-\varphi_n^0)\right.$$
$$\left.-(\nu_{n+\delta}-\nu_n)m_n\frac{m_{\perp n+\delta}}{m_{\perp n}}\sin(\varphi_{n+\delta}^0-\varphi_n^0)\right]$$
$$-\mu_{n+\delta}\left[\frac{m_n m_{n+\delta}}{m_{\perp n}m_{\perp n+\delta}}\cos(\varphi_{n+\delta}^0-\varphi_n^0)+\lambda\right], \qquad (6)$$

$$\frac{d\mu_n}{dt}=\sum_{\delta}\left\{(\nu_{n+\delta}-\nu_n)m_{\perp n}m_{\perp n+\delta}\cos(\varphi_{n+\delta}^0-\varphi_n^0)\right.$$
$$+\left[\mu_n m_n\frac{m_{\perp n+\delta}}{m_{\perp n}}+\mu_{n+\delta}m_{n+\delta}\frac{m_{\perp n}}{m_{\perp n+\delta}}\right]$$
$$\left.\times\sin(\varphi_{n+\delta}^0-\varphi_n^0)\right\}, \qquad (7)$$

where $n=1-4$, $m_n=0$ for the IP and m for the OP configuration, $m_{n+\delta}=0$ for the spins of the outer coordination spheres and for the spins with $n+\delta=1-4$ in the IP configuration, and $m_{n+\delta}=m$ for $n+\delta=1-4$ in the OP configuration. The spectrum of system (6), (7) for a plaquette in the region of stability of the IP vortex configuration ($\lambda<\lambda_c$) contains three branches. (The total number of modes is equal to the number of degrees of freedom of the Hamiltonian system, i.e., the number of free spins, but for an in-plane vortex one of the modes is twofold degenerate.) The lowest branch (see Fig. 2) corresponds to a symmetric mode with $\mu_n(t)\mu^0\cos\Omega_0 t$, $\nu_n(t)=\nu^0\sin\Omega_0 t$, and the dependence of its frequency on the parameter λ is given by the formula

$$\Omega_0^{IP}(\lambda)=2\sqrt{\lambda_c(\lambda_c-\lambda)}, \qquad (8)$$

and the ratio of the amplitudes of the oscillations of the spins in the two perpendicular directions is given by

$$\nu^0/\mu^0=\sqrt{1-\lambda/\lambda_c}\ . \qquad (9)$$

This mode, denoted here by the index 0, corresponds to the symmetric mode with index 2 considered in our previous paper.[10] We see that at the critical point $\lambda\to\lambda_c$ the spins oscillate perpendicular to the easy plane.

The next mode is the twofold degenerate first azimuthal mode: $\mu_n=\mu^{1,2}\cos(\chi_n-\Omega_{1,2}t)$, $\nu_n=\nu^{1,2}\sin(\chi_n-\Omega_{1,2}t)$

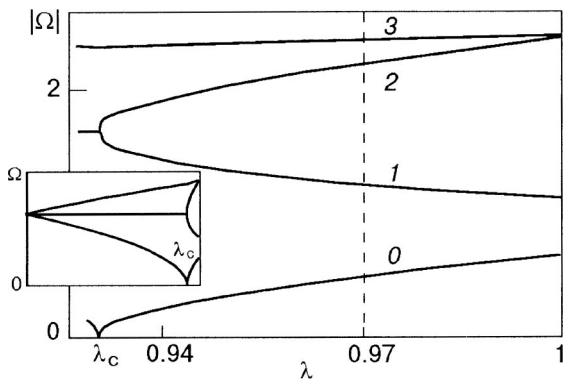

FIG. 2. Spectrum of eigenmodes of a spin plaquette in a vortex configuration in the OP region: symmetric mode (*0*); doublet of first azimuthal modes with different directions of rotation of the spin wave (*1,2*); second azimuthal mode (*3*). The inset shows the total spectrum in the whole range of variation of the anisotropy parameter.

(where χ_n is the azimuthal coordinate of the nth spin). Its frequency for $\lambda<\lambda_c$ is independent of the parameter λ_c:

$$\Omega_{1,2}^{IP}=2\lambda_c, \qquad (10)$$

and

$$\nu^{1,2}/\mu^{1,2}=\mp 1. \qquad (11)$$

Finally, the highest-frequency mode, the second azimuthal mode with antiphase oscillations of neighboring spins, corresponds to a solution with $\mu_n=\mu^3\cos(2\chi_n-\Omega_3 t)$, $\nu_n=\nu^3\sin(2\chi_n-\Omega_3 t)$, the frequency is

$$\Omega_3^{IP}(\lambda)=2\sqrt{\lambda_c(\lambda_c+\lambda)}, \qquad (12)$$

and the amplitude ratio

$$\nu^3/\mu^3=\sqrt{1+\lambda/\lambda_c}. \qquad (13)$$

For the OP region ($\lambda>\lambda_c$) we have an analogous classification of modes, with the only difference being that now, thanks to the lowering of the symmetry of the system, the degeneracy of the first two azimuthal modes is lifted. The corresponding wave parameters of the oscillatory modes have the following dependence on λ:

for the symmetric mode

$$\Omega_0^{OP}(\lambda)=2\sqrt{\lambda^2-\lambda_c^2}, \qquad (14)$$

$$\nu^0/\mu^0=\frac{\lambda}{\lambda_c}\sqrt{\left(\frac{\lambda_c}{\lambda}\right)^2-1}; \qquad (15)$$

for the lower first azimuthal mode

$$\Omega_1^{OP}(\lambda)=2(\lambda-\sqrt{1-(\lambda_c/\lambda)^2}), \qquad (16)$$

$$\nu^1/\mu^1=-\frac{\lambda(\lambda-\sqrt{1-(\lambda_c/\lambda)^2})}{\lambda_c^2+\lambda\sqrt{1-(\lambda_c/\lambda)^2}}; \qquad (17)$$

for the upper first azimuthal mode

$$\Omega_2^{OP}(\lambda)=2(\lambda+\sqrt{1-(\lambda_c/\lambda)^2}), \qquad (18)$$

$$\nu^2/\mu^2=-\nu^1/\mu^1=\frac{\lambda(\lambda-\sqrt{1-(\lambda_c/\lambda)^2})}{\lambda_c^2+\lambda\sqrt{1-(\lambda_c/\lambda)^2}}; \qquad (19)$$

and for the second azimuthal mode

$$\Omega_3^{OP}(\lambda)=2\sqrt{\lambda^2+\lambda_c^2}, \qquad (20)$$

$$\nu^3/\mu^3=\frac{\lambda}{\lambda_c}\sqrt{\left(\frac{\lambda_c}{\lambda}\right)^2+1}. \qquad (21)$$

The total spectrum of oscillation frequencies of the plaquette in the OP region is shown in Fig. 2. We see that it does in fact have a qualitative similarity to the low-frequency part of the spectrum of systems of large size (for a fixed boundary),[14,18] but there are several differences. For example, in a large system for $\lambda>\lambda_c$ the symmetric and lower first azimuthal modes cross, and at large values of λ the latter becomes the lowest in frequency. This is the reason for the change in the numbering of the modes in Part I of this study:[10] the zeroth mode of the plaquette corresponds to the second mode of a large system, the first mode of the plaquette, to the first mode, and the second mode of the plaquette, to the third mode (see Fig. 4b of Ref. 10). Furthermore, it should be noted that the second azimuthal mode (the

highest in frequency) in the plaquette corresponds in a large system to a solution with four nodes in the azimuthal direction. In Fig. 4b in Ref. 10 this frequency dependence is not shown, and the curve (*4*) in that figure corresponds to the first azimuthal mode (with two nodes in the azimuthal direction), but with an additional node in the radial direction. Below we will be interested in the vortex dynamics only in the OP region, and we shall drop the superscript OP from all the quantities.

It will be convenient below to change over from equations for the oscillations of individual spins to equations for the characteristics of the collective modes discussed above. We expand the Hamiltonian of the system (see Ref. 10) to terms of second order in the small deviations μ_n and ν_n from the OP solution. For a plaquette, with the the symmetry properties of the static OP solution taken into consideration, the Hamiltonian is written explicitly as a positive definite quadratic form:

$$\mathcal{H}_o=\frac{\lambda_c}{m_\perp^3}\sum_{n=1}^{4}\mu_n^2+\lambda_c m_\perp\sum_{n=1}^{4}\nu_n^2-\lambda(\mu_1\mu_2+\mu_1\mu_4+\mu_2\mu_3+\mu_3\mu_4)+m(\mu_2\nu_1-\mu_1\nu_2+\mu_1\nu_4-\mu_4\nu_1+\mu_3\nu_2-\mu_2\nu_3+\mu_4\nu_3-\mu_3\nu_4), \tag{22}$$

and the dynamical equations (6), (7), for the Hamiltonian (22), will be Hamilton's equations for four coupled oscillators with effective momenta μ_n and effective coordinates ν_n conjugate to them. To explain the process of activation of the normal modes of a plaquette by a circular magnetic field, it is necessary to diagonalize the Hamiltonian (22) (change to normal modes) and write the correction to it due to the influence of the external field, $\mathcal{H}_{\rm int}(t)$, in terms of the normal momenta and coordinates for each of the modes. We reduce the quadratic form (22) to the principal axes:

$$\mathcal{H}_0=\frac{1}{2}\sum_{n=0}^{3}(\alpha_n P_n^2+\beta_n Q_n^2), \tag{23}$$

where α_n and β_n are the coefficients of the reciprocal mass and stiffness of the nth effective oscillator, which depend on the anisotropy parameter λ in the following way:

$$\alpha_0=2\lambda_c(1-m_\perp^4)/m_\perp^3,\quad \beta_0=\beta_3=2\lambda_c m_\perp,$$
$$\alpha_1=\beta_1=\Omega_1=2(\lambda-m),\quad \alpha_2=\beta_2=\Omega_2=2(\lambda+m),$$
$$\alpha_3=2\lambda_c(1+m_\perp^4)/m_\perp^3.$$

(We recall that the quantities m and $m_\perp$ appearing in these formulas are functions of λ.) The frequencies of the normal modes (effective oscillators) Ω_n^2 are expressed in terms of the parameters α_n and β_n as follows: $\Omega_n^2=\alpha_n\beta_n$, and the initial variables μ and ν are expressed in terms of the normal "coordinates" and "momenta" as

$$\mu_1=\frac{1}{2}(P_0+P_3+m_\perp Q_1+m_\perp Q_2),$$
$$\mu_2=\frac{1}{2}(P_0+m_\perp P_1-m_\perp P_2-P_3),$$
$$\mu_3=\frac{1}{2}(P_0+P_3-m_\perp Q_1-m_\perp Q_2),$$
$$\mu_4=\frac{1}{2}(P_0-m_\perp P_1+m_\perp P_2-P_3),$$
$$\nu_1=\frac{1}{2}(P_0/m_\perp+P_2/m_\perp+Q_0+Q_3),$$
$$\nu_2=\frac{1}{2}(Q_0-Q_1/m_1+Q_2/m_\perp-Q_3),$$
$$\nu_3=\frac{1}{2}(-P_1/m_\perp-P_2/m_\perp+Q_0+Q_3),$$
$$\nu_4=\frac{1}{2}(Q_0+Q_1/m_\perp-Q_2/m_\perp-Q_3). \tag{24}$$

2. DYNAMICS OF A SPIN PLAQUETTE IN AN EXTERNAL CIRCULAR FIELD

Let us take into account the presence of a circular magnetic field and analyze the resonances arising in the initial stage of activation of the eigenmodes of the plaquette by a field of a given symmetry.

We expand out the interaction Hamiltonian of the plaquette with the external circular field, $\mathcal{H}_{\rm int}(t)=-h\Sigma_n m_{\perp n}\cos(\varphi_n-\omega t)$, to terms of first order (in the small corrections μ and ν) and, going over to a description in terms of the normal modes (24), we have

$$\mathcal{H}_{\rm int}^d=h[(1-m)P_1-(1+m)P_2]\sin\left(\frac{\pi}{4}-\omega t\right)-h[(1-m)Q_1-(1+m)Q_2]\cos\left(\frac{\pi}{4}-\omega t\right). \tag{25}$$

The superscript d (for "direct") is introduced in order to emphasize that this part of the interaction Hamiltonian is responsible for the "direct" resonant influences on the system. To second order in μ and ν, after an analogous procedure, we obtain

$$\mathcal{H}_{\rm int}^p=h\left\{\left[1-\frac{m}{2}\right]\left[\frac{P_1P_3+P_0P_2}{m_\perp^2}+Q_0Q_1+Q_2Q_3\right]-\left[1+\frac{m}{2}\right]\left[\frac{P_0P_1+P_2P_3}{m_\perp^2}+Q_0Q_2+Q_1Q_3\right]\right\}\times\sin\left(\frac{\pi}{4}-\omega t\right)+h\left\{\left[1-\frac{m}{2}\right]\left[\frac{P_0Q_2+P_3Q_1}{m_\perp^2}+P_1Q_0+P_2Q_3\right]+\left[1+\frac{m}{2}\right]\left[\frac{P_0Q_1+P_3Q_2}{m_\perp^2}+P_2Q_0+P_1Q_3\right]\right\}\cos\left(\frac{\pi}{4}-\omega t\right). \tag{26}$$

Since Eq. (25) contains only quantities with indices 1 and 2, only the first azimuthal modes are excited in a direct resonance manner. The part of Hamiltonian (26) with superscript p ("parametric") is responsible for the parametric excitation of the system, but, as we have pointed out previously[10] and will show in detail below, the parametric excitation in this case is rather unusual.

The calculations below are less awkward to do if we go over to a description of the dynamics in terms of complex quantities:

$$\psi_n = \sqrt[4]{\frac{\alpha_n}{\beta_n}}\frac{P_n}{\sqrt{2}} + i\sqrt[4]{\frac{\beta_n}{\alpha_n}}\frac{Q_n}{\sqrt{2}}, \tag{27}$$

where ψ and ψ^* play the role of classical analogs of creation and annihilation operators, creating and annihilating normal modes. Here the total Hamiltonian of the system in the approximation quadratic in ψ_n is written as follows:

$$\begin{aligned}\mathcal{H} = {} & \frac{1}{2}\sum_{n=0}^{3}\Omega_n|\psi_n|^2 + h\frac{1-i}{2}[(1-m)\psi_1^* e^{-i\omega t} \\ & -(1+m)\psi_2^* e^{i\omega t}] - h\psi_1\frac{e^{i\omega t}(1+i)}{2\sqrt{2}} \\ & \times\left\{\psi_0\left[\frac{1+m/2}{m_\perp^2}\sqrt[4]{\frac{\beta_0}{\alpha_0}} + \left(1-\frac{m}{2}\right)\sqrt[4]{\frac{\alpha_0}{\beta_0}}\right]\right. \\ & \left. + \psi_0^*\left[\frac{1+m/2}{m_\perp^2}\sqrt[4]{\frac{\beta_0}{\alpha_0}} - \left(1-\frac{m}{2}\right)\sqrt[4]{\frac{\alpha_0}{\beta_0}}\right]\right\} \\ & + h\psi_2\frac{e^{-i\omega t}(1-i)}{2\sqrt{2}}\left\{\psi_0\left[\frac{1-m/2}{m_\perp^2}\sqrt[4]{\frac{\beta_0}{\alpha_0}}\right.\right. \\ & \left.\left. + \left(1+\frac{m}{2}\right)\sqrt[4]{\frac{\alpha_0}{\beta_0}}\right] + \psi_0^*\left[\frac{1-m/2}{m_\perp^2}\sqrt[4]{\frac{\beta_0}{\alpha_0}} - \left(1+\frac{m}{2}\right)\right. \right. \\ & \left.\left. \times\sqrt[4]{\frac{\alpha_0}{\beta_0}}\right]\right\} - h\psi_2\frac{e^{i\omega t}(1+i)}{2\sqrt{2}}\left\{\psi_3\left[\frac{1+m/2}{m_\perp^2}\right.\right. \\ & \left.\left. \times\sqrt[4]{\frac{\beta_3}{\alpha_3}} + \left(1-\frac{m}{2}\right)\sqrt[4]{\frac{\alpha_3}{\beta_3}}\right] + \psi_3^*\left[\frac{1+m/2}{m_\perp^2}\right.\right. \\ & \left.\left. \times\sqrt[4]{\frac{\beta_3}{\alpha_3}} - \left(1-\frac{m}{2}\right)\sqrt[4]{\frac{\beta_3}{\beta_3}}\right]\right\} \\ & + h\psi_1\frac{e^{-i\omega t}(1-i)}{2\sqrt{2}}\left\{\psi_3\left[\frac{1-m/2}{m_1^2}\sqrt[4]{\frac{\beta_3}{\alpha_3}} + \left(1+\frac{m}{2}\right)\right.\right. \\ & \left.\left. \times\sqrt[4]{\frac{\alpha_3}{\beta_3}}\right] + \psi_3^*\left[\frac{1-m/2}{m_\perp^2}\sqrt[4]{\frac{\beta_3}{\alpha_3}} - \left(1+\frac{m}{2}\right)\sqrt[4]{\frac{\alpha_3}{\beta_3}}\right]\right\} \\ & + \text{c.c.}, \end{aligned} \tag{28}$$

where c.c. stands for the complex conjugate of the entire expression preceding it. Accordingly, the dynamical equations (LLEs) are now written as

$$i\frac{d\psi_n}{dt} = \frac{\partial\mathcal{H}}{\partial\psi_n^*} \tag{29}$$

(and the anomalous set of complex-conjugate equations) or, in explicit form,

$$\begin{aligned} i\frac{d\psi_0}{dt} - \Omega_0\psi_0 = {} & h(a_1\psi_1 e^{i\omega t} + a_2\psi_1^* e^{-i\omega t} + a_3\psi_2 e^{-i\omega t} \\ & + a_4\psi_2^* e^{i\omega t}), \end{aligned} \tag{30}$$

$$\begin{aligned} i\frac{d\psi_1}{dt} - \Omega_1\psi_1 = {} & h(a_1^*\psi_0 e^{-i\omega t} + a_2\psi_0^* e^{-i\omega t} + b_1^*\psi_3 e^{i\omega t} \\ & + b_2\psi_3^* e^{i\omega t}) + h\zeta e^{-i\omega t}, \end{aligned} \tag{31}$$

$$\begin{aligned} i\frac{d\psi_2}{dt} - \Omega_2\psi_2 = {} & h(a_3^*\psi_0 e^{i\omega t} + a_4\psi_0^* e^{i\omega t} + b_3^*\psi_3 e^{-i\omega t} \\ & + b_4\psi_3^* e^{-i\omega t}) + h\xi e^{i\omega t}, \end{aligned} \tag{32}$$

$$\begin{aligned} i\frac{d\psi_3}{dt} - \Omega_3\psi_3 = {} & h(b_1\psi_1 e^{-i\omega t} + b_2\psi_1^* e^{i\omega t} + b_3\psi_2 e^{i\omega t} \\ & + b_4\psi_2^* e^{-i\omega t}), \end{aligned} \tag{33}$$

where for convenience of notation we have introduced the simplified notation for the coefficients, which are related to the original ones in the obvious way:

$$\begin{aligned} a_1 = {} & \frac{e^{-i\omega t}}{h}\frac{\partial^2\mathcal{H}}{\partial\psi_0^*\partial\psi_1} \\ = {} & -\frac{1+i}{2\sqrt{2}}\left[\frac{1+m/2}{m_\perp^2}\sqrt[4]{\frac{\beta_0}{\alpha_0}} - \left(1-\frac{m}{2}\right)\sqrt[4]{\frac{\alpha_0}{\beta_0}}\right],\ldots, \\ \zeta = {} & \frac{e^{i\omega t}}{h}\frac{\partial\mathcal{H}_{\text{int}}^d}{\partial\psi_1^*} = \frac{1-i}{2}(1-m), \\ \xi = {} & \frac{e^{-i\omega t}}{h}\frac{\partial\mathcal{H}_{\text{int}}^d}{\partial\psi_2^*} = -\frac{1-i}{2}(1+m) \end{aligned}$$

etc. We see that taking the circular magnetic field into account gives rise to terms responsible for both the direct and the parametric excitation of the eigenmodes. It should be noted that, as is seen from the structure of the system of equations obtained, the parametric excitation of each individual mode in a linear approximation occurs only on account of the remaining modes of the system, which can lead to parametric resonance at combination frequencies (see Part I).[10] This fact was not pointed out in Ref. 12, where the authors did not take into account the influence of the first azimuthal mode on the fundamental symmetric mode, i.e., they neglected terms of the form $\psi_0\psi_k$, $\psi_0\psi_k^*$, $\psi_0^*\psi_k$, and $\psi_0^*\psi_k^*$ with $k\neq 0$ in the Hamiltonian. Another interesting fact is that for a vortex at the center of the system, a circular magnetic field can lead to direct resonance only at the frequencies of the first azimuthal modes. In turn, owing to the presence of the cross terms in the phenomenological equations for the zeroth mode, direct resonance at the frequency of the first azimuthal mode can also lead to activation of the zeroth mode.

The resonance pattern of the inhomogeneous system of equations (30)–(33) with periodic coefficients can be obtained by using the method of multiple scales.[19] In the general case for correctness of the expansion obtained it is necessary that the modulus of the periodic coefficients be much less than the moduli of the constant coefficients of the equations. This is correct when the inequality $h \ll \Omega_n$ holds. Since in the case of a plaquette the eigenfrequencies are of the order of unity, it is sufficient to satisfy the inequality $h \ll 1$, i.e., the condition of weak pumping.

In accordance with the method of multiple scales, we replace the true time t by a set of "times" T_k, assuming that

$$\psi_n(h;t)=\psi_n^0(T_0,T_1,T_2\ldots)+h\psi_n^1(T_0,T_1,T_2\ldots)+\ldots, \tag{34}$$

where $T_k=h^kT_0$ are the different time scales, and

$$\frac{d}{dt}=\frac{\partial}{\partial T_0}+h\frac{\partial}{\partial T_1}+\ldots=\hat{D}_0+h\hat{D}_1+\ldots\ . \tag{35}$$

Substituting (34) and (35) into (30)–(33), we obtain in the zeroth approximation

$$i\hat{D}_0\psi_n=\Omega_n\psi_n \quad \text{and} \quad \psi_n^0=A_n(T_1,T_2)\exp(-i\Omega_nT_0).$$

To first order in h we obtain an inhomogeneous system of the form

$$\begin{aligned} i\hat{D}_0\psi_0^1-\Omega_0\psi_0^1=&-i\hat{D}_1A_0e^{-i\Omega_0T_0}+a_1A_1e^{i(\omega-\Omega_1)T_0}\\ &+a_2A_1^*e^{i(\Omega_1-\omega)T_0}+a_3A_2e^{-i(\omega+\Omega_2)T_0}\\ &+a_4A_2^*e^{i(\omega+\Omega_2)T_0} \end{aligned} \tag{36}$$

and the other analogous equations for ψ_n^1, $n=1,2,3$. According to Floquet theory,[19] at a boundary separating a region of exponentially growing solutions from a region of nongrowing solutions of a system of equations with periodic coefficients, the solution is a purely periodic function of time. To arrive at the curve (in terms of $\omega=\omega(h)$) on which the solution is purely periodic, it is necessary to eliminate the secular terms from the right-hand side of equations (36). If the combination frequencies of the inhomogeneous terms $\pm\omega\pm\Omega_n$ are far from the eigenfrequencies, then $\hat{D}_1A_n=0$ and $A_n=A_n(T_2,\ldots)$. We assume that the external pumping frequency is such that the following inequality holds:

$$\omega=\Omega_0+\Omega_1+h\sigma, \tag{37}$$

where σ is the detuning parameter. Then from the condition that the resonance terms be eliminated, we obtain from (36)

$$-i\hat{D}_1A_0+a_2A_1^*e^{-i\sigma T_1}=0, \tag{38}$$

$$-i\hat{D}_1A_1+a_2A_0^*e^{-i\sigma T_1}=0 \tag{39}$$

or

$$\hat{D}_1^2A_1^*+i\sigma\hat{D}_1A_1^*-|a_2|^2A_1^*=0,$$

where it is taken into account that $T_1=hT_0$, and also the remaining equations $\hat{D}_1A_n=0$, $n=2,3$. Hence, assuming $A_1^*=A_1^*(T_2,\ldots)\exp(i\epsilon T_1)$, we have

$$\varepsilon=\frac{\sigma}{2}\pm\sqrt{\frac{\sigma^2}{4}-|a_2|^2}. \tag{40}$$

We see that the increasing solutions (i.e., parametric resonance at the given combination frequency) exist under the condition $|a_2|^2>0$, which obviously holds, and the form of the resonance curve $\omega=\omega(h)$, separating the region of stable oscillations from the exponentially growing solutions, in a first approximation in h has the form

$$\omega(h)=\Omega_0+\Omega_1\pm2h|a_2|. \tag{41}$$

Thus a parametric resonance is observed at the positive combination frequency $\Omega_0+\Omega_1$. By doing an analogous treatment of all the remaining cases, one can show the following:

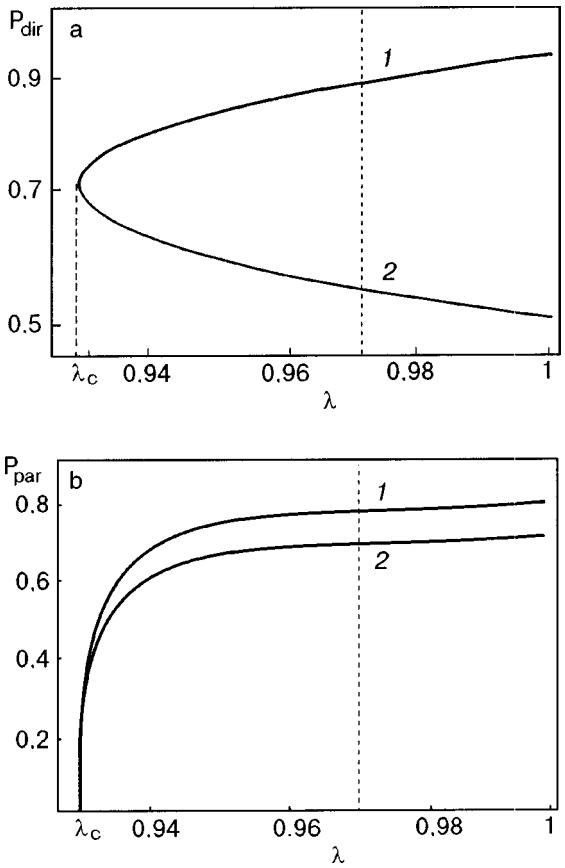

FIG. 3. The "power" of the direct (a) and parametric (b) resonances as functions of the anisotropy parameter in the OP region. The dotted line corresponds to the value $\lambda=0.97$ for which the numerical calculations were done.

(1) There is no parametric resonance at the positive frequency $\omega=\Omega_1-\Omega_0$.
(2) Similarly, there is no parametric resonance at the negative frequency $\omega=\Omega_0-\Omega_2$.
(3) The parametric resonance at the negative frequency $\omega=-\Omega_0-\Omega_2$ does exist, and the resonance curve has the form

$$\omega(h)=-\Omega_0-\Omega_2\pm2h|a_4|. \tag{42}$$

Thus parametric resonances can occur in a plaquette only at the frequencies $\Omega_0+\Omega_1$ and $-\Omega_0-\Omega_2$. Since $\Omega_1\neq\Omega_2$ for any λ from the region $\lambda>\lambda_c$, the asymmetry of the resonance curve with respect to a change in sign of the external pump frequency is obvious. The conclusions as to the presence of parametric resonances of the first order (in the field amplitude) at combination frequencies, including the sum (with the appropriate sign) of the frequencies of the symmetric and first azimuthal modes, are in agreement with the data from the analysis in Part I,[10] but the frequency asymmetry was not discussed there.

In system (30)–(33) there also exist direct resonances of first order in h: at the frequency $\omega=-\Omega_2$ and at the frequency $\omega=\Omega_1$ with different "powers"—amplitude factors $|\xi|\sim(1-m)$ and $|\zeta|\sim(1+m)$ from Eqs. (31), (32) (see Fig. 3a). Thus the pattern of direct resonances is also asymmetric with respect to a change in sign of the pump frequency. Figure 3b shows the "power" of the parametric resonances in the system as a function of the anisotropy parameter λ in

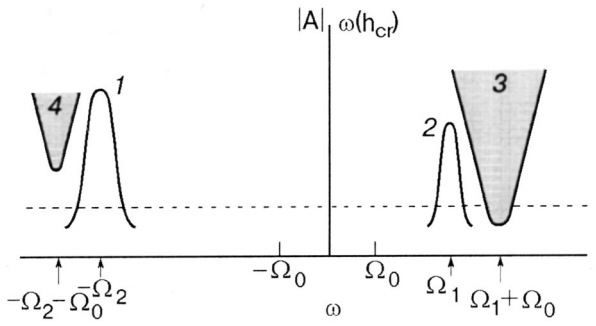

FIG. 4. Illustrative scheme of the main resonances of a plaquette containing a vortex: for direct resonances the dependence of the oscillation amplitudes of the spins on the pump frequency is shown, and for the parametric resonances, the characteristic curves $\omega(h_{cr})$ and the regions of instability (shaded). For each of the resonance curves the presence of finite damping is taken into account. The labels *1,2,3,4* correspond to Fig. 3. The dotted line corresponds to resonances found in the numerical study.

the existence region of the out-of-plane vortex (i.e., the dependence on λ of the opening angle of the curve $\omega=\omega(h_{cr})$, which bounds the regions of exponential instability). The power of the parametric resonance is defined as $P_{par}=\pi-2\tan^{-1}(2|a_2|)$ for resonance *3* at the frequency $\Omega_0+\Omega_1$, and by the same expression but with $|a_4|$ for resonance *4* at the frequency $-\Omega_0-\Omega_1$, $P_{1,2}^{par}(\lambda_c)=0$. From the curves given it is easy to determine the sequence in which the resonances should arise (when damping is taken into account) as the amplitude h of the external influence increases. The first of the direct resonances to appear should be the resonance at the frequency $\omega=-\Omega_2$, which has a high power. The first of the parametric resonances is that at the frequency $\omega=\Omega_0+\Omega_1$. Figure 4 shows the frequency dependence of the oscillation amplitude (the amplitude–frequency characteristics) for the direct resonances and the curves of the critical value of the amplitude of the external field as a function of the pump frequency (the critical characteristics) for the parametric resonances. Performing the expansion by the method of multiple scales, one can show that in the second order in h only a renormalization of the resonances frequencies, of order h^2, arises, and no additional resonances appear.

Thus in the activation of the low-frequency modes the following pattern arises: upon a change in the direction of rotation of the external circular field, the role of the lowest first azimuthal mode begins to be played by the next azimuthal mode (as has been noted in a number of previous papers, these modes can be regarded as spin waves rotating in opposite directions), and that leads to a frequency asymmetry of the observed resonance interaction upon a change in the sign of ω. In the general case the ''power'' of the resonance (determined by the value of the amplitude factors for a direct resonance and by the opening angle of the characteristic $\omega=\omega(h_{cr})$ of the form (41), (42) for a parametric resonance) is also different for different directions of rotation of the pump field even in the linear approximation. It should be noted that the remarks concerning the presence of a direct resonance are also correct in the case of an arbitrary system with a fixed boundary, since in the derivation of the dynamical equations only the symmetry of the modes themselves and of the external field was taken into account. The presence of a parametric resonance, on the other hand, is determined by the sign in front of the coefficient $|a_i|^2$ in conditions of the form (40) for the different modes, and the power of a particular parametric resonance (if it exists) depends only on the value of $|a_i|^2$, which in turn depends on the configuration of the static vortex solution in the system (and, hence, on the system itself) and the value of the anisotropy. Therefore, in going from a small plaquette to a macroscopic system only a quantitative change in the results is possible. However, by using the procedure described above, it is straightforward to derive a set of criteria (similar to those which we derived for the case of the interaction of the zeroth and azimuthal modes) that will predict the existence of a parametric resonance at combination frequencies by starting from the value of the static discrete distribution of spins in the OP vortex. The results regarding the presence of a direct resonance at the frequencies of the first azimuthal modes also remain valid for considering systems with a free boundary. In that case, however, the lowest zeroth mode is absent (its frequency is identically equal to zero), so that the pattern of the combination parametric resonances in the system is qualitatively altered. However, as was pointed out in Ref. 12, a change in the form of the boundary conditions does not entail a substantial rearrangement of the resonance pattern. Therefore, it can be stated that the main effect should be a direct resonance at the frequencies of the first azimuthal modes, and that has been confirmed in our subsequent numerical studies.

3. NUMERICAL ANALYSIS OF THE DYNAMICS OF A SPIN PLAQUETTE IN A CIRCULAR MAGNETIC FIELD

To confirm and check the results of the analytical treatment of the mechanism of vortex switching in Sec. 2 and also to get an understanding of the relation of the linear analysis to the true physical picture (since the switching itself is a substantially nonlinear phenomenon, the resonant activation of the eigenmodes of the system by an external field is not guaranteed to lead to a change in polarization of the OP vortex, since here a linear treatment is insufficient), we carried out a series of numerical simulations and modeled the process of switching of an OP vortex for a plaquette. The system of eight nonlinear equations (1), (2) for the plaquette was integrated by the Runge–Kutta method for different values of the frequency and amplitude of the external field. At the chosen value of the anisotropy parameter $\lambda=0.97$ the total z projection of the magnetization in the OP vortex configuration, $|M|=4|m|\approx 1.12$, is large enough for a precise and unambiguous determination of the polarization of the vortex. At the same time, the static value $m\approx 0.28$, which is much smaller than unity, allows one to do the integration by determining the direction of the spin vector in spherical projections, making it possible to satisfy the condition $|\mathbf{S}_n|=1$ without additional procedures and expenditure of computer time. As the initial configuration we chose the static distribution (5) with $p=1$ (spins directed upward) for an OP vortex found precisely at the center of the plaquette, and then an external field was turned on and the dynamic behavior of each of the four spins was tracked. For stabilization of the system a weak damping $\gamma=6\times 10^{-3}$ was taken into account

(this led only to an insignificant renormalization, of order γ^2, of the eigenfrequencies of the system). The eigenfrequencies for a value of the anisotropy parameter $\lambda = 0.97$ are as follows: frequency of the zeroth mode (14) $\Omega_0 \approx 0.55$; frequency of the lower first azimuthal mode (16) $\Omega_1 \approx 1.38$; frequency of the upper first azimuthal mode (18) $\Omega_2 \approx 2.5$; frequency of the second azimuthal mode (20) $\Omega_3 \approx 2.68$ (see Fig. 1). The dependence of the vortex switching time τ on the frequency of the circular pump was found to first order for different values of the amplitude h of the external circular field h. The corresponding curves are shown in Fig. 5. The switching time was considered to be that time at which the total z projection of the magnetization of the system became equal to the initial value but with the opposite sign: $M = -1.12$. It is seen in Fig. 5a,b,c that initially (at small values of h) the first switching occurs at a negative frequency $\omega \approx -2.43$ (Fig. 5a). With increasing field amplitude another region, at positive frequencies with $\omega \approx 1.46$ is added (Fig. 5b). Finally, at still larger values of the external field a third switching region arises, at positive frequencies with $\omega \approx 1.92$ (Fig. 5c).

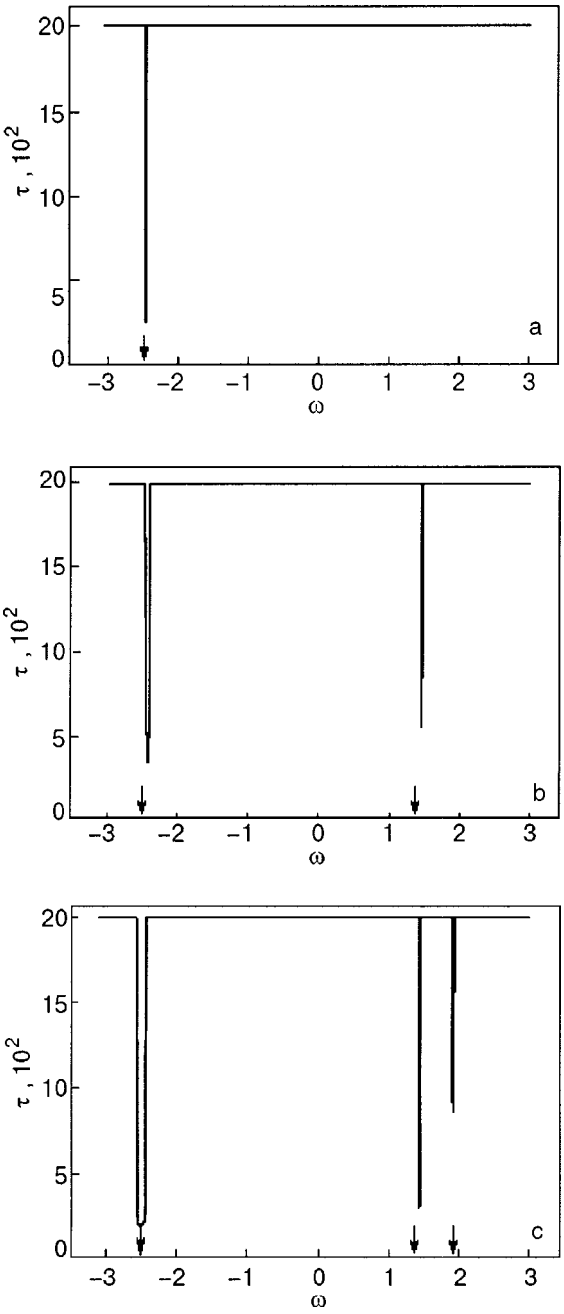

FIG. 5. Numerically obtained dependence of the vortex switching time on the frequency of the external field for different values of its amplitude h, 10^{-2}: 0.65 (a), 0.8 (b), 1.05 (c). The value of the damping used was $\gamma = 0.6 \times 10^{-2}$. The arrows indicate the values of the resonance frequencies predicted analytically.

By comparing the results of the numerical analysis with the data from the analytical treatment of the mechanism of activation of the eigenmodes of the plaquette and also taking into account the values of the eigenfrequencies of the system for $\lambda = 0.97$, one can conclude that the most pronounced switching is that due to the direct resonance at a negative frequency of the upper first azimuthal mode $\omega \approx -\Omega_2$, then the weaker direct resonance at the frequency of the lower azimuthal mode $\omega \approx \Omega_1$, and then the strongest parametric resonance is seen, at the combination frequency $\omega \approx \Omega_0 + \Omega_1$. The slight difference between the values of the frequencies at which switching was observed and the values of the eigenfrequencies is apparently due to the deformation of the amplitude–frequency characteristics for the direct resonance and of the $\omega(h_{cr})$ curves for the parametric resonance on account of nonlinearity, and also to the nonlinear frequency shift (the change, of order h^2, in the eigenfrequencies can also be neglected, since the amplitude of the applied field is rather small). Figure 6a, b shows the curve of $M(t) = m_1(t) + m_2(t) + m_3(t) + m_4(t)$ for the switching regions $\omega = -2.43$ and 1.92. (The form of the $M(t)$ curve for

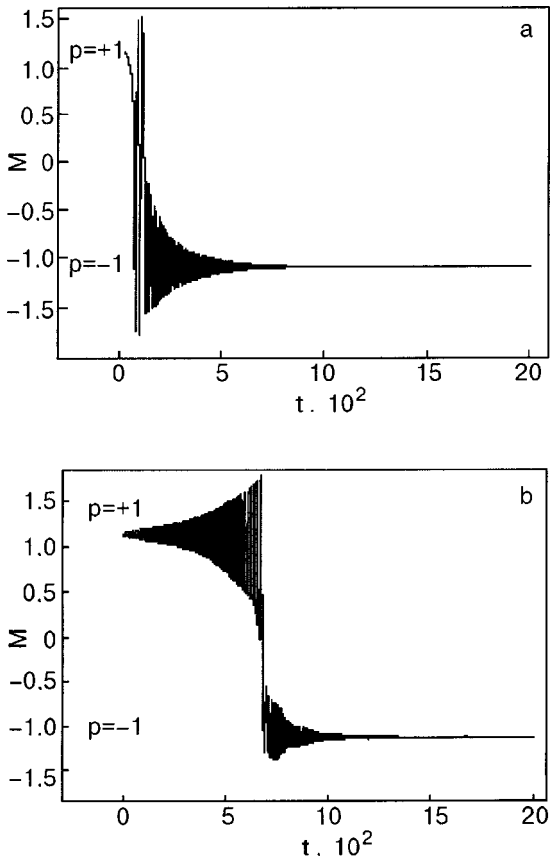

FIG. 6. Time dependence of the total z component of the magnetization for a direct resonance (a) and a parametric resonance (b). The value of the field amplitude was $h = 1.1 \times 10^{-2}$.

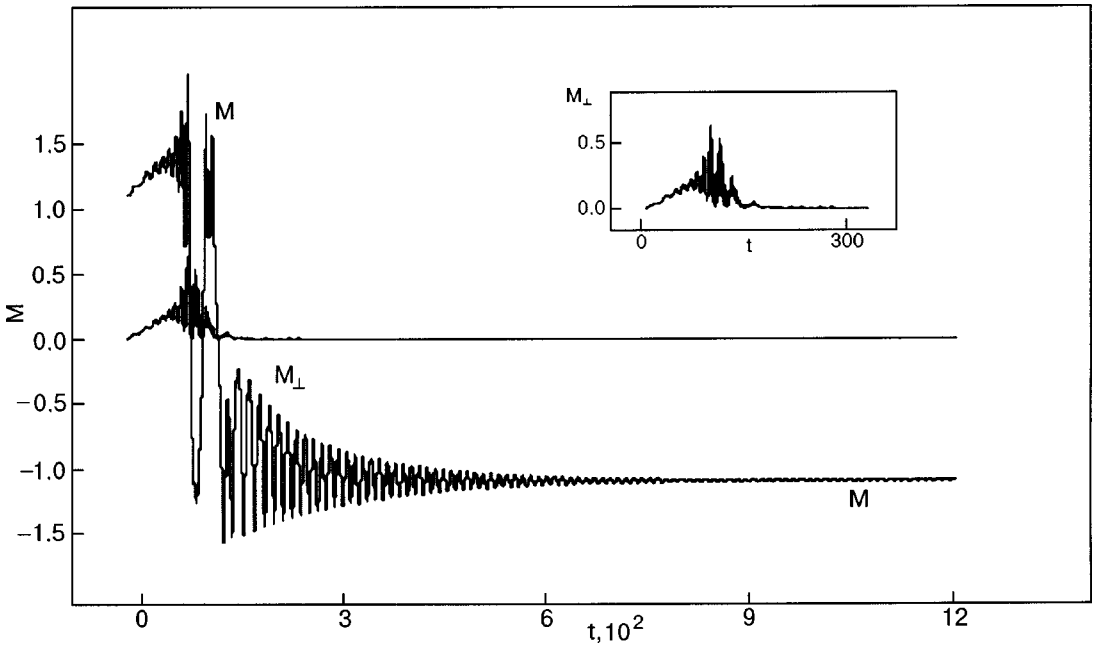

FIG. 7. Time dependence of the total z component M and the in-plane component $M_\perp$ (see also the inset) of the magnetization. The field amplitude $h=0.9\times10^{-2}$.

switching at $\omega=1.46$ is basically the same as that shown in Fig. 6a). From a comparison of these figures one can see the qualitative difference of the activation process for these regions—the switching at the direct resonance frequencies $\omega\approx\Omega_1$ and $-\Omega_2$ occurs rapidly, with a very short activation time, as should be observed at a direct resonance. At the parametric resonance frequency a slower, exponential growth of the oscillations amplitude takes place.

In Fig. 7 the time dependences of the total z projection of the spins and of the in-plane component of the total magnetization $M_\perp(t)=\sqrt{(\Sigma_n S_n^x)^2+(\Sigma_n S_n^y)^2}$ for switching at the frequency $\omega=-2.43$ (for $\omega=1.46$ the form of these curves is basically the same) are shown on one graph. If the vortex switching is due to activation of only a symmetric mode, then in the course of the switching one should observe the equality $M_\perp\approx0$. If azimuthal modes are involved in it, then the total in-plane magnetization should be nonzero. The form of the curves obtained suggests that at least in the initial stage of the switching the first azimuthal modes are sharply excited. Subsequently the switching itself takes on the symmetry of the zeroth mode, a circumstance that confirms the analytical conclusion that the first azimuthal modes play a sort of ''catalytic'' role in the switching process: the growth of the amplitude of these modes leads to activation of the zeroth mode, as a consequence of the presence of crossing terms in the dynamical equations (30)–(33) and also because of the nonlinear mode–mode coupling (when the amplitudes of the modes become sufficiently large). In turn, for systems with a fixed boundary the switching due to activation of the symmetric mode is energetically most favorable, in agreement with what was stated in Ref. 12.

The numerical analysis permits the conclusion that the most important element of the activation process is the direct excitation at the azimuthal mode frequencies, which leads to secondary activation of the zeroth mode, and the switching process itself basically acquires the symmetry of this zeroth mode.

In studying the dynamics of a spin plaquette we did not discern any destruction of the vortex configuration by large-amplitude oscillations in the case of a positive sign of the frequency of the circular pump (as had been observed in the numerical simulations by the authors of Ref. 12). Apparently this is because in our plaquette treatment there is practically no difference in the amplitudes of the switching field for the case of switching at positive and negative frequencies, and this effect becomes noticeable only for systems of large size. However, the plaquette treatment obviously gives an explanation for the nonequivalence of the signs of the frequency in the switching process. In the numerical simulation we also did not attain the values of the field amplitude at which the parametric resonance at the negative frequency $\omega=-\Omega_0-\Omega_2$ would be noticeable. However, as was shown in Sec. 2, the parametric resonance at that frequency has a lower power than the resonance at $\omega=\Omega_0+\Omega_1$.

CONCLUSION

In this paper we have presented a detailed study of a new mechanism for the process by which the polarity of an OP vortex in an easy-plane ferromagnet is switched in a circular field; this mechanism, which was proposed in Part I of this study,[10] differs fundamentally from that considered earlier in Ref. 12. The approximate qualitative treatment of the vortex switching process from Ref. 10 is bolstered by an analysis of this process in a small spin plaquette, for which an exact analytical treatment of the linear problem of the activation of eigenmodes by a circular pump is possible. The essence of the proposed mechanism of activation of the system is that the low-frequency circular external field excites the lowest-lying azimuthal modes, which, in turn, act as a ''catalyst'' for

growth of the amplitude of the zeroth ''symmetric'' mode, which is what leads to vortex switching. The studies done and a comparison of the data of the present study with the results of the Part I[10] show that this unusual mechanism for a change of polarity is dominant for vortices found far from the center of the system, and it completely suppresses the mechanism of direct activation of the symmetric mode which was proposed in Ref. 12, involving the asymmetry of the vortex due to its displacement from the center of the system. We have proposed a scheme for constructing a criterion by which one could predict the possibility of parametric resonances at combination frequencies from the coefficients of the linear equations (which are determined solely by the static distribution of the magnetization in the OP vortex). We note in this regard that by considering a plaquette one can make a generalization to the case of an arbitrary system with a fixed boundary, and the conclusions as to the direct resonance at the frequency of the azimuthal modes with the corresponding sign are applicable to an arbitrary system with boundary conditions of any type; this agrees with the conclusions stated in Ref. 10. The data obtained, and a comparison with the previous numerical results,[12] make it possible to construct a more correct (applicable to a vortex found close to the center of the system) two-mode model for describing the process of change of the vortex polarization: the simplest model, which in the linear limit must give the results of our linear treatment, should take into account in a phenomenological way the presence of nonlinear terms of the form $|\psi_n|^2|\psi_k|^2$, $n,k=0,1$ in the Hamiltonian. However, in constructing such models it is necessary to keep in mind that, despite the formal equivalence of the mechanism for the switching from the state with $p=1$ to $p=-1$ and vice versa (with the lowest azimuthal mode replaced by the next, rotating in the opposite direction), switching under an asymmetric influence (in particular, during pumping by a circular field) has a preferred direction, and so modes of that kind can describe adequately only the switching in one direction. In the final analysis the asymmetry of the process by which the polarization of the vortex is switched is due to the lifting of the degeneracy of the frequency dependence of the azimuthal modes in the OP configuration, and thus it is of paramount importance to take them into account.

The authors are grateful to Yu. B. Gaididei and A. M. Kosevich for some stimulating discussions and helpful comments, and to N. N. Korabl' for assistance in the numerical investigations. We also express our gratitude to the INTAS program for partial support of this study under the grant INTAS No. 99-0167.

Material in this paper was presented at the Conference on Nonlinear Lattice Structure and Dynamics, Dresden, 2001.

*E-mail: kovalev@ilt.kharkov.ua

[1] R. P. Cowburn, D. K. Koltsov, A. O. Adeyeye, M. E. Welland, and D. M. Tricker, Phys. Rev. Lett. **83**, 1042 (1999); R. P. Cowburn, J. Phys. D **33**, R1 (2000).
[2] T. Shinjo, T. Okuno, R. Hassdorf, K. Shigeto, and T. Ono, Science **289**, 930 (2000); ICR Ann. Rep. **7**, 16 (2000).
[3] L. Thomas, F. Lionti, R. Ballou, D. Gatteschi, R. Sessoli, and B. Barbara, Nature (London) **383**, 145 (1996).
[4] J. Kortus, M. R. Pedersen, C. S. Hellberg, and S. N. Khanna, Eur. Phys. J. D **16**, 177 (2001); N. Fujima, *ibid.* **16**, 185 (2001).
[5] A. M. Kosevich, B. A. Ivanov, and A. S. Kovalev, *Nonlinear Magnetization Waves. Dynamic and Topological Solitons* [in Russian], Naukova Dumka, Kiev (1983).
[6] M. Kosevich, B. A. Ivanov, and A. S. Kovalev, Phys. Rep. **194**, 117 (1990).
[7] A. M. Kosevich, V. P. Voronov, and I. V. Manzhos, Zh. Éksp. Teor Fiz. **84**, 148 (1983) [Sov. Phys. JETP **57**, 87 (1983)].
[8] A. V. Nikiforov and É. B. Sonin, Zh. Éksp. Teor Fiz. **85**, 148 (1983) [Sov. Phys. JETP **58**, 373 (1983)].
[9] F. G. Mertens and A. R. Bishop, *Nonlinear Sciences at the Dawn of the 21st Century*, Lecture Notes in Physics, P. L. Christiansen, M. P. Soerensen, and A. C. Scott (eds.), Springer, Berlin (2000), p. 137.
[10] A. S. Kovalev and J. E. Prilepsky, Fiz. Nizk. Temp. **28**, 921 (2002) [Low Temp. Phys. **28**, 921 (2002)].
[11] Yu. Gaididei, T. Kamppeter, F. G. Mertens, and A. R. Bishop, Phys. Rev. B **59**, 7010 (1999).
[12] Yu. Gaididei, T. Kamppeter, F. G. Mertens, and A. R. Bishop, Phys. Rev. B **61**, 9449 (2000).
[13] A. S. Kovalev and J. E. Prilepsky, Vestn. KhGU Ser. Fiz. **417**, 32 (1998).
[14] A. S. Kovalev and J. E. Prilepsky, Vestn. KhGU Ser. Fiz. **440**, 25 (1999).
[15] G. M. Wysin, Phys. Lett. A **240**, 95 (1998).
[16] M. E. Gouvea, G. M. Wysin, A. R. Bishop, and F. G. Mertens, Phys. Rev. B **39**, 11840 (1989).
[17] G. M. Wysin and A. R. Völkel, Phys. Rev. B **52**, 7412 (1995).
[18] B. A. Ivanov, H. J. Schnitzer, F. G. Mertens, and G. M. Wysin, Phys. Rev. B **58**, 8464 (1998).
[19] H. Nayfeh and D. Mook, *Nonlinear Oscillations*, Wiley, New York (1995).

Translated by Steve Torstveit

Effective equations of motion for solitons in two-sublattice isotropic magnets

E. G. Galkina

Institute of Physics, National Academy of Sciences of Ukraine, pr. Nauki 46, 03028 Kiev, Ukraine

B. A. Ivanov*

Institute of Magnetism of the National Academy of Sciences and Ministry of Science and Education of Ukraine, bul'v. Vernadskogo 36b, 03142 Kiev, Ukraine; Radio Physics Department, Taras Shevchenko Kiev National University, pr. Glushkova 2, 03127 Kiev, Ukraine

V. M. Murav'yov

Institute of Magnetism of the National Academy of Sciences and Ministry of Science and Education of Ukraine, bul'v. Vernadskogo 36b, 03142 Kiev, Ukraine; National Aviation University, pr. Kosmonavta Komarova 1, 03058 Kiev, Ukraine

(Submitted July 16, 2002)
Fiz. Nizk. Temp. **29**, 84–92 (January 2003)

A solution of the problem of magnon scattering on Belavin–Polyakov solitons in two-dimensional magnets is constructed in the framework of a generalized σ model. This model can serve as a basis for describing both ferromagnets and antiferromagnets, and it can also describe ferrimagnets near the point of compensation of the sublattice spins. The problem of magnon scattering on a soliton is formulated‘ for this model, and its exact solution is obtained for a partial mode with azimuthal quantum number $m=1$. It is shown that in a linear approximation this mode completely describes the dynamics of the center of the soliton in a magnet of finite size. Effective equations of motion for solitons in different magnets are constructed on the basis of this analysis. © *2003 American Institute of Physics.*
[DOI: 10.1063/1.1542379]

It is well known that in low-dimensional magnets a special role can be played by nonlinear elementary excitations—solitons. In some cases the thermodynamic properties of one-dimensional and two-dimensional magnets are governed by the soliton contribution. Solitons are responsible for the lack of long-range order at nonzero temperatures in one-dimensional and isotropic two-dimensional magnets. In one-dimensional magnets this is due to kinks (see, e.g., the reviews[1–3]) and in two-dimensional magnets, to localized Belavin–Polyakov solitons. For two-dimensional easy-plane ferromagnets it has been shown that the presence of nonlocal solitons (vortices) leads to a special form of phase transition—a Berezinskiĭ–Kosterlitz–Thouless phase transition.[5,6] The motion of solitons and the soliton–magnon interaction lead to a soliton contribution to the dynamic response function, which can be investigated experimentally by neutron scattering[7] and spin-wave damping[8–10] studies.

The dynamic description of a wide class of classical two-dimensional isotropic Heisenberg magnets can be given in terms of the classical unit vector order parameter $\mathbf{n}$, $n_x+in_y=\sin\theta e^{i\varphi}$, $n_z=\cos\theta$.[1,11] The dynamics of a classical ferromagnet is described by the Landau–Lifshitz equation for the normalized magnetization, which in this case plays the role of the dynamical variable $\mathbf{n}$. In a classical antiferromagnet the dynamical variable is the antiferromagnetic vector, which in the long-wavelength approximation can be treated as a unit vector. The dynamics of an antiferromagnet is described by the Lorentz invariant σ model of the $\mathbf{n}$ field. Both types of magnets will be treated in the framework of a unified approach, based on the the generalized σ model, the dynamical equations of which have the form

$$\nabla^2 0-\sin\theta\cos\theta\left[\frac{1}{c^2}\left(\frac{\partial p}{\partial t}\right)^2-(\nabla\varphi)^2\right]=\frac{1}{c^2}\frac{\partial^2\theta}{\partial t^2}+\frac{\zeta\sin\theta}{D}\frac{\partial\varphi}{\partial t}, \tag{1}$$

$$\nabla(\sin^2\theta\nabla\varphi)=\frac{1}{c^2}\frac{\partial}{\partial t}\left(\sin^2\theta\frac{\partial\varphi}{\partial t}\right)-\frac{\zeta\sin\theta}{D}\frac{\partial\theta}{\partial t}. \tag{2}$$

Here the parameter D has the meaning of the coefficient of spin stiffness of the ferromagnet, and c is the spin-wave velocity in the antiferromagnet. In the nearest-neighbor interaction approximation one has $D=JSa^2/\hbar$ and $c=2JSa\sqrt{Z}/\hbar$, where J is the modulus of the exchange integral, S is the spin of the atom, a is the lattice constant, and Z is the number of nearest neighbors. The particular type of magnet is determined by the relationship between the parameters c and D/ζ. For finite D and c the generalized σ model describes a ferrimagnet near the compensation point of the mechanical moments of the sublattices. For such a magnet the gyroscopic term (the term linear in the time derivative) in the equations has the same structure as in a ferromagnet but is proportional to the small parameter $\zeta=(S_1-S_2)/(S_1+S_2)$, where S_1 and S_2 are the average values of the mechanical moments of the atoms of the two sublattices.[11] For describing a ferromagnet one should drop the second derivatives with respect to time from the equations, i.e., formally let c tend to infinity and set $S_2=0$, i.e., $\zeta=1$. The dynamic

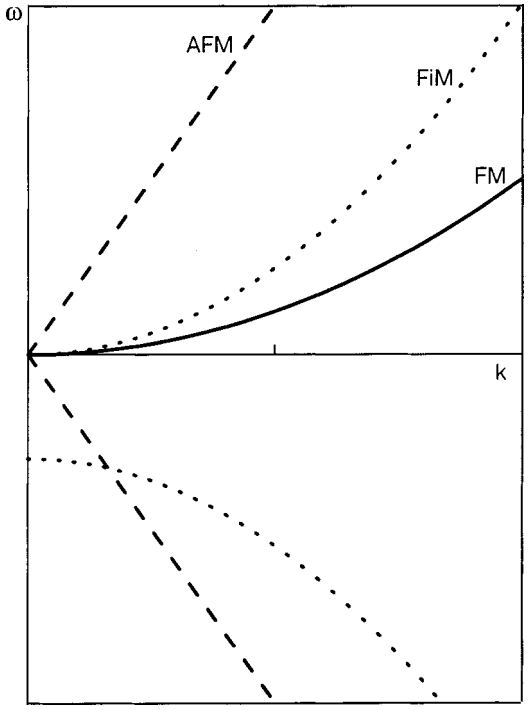

FIG. 1. Magnon dispersion relations for various isotropic magnets described by the generalized σ model: ferromagnet (FM), antiferromagnet (AFM), ferrimagnet (FiM).

term in the Lagrangian of a ferromagnet is of a purely gyroscopic nature. The dynamics of the isotropic σ model, which describes an antiferromagnet, has a Lorentz invariant form with a characteristic velocity parameter c. For an antiferromagnet the gyroscopic term is absent (one must set $\zeta=0$).

The simplest linear elementary excitation of an isotropic magnet, arising against the background of the uniform ground state, are magnons of the continuum spectrum. By choosing an orientation of the order parameter **n** along the polar axis, we obtain magnon solutions in the form of circularly polarized waves with $\theta=\text{const}\ll 1$, $\varphi=\mathbf{k}\cdot\mathbf{r}-\omega(k)t$. The dispersion relation for a ferromagnet is quadratic: $\omega_{FM}(k)=Dk^2$ (see Fig. 1).

In the case of an antiferromagnet the dispersion relation is linear, $|\omega_{AFM}(k)|=ck$; it has two degenerate branches with opposite circular polarizations, $\omega=\pm ck$, which means that linear polarization of the magnons is possible. For a ferrimagnet there are two branches, as in the antiferromagnet, but here the two branches are nondegenerate, their frequencies being given by

$$\omega^{(\pm)}=-\zeta\frac{c^2}{2D}=\sqrt{\left(\zeta\frac{c^2}{2D}\right)^2+c^2k^2}. \tag{3}$$

For small k one branch of magnons, as in a ferromagnet, has a gapless dispersion relation $\omega_{1,FIM}(k)=Dk^2/\zeta$, while the second has a nonzero activation $\omega_{2,FIM}\to-\zeta c^2$ for $k\to 0$.

For an isotropic magnet in the two-dimensional case an exact analytical solution is known, describing the Belavin–Polyakov soliton:[4]

$$\tan\frac{\theta_0}{2}=x^{-|\nu|},\quad \varphi_0=\alpha+\nu\chi,\quad x=\frac{r}{R}. \tag{4}$$

Naturally, this solution has the same form for both the ferro- or antiferromagnet and the ferrimagnet. Here r and χ are the polar coordinates in the plane of the magnet, the integer ν is the topological charge of the soliton, and R and α are arbitrary parameters.

The energy of such a soliton is determined by the formula

$$E_0=4\pi JS^2|\nu|$$

and is independent of R and α. The nonuniqueness in the choice of α is characteristic for many models and is a consequence of the isotropicity of the Heisenberg exchange. The existence of an arbitrary parameter R (soliton radius) and the fact that the energy is independent of R are due to the scale invariance of the static two-dimensional σ model.[4] It is clear that this symmetry is broken in dynamics, except for the trivial case of a pure antiferromagnet and translational motion, where everything reduces to a Lorentz transformation.

The equations of the nonlinear σ model for an antiferromagnet are formally Lorentz invariant with a characteristic velocity c—the magnon phase velocity. Consequently, the dynamical properties of solitons in antiferromagnets can be analyzed using a Lorentz transformation with respect to the nonmoving soliton. In particular, in antiferromagnets the energy and momentum of solitons moving at an arbitrary velocity **v** is given by

$$E(v)=\frac{E_0}{\sqrt{1-v^2/c^2}},\quad \mathbf{P}(v)=\frac{\mathbf{v}}{c}\frac{E_0}{\sqrt{c^2-v^2}}$$

with a dispersion relation having the standard Lorentz invariant form, $E(P)=\sqrt{E_0^2+c^2P^2}$, where E_0 is the energy of the nonmoving soliton. In the case of interest here, that of low soliton velocities $v\ll c$, this means that in the leading approximation the soliton coordinate **X** in the case of an antiferromagnet satisfies a Newton equation with a completely determinate mass M, $M_{AFM}=E_0/c^2$:

$$M\frac{d^2\mathbf{X}}{dt^2}=\mathbf{F}_e, \tag{5}$$

where $\mathbf{F}_e$ is the external force acting on the soliton.

The dynamical properties of solitons in ferromagnets have not been adequately studied. It has only been established for them that the dynamical equations contain a gyroscopic term $G[\mathbf{e}_z,d\mathbf{X}/dt]$, the value of which is determined by the topology. For a soliton $G=4\pi\nu JS^2/D$. Of course, the combination of this term with the Newton equations (5) should lead to Larmor precession of the soliton center with a frequency $\omega_L=G/M$. However, the situation turns out to be more complicated than that. Both for a soliton in an isotropic magnet and for a vortex in an easy-plane magnet the magnon spectrum is gapless. This implies that for soliton motion of the Larmor precession type with a finite frequency ω_L, that frequency inevitably falls in a magnon continuum. As a result, soliton motion excites magnon modes, and that will lead to fundamentally different consequences for soliton motion in an unbounded medium and in a finite sample. For the case of interest, a magnet of finite size, one expects that the radiation of magnons, their reflection off the boundary, and their effect back on the soliton will result in the establishment of a dynamical state of the magnet which includes both

the moving soliton and the coherent magnetization oscillations matched to the soliton motion. For understanding this complex picture, direct numerical simulations of soliton motion for ferromagnets of approximately circular shape (cut out from a square lattice up to 200×200 in size) under the influence of image forces exerted by the boundary[12,13] have proved to be extremely important. In those studies it was shown that the soliton motion is not described by simple second-order equations of the Newton type, and it is necessary to introduce dynamical equations of higher order in the time derivatives. Following this idea, the authors of Ref. 14 state that an adequate description of the dynamics of a magnetic vortex in an easy-plane ferromagnet can be obtained only with the use of a complicated hierarchy of equations of motion, containing all the higher time derivatives. To understand this, we must address the question of in what sense it is meaningful to speak of nonuniform motion of a vortex (which is not a localized disturbance of the field) in an easy-plane magnet or of a Belavin–Polyakov soliton (in which the localization is weak) in an isotropic magnet.

For calculating the soliton contribution to the response function of a magnet, it is the coordinate of the center of the soliton that is important. The behavior of this coordinate has been analyzed in numerical simulations.[12,13] Thus we arrive at the problem of constructing effective equations of soliton dynamics, i.e., equations describing the motion of a certain point **X**, chosen as the center of the soliton, without taking into consideration that magnon modes linked to the time evolution of $\mathbf{X}(t)$ can be excited far from the soliton. In this approach the soliton coordinate $\mathbf{X}=\mathbf{X}(t)$ plays the role of a *collective variable* describing both the dynamics of a finite number of spins coupled to the soliton as such and also the dynamics of the magnon modes far from the soliton. It is clear that such equations can be constructed only approximately, and it is important to establish how the form of those equations will change as the accuracy is increased (e.g., as an ever greater number of spins are taken into account). In addition, it is clear that such equations at a certain level become *nonlocal*, i.e., the coefficients in them will depend substantially on the size and shape of the system. Just such a situation arose in the construction of the effective equations for magnetic vortices proposed in Ref. 12. On the other hand, analysis of the data from a numerical simulation has established that the equations linear in the time derivative of the displacement of the soliton from the center of the system give an adequate description of the dynamics of the soliton center, even when the initial displacement is not small (10–20% of the dimension of the system). This means that in practice the only source of nonlinearity in the equations is due to the static term—an external force, e.g., an image force. This led to the idea of recovering the dynamical equations describing the soliton motion from data on small oscillations of the magnetization against the background of the soliton. Indeed, since the image force acting on a magnetic vortex is easily calculated, the frequencies of several magnon modes can be coupled with the dynamic terms in the equations of motion.

Thus we arrive at the problem of small oscillations of the magnetization against the background of the soliton (this approach was developed by Wysin[15]). Analysis of this problem is complicated considerably in comparison with the one-dimensional case by the fact that numerical methods are used even for studying nonmoving solitons, which is an obvious first stage in the analysis of the dynamics. Here again the most interesting case is the isotropic σ model, for which not only is the nonmoving soliton solution known but substantial progress has been made in the analysis of magnons against the background of the soliton.

For the analysis of small oscillations of the magnetization against the background of the Belavin Polyakov soliton it is necessary to consider the deviation of the angle variables θ and φ from their values in the soliton θ_0 and φ_0, respectively. It is convenient to introduce $\vartheta=\theta-\theta_0$ and the variable $\mu=(\varphi-\varphi_0)\sin\theta_0$ and then change to the complex variable $\psi=\vartheta+i\mu$. After straightforward transformations the problem reduces to a complex equation of the form

$$\hat{H}\psi+\Delta U\psi^*-\frac{2\cos\theta_0}{x^2}i\frac{\partial\psi}{\partial\chi}=-i\frac{DR^2}{\zeta}\frac{\partial\psi}{\partial t}-\frac{R^2}{c^2}\frac{\partial^2\psi}{\partial t^2}, \tag{6}$$

where $\hat{H}$ is the Schrödinger operator with a potential

$$U=\frac{2\nu^2\cos^2\theta_0+(\theta_0')^2-\nu^2\sin^2\theta_0}{2x^2},$$

$$2\Delta U=(\theta_0')^2-\left(\frac{\nu^2}{x^2}\right)\sin^2\theta_0;$$

the prime denotes a derivative with respect to the variable $x=r/R$. For a soliton in an isotropic magnet one has $\theta_0'=-(\nu/x)\sin\theta_0$, and the term with ΔU goes to zero. The value of ΔU is nonzero both for magnetic vortices and for precessional solitons in easy-axis magnets. Although our problem does not require studying anisotropic magnets, for which $\Delta U\neq0$, we shall begin by discussing the general properties of that problem, since they are important for choosing the modes corresponding to the motion of the soliton center.

The solution of Eq. (6) can be sought in the form $\psi=\vartheta+i\mu=u(r)e^{i\Phi}+v(r)e^{-i\Phi}$, with $\Phi=m\chi+\omega t$, where m is the azimuthal quantum number. Then for the functions $u(r)$ and $v(r)$ one obtains an eigenvalue problem in the form of two coupled Schrödinger equations:

$$\begin{aligned}\left[\hat{H}+\frac{2m\nu\cos\theta_0}{x^2}\right]u+(\Delta U)_v=\Omega u,\\ \left[\hat{H}-\frac{2m\nu\cos\theta_0}{x^2}\right]v+(\Delta U)u=-\Omega v,\end{aligned} \tag{7}$$

where $\Omega=R^2[\omega D/\zeta+\omega^2/c^2]$ for the generalized σ model. However, if $\Delta U=0$, then the system decomposes into two independent equations of the Schrödinger type for u and v:

$$\hat{H}_{(+)}u=\Omega u,\quad \hat{H}_{(-)}v=-\Omega v, \tag{8}$$

$$\hat{H}_{(\pm)}=-\nabla_x^2+\frac{(m\pm\nu\cos\theta_0)^2-\nu^2\sin^2\theta_0}{r^2}. \tag{9}$$

These two equations are not equivalent; in particular, they have different asymptotics of the solution at zero: $u=c_1r^{m-\nu}+c_2r^{-(m-\nu)}$, and $v=c_3r^{m+\nu}+c_4r^{-(m+\nu)}$. Therefore the equations for u and v play different roles in

the description of the soliton dynamics. It is easy to see that the operators $\hat{H}_{(\pm)}$ do not have negative eigenvalues. Therefore, in the case $\Delta U=0$ the equation for v need not be considered at all—one can set $v=0$ in the solution. Then we arrive at the conclusion that small oscillations against the background of the soliton in an isotropic magnet are described by a single equation of the Schrödinger type (8) with the operator $\hat{H}_{(+)}$ for the variable u.

Solutions of this problem were found in Ref. 16 for $\Omega=0$ and any value of the azimuthal number m. These zeroth solutions $u_m^{(0)}$ have the form $u_m^{(0)}=\sin\theta_0/x\propto d\theta_0/dx$. For $-\nu+1\leqslant m\leqslant\nu$ they describe quasilocal modes of this task. It is particularly important that a mode with $m=1$ exists among them, and the mode conists of $u_1^{(0)}=\sin\theta_0/x\propto d\theta_0/dx$. It is clear that this is the mode that describes the soliton motion and is the mode of greatest interest to us.

For any arbitrarily small but nonzero value of ΔU the situation is fundamentally altered. In this case the equations for u and v form a coupled system. The formal solution for the second equation of system (7) at small ΔU and a finite value $\Omega>0$ can be written in the form

$$v=\frac{1}{\hat{H}_{(-)}+\Omega}(\Delta U)u.$$

This quickly leads to the possibility of not two but four types of behavior of $u(r)$ and the same types of behavior for $v(r)$ for $r\to 0$, i.e., for any m both asymptotic forms can appear: $\psi=c_1r^{m-\nu}+c_2r^{-(m-\nu)}+c_3r^{m+\nu}+c_4r^{-(m+\nu)}$. From this we immediately see that in the case of a coupled system of general form the soliton dynamics as a whole is associated with modes both with $m=-1$ and $m=+1$. In a certain sense, in this case the symmetry with respect to the substitution $m\to -m$ is restored. In particular, the scattering amplitude for spin waves with a small wave number k on a magnetic vortex ($\Delta U\neq 0$) for $m=+1$ and $m=-1$ differ only in the sign,[14] whereas for a soliton in an isotropic ferromagnet $\Delta U=0$, and those amplitudes have different functional dependence on k.[17]

Thus we come to the conclusion that for a general magnet model, when constructing effective equations for the vortex center coordinate, which plays the role of a collective variable, one should use the frequencies of the modes with $m=+1$ and $m=-1$ the higher modes, both single modes and modes joined into doublets. For isotropic magnets only modes with $m=+1$ are important in this problem, which in the limit $\Omega\to 0$ have the asymptotic form $d\theta_0/dr$ and describe the displacement of the soliton. However, we are interested in the motion with nonsmall velocity, which corresponds to finite frequencies in equations (8).

A remarkable property of isotropic magnets with a Belavin–Polyakov soliton is that for them there exists an exact solution for the translational mode with azimuthal number $m=1$ for arbitrary k, and not only of its $k\to 0$ ($\omega\to 0$) asymptotics; this solution corresponds to a shift of the soliton as a whole with an infinitesimal velocity. For our analysis this is very important, since for elucidating the question of whether the soliton motion is of a local or nonlocal character it is necessary to study the dynamics in a magnet of finite size L and not only in the limit $L\to\infty$. This solution was obtained in Ref. 17 and can be written in the form

$$u_1^{\kappa}=J_{\nu+1}(kr)+\frac{J_\nu(kr)}{k(r/R)^\nu}\frac{d\theta_0}{dr}, \tag{10}$$

which emphasizes that at short distances this mode describes the displacement of the soliton. Apparently the presence of such a solution is not due to the exact integrability of the problem. Indeed, an isotropic magnet model is exactly integrable in the static two-dimensional case, $\mathbf{n}=\mathbf{n}(x,y)$, but nothing is known about its integrability in the dynamic $(2+1)$ case, for $\mathbf{n}=\mathbf{n}(x,y,t)$.

Let us study a simple case that permits recovering the soliton equation of motion. We consider oscillations of the magnetization in a circular magnet with a finite radius L and a soliton at the center. We shall discuss the Dirichlet boundary conditions corresponding to a fixed value of the magnetization at the boundary:

$$\psi(r,\chi)|_{r=L}=0, \tag{11}$$

which models the case of repulsion of the soliton from the boundary on account of the image forces.[17] We are interested only in those magnetization oscillations which are due the displacement of the soliton, i.e., which have azimuthal quantum number $m=1$. When the boundary conditions (11) and the explicit form of the eigenfunction (10) are taken into account, the spectrum of the problem is discrete. In the region of small wave vectors $kL\ll 1$ the solution of equation (10) has the form

$$\psi(x)\propto r^{\nu-1}\left(1-\frac{4\nu(\nu+1)}{(kr)^2}\frac{1}{(r/R)^{2\nu}+1}\right),$$

from which we find that for fixed boundary conditions there exists a solution of the spectral problem with an anomalously low frequency corresponding to this inequality. For it

$$k_0^2=\frac{4\nu(\nu+1)}{L^2}\left(\frac{R}{L}\right)^{2\nu}. \tag{12}$$

The next roots of the equation already correspond to the condition $kL\approx 1$, $k_n=j_n/L$, where j_n is the nth root of the Bessel function. Thus the spectrum of eigenfrequencies of the translational mode with $m=1$ contains an anomalously low frequency, which should be manifested in a slow motion of the soliton, and a discrete set of higher frequencies of the same order of magnitude as for the magnet without the soliton. It is important to note that for all these frequencies the corresponding solution clearly exhibits a characteristic peak corresponding to soliton displacement. For an anomalously low frequency the solution is practically indistinguishable from the function $d\theta_0/dr$ in the whole magnet (see Fig. 2a). For the next mode the difference from $d\theta_0/dr$ is noticeable far from the soliton, but the translational maximum, as before, is clearly discernable in the region of localization of the soliton.

For a ferromagnet and antiferromagnet these solutions lead to fundamentally difference physical pictures of the soliton dynamics, and these cases must therefore be analyzed separately. In the case of an antiferromagnet there are two frequencies corresponding to the translational Goldstone mode:

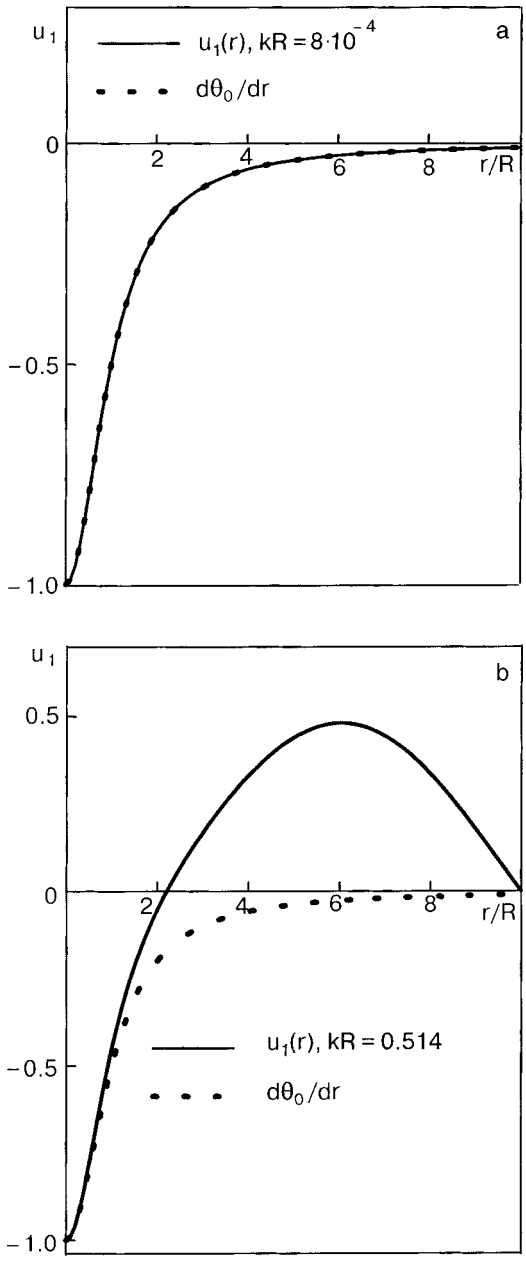

FIG. 2. The function $u_{m=1}(r)$ for a translational Goldstone mode (a) and the next translational mode (b) in an isotropic magnet with $L=10R$.

$$\omega_0^2=c^2k_0^2=\frac{4\nu(\nu+1)c^2}{L^2}\left(\frac{R}{L}\right)^{2\nu}. \tag{13}$$

These frequencies can easily be explained on the basis of a simple physical picture for the motion of a soliton under the image force $\mathbf{F}_e=-\alpha\mathbf{X}/L^p$, where $p=2(\nu-1)$ and $\alpha=16\pi\nu^2(\nu-1)JS^2R^{2\nu}$ (Ref. 17). For the Dirichlet boundary conditions considered here, the force is a restoring force (repulsion from the boundary), and the motion is stable.

It is extremely important that even for the simple case of an antiferromagnet, for which a Lorentz invariant or (at low velocities) Newtonian dynamics should be realized, in the case of a soliton in a magnet of finite size the effective equations turn out to be more complicated than Newton equations. Indeed, the oscillations of the soliton under the influence of the image force has a finite frequency and falls in the continuum. Because of this, magnon modes which in a circular magnet correspond to higher values of k_n are excited. Taking k_n into account for $n>0$ can also be done on the basis of the effective equations for $\mathbf{X}$. A hierarchy of effective equations of motion appears, containing only even-numbered time derivatives. For describing the dynamics with allowance for a single higher mode it is sufficient to write the fourth-order equation in the form

$$M_2\frac{d^4\mathbf{X}}{dt^4}+M\frac{d^2\mathbf{X}}{dt^2}+\frac{\alpha\mathbf{X}}{L^p}=0, \tag{14}$$

the coefficients in which can be found by comparing the frequencies $\omega_1^2=c^2k_1^2$, $k_1=j/L$. For large $L\gg R$ it is found that $M_2\cong M/\omega_1^2$, i.e., M_2 diverges with increasing L,

$$M_2=\frac{E_0L^2}{c^4j^2}, \tag{15}$$

and taking this mode into account gives nonlocal equations for the soliton in an antiferromagnet. The soliton motion with allowance for this term will have the form of a superposition of oscillations of the slow motion with frequencies $\pm\omega_0$ and a fast motion with frequencies $\pm\omega_1$. In the general case one can write for components of the $\mathbf{X}$ vector

$$X=A\cos\omega_0t+C\cos(\omega_1t+\varphi_1),$$

$$Y=B\sin(\omega_0t+\varphi_0)+D\sin(\omega_1t+\varphi_2).$$

Depending on the relationships of the amplitudes A, B, C, D and the phases φ_0, φ_1, φ_2 both the fast and slow motion can be characterized by both linear and elliptical (or circular) polarization. Such a great diversity of the solutions is unsurprising for a fourth-order equation, in which as initial conditions one must specify the value of $\mathbf{X}$ and its time derivatives up to the third, inclusive.

Let us discuss how soliton motion is obtained from this equation under the conditions for which the numerical simulation was done.[13] In this case the initial state corresponded to a static spin configuration with a soliton, which was initially at rest at a certain point $\mathbf{X}(0)=a\mathbf{e}_0$, where $\mathbf{e}_0$ is an arbitrary unit vector. Since a static configuration was used at the initial time, it should be assumed that $d\mathbf{X}/dt|_{t=0}=0$, $d^2\mathbf{X}/dt^2|_{t=0}=0$, and $d^3\mathbf{X}/dt^3|_{t=0}=0$. Hence we find that the soliton moves along a straight line parallel to $\mathbf{e}_0$, and its displacement $\mathbf{X}(t)$ has the form of a superposition of two oscillations:

$$\mathbf{X}(t)=a\mathbf{e}_0\frac{\omega_1^2\cos\omega_0t-\omega_0^2\cos\omega_1t}{\omega_1^2-\omega_0^2}.$$

Thus, by analyzing the simplest case of an antiferromagnet, for which it would seem that the dynamics of solitons of any type should have a Lorentz invariant character, we have established that the center of the soliton should execute a rather complex motion, which, in turn, should be reflected in the response functions of the magnet. This can be verified by numerical modeling. Unfortunately, such studies have not been done.

Thus, starting only from linear equations for the soliton coordinate, we have obtained a relation between the amplitudes of the different modes excited in the system. To check the validity of this approach, let us apply it to a problem that has been analyzed in detail both analytically and numeri-

cally. Let us consider the motion of a vortex in an easy-plane magnet of circular shape with radius L. In such a system there is a lowest mode with $m=1$ and a frequency $\omega_0 \propto 1/L^2$. The next modes are joined into doublets with $m=\pm 1$, and their frequencies ω_1 and ω_2 are close in modulus. The lowest doublet corresponds to $\omega_1=-\tilde{\omega}+\delta$, $\omega_2=\tilde{\omega}+\delta$, $\omega_0 \leqslant \delta \ll \tilde{\omega} \propto 1/L$. This picture is obtained for a numerical study of magnon modes against the background of a vortex in a discrete magnet model[15,14] and analytically from an analysis of the data for magnon scattering on a vortex.[14] The presence of these three modes has been observed in a numerical simulation of the vortex dynamics, while the higher doublets were ordinarily not visible.[13] When only these three frequencies are taken into account, the vortex motion is described by an equation that can be obtained both by a generalization of the phenomenological data[13] and on the basis of the method of collective variables with the use of the generalized substitution of the traveling-wave type:[18]

$$G_3[d^3\mathbf{X}/dt^3,\mathbf{e}_z]+Md^2\mathbf{X}/dt^2+G[d\mathbf{X}/dt,\mathbf{e}_z]+\kappa\mathbf{X}=0.$$

Here the coefficients of the gyroforce G and mass M are finite, the coefficient of elasticity $\kappa \propto 1/L^2$, and the coefficient of the ''higher'' gyroforce G_3 diverges as L^2 with increasing size of the system.[14] The general solution of this equation can be written in the form

$$X=A_0\cos\omega_0 t+A_t\cos(\omega_1 t+\varphi_1)+A_2\cos(\omega_2 t+\varphi_2),$$

$$Y=A_0\sin\omega_0 t+A_1\sin(\omega_1 t+\varphi_1)+A_2\sin(\omega_2 t+\varphi_2).$$

For a description of the numerical studies, let us assume that the vortex is at rest in the initial state, i.e., $d\mathbf{X}/dt|_{t=0}=0$, $d^2\mathbf{X}/dt^2|_{t=0}=0$. Assuming for specificity that $X(0)=a$, $Y(0)=0$, we find that all three coefficients A_0, A_1, and A_2 are nonzero. In the linear approximation in the small parameter $\omega_0/\tilde{\omega}$ we have

$$A_0 \approx a, \quad A_1 \approx -A_2 \approx a\omega_0/2\tilde{\omega}.$$

Here one obtains a trajectory which is extremely similar to that which is observed in numerical simulations and to that described analytically by Kovalev, Mertens, and Schnitzer on the basis of an analysis of the conservation laws for a soliton interacting with a magnon cloud.

For localized topological solitons in ferromagnets no numerical simulation of the soliton motion has been done. In Ref. 17, from an analysis of small oscillations, it was proposed to describe the motion of such solitons on the basis of a Newton equation with a gyroforce:

$$Md^2\mathbf{X}/dt^2+G[d\mathbf{X}/dt,\mathbf{e}_z]=-\alpha\mathbf{X}/L^p.$$

It was found that for a Belavin–Polyakov soliton in a ferromagnet the nonlocality is manifested even in a second-derivative analysis, i.e., in the standard equations of the Newtonian type the effective mass M_{FM} diverges as L^2, $M_{FM}=-4\pi\nu JS^2(L/jD)^2$, its sign depending on the character of the boundary conditions.[17] For fixed boundary conditions the sign of the mass is negative, and for a magnet with a free boundary the mass becomes positive.

The transition from local to nonlocal dynamics is conveniently traced for the example of the generalized σ model (1), (2), which in the antiferromagnet limit (for $\zeta \to 0$) and when only the two lowest modes are taken into account gives local Newton equations with a finite mass $M=E_0/c^2$, and for $1/c^2 \to 0$ it goes over to the Landau–Lifshitz equation for a ferromagnet. We restrict the analysis below to the most interesting case, that with topological charge $\nu=1$.

Let us discuss the dynamical equations with allowance for the two lowest eigenvalues k_0^2 and k_1^2, $k_0^2 \ll k_1^2$ under the condition $R \ll L$, which is written in the form

$$k_0^2=\frac{8R^2}{L^4}, \quad k_1^2=\left(\frac{j}{L}\right)^2.$$

In contrast to the case of a ferromagnet, they correspond to four frequencies, the absolute values of which, unlike the case of an antiferromagnet, can be different. Two frequencies $\omega_0^{(+)}$ and $\omega_0^{(-)}$ correspond to $k^2=k_0^2$,

$$\omega_0^{(\pm)}=-\zeta\frac{c^2}{2D}\pm\sqrt{\left(\zeta\frac{c^2}{2D}\right)^2+c^2k_0^2}, \tag{16}$$

and the other two, $\omega_1^{(+)}$ and $\omega_1^{(-)}$, are related to k_1^2:

$$\omega_1^{(\pm)}=-\zeta\frac{c^2}{2D}\pm\sqrt{\left(\zeta\frac{c^2}{2D}\right)^2+c^2k_1^2}, \tag{17}$$

where the symbols $(\pm)$ in the notation for the frequencies must be chosen the same as the signs in front of the square root in the formulas. These expressions contains three dimensionless small parameters: ζ, $(R/L)^2$, and D/cL. Let us assume that the quantity ck_0, containing the product of two of them, is much less than ck_1, but we shall not yet fix the relative values of $\zeta c^2/D$ and ck_0 or ck_1. It is clear that such an inequality does not rule out the case of a ''pure'' antiferromagnet, for which $\zeta=0$.

If the value of ζ is large enough or the size L of the system small, so that $\zeta c > D/L$, then the following inequality holds:

$$\omega_0^{(+)} \ll \omega_1^{(+)} \ll \omega_0^{(-)} \cong |\omega_1^{(-)}| \cong \zeta c^2/D.$$

In this limiting case one should throw out the maximum frequencies of the order of $\zeta c^2/D$. The point is that for a ''pure'' ferromagnet $\zeta \sim 1$, and these frequencies are large, of the order of the exchange integral. More importantly, a whole series of quasi-doublets, corresponding to the values $c^2k_2^2$, $c^2k_2^3$, ..., $k_n^2 \sim j_n/L$, where j_n are the next roots of the Bessel function, lie between $\omega_1^{(\pm)}+$ and $\omega_{0,1}^{(-)}$, by virtue of which it is inconsistent to take $\omega_{0,1}^{(-)}$ into account. Then the the relationship of the two frequencies $\omega_1^{(+)}$ and $\omega_0^{(+)}$, which are important for the problem, are the same as for a soliton in a ferromagnet: $\omega_0^{(-)} \ll \omega_1^{(+)}$. One expects that the equation of motion, as in a ferromagnet, will have Newtonian form:

$$M\frac{d^2\mathbf{X}}{dt^2}+G\left[\mathbf{e}_z,\frac{d\mathbf{X}}{dt}\right]=\mathbf{F}_e. \tag{18}$$

Here $\mathbf{F}_e=-\alpha\mathbf{X}/L^p$ is the external force, which has the same form as for an antiferromagnet; G is the gyroscopic constant. Let us consider how these equations jibe with the regularities of soliton dynamics obtained from an analysis of small oscillations. In the leading approximation in the small parameters ζ and $(R/L)^2$, we obtain two values of the frequencies: G/M and α/GL^p. Comparing these frequencies with the quantities $\omega_0^{(+)}$ and $\omega_1^{(+)}$, we arrive at a formula for the

effective mass and gyroforce, which differ from those obtained above for a ferromagnet only by the presence of a factor ζ:

$$M = -\frac{4\pi\zeta^2 JS^2}{D^2}\left(\frac{L}{j}\right)^2, \quad G = \frac{4\pi\zeta JS^2}{D}. \tag{19}$$

We note that the value of the gyroforce is easily obtained in the usual way, by direct analysis of the equations of the σ model.

To summarize, in the ''ferromagnetic'' limiting case $\zeta c > D/L$ the value of the effective mass turns out to diverge as L^2, just as in a ''pure'' ferromagnet. However, the coefficient in front of L^2 falls off with decreasing ζ, and in the actual case $\zeta \ll 1$ the value of M for finite L is of order ζ in smallness.

Let us now consider the other interesting limiting case, the ''antiferromagnetic,'' $\zeta c < D/L$. In this limiting case the inequality $|\omega_0^{(\pm)}| \ll |\omega_1^{(\pm)}|$ holds, and the leading approximation corresponds to two frequencies, $\omega_0^{(+)} \cong \alpha R^2/L^4 G$, and $\omega_0^{(-)} \cong -\zeta c^2/D$, and the frequencies $\omega_1^{(\pm)}$ form a high-lying doublet. It is clear that in this leading approximation we again obtain the usual Newton dynamical equation with the gyroforce (18). Comparing its roots with the quantities $\omega_0^{(-)}$ and $\omega_0^{(-)}$ from Eq. (16), we find that the value of the effective mass is finite and positive:

$$M = \frac{4\pi JS^2}{c^2}.$$

This value literally reproduces the Lorentz invariant answer, but in this case the value of the gyroforce is finite. Taking the limit $\zeta \to 0$ in the formulas obtained gives a purely antiferromagnetic Lorentz invariant dynamics. Taking the higher doublet into account leads to the appearance of fourth-order equations with the same structure as for a ''pure'' antiferromagnet but with an additional term proportional to $\zeta d^3\mathbf{X}/dt^3$ (we shall not discuss them here).

Thus, for the most general but physically interesting two-dimensional model of an isotropic magnet, we have analyzed the dynamics of Belavin–Polyakov solitons and tracked the transition from local dynamics—Lorentz invariant for an antiferromagnet or purely gyroscopic (inertialess) for the ferromagnet—to nonlocal dynamics. We have shown that the nonlocal nature necessarily arises in an analysis of the motion of the coordinate of the center of the soliton, considered as a collective variable, and as necessary take into account a sufficient number of eigenfrequencies of the system. In a ferromagnet the standard inertial term in the Newton equation is already nonlocal, while for a pure antiferromagnet the nonlocality appears when the first non-Goldstone doublet is taken into account. In the intermediate case of a ferrimagnet with a small but nonzero decompensation of the spins, $\zeta \gg (D/cL)(R/L)^2$, for a soliton in the simplest approximation one obtains typical Newtonian dynamics with a gyroscopic force. Under the inequality $\zeta \ll D/cL$ the effective mass is finite for $L \to \infty$. The condition for realization of such behavior is that the inequalities $\zeta \ll D/cL$ hold. Since $D/c \sim a$ (a is the lattice constant), this may reasonably be reconciled with the point of view of the microscopic approximation (which requires the condition $R \gg a$) only in a finite magnet at sufficiently low values of ζ:

$$\zeta \ll \frac{1}{L}\frac{D}{c} \approx \frac{a}{L}.$$

In the other limiting case, $\zeta > D/cL$, the effective mass, as in the case of a ferromagnet, diverges as L^2 as the size of the system increases, but with a much smaller coefficient, which goes to zero in the limit $\zeta \to 0$. Thus a transition from local to typically nonlocal behavior occurs upon variations in the size of the system or the decompensation parameter ζ.

*E-mail: bivanov@i.com.ua

[1] Yu. A. Izyumov, Usp. Fiz. Nauk **155**, 553 (1988) [Sov. Phys. Usp. **31**, 689 (1988)].
[2] H.-J. Mikeska and M. Steiner, Adv. Phys. **40**, 191 (1991).
[3] V. G. Bar'yakhtar and B. A. Ivanov, ''Soliton thermodynamics of low-dimensional magnets,'' Sov. Sci. Rev. Sec. A: Phys. Reviews (edited by I. Khalatnikov, Amsterdam) **16**, 3 (1993).
[4] A. A. Belavin and A. M. Polyakov, JETP Lett. **22**, 245 (1975).
[5] V. L. Berezinskiĭ, Zh. Éksp. Teor. Fiz. **59**, 907 (1970) [Sov. Phys. JETP **32**, 493 (1971)]; Zh. Éksp. Teor. Fiz. **61**, 1144 (1971) [Sov. Phys. JETP **34**, 610 (1972)].
[6] J. M. Kosterlitz and D. J. Thouless, J. Phys. C **6**, 1181 (1973).
[7] D. D. Wiesler, H. Zabel, and S. M. Shapiro, Z. Phys. B: Condens. Matter **93**, 277 (1994).
[8] F. Waldner, J. Magn. Magn. Mater. **31–34**, 1203 (1983); *ibid.* **54–57**, 873 (1986); *ibid.* **104–107**, 793 (1992).
[9] C. E. Zaspel, T. E. Grigereit, and J. E. Drumheller, Phys. Rev. Lett. **74**, 4539 (1995); K. Subbaraman, C. E. Zaspel, and J. E. Drumheller, *ibid.* **80**, 2201 (1998).
[10] C. E. Zaspel and J. E. Drumheller, Int. J. Mod. Phys. **10**, 3649 (1996).
[11] B. A. Ivanov and A. L. Sukstanskiĭ, Zh. Éksp. Teor. Fiz. **84**, 370 (1983) [Sov. Phys. JETP **57**, 214 (1983)].
[12] F. G. Mertens, H. J. Schnitzer, and A. R. Bishop, Phys. Rev. B **56**, 2510 (1997).
[13] F. G. Mertens and A. R. Bishop, in *Nonlinear Science at the Dawn of the 21st Century*, edited by L. Christiansen, M. Soerensen, and A. C. Scott, Lecture Notes in Physics, Springer, Berlin (2000).
[14] B. A. Ivanov, H. J. Schnitzer, F. G. Mertens, and G. M. Wysin, Phys. Rev. B **58**, 8464 (1998).
[15] G. M. Wysin, Phys. Rev. B **54**, 15156 (1996).
[16] B. A. Ivanov, JETP Lett. **61**, 917 (1995).
[17] B. A. Ivanov, V. M. Murav'ev, and D. D. Sheka, Zh. Éksp. Teor. Fiz. **116**, 1091 (1999) [JETP **89**, 583 (1999)].
[18] H. J. Schnitzer, F. G. Mertens, and A. R. Bishop, Physica D **141**, 261 (2000).

Translated by Steve Torstveit

LATTICE DYNAMICS

Elastic constants of borocarbides. New approach to acoustic measurement technique

E. A. Masalitin, V. D. Fil,' K. R. Zhekov, A. N. Zholobenko, and T. V. Ignatova

B. Verkin Institute for Low Temperature Physics and Engineering, National Academy of Sciences of Ukraine, pr. Lenina 47, 61103 Kharkov, Ukraine

Sung-Ik Lee

Department of Physics, Pohang University of Science and Technology, Pohang 790-784, Korea
(Submitted July 15, 2002)
Fiz. Nizk. Temp. **29**, 93–98 (January 2003)

A new version of the phase method of determining the sound velocity is proposed and implemented. It utilizes the ''Nonius'' measurement technique and can give acceptable accuracy ($\leqslant 1\%$) in samples of submillimeter size. Measurements of the sound velocity are made in single-crystal samples of the borocarbides RNi_2B_2C (R=Y, Lu, Ho). The elastic constants and the Debye temperature are calculated. © *2003 American Institute of Physics.*
[DOI: 10.1063/1.1542380]

1. INTRODUCTION

An important problem of physical acoustics is to obtain reliable data on the elastic constants of newly synthesized compounds. These data, while being of independent interest, also serve as tests for theoretical calculations of band structures, force constants, and phonon spectra. As a rule, newly synthesized materials come either in the form of products of solid-phase synthesis (i.e., more or less porous ceramics) or in the form of fine single crystals. Objects of the first group are characterized by appreciable scattering of elastic vibrations, making it practically impossible to use some version of a resonance or quasiresonance (of the long-pulse type) method to determine the absolute values of the sound velocity in them. Single crystals most often are of millimeter or submillimeter size; besides, in layered crystals the characteristic size in the direction perpendicular to the layers is often 100–200 μm or even less. To determine the elastic constants of such objects the method of ultrasonic resonance spectroscopy[1] was developed, which consists in measurement of the spectrum of resonance frequencies of a sample and subsequent solution of the inverse problem of recovering all the components of the tensor of elastic constants. The technique is inherently a resonance method, i.e., it applies only to objects with small scattering (damping), a condition which is not always possible to satisfy even in small single crystals, e.g., near points of phase transitions. In addition, it can be implemented only in samples having a definite simple geometric shape (rectangular parallelepiped). The lucidity of this method is compromised by the complexity of the mathematical processing, making it hard to spot possible errors.

We have implemented a new version of the phase method of measuring sound velocities; it is applicable both to ceramic samples with strong scattering and to single crystals of submillimeter size. Utilizing a kind of ''Nonius'' measurement procedure, the method permits one to achieve acceptable accuracy (as a rule, better than 1%) in both cases. It has been used to measure the sound velocity in MgB_2 polycrystals[2] and in VSe_2 layered single crystals.[3] Furthermore, being completely independent of the nature of the signals to be analyzed, the instrumental implementation of the method enables one to study the variation of the amplitude and phase of any pulsed high-frequency signals. In particular, it has been used to measure the characteristics of an electric field accompanying a longitudinal sound wave in a metal.[4]

Section 2 of this paper is devoted to a description of the basic principles of implementation of the ''Nonius'' method of phase measurements of sound velocity. In Sec. 3 we present the results of measurements of the elastic constants in single crystals of the borocarbides RNi_2B_2C (R=Y, Lu, Ho).

2. "NONIUS" METHOD OF SOUND VELOCITY MEASUREMENT. PRINCIPLES AND INSTRUMENTAL IMPLEMENTATION

A block diagram of a device implementing the technique is presented in Fig. 1. It is essentially a standard compensation or bridge circuit, depending on the algorithm used for process the pulsed signals, which is set by the pulse code modulation unit. In the bridge mode the signal that has passed through the sample channel is summed with the antiphase comparison signal, which is equal in absolute value. The amplitude and phase of the latter are regulated by the receiver, which functions as a null device. The unbalance signal is separated into amplitude and phase components by high-frequency synchronous detectors.[5] In the compensation mode the receiver, with the aid of sampling–storage devices, matches the amplitudes of the signals arriving at its input at different times. In this case the noncompensation signals with respect to amplitude and phase are produced through a special code modulation of the pulse trains of the signals in the two channels. In any variant the data input to the com-

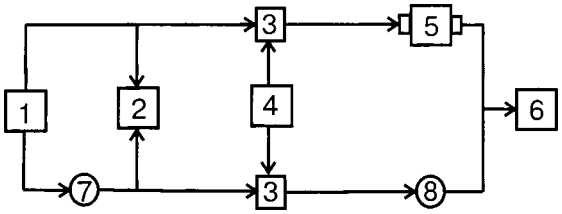

FIG. 1. Block diagram of the instrument: 1—frequency synthesizer, 2—phase meter, 3—switches, 4—pulse-code modulation unit, 5—sample with piezotransducers, 6—receiver, 7—electronically tunable phase shifter, 8—smoothly adjustable attenuator.

puter are the readings of an attenuator (amplitude of the comparison signal) and phase meter (phase difference of the signal to be analyzed and the comparison signal).

Two original developments employed in the implementation of this standard scheme have substantially expanded its operational capabilities: an electronically controlled (linear) phase shifter with a practically unlimited tuning range, and a new data processing algorithm, which maintains a phase shift of 120° (or 240°) between the signals being analyzed. The advantages of the new phase shifter are quite obvious. In particular, in relative measurements this phase shifter provides a practically unlimited dynamic range while maintaining an extremely high accuracy of measurement, which is actually determined by the resolution of the phase meter (at a signal-to-noise ratio $\geqslant 5$). Let us discuss the second development in somewhat more detail. In the bridge mode the working algorithm of the circuit consists in maintaining a null signal at the input of the receiver upon changes in the sound velocity and damping in the sample. In inhomogeneous (e.g., polycrystalline) samples, internal rereflections and mutual conversion of different modes at inhomogeneities lead to nonconstancy of the phase of the signal over the duration of the rf pulse envelope. The same situation is observed in short single crystals due to the superposition of secondary reflections. In this case the length of the time interval during which the sum of the two signals has zero amplitude turns out to be short ($\leqslant 10^{-7}$ s). For analysis of such narrow features the receiving system should have a rather wide passband and not allow any overshoots in reproducing steep signal fronts.

For the 120° algorithm the sum of two signals of identical amplitude (their equality is maintained by an independent channel) is equal to the amplitude of each of the signals (equilateral triangle). In this case at the time of sampling–storage there are no sharp amplitude drops at the input of the receiver; this substantially improves the working of the system as a whole. A distinct advantage of the 120° algorithm is that it is unnecessary to have frequency (phase) modulation of the master oscillator in order to obtain unbalance signals of different polarity upon passage through the compensation point, as one must have for self-balancing of the circuit. Furthermore, the usual amplitude detection used in the 120° algorithm allows one to use as the signals of the two channels any two reflections that have traveled different distances in the sample.

The measurement algorithm in part resembles one proposed earlier.[6] First the phase–frequency (P–F) characteristic of an acoustic circuit consisting of two delay lines is

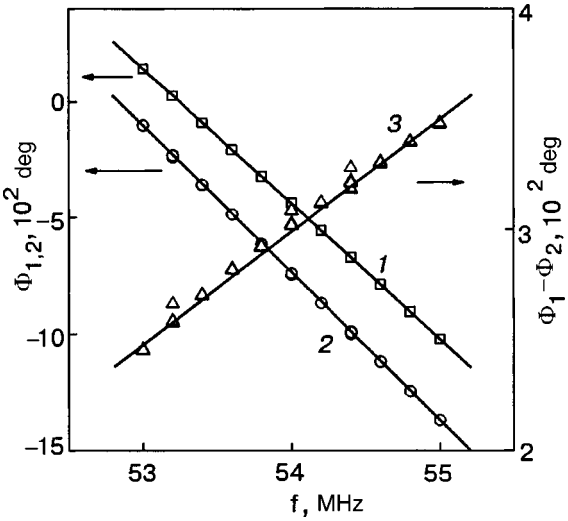

FIG. 2. Phase–frequency characteristics of the delay lines (*1*), of a sandwich consisting of the sample ($LuNi_2B_2C$, $\mathbf{q}\|[100]$, $\mathbf{u}\|[100]$, $L=0.835$ mm) and the delay lines (*2*), and the difference function, i.e., the P–F characteristic of the sample (*3*). Note the difference in the scales of the vertical axes.

measured at fixed frequency points (step 1). Then the P–F characteristic of a sandwich consisting of the same delay lines but with the sample between them (Fig. 2) is measured at the same temperature (step 2).[1)]

Because the signal circuits contain elements capable of resonating (piezotransducers, imperfectly matched feeders), each of these characteristics is not necessarily a straight line. However, their difference, i.e., the P–F characteristic of the sample, in the absence of interference distortions in it, should form a strictly straight line, the slope of which determines the phase velocity of the sound,

$$v=\frac{360L}{S}, \tag{1}$$

where v is the sound velocity (cm/s), L is the thickness of the sample (cm), and S is the slope of the P–F difference characteristic (deg/Hz). It is easily seen by a direct calculation that when the P–F characteristics *1* and *2* are approximated by straight lines by the least-squares method (the slopes are S_1 and S_2, respectively), then

$$S=S_2-S_1 \tag{2}$$

for any deviations of the P–F characteristics *1* and *2* from straight lines. This relation is valid only if the frequency points at which the P–F characteristics *1* and *2* are measured are coincident. In Ref. 6 essentially the same procedure was used to determine S, but since the technique used there did not guarantee the required coincidence, additional errors could have been introduced.

If S is comparable to S_1 (0.3 or larger), then in homogeneous materials the measurements can be limited to this step with completely acceptable accuracy (0.3% or better).

However, in homogeneous but rather thin samples the superposition of secondary reflections distorts the main part of the measurement signal. Because of this, the parts of the pulse that coincide with the leading edge are customarily used for measurements. An analogous procedure, as a rule,

should be used in inhomogeneous materials for the reasons already mentioned, even though the acoustic path length in them may be comparatively large.

As a result of the occurrence of various kinds of transient processes, the rate of which depends on the carrier frequency of the pulses, the slopes of the P–F characteristics *1* and *2* become functions of the temporal position of the strobe readout pulse at the leading edge of the measurement signal. The variation of $S_{1,2}$, depending on the type of piezotransducers, is 2–4% (for comparison, in extended samples the variation of $S_{1,2}$ at the steady part of the pulse is at the 0.1% level). This means that in going from step 1 to step 2 the readout pulse should be shifted precisely by the sound delay time τ_0 in the sample. Since the latter is initially unknown and also because of the discreteness of the step for the time shift of the strobe signal (5×10^{-8} s in our experiments), it was practically impossible to satisfy this condition. For finding τ_0 (and, hence, the sound velocity) we used the following interpolation procedure.

For each series of measurements with a definite mode (longitudinal or transverse) we calibrated the dependence of S_1 on the temporal position t_x of the readout pulse. Then for a given sample we measured S_2 at some known position t_c of the readout pulse at the leading edge of the signal. It is easy to see from Eqs. (1) and (2) that τ_0 is a solution of the equation $S(x)=360x$, where $x\equiv t_c-t_x$ is the time shift of the readout pulse between the set of calibration measurements S_1 and the measurements with the sample, S_2. An example of the graphical solution of the interpolation equation for several values of t_c is presented in Fig. 3. The results of the interpolation (the value of τ_0) coincide regardless of the choice of t_c.

At this step of the procedure the ''rough'' determination of the sound velocity is completed. To refine the values we use the ''Nonius'' method. Let the phase of the signal registered at some definite frequency f_0 by the phase meter in step 1 be equal to Φ_1. In step 2 at the same frequency the phase of the signal will be Φ_2. The total phase inserted by

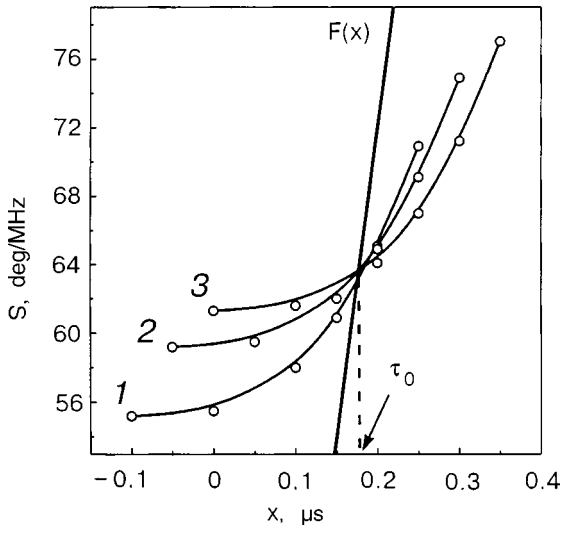

FIG. 3. Example of the interpolation procedure for finding the sound delay time τ_0. YNi_2B_2C sample ($\mathbf{q}\|[100]$, $\mathbf{u}\|[010]$, $L=0.885$ mm) for several values of t_c (see text). At $x=0$ the values of t_c increase from bottom to top with a step of 5×10^{-8} s. The linear function $F(x)=360x$.

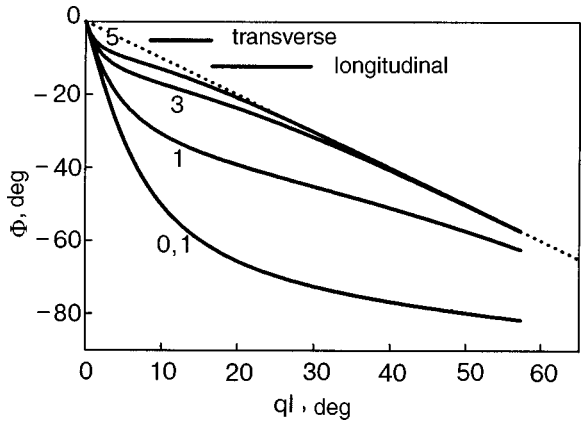

FIG. 4. Diagram pertaining to the calculation of the additional phase shift inserted by the grease layer. The reflection coefficient at the grease–sample boundary $k=0.85$, and the numbers on the curves give the sound damping coefficient in the grease layer (neper/cm). The dotted curve corresponds to $\Phi=-ql$. The horizontal lines indicate the regions of the actual values of the parameter ql for the corresponding mode.

the sample is $\Phi_0=360n+(\Phi_2-\Phi_1)$, where $n=0,1,2,\ldots$. Since $\Phi_0=360f_0L/v$, by trying values of n we find the refined value of v that is closest to the ''rough'' estimate.

In the above discussion it was tacitly assumed that on going from step 1 to step 2 the phase of the signal changes only because of the addition of the sample. Actually, however, besides the sample we also had an additional layer of grease in step 2. During measurements in very thin samples the contribution of the grease layer can become noticeable. In our experiments GKZh-94 silicone oil was used as the bonding agent, forming a layer $\sim1-2$ μm thick between the ground surfaces. The passage of an elastic wave through such a thin layer is described by the sum of an infinite geometric progression with the denominator $q=k^2e^{-2l(\alpha+iq)}$, where k is the reflection coefficient at the boundary (we assume that the wave impedances of the delay line and sample are close in value), l is the thickness of the grease layer, α is the damping coefficient, and q is the wave number.

An estimate of the propagation velocity of sound in the grease gave $v_l\sim2.1\times10^5$ cm/s, $v_t\sim1.2\times10^5$ cm/s, which correspond to reflection coefficients $k\sim0.85$ for our samples. In Fig. 4 we present the calculated dependence of the phase of the wave passing through the grease layer on the thickness for various damping coefficients. The regions of ql corresponding to the conditions of the experiment are also indicated in Fig. 4. At low damping the correction can be rather large. We were unable to estimate the value of the sound damping in the grease—in thick layers (~0.5 mm) it was very large, probably because of cracking—but we assume that its value is found at the 20 dB/cm level or higher, i.e., the phase inserted by the grease layer is close to ql. In processing the results of the measurements we introduced a correction for the additional grease layer—10° for longitudinal sound and 20° for transverse sound. In thin samples the effect of this correction was not over 1%. We suppose that this correction can be eliminated by making comparative measurements on two samples of different thickness.[3] In that case the length difference δL should be comparable to L, since otherwise the contribution of possible nonuniformities of the sound velocity over the whole length of the sample

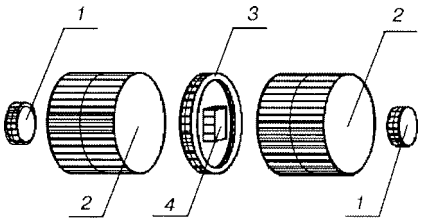

FIG. 5. Diagram of the mounting of the sample: 1—piezotransducers, 2—delay lines, 3—brass support ring, 4—sample.

would be attributed to the small difference δL.

Let us conclude with an estimate of the potential accuracy of a single measurement. Special studies have established that the irreducibility of the phase upon the remounting (regluing) of the acoustic circuit is at the level of 20°. We estimate the indeterminacy of the correction for the additional grease layer to be 10°. Assuming that the accuracy of the ''rough'' estimate of the velocity is sufficient for determining the necessary value of n, we obtain for the measurement error (at $f_0 \sim 50$ MHz)

$$\frac{\delta v}{v} = \frac{30}{\Phi_0} \approx 2 \times 10^{-9} \frac{v}{L}.$$

TABLE I. Sound velocity in single crystals of borocarbides ($T = 77$ K).

Polarization		v, 10^5 cm/s		
q ∥	u ∥	YNi_2B_2C	$LuNi_2B_2C$	$HoNi_2B_2C$
[100]	[100]	6.78 (0.885)	5.88 (0.8)	6.04 (0.606)
	[001]	3.25 (0.885)	2.65 (0.8)	2.73 (0.606)
	[010]	4.80 (0.885)	4.30 (0.8)	4.33 (0.606)
[110]	[110]*	7.55 (0.59)	6.64 (0.988)	6.86 (0.525)
	[001]*	3.26 (0.59)	2.64 (0.988)	–
	[1$\bar{1}$0]	3.34 (0.59)	2.77 (0.988)	2.83 (0.525)
[001]	[001]	6.49 (0.84)	6.01 (0.4)	5.91 (0.23)
	[100]*	3.26 (0.84)	2.70 (0.4)	2.81 (0.23)
	[010]*	3.28 (0.84)	2.70 (0.4)	2.83 (0.23)
45° from the [001] axis in the (110) plane	QL*	7.28 (0.303)	–	–
	QT	3.18 (0.465)	–	–
	[110]*	3.31 (0.303)	–	–
45° from the [001] axis in the (100) plane	QT	–	2.01 (0.27)	–

Note: The ''superfluous'' data are denoted by an asterisk (*). QL and QT are the quasilongitudinal and quasitransverse modes; the thickness of the sample in mm is given in parentheses.

3. ELASTIC CONSTANTS OF BOROCARBIDES RNi_2B_2C (R=Y, Lu, Ho)

In spite of the significant interest in the family of superconducting borocarbides, very little information about their elastic properties can be found in the literature. We know of only one ''acoustical'' study,[7] devoted to YNi_2B_2C, in which the sound velocity was measured by a time-of-flight method. Single crystals of borocarbides were grown by the method described in Ref. 8 and had the shape of a slab with a maximum dimension along the [001] axis of ~0.8 mm (R=Y), ~0.2 mm (R=Ho), and ~0.4 mm (R=Lu). They were quite brittle, and therefore the mounting of the samples between the delay lines was done with the aid of a special brass ring, which acted as a holder and reinforcer; the ring was ground simultaneously with the preparation of the working faces (Fig. 5). The diameter of the ring was chosen larger than the diameter of the piezotransducers to prevent spurious signals.

All of the measurements were made at liquid nitrogen temperature. The results are presented in Table I. It contains some ''superfluous'' data, marked by an asterisk (*). For example, for C_{44} it was sufficient to make a single measurement $\mathbf{q} \| [100]$, $\mathbf{u} \| [001]$ ($\mathbf{u}$ is the polarization vector of the elastic wave). We assume, however, that having the ''superfluous'' data will make it possible to get an idea of the accuracy of the measurements in this case.

One can also see that certain relations which follow from the general theory of elasticity[9] are well satisfied. For example, in a tetragonal crystal the sum of the squares of the velocities of the three modes remains constant under rotation of the wave vector $\mathbf{q}$ in the (001) plane.

The elastic constants of the single crystals studied are presented in Table II. The x-ray densities were used in calculating them. For R=Y the agreement with the results of Ref. 7 is poor, although the relationships among the various

TABLE II. Calculated parameters for borocarbides ($T = 77$ K).

Parameters	YNi_2B_2C		$LuNi_2B_2C$	$HoNi_2B_2C$
C_{11}	27.94	22 [7]	29.39	29.47
C_{12}	14.39	9.84 [7]	16.34	16.53
C_{13}	17.81	–	23.15	–
C_{33}	25.61	21.1 [7]	30.68	28.20
C_{44}	6.43	5.42 [7]	5.97	6.02
C_{66}	14.0	13.1 [7]	15.71	15.15
B	20.16	–	20.27	23
θ_D, K	501	490 [10]	409 (360 [10])	404
ρ, g/cm^3	6.08	6.05 [7]	8.5	8.08

Note: C_{ik} are elastic constants (in units of 10^{11} dyn/cm^2), θ_D is the Debye temperature, and B is the bulk modulus. For Ho the modulus C_{13} was not measured, and in the calculation of θ_D and B it was assumed equal to 23.15 (see text).

constants are preserved on the whole. The Debye temperature was calculated according to the formula[9]

$$\Theta_D = 1146.8\left(\frac{\rho s}{AI}\right)^{1/3},$$

where A is the molecular weight, s is the number of atoms in the molecule, ρ is the mass density, and I is the sum of the inverse cubes of the phase velocities of the elastic waves, averaged over all directions of the wave normal. For R=Ho, because of the difficulty of preparing a sample of the required orientation, the elastic constant C_{13} was not measured, and in the calculation of the bulk modulus and Debye temperature it was assumed equal to the value of C_{13} in lutecium borocarbide. For R=Y the calculated value of Θ_D is close to the thermodynamic estimate.[10] For R=Lu the deviation of the calculated value of Θ_D from the thermodynamic value is, generally speaking, greater than the allowable error. That may be an indication of the existence in lutecium borocarbide of a low-temperature ferroelastic structural transition, accompanied by a significant softening of some elastic constant. Our preliminary measurements in holmium borocarbide have shown that at 5.2 K the velocity of the C_{66} mode falls to $\sim 3.3\times 10^5$ cm/s. When this softening is taken into account, one obtains $\Theta_D = 383$ K for R=Ho.

This study was supported in part by the Government Foundation for Basic Research of the Ministry of Education and Science of Ukraine (Grant No. 0207/00359).

*E-mail: fil@ilt.kharkov.ua

[1)] At the frequencies we used the scale of the phase variations of the signal are much greater than 360°. The phase meter, of course, measures phase differences in the interval 0–360°, and the absence of discontinuities (360° jumps) in Fig. 2 is achieved through programming.

[1] A. Migliory, J. L. Sarrao, W. M. Visscher, T. M. Bell, M. Lei, Z. Fisk, and R. G. Leisure, Physica B **183**, 1 (1993).
[2] T. V. Ignatova, G. A. Zvyagina, I. G. Kolobov, E. A. Masalitin, V. D. Fil', Yu. B. Paderno, A. N. Bykov, V. N. Paderno, and V. I. Lyashenko, Fiz. Nizk. Temp. **28**, 270 (2002) [Low Temp. Phys. **28**, 190 (2002)].
[3] I. A. Gospodarev, A. V. Eremenko, T. V. Ignatova, G. V. Kamarchuk, I. G. Kolobov, P. A. Minaev, E. S. Syrkin, S. B. Feodos'ev, V. D. Fil, A. Soreau-Leblanc, P. Molinie, and E. C. Faolques, Fiz. Nizk. Temp. [Low Temp. Phys.] (in press).
[4] Yu. A. Avramenko, E. V. Bezuglyi, N. G. Burma, V. M. Gokhfeld, I. G. Kolobov, V. D. Fil', and O. A. Shevchenko, Fiz. Nizk. Temp. **28**, 469 (2002) [Low Temp. Phys. **28**, 328 (2002)].
[5] V. D. Fil', P. A. Bezuglyĭ, E. A. Masalitin, and V. I. Denisenko, Prib. Tekh. Éksp. No. 3, 210 (1973).
[6] E. V. Bezuglyĭ, N. G. Burma, I. G. Kolobov, V. D. Fil', I. M. Vitebskiĭ, A. N. Knigavko, N. M. Lavrinenko, S. N. Barilo, D. I. Zhigunov, and L. E. Soshnikov, Fiz. Nizk. Temp. **21**, 86 (1995) [Low Temp. Phys. **21**, 65,452 (1995)].
[7] S. Isida, A. Matsushita, H. Takeya, and M. Suzuki, Physica C **349**, 150 (2001).
[8] M. O. Mun, S. I. Lee, W. C. Lee, P. C. Canfield, B. K. Cho, and D. C. Johnston, Phys. Rev. Lett. **76**, 2790 (1996).
[9] F. I. Fedorov, *Theory of Elastic Waves in Crystals*, Plenum Press, New York (1968), Nauka, Moscow (1965).
[10] H. Michor, T. Holubar, C. Dusek, and G. Hilscher, Phys. Rev. B **52**, 16165 (1995).

Translated by Steve Torstveit